https://ntrs.nasa.gov/search.jsp?R=19830002119 2020-03-21T06:55:31+00:00Z

General Disclaimer

One or more of the Following Statements may affect this Document

- This document has been reproduced from the best copy furnished by the organizational source. It is being released in the interest of making available as much information as possible.

- This document may contain data, which exceeds the sheet parameters. It was furnished in this condition by the organizational source and is the best copy available.

- This document may contain tone-on-tone or color graphs, charts and/or pictures, which have been reproduced in black and white.

- This document is paginated as submitted by the original source.

- Portions of this document are not fully legible due to the historical nature of some of the material. However, it is the best reproduction available from the original submission.

Produced by the NASA Center for Aerospace Information (CASI)

NASA Technical Memorandum 82876

(NASA-TM-82876) IMPLICIT MARCHING SOLUTION OF COMPRESSIBLE VISCOUS SUBSONIC FLOW IN PLANAR AND AXISYMMETRIC DUCTS Ph.D. Thesis (NASA) 222 p HC A10/MF A01 CSCL 20D N83-10389
Unclas
G3/34 38398

Implicit Marching Solution of Compressible Viscous Subsonic Flow in Planar and Axisymmetric Ducts

Charles E. Towne
Lewis Research Center
Cleveland, Ohio

and

Joe D. Hoffman
Purdue University
West Lafayette, Indiana

September 1982

NASA

TABLE OF CONTENTS

PRINCIPAL NOTATION

Symbols

a	Coefficient of velocity in uncoupled streamwise momentum equation
A	Area
$\tilde{\tilde{A}}$	Coefficient matrix in coupled equations
b	Coefficient of velocity in uncoupled streamwise momentum equation
$\tilde{\tilde{B}}$	Coefficient matrix in coupled equations
c	Coefficient of velocity in uncoupled streamwise momentum equation
c_f	Skin friction coefficient
c_p	Specific heat at constant pressure
c_P	Pressure coefficient
c_v	Specific heat at constant volume
c_C	Coefficient in coupled continuity equation
c_E	Coefficient in coupled energy equation
c_W	Coefficient in cross-flow momentum equation evaluated at a wall
c_X	Coefficient in coupled streamwise momentum equation
c_Y	Coefficient in coupled cross-flow momentum equation
$\tilde{\tilde{C}}$	Coefficient matrix in coupled equations
d	Coefficient of viscous pressure correction in uncoupled streamwise momentum equation
D	Pipe diameter
D_S	Parameter controlling grid packing

e	Coefficient of velocity in total mass flow rate equation
e_{mn}	Strain rate tensor (m and n = 1, 2, 3)
f	Coefficient of viscous pressure correction in total mass flow rate equation
h	Static enthalpy
h_1, h_2, h_3	Metric scale coefficients
i	Grid index in streamwise (ξ) direction
j	Grid index in cross-stream (η) direction
J	Value of j at upper wall
k	Thermal conductivity coefficient
ℓ	Mixing length
L_e	Entrance length in developing pipe flow
L_r	Reference length
$\dot{m}$	Mass flow rate
M	Mach number
M_1	Nominal inlet Mach number
$\mathcal{O}$	Symbol for "order of"
p	Static pressure
p_0	Total pressure
p_{ref}	Reference pressure in definition of pressure coefficient
p'	Viscous static pressure correction
$\bar{p}$	Imposed static pressure
Pr	Prandtl number
q_m	Heat flux vector (m = 1, 2, 3)
r	Absolute Cartesian or polar coordinate
r_F	Recovery factor

R	Gas constant; Pipe radius
Re_0	Reynolds number based on pipe diameter and average velocity
Re_r	Reference Reynolds number
Re_R	Reynolds number based on pipe radius and average velocity
s_M	Source term in total mass flow rate equation
s_X	Source term in uncoupled streamwise momentum equation
S_C	Source term in coupled continuity equation
S_E	Source term in coupled energy equation
S_W	Source term in cross-flow momentum equation evaluated at a wall
S_X	Source term in coupled streamwise momentum equation
S_Y	Source term in coupled cross-flow momentum equation
$\vec{S}$	Source term vector in coupled equations
t	Time
T	Static temperature
T_0	Total temperature
T_{AW}	Adiabatic wall temperature
T_r	Reference temperature
T^+	Law-of-the-wall temperature
u	Streamwise velocity
u_0	Average streamwise velocity in pipe
u_τ	Friction velocity
u^+	Law-of-the-wall streamwise velocity
u^*	Streamwise velocity from preliminary marching step

U_r	Reference velocity
v	Cross-flow, or normal, velocity
V_p	Potential flow velocity
w	Implicit weighting factor
$\tilde{X}$	Solution vector in coupled equations
y	Distance from wall
y^+	Law-of-the-wall coordinate
Y	Transformed (equally spaced) cross-stream coordinate
z	Absolute Cartesian or polar coordinate
γ	Ratio of specific heats, c_p/c_v
δ	Boundary layer thickness
δ_{mn}	Kronecker delta (m and n = 1, 2, 3)
δ_Y	Difference operator for first derivative in Y-direction
δ_Y^2	Difference operator for second derivative in Y-direction
δ^*	Boundary layer displacement thickness
ϵ_i	Inner region eddy viscosity
ϵ_o	Outer region eddy viscosity
η	Computational cross-stream coordinate
θ	Boundary layer momentum thickness
κ	Von Karman constant
λ	Ratio of successive streamwise step sizes
μ	Viscosity coefficient
ν	Kinematic viscosity coefficient
ξ	Computational streamwise coordinate
ρ	Static density
ρ_r	Reference density

τ_{mn}	Stress tensor (m and n = 1, 2, 3)
Φ	Viscous dissipation

Subscripts

AVE	Average at inlet station
C-BODY	Along centerbody
COWL	Along cowl
e	At edge of boundary layer
E	Effective (laminar plus turbulent)
F-D	Fully-developed
i	Grid location in streamwise (ξ) direction
j	Grid location in cross-stream (η) direction
L	Laminar
r	Reference
T	Turbulent
W	Wall
η	Partial differentiation in η-direction
ξ	Partial differentiation in ξ-direction

Superscript

T	Vector transpose

IMPLICIT MARCHING SOLUTION OF COMPRESSIBLE VISCOUS SUBSONIC FLOW IN PLANAR AND AXISYMMETRIC DUCTS

Charles E. Towne

National Aeronautics and Space Administration
Lewis Research Center
Cleveland, Ohio

and

Joe D. Hoffman
Purdue University
West Lafayette, Indiana

SUMMARY

A new streamwise marching procedure has been developed and coded for compressible viscous subsonic flow in planar or axisymmetric ducts with or without centerbodies. The continuity, streamwise momentum, cross-flow momentum, and energy equations are written in generalized orthogonal curvilinear coordinates. To allow the use of a marching procedure, second derivatives in the streamwise direction are neglected, and the pressure in the streamwise momentum equation is written as the sum of a known two-dimensional imposed pressure field and an unknown one-dimensional viscous correction. For turbulent flow, the Reynolds stress and turbulent heat flux terms are modeled using two different two-layer eddy viscosity turbulence models.

Prior to each main marching step, a preliminary marching step is taken in which the integral mass flow rate equation and an uncoupled form of the streamwise momentum equation are solved simultaneously to obtain the viscous pressure correction. During the main marching step the four governing equations are solved simultaneously as a coupled system using an implicit finite-difference method, with the viscous

PRECEDING PAGE BLANK NOT FILMED

pressure correction treated as a source term. The equations are linearized to second-order accuracy without using iteration by expanding each unknown term in a Taylor series in the streamwise direction.

Results are presented for developing laminar flow in a circular pipe, laminar flow in a two-dimensional converging channel (Jeffery-Hamel flow), developing turbulent flow in a circular pipe, turbulent flow in a two-dimensional S-duct, and turbulent flow in a typical subsonic diffuser for a supersonic inlet. For all test cases, the results are compared with data and/or exact solutions.

The computed results agree very well with the data and exact solutions for the laminar cases studied. The results for the turbulent cases also agree well with the data, although not quite as well as for laminar flow. The viscous pressure correction properly accounts for the effect of viscous blockage on the streamwise pressure gradient.

SECTION 1

INTRODUCTION

1.1 GENERAL BACKGROUND

The computation of viscous subsonic internal flow has many engineering applications. The design or analysis of a subsonic jet engine system, for example, requires the computation of flow through the inlet and nozzle. Even a supersonic inlet requires a subsonic solution in the diffuser.

The traditional method for computing subsonic flow in a duct is to first use an inviscid analysis to get a pressure field in the main core flow region, and then to use a boundary layer analysis to account for the viscous effects near the walls. If the boundary layers grow large enough to have a blockage effect on the core flow, however, some type of patching or iteration between the inviscid and boundary layer analyses must be done. If the boundary layers grow further, so that they merge and fill the duct with viscous flow, this method breaks down completely.

One approach that can be used in this situation is to solve the complete Navier-Stokes equations. Since these equations are elliptic, they are usually solved by time-dependent or relaxation techniques, requiring large amounts of computer time and storage.

For many flows, however, a complete Navier-Stokes solution is not necessary. If the flow conditions and geometry are such that elliptic effects in one of the coordinate directions can either be ignored or assumed known a priori, a marching solution procedure can be used. This requires that viscous and thermal diffusion in the streamwise direction be neglected. In addition, special treatment of the streamwise pressure gradient is normally required, since the pressure field in subsonic flow is inherently elliptic. Physically, these assumptions imply a relatively high Reynold's number flow without abrupt changes in geometry and without flow separation.

1.2 EARLIER WORK

All previously published marching methods for viscous internal flow, of course, neglect streamwise diffusion. However, they differ considerably in several details, including the form of the equations being solved, the degree of approximations and/or simplifications involved, the treatment of the streamwise pressure gradient, the degree of coupling between equations, the treatment of compressibility, and the numerical method used.

An early effort in this area was that of Anderson (Refs. 1-3). He developed a method for analyzing compressible axisymmetric flow with or without swirl by assuming that the cross-flow velocity v is of order δ and then neglecting all $\mathcal{O}(\delta^2)$ terms. In addition, several other terms are neglected that involve either derivatives of metric scale coefficients or streamwise derivatives of v. An inviscid cross-flow momentum equation is used, with all of the convective terms

neglected (for zero swirl) except the one involving the derivative of the metric scale coefficient in the cross-flow direction. Thus, the cross-flow pressure gradient is balanced by the curvature of the coordinate lines parallel to the wall. The coordinate lines are given by the streamlines and potential lines from a planar potential flow solution. In his original work (Ref. 1), Anderson uncoupled the equations and solved them using an explicit numerical method. He later modified the analysis by expanding the dependent variables in a Taylor series in the marching direction and solving the resulting equations implicitly (Refs. 2-3). In this formulation, the equation of state and the definitions of the two shear stresses, heat flux, and entropy (the energy equation dependent variable) are treated as independent equations. The implicit solution is thus accomplished by the inversion of a block tri-diagonal matrix with 10x10 sub-matrices. This method has been widely applied to flows in subsonic diffusers (Refs. 4-7).

In Anderson's method, because of the simplifications made to the governing equations, the streamwise pressure gradient p_ξ can be treated like any other term. However, as demonstrated by several other authors (Refs. 8-11), when a more complete form of the cross-flow momentum equation is solved, special treatment of the streamwise pressure gradient is required.

In the three-dimensional method of Patankar and Spalding (Ref. 9), the streamwise pressure gradient p_ξ is assumed to be a function of streamwise distance only. Thus, the pressure gradient in the streamwise momentum equation is uncoupled from those in the cross-flow momentum equations. To advance the solution one marching station using the Patankar-Spalding method, the procedure is as follows:

1. Guess a value for $p_\xi(\xi)$. In practice the value for the preceding step would normally be used.

2. Solve the streamwise momentum equation, uncoupled from the rest of the equations, for the streamwise velocity u using an implicit numerical method. Since the continuity equation has not yet been used, the computed mass flow rate will, in general, be incorrect.

3. Correct p_ξ, using an integral equation derived from an approximate inviscid form of the streamwise momentum equation, to get the correct total mass flow rate.

4. Correct u to be consistent with step 3.

5. Guess a pressure distribution in the new cross-flow plane. Again, in practice the values at the preceding station would be used.

6. Solve the cross-flow momentum equations, uncoupled, for the cross-flow velocities v and w.

7. Correct the cross-flow pressures by solving a two-dimensional Poisson equation derived from the continuity equation and approximate forms of the inviscid cross-flow momentum equations.

8. Correct v and w to be consistent with step 7.

9. Solve the energy equation, uncoupled, for the temperature distribution at the new station.

If the flow is compressible, the density would presumably be updated after step 9, although this is not clear in Reference 9. Multiple-sweep variations of this method, termed "partially-parabolic" procedures, have also been used (Refs. 12-14). However, by sweeping the entire flow field several times, much of the advantage of a marching solution over a complete Navier-Stokes solution is lost. The Patankar-Spalding

method has been applied to straight pipes with circular, square, and polar cross-sections (Refs. 9, 11, 15-16), to curved circular pipes (Refs. 17-19), and, with iteration at each station to reduce linearization errors, to a D-shaped transitioning duct (Ref. 15).

The method of Briley (Ref. 20) is similar in concept to that of Patankar and Spalding, but is somewhat more rigorous and differs considerably in detail. He splits the pressure into an inviscid contribution P and a viscous correction p'. The inviscid contribution is assumed to be known a priori, and is used to bring elliptic effects of the geometry into the solution. The pressure correction term in the streamwise momentum equation is uncoupled from the correction terms in the cross-flow momentum equations in the manner suggested by Patankar and Spalding. The method for computing this pressure, however, is different. Briley's procedure for advancing the solution one step is as follows:

1. Guess a value for $p'_\xi(\xi)$. Again, in practice it would be lagged one step.

2. Solve the streamwise momentum equation, uncoupled, by an implicit method.

3. Correct p'_ξ, using secant iteration on steps 1 and 2, to get the correct total mass flow rate.

4. Solve the cross-flow momentum equations (uncoupled), using a lagged pressure field, to get predicted cross-flow velocities v_P and w_P.

5. Solve a two-dimensional Poisson equation for φ, where φ is a velocity potential for the cross-flow velocity corrections v_C

and w_C. This Poisson equation is derived from the continuity equation by assuming the cross-flow velocity corrections are irrotational.

6. Compute v_C and w_C from ϕ. Note that with this formulation v_C and w_C will have non-zero values at the wall, and therefore the final cross-flow velocities will not satisfy the no-slip boundary condition.

7. Correct the pressure field used in the cross-flow momentum equations by solving a two-dimensional Poisson equation derived from the cross-flow momentum equations.

8. Solve the energy equation for the temperature at the new station.

As presented in Reference 20, Briley's method is for incompressible flow, so the requirement for updating the density does not arise.

This method was later improved by Briley and McDonald (Ref. 21) and by Levy, McDonald, Briley, and Kreskovsky (Ref. 22). In the newer method, the velocity is split into a primary (streamwise) component and a secondary (cross-flow) component. The secondary flow component is split further into irrotational and rotational contributions, which are presumed derivable from a secondary flow velocity potential and stream function, respectively. The pressure is split as in Briley's original method. To march one step with this method, the procedure is as follows:

1. Guess $p'_\xi(\xi)$.

2. Solve the streamwise momentum equation, the energy equation, and an approximate equation of state for the primary velocity u, the static enthalpy h, and the density ρ. In many applications, the

total enthalpy is assumed constant, which eliminates the requirement for solving the energy equation.

3. Correct p'_ξ, using secant iteration on steps 1 and 2, to get the correct total mass flow rate.

4. Solve a two-dimensional Poisson equation for ϕ, where ϕ is the velocity potential for the irrotational component of the cross-flow velocity. This Poisson equation is derived from the continuity equation.

5. Solve an approximate transport equation for Ω and a two-dimensional Poisson equation for ψ as a coupled system, where Ω is the streamwise vorticity and ψ is the stream function for the rotational component of the cross-flow velocity. The streamwise vorticity equation can be derived from the cross-flow momentum equations. The Poisson equation for ψ is simply the definition of streamwise vorticity written in terms of the secondary flow stream function.

6. Compute the cross-flow velocities from ϕ and ψ.

With this formulation, no explicit correction is made to the pressure in the cross-flow momentum equations, since it does not appear in the vorticity transport equation. At the end of a calculation one could solve a three-dimensional Poisson equation for the pressure field since the velocities are known. In practice, however, this has not been done. The method has been applied to straight circular pipes (Ref. 22), curved ducts of rectangular cross-section (Refs. 21,23), a turbine blade passage (Ref. 21), and mixer nozzles (Refs. 24-26).

A method has been developed by Dodge (Ref. 27) for three-dimensional incompressible flow that is quite different from the preceding methods. He splits the velocity into inviscid and viscous components V_i and V_v, respectively, and assumes that the inviscid component is derivable from a velocity potential φ. That is,

$$\vec{V} = \vec{V}_i + \vec{V}_v = \nabla\varphi + \vec{V}_v$$

This expression is substituted into the three momentum equations. It is then assumed that the pressure gradients in all three directions are balanced by the purely potential terms. Thus, the pressure gradients are eliminated from the momentum equations, which can then be solved for $\vec{V}_v$ by a marching technique if φ is known. When the assumed velocity split is substituted into the continuity equation, the result is a three-dimensional Poisson equation for φ if $\vec{V}_v$ is known. The numerical procedure is thus:

1. Guess a three-dimensional potential field (or, equivalently, a pressure field).

2. Solve the three momentum equations throughout the flow field for $\vec{V}_v$ using a marching procedure. It is not clear in Reference 27 whether an explicit or implicit method is used.

3. Solve the three-dimensional Poisson equation, using the results for $\vec{V}_v$ from step 2, to get a new potential field.

4. Iterate steps 2 and 3 until convergence.

Note that this method involves multiple sweeps of the computational domain. As with the "partially-parabolic" variations of the Patankar-

Spalding method, if more than a few sweeps are needed, a complete Navier-Stokes solution might be preferred.

1.3 PRESENT WORK

In the present study, a new streamwise marching procedure was developed and coded for compressible viscous subsonic flow in planar or axisymmetric ducts with or without centerbodies. As in the previously described methods, second derivatives in the marching direction are neglected. The remaining second-order viscous terms are retained, however, since they can be included within the framework of a marching procedure.

Following Briley (Ref. 20), the pressure in the streamwise momentum equation is written as the sum of a known two-dimensional inviscid contribution P and an unknown one-dimensional viscous correction p'. However, this form for the pressure is used only in the streamwise momentum equation, not in the cross-flow momentum equation. This is sufficient to remove the streamwise elliptic character of the pressure field and allow the use of a marching solution procedure. The pressure in the cross-flow momentum equation is simply treated as an unknown dependent variable, thus eliminating the requirement for a separate correction procedure for the cross-flow pressure field. Since elliptic effects due to geometry are included in the known inviscid pressure field, only one sweep through the flow field is required.

In order to rigorously model the relationships between dependent variables, the four governing equations (continuity, streamwise momentum, cross-flow momentum, and energy) are solved simultaneously at each station as a coupled system. Since the continuity equation is one of the equations in the system, however, conservation of total mass flow rate cannot be used during or after a marching step to compute the pressure correction p'. Therefore, a preliminary marching step is taken using the integral mass flow rate equation and an uncoupled form of the streamwise momentum equation. Instead of iterating to find the value of p' that gives the correct mass flow rate, these two equations are solved simultaneously as a coupled system to get p' directly. Then, with p' known, the four governing equations are solved simultaneously with p'_ξ treated as a source term.

The equations are solved by an implicit finite-difference procedure. A weighting factor is used to allow the degree of implicitness to vary from Crank-Nicholson type to fully implicit. The equations are linearized by expanding each unknown term in a Taylor series in the streamwise direction. This allows the inherent nonlinearities of the governing differential equations to be modeled with second-order accuracy without using iteration. Cross-flow derivatives are represented by second-order accurate centered differences. The difference form of the streamwise derivatives is second-order accurate when Crank-Nicholson differencing is used and first-order accurate when fully implicit differencing is used. The resulting set of coupled, linear algebraic equations has a block tri-diagonal coefficient matrix with 4x4 sub-matrices. The equations are solved using a standard tri-diagonal matrix inversion method.

SECTION 2

ANALYSIS

2.1 COORDINATE SYSTEM

In this analysis, the equations of motion are to be solved using a finite difference method. The contours of the duct being studied are usually specified in physical space in Cartesian or polar coordinates, both designated (z,r). Using physical coordinates for computational coordinates, however, is very inconvenient in a finite difference method because of difficulties in applying Neumann boundary conditions. In addition, the assumptions to be made in deriving a set of equations that can be solved by forward marching (see Section 2.2) would, in general, be questionable.

Therefore, an orthogonal, body-fitted, curvilinear system is used for the computational (ξ,η) coordinates. The flow domain in the physical plane is mapped into a rectangular domain in the computational plane, as shown in Figure 2-1.

Since the governing equations will be written in a general form, any orthogonal, body-fitted coordinate system can be used. For the results presented in Sections 4.4 and 4.5, an existing computer code that employs the coordinate generation method of References 2 and 3 was used. In this method, the coordinates are generated by solving for the planar potential flow through the duct. The computational

coordinates are chosen as the velocity potential ξ and stream function η obtained from the potential flow solution.

The computational and physical coordinates are thus related through Laplace's equation,

$$\frac{\partial^2 \xi}{\partial z^2} + \frac{\partial^2 \xi}{\partial r^2} = 0 \tag{2.1}$$

$$\frac{\partial^2 \eta}{\partial z^2} + \frac{\partial^2 \eta}{\partial r^2} = 0 \tag{2.2}$$

These equations could be solved directly to get ξ and η as functions of z and r. The method used in References 2 and 3, however, is to solve the inverse problem, getting z and r as functions of ξ and η. This is accomplished by a conformal mapping technique using the Schwartz-Christoffel transformation.

In order to use this potential flow solution as a coordinate system, the metric scale coefficients h_1, h_2, and h_3 must be determined. From the definition of velocity potential and stream function, it can be shown that differential distances along a streamline and a potential line are given by

$$dS_\xi = \frac{1}{V_p} d\xi$$

and

$$dS_\eta = \frac{1}{V_p} d\eta$$

respectively, where V_p is the potential flow velocity. The differential distance along a general line in this coordinate system is then given by

ORIGINAL PAGE IS
OF POOR QUALITY

$$dS^2 = dS_\xi^2 + dS_\eta^2 = \left(\frac{1}{V_p}\right)^2 d\xi^2 + \left(\frac{1}{V_p}\right)^2 d\eta^2$$

But this is the definition of the metric scale coefficients h_1 and h_2. Therefore, with this coordinate system,

$$h_1 = h_2 = \frac{1}{V_p} \tag{2.3a}$$

Note that although these coordinates are determined by a planar potential flow solution, they can also be used for axisymmetric flow simply by rotation around the axis of symmetry. The third metric scale coefficient h_3 determines whether the coordinate system is planar or axisymmetric. For a planar coordinate system,

$$h_3 = 1 \tag{2.3b}$$

and for an axisymmetric coordinate system,

$$h_3 = r \tag{2.3c}$$

where r is the absolute radial coordinate.

2.2 GOVERNING EQUATIONS

2.2.1 Equations of Motion

The governing equations for steady, viscous, compressible, laminar or turbulent flow in a two-dimensional orthogonal coordinate system are derived in Appendix A as equations (A.29)-(A.32). They are repeated here.

ORIGINAL PAGE IS
OF POOR QUALITY

CONTINUITY

$$\frac{1}{h_1 h_2 h_3}\left[(h_2 h_3 \rho u)_\xi + (h_1 h_3 \rho v)_n\right] = 0 \tag{2.4}$$

STREAMWISE MOMENTUM

$$\frac{1}{h_1}\rho u u_\xi + \frac{1}{h_2}\rho v u_n - \frac{h_{2_\xi}}{h_1 h_2}\rho v^2 + \frac{h_{1_n}}{h_1 h_2}\rho u v = -\frac{1}{h_1}p_\xi + \frac{1}{h_1 h_2 h_3}\left[(h_2 h_3 \tau_{E_{11}})_\xi + (h_1 h_3 \tau_{E_{12}})_n\right] + \frac{h_{1_n}}{h_1 h_2}\tau_{E_{12}} - \frac{h_{2_\xi}}{h_1 h_2}\tau_{E_{22}} - \frac{h_{3_\xi}}{h_1 h_3}\tau_{E_{33}} \tag{2.5}$$

CROSS-FLOW MOMENTUM

$$\frac{1}{h_1}\rho u v_\xi + \frac{1}{h_2}\rho v v_n + \frac{h_{2_\xi}}{h_1 h_2}\rho u v - \frac{h_{1_n}}{h_1 h_2}\rho u^2 = -\frac{1}{h_2}p_n + \frac{1}{h_1 h_2 h_3}\left[(h_2 h_3 \tau_{E_{12}})_\xi + (h_1 h_3 \tau_{E_{22}})_n\right] + \frac{h_{2_\xi}}{h_1 h_2}\tau_{E_{12}} - \frac{h_{3_n}}{h_2 h_3}\tau_{E_{33}} - \frac{h_{1_n}}{h_1 h_2}\tau_{E_{11}} \tag{2.6}$$

ENERGY

$$\frac{1}{h_1}\rho u c_v T_\xi + \frac{1}{h_2}\rho v c_v T_n = -\frac{1}{h_1 h_2 h_3}p\left[(h_2 h_3 u)_\xi + (h_1 h_3 v)_n\right] - \frac{1}{h_1 h_2 h_3}\left[(h_2 h_3 q_{E_1})_\xi + (h_1 h_3 q_{E_2})_n\right] + \varphi_E \tag{2.7}$$

In these equations, h_1, h_2, and h_3 are the metric scale coefficients for the orthogonal curvilinear coordinate system; ξ and n are the coordinate directions; u and v are the velocities in the ξ and n directions, respectively; ρ, p, and T are the static density, pressure, and temperature, respectively; and c_v is the specific heat at constant volume. The subscripts ξ and n denote partial differentiation.

ORIGINAL PAGE IS
OF POOR QUALITY

The effective shear stresses are:

$$\left.\begin{aligned}
\tau_{E_{11}} &= 2\mu_E\left(\frac{1}{h_1}u_\xi + \frac{h_{1_n}}{h_1h_2}v\right) - \frac{2}{3}\mu_E\,\nabla\cdot\vec{V} \\
\tau_{E_{22}} &= 2\mu_E\left(\frac{1}{h_2}v_n + \frac{h_{2_\xi}}{h_1h_2}u\right) - \frac{2}{3}\mu_E\,\nabla\cdot\vec{V} \\
\tau_{E_{33}} &= 2\mu_E\left(\frac{h_{3_\xi}}{h_1h_3}u + \frac{h_{3_n}}{h_2h_3}v\right) - \frac{2}{3}\mu_E\,\nabla\cdot\vec{V} \\
\tau_{E_{12}} &= \mu_E\left[\frac{h_2}{h_1}\left(\frac{v}{h_2}\right)_\xi + \frac{h_1}{h_2}\left(\frac{u}{h_1}\right)_n\right]
\end{aligned}\right\} \qquad (2.8)$$

where

$$\nabla\cdot\vec{V} = \frac{1}{h_1h_2h_3}\left[(h_2h_3u)_\xi + (h_1h_3v)_n\right]$$

For laminar flow, μ_E is simply the molecular viscosity μ_L. For turbulent flow, it is an effective viscosity given by the sum of the molecular and turbulent viscosities,

$$\mu_E = \mu_L + \mu_T$$

where $\mu_T = \rho\epsilon$, and ϵ, the eddy viscosity, comes from some appropriate turbulence model.

The effective heat fluxes are:

$$\left.\begin{aligned}
q_{E_1} &= -\frac{1}{h_1}k_E T_\xi \\
q_{E_2} &= -\frac{1}{h_2}k_E T_n
\end{aligned}\right\} \qquad (2.9)$$

ORIGINAL PAGE IS
OF POOR QUALITY

where, analogous to viscosity, k_E for laminar flow is the molecular coefficient of thermal conductivity k_L, and for turbulent flow it is given by

$$k_E = k_L + k_T$$

where k_T is the turbulent thermal conductivity. Here k_T is related to μ_T by

$$k_T = \frac{c_p \mu_T}{Pr_T}$$

where c_p is the specific heat at constant pressure and Pr_T is the turbulent Prandtl number, which is assumed known.

The effective dissipation φ_E, when written out in full, is given by:

$$\varphi_E = \varphi_L + \varphi_T = 2\mu_E \left\{ \left(\frac{1}{h_1} u_\xi + \frac{h_{1_\eta}}{h_1 h_2} v \right)^2 + \left(\frac{1}{h_2} v_\eta + \frac{h_{2_\xi}}{h_1 h_2} u \right)^2 \right.$$

$$\left. + \left(\frac{h_{3_\xi}}{h_1 h_3} u + \frac{h_{3_\eta}}{h_2 h_3} v \right)^2 + \frac{1}{2} \left[\frac{h_2}{h_1} \left(\frac{v}{h_2} \right)_\xi + \frac{h_1}{h_2} \left(\frac{u}{h_1} \right)_\eta \right]^2 \right\}$$

$$- \frac{2}{3} \mu_E \left(\frac{1}{h_1} u_\xi + \frac{h_{1_\eta}}{h_1 h_2} v + \frac{1}{h_2} v_\eta \right.$$

$$\left. + \frac{h_{2_\xi}}{h_1 h_2} u + \frac{h_{3_\xi}}{h_1 h_3} u + \frac{h_{3_\eta}}{h_2 h_3} v \right)^2 \qquad (2.10)$$

Along with the governing differential equations, the perfect gas equation of state is used to relate pressure, density, and temperature. Thus,

$$p = \rho RT \tag{2.11}$$

where R is the gas constant.

The preceding equations form a set of elliptic, nonlinear, coupled partial differential equations to be solved for ρ, u, v, and T. Such a solution is referred to as a complete Navier-Stokes solution and can be accomplished using time-dependent or relaxation numerical techniques. However, large amounts of computer time and storage are required.

Fortunately, for many flows a complete Navier-Stokes solution is not needed. If the flow conditions and geometry are such that elliptic effects in one of the coordinate directions can either be ignored or assumed known a priori, a marching solution procedure can be used. Starting with known profiles at some initial station, the flowfield can be computed by integrating the equations one station at a time in the marching direction. The flow field can be computed in one pass, and large amounts of computer storage are not needed.

Therefore, it is assumed that a primary, or streamwise, flow direction can be identified (in this case, the ξ direction). An order-of-magnitude analysis is used to simplify the governing equations (see Appendix B). Viscous and thermal diffusion in the streamwise direction are neglected. Physically, this assumption holds best for flows with relatively high Reynolds numbers in which there are no abrupt changes in geometry. Separated flow regions cannot be analyzed by this technique.

The above assumptions remove some of the elliptic character of the governing equations, but not all. As shown by several authors (Refs. 8-11), the pressure field is also elliptic in nature for subsonic flow.

Upstream influence can be important, sometimes very important. Removing the elliptic character of the pressure field could result in physically unrealistic solutions when using a marching procedure.

In conventional boundary layer theory, the streamwise pressure gradient is assumed to be imposed on the viscous boundary layer by the inviscid core flow, and the cross-flow pressure gradient is neglected. The imposed pressure gradient usually comes from either an elliptic inviscid analysis or experimental data. A similar procedure is used in this analysis, but without neglecting the cross-flow pressure gradient.

First, the streamwise pressure gradient p_ξ is uncoupled from the cross-flow pressure gradient p_η as first suggested by Patankar and Spalding (Ref. 9). No assumptions are made regarding p_η, and it is treated as an unknown in the marching solution algorithm. The streamwise pressure gradient p_ξ is written as:

$$p_\xi = P_\xi(\xi,\eta) + p'_\xi(\xi) \tag{2.12}$$

where $P(\xi,\eta)$ is a known two-dimensional pressure field that is "imposed" onto the flow and $p'(\xi)$ is a correction to P that is computed as part of the marching solution to account for viscous blockage effects. Note that $p'(\xi)$ has been written as a function of ξ only, that is, it is assumed constant over any given cross-section of the duct being analyzed. The $P(\xi,\eta)$ term can come from any available source. Normally, it would be computed using an elliptic inviscid analysis.

Note that this procedure introduces an inconsistency in the treatment of the pressure in the two momentum equations. As pointed out in Reference 9, this inconsistency is part of the price that must be paid

ORIGINAL PAGE IS
OF POOR QUALITY

in deriving a set of equations that can be solved by a forward marching technique.

With the above assumptions, and the equation of state, equations (2.4)-(2.7) can be written in dimensionless form as:

CONTINUITY

$$\frac{1}{h_1}\left(u\rho_\xi + \rho u_\xi\right) + \frac{1}{h_2}\left(\rho v\right)_\eta + \frac{1}{h_1 h_2 h_3}\left[\left(h_2 h_3\right)_\xi \rho u + \left(h_1 h_3\right)_\eta \rho v\right] = 0 \qquad (2.13)$$

STREAMWISE MOMENTUM

$$\frac{1}{h_1}\rho u u_\xi + \frac{1}{h_2}\rho v u_\eta - \frac{h_{2_\xi}}{h_1 h_2}\rho v^2 + \frac{h_{1_\eta}}{h_1 h_2}\rho u v = -\frac{1}{h_1}\left(p_\xi + p'_\xi\right) + \frac{1}{Re_r}\frac{1}{h_1 h_2 h_3}$$

$$\times \left(h_1 h_3 \tau_{E_{12}}\right)_\eta + \frac{1}{Re_r}\left(\frac{h_{1_\eta}}{h_1 h_2}\tau_{E_{12}} - \frac{h_{2_\xi}}{h_1 h_2}\tau_{E_{22}} - \frac{h_{3_\xi}}{h_1 h_3}\tau_{E_{33}}\right) \qquad (2.14)$$

CROSS-FLOW MOMENTUM

$$\frac{1}{h_1}\rho u v_\xi + \frac{1}{h_2}\rho v v_\eta + \frac{h_{2_\xi}}{h_1 h_2}\rho u v - \frac{h_{1_\eta}}{h_1 h_2}\rho u^2 = -\frac{1}{h_2}R(\rho T)_\eta + \frac{1}{Re_r}\frac{1}{h_1 h_2 h_3}$$

$$\times \left[\left(h_2 h_3 \tau'_{E_{12}}\right)_\xi + \left(h_1 h_3 \tau_{E_{22}}\right)_\eta\right] + \frac{1}{Re_r}\left(\frac{h_{2_\xi}}{h_1 h_2}\tau_{E_{12}} - \frac{h_{3_\eta}}{h_2 h_3}\tau_{E_{33}}\right) \qquad (2.15)$$

ENERGY

$$\frac{1}{h_1}\rho u c_v T_\xi + \frac{1}{h_2}\rho v c_v T_\eta = -\frac{1}{h_1 h_2 h_3}\rho R T\left[\left(h_2 h_3 u\right)_\xi + \left(h_1 h_3 v\right)_\eta\right]$$

$$- \frac{1}{Re_r Pr_r}\frac{1}{h_1 h_2 h_3}\left(h_1 h_3 q_{E_2}\right)_\eta + \varphi_E \qquad (2.16)$$

In these equations, length has been nondimensionalized by L_r, velocity by U_r, density by ρ_r, temperature by T_r, viscosity by μ_r, thermal conductivity by k_r, pressure by $\rho_r U_r^2$, and specific heat by U_r^2/T_r. The reference Reynolds and Prandtl numbers, then, are given by

$$Re_r = \frac{\rho_r U_r L_r}{\mu_r}$$

and

$$Pr_r = \frac{c_{p_r} \mu_r}{k_r} = \frac{U_r^2 \mu_r}{k_r T_r}$$

When nondimensionalized, the shear stresses (except for the $\tau'_{E_{12}}$ in the cross-flow momentum equation), the heat flux, and the dissipation are still given by equations (2.8)-(2.10). In the $\tau'_{E_{12}}$ term, the higher-order $(v/h_2)_\xi$ half has been dropped, since leaving it in would make the equation elliptic. As shown in Appendix B, many of the shear stress terms in equations (2.14) and (2.15) are actually higher-order terms that could reasonably be eliminated. They have been left in for completeness, however, since they can be handled within the framework of a numerical marching solution. In the computer code used to solve these equations, the user can control which viscous terms are included in the solution.

ORIGINAL PAGE IS
OF POOR QUALITY

2.2.2 Boundary Conditions

Boundary conditions are needed for the dependent variables ρ, u, v, and T at a symmetry line and at a wall. At a symmetry line, the boundary conditions are

$$\left.\begin{aligned} \frac{\partial \rho}{\partial n} = \frac{\partial u}{\partial n} = \frac{\partial T}{\partial n} = 0 \\ v = 0 \end{aligned}\right\} \tag{2.17}$$

At a wall, the conditions normally used are

$$\left.\begin{aligned} u = u_W \\ v = v_W \\ T = T_W \quad \text{or} \quad \frac{\partial T}{\partial n} = \left(\frac{\partial T}{\partial n}\right)_W \end{aligned}\right\} \tag{2.18}$$

The density boundary condition is found by writing the cross-flow momentum equation at the wall, using the equation of state to rewrite $\partial p/\partial n$ in terms of ρ and T. The resulting equation, when written in difference form, can be solved for ρ_W in terms of the other dependent variables.

The above velocity boundary conditions are general to allow for slip or a moving wall, and to allow for bleed or blowing. For no slip and no bleed, $u_W = v_W = 0$. The temperature gradient boundary condition is also general. For an adiabatic wall, the temperature gradient normal to the wall would be set equal to zero. Details on the implementation of these boundary conditions in the finite-difference equations are presented in Section 3.3.3.

In turbulent flow, when equations (2.18) are used as boundary conditions at a wall, the finite-difference grid must be very dense near the wall to resolve the steep velocity gradients expected there. This can be avoided, however, by making use of the experimentally observed properties of turbulent boundary layers (Ref. 38). A typical unseparated turbulent boundary layer can be divided into an inner region, where the total shear stress is essentially constant, and an outer region, where the total shear stress decreases with distance from the wall. The inner region can be further divided into a laminar sublayer where the laminar shear stress dominates, a transition or buffer region where both laminar and turbulent shear stress are important, and a fully turbulent region where turbulent shear stress dominates.

In the fully turbulent part of the inner region, a universal velocity distribution law exists, given by Reference 38 as

$$u^+ = \frac{1}{\kappa} \ln y^+ + B \tag{2.19}$$

where κ is the von Karman constant (about 0.4) and B is a constant between 4.9 and 5.5. The variables u^+ and y^+ are defined by

$$u^+ = \frac{u}{u_\tau}$$

$$y^+ = \frac{u_\tau y}{\nu_w}$$

where y is the distance from the wall, ν_w is the kinematic viscosity at the wall, and u_τ is the friction velocity defined by

$$u_\tau = \sqrt{\frac{\tau_w}{\rho}}$$

Equation (2.19) is often referred to as the logarithmic law-of-the-wall. It is valid for y^+ between about 35 and 350 (Ref. 28). The upper limit on y^+ actually depends on the streamwise pressure gradient, but 350 is a conservative value. If it is assumed that the first grid point away from the wall is in the law-of-the-wall region, a slip velocity (or wall function) boundary condition can be derived. The laminar sublayer is not resolved, thus fewer grid points are needed in the η direction.

To use the law-of-the-wall as a boundary condition, equation (2.19) is differentiated with respect to η, giving

$$\frac{\partial u}{\partial \eta} = \pm h_2 \frac{u_\tau}{\kappa} \frac{1}{y} \tag{2.20}$$

where the $+$ sign is used for a lower wall and the $-$ sign is used for an upper wall. This equation is the one actually used to specify the boundary condition on u.

It should be noted that equation (2.19) was developed for incompressible flow. Very little error is introduced, however, by using it for compressible subsonic flow, as will now be shown. Several methods have been proposed to extend equation (2.19) to compressible flow (Ref. 29). Maise and McDonald (Ref. 30) suggested using equation (2.19) with u replaced by a generalized velocity u'. For adiabatic flow they used

$$u' = u_e \frac{1}{\sqrt{\sigma}} \sin^{-1}\left(\sqrt{\sigma}\frac{u}{u_e}\right) \tag{2.21}$$

ORIGINAL PAGE IS
OF POOR QUALITY

where

$$\sigma = \frac{\frac{\gamma - 1}{2} M_e^2}{1 + \frac{\gamma - 1}{2} M_e^2}$$

Here u_e and M_e are the velocity and Mach number, respectively, at the edge of the boundary layer. For $M_e = 0$ (incompressible flow), equation (2.21) gives $u' = u$. As M_e increases, the value of u' increases for a given value of u. But, for $u/u_e = 0.4$, for example, the value of u'/u_e is only 0.4018 at $M_e = 1$, which is less than a one percent increase. Since the present analysis is for subsonic flow, equation (2.19) can be used as is, with no modification for compressibility.

When a wall function boundary condition is used for u, and the wall temperature is specified, a wall function boundary condition must also be used for temperature since the sublayer region is not resolved. (If the temperature gradient normal to the wall is specified, the implicit assumption that $q = q_w$ in the law-of-the-wall region means the temperature gradient boundary condition of equation (2.18) can still be used). Following White (Ref. 28), but without assuming $Pr_T = 1$, a temperature law-of-the-wall can be written as

$$T^+ = Pr_T \frac{1}{\kappa} \ln y^+ + c_1 \qquad (2.22)$$

where

$$T^+ = \frac{\rho_w c_p u_\tau (T - T_w)}{q_w}$$

$$c_1 = 12.8\, Pr_L^{0.68} - 7.3$$

ORIGINAL PAGE IS
OF POOR QUALITY

Here $Pr_L = c_p \mu_L / k$ is the laminar Prandtl number and q_w is the heat flux at the wall. Equation (2.22) is differentiated with respect to n to give

$$\frac{\partial T}{\partial n} = \pm h_2 \frac{T - T_w}{\kappa y \left(Pr_T \frac{1}{\kappa} \ln y^+ + c_1 \right)} \tag{2.23}$$

Details on the use of equations (2.20) and (2.23) as boundary conditions are presented in Section 3.3.4.

2.2.3 Initial Profiles

To start the marching procedure, profiles of ρ, u, v, and T must be specified at some initial station. Two options are available in the computer program written for this study. A uniform free stream can be specified, with boundary layers computed for each wall from input boundary layer parameters. Or, complete nonuniform initial profiles of ρ, u, v, and T can be read in, with the option of computing boundary layers at the walls from input boundary layer parameters. In either case, the procedure for computing the profiles in the boundary layers is the same.

In laminar flow, the boundary layer thickness δ and the displacement thickness δ^* are specified. The streamwise velocity in the boundary layer is computed by assuming a von Karman-Pohlhausen profile, that is,

$$\frac{u}{u_e} = \frac{y}{\delta}\left[\left(\frac{y}{\delta}\right)^3 - 2\left(\frac{y}{\delta}\right)^2 + 2\right] + \frac{\Lambda}{6}\frac{y}{\delta}\left(1 - \frac{y}{\delta}\right)^3 \tag{2.24}$$

ORIGINAL PAGE IS
OF POOR QUALITY

where

$$A = 36 - 120 \frac{\delta^*}{\delta}$$

Although equation (2.24) was originally developed for incompressible flow, it can be used in compressible flow as well (Ref. 31).

For turbulent flow, the situation is more complicated. Coles (Ref. 32) developed an expression for the velocity profile in the fully turbulent part of the boundary layer. This was modified by Walz (Ref. 31) to include the laminar sublayer and the transitional region. Walz' expression is

$$u^+ = \frac{u}{u_\tau} = \left[\left(1 - \frac{1}{\kappa} - Ba\right) y^+ - B\right] e^{-ay^+} + \frac{1}{\kappa} \ln(1 + y^+) + B + \frac{1}{\kappa} \omega f^* \tag{2.25}$$

where

$$\omega = 1 + \sin\left[\frac{\pi}{2}\left(2 \frac{y}{\delta} - 1\right)\right]$$

$$f^* = \frac{\kappa}{2}\left(\frac{u_e}{u_\tau} - \frac{1}{\kappa} \ln \frac{\rho_w u_\tau \delta}{\nu_w} - B\right)$$

The only symbol in these equations not previously defined is the constant a, which Walz sets equal to 0.3.

Before equation (2.25) can be used, the shear stress, viscosity, and density at the wall must be found. The boundary layer parameters specified are the thickness δ, displacement thickness δ^*, and momentum thickness θ. The wall shear stress is found from the Ludweig-Tillman skin friction formula, as written by Sasman and Cresci (Ref. 33). Thus,

ORIGINAL PAGE IS
OF POOR QUALITY

$$c_f = \frac{\tau_w}{\frac{1}{2}\rho_e u_e^2} = 0.246\, e^{-1.561 H_i} \left(\frac{u_e \theta}{\bar{\nu}}\right)^{-0.268} \left(\frac{T_e}{\bar{T}}\right)^{1.268} \tag{2.26}$$

where $\bar{T}$ is a reference temperature given by

$$\frac{\bar{T}}{T_{0_e}} = \frac{1}{2}\frac{T_w}{T_{0_e}} + 0.22\, r_F + (0.5 - 0.22\, r_F)\frac{T_e}{T_{0_e}} \tag{2.27}$$

T_{0_e} is the total temperature at the edge of the boundary layer and r_F is the recovery factor, assumed equal to $\sqrt[3]{Pr_L}$. The parameter $\bar{\nu}$ is the kinematic viscosity evaluated at $T = \bar{T}$. The incompressible shape factor H_i is computed from

$$H = \frac{T_w}{T_{0_e}} H_i \left(1 + \frac{\gamma - 1}{2} M_e^2\right) + \frac{\gamma - 1}{2} M_e^2 \tag{2.28}$$

where

$$H = \frac{\delta^*}{\theta}$$

The wall temperature is either given, or computed assuming an adiabatic wall from

$$T_{AW} = T_e + r_F \frac{u_e^2}{2c_{p_e}} \tag{2.29}$$

The viscosity at the wall is then found from Sutherland's formula, equation (2.32). Finally, the wall density is computed from the equation of state by assuming $\partial p/\partial y = 0$ across the initial boundary layer.

For both laminar and turbulent flow, the temperature profile in the boundary layer is given by the Crocco-Busemann relation (Ref. 28),

ORIGINAL PAGE IS
OF POOR QUALITY

$$\dot{T} = T_W + (T_{AW} - T_W)\frac{u}{u_e} - r_F \frac{u_e^2}{2c_{p_e}} \tag{2.30}$$

where $r_F = \sqrt{Pr_L}$ for laminar flow and $\sqrt[3]{Pr_L}$ for turbulent flow. The density profile is then found by assuming $\partial p/\partial y = 0$ across the boundary layer. That is,

$$\rho = \frac{p_e}{RT} \tag{2.31}$$

Finally, the cross-flow velocity v is set equal to 0.0.

2.2.4 Molecular Transport Properties

In addition to equations (2.13)-(2.16), equations are needed relating μ_L, k_L, and c_v to temperature. The molecular viscosity is determined from Sutherland's formula,

$$\frac{\mu_L}{\mu_r} = \frac{T_r + 110.3}{T + 110.3}\left(\frac{T}{T_r}\right)^{3/2} \tag{2.32}$$

where T is in K. The specific heat at constant volume is found from the empirical formula of Reference 34, which for air with an average molecular weight of 28.97 kg/mole can be written as:

$$c_v = 1.44\text{x}10^3 - 3.94\text{x}10^3\, T^{-1/2} - 1.943\text{x}10^5\, T^{-1} + 4.09\text{x}10^7\, T^{-2} - R \tag{2.33}$$

where T is in K and c_v and R are in $m^2/sec^2 - K$. The molecular coefficient of thermal conductivity is given by the empirical formula of Reference 35:

ORIGINAL PAGE IS
OF POOR QUALITY

$$k_L = \frac{a\sqrt{T}}{1 + \frac{b}{T} \times 10^{-c/T}} \tag{2.34}$$

where, for T in K and k in kg-m/sec^3 - K, $a = 0.002646$, $b = 245.4$, and $c = 12$.

2.3 STREAMWISE PRESSURE GRADIENT

2.3.1 Viscous Pressure Correction

Equations (2.13)-(2.16) form a set of four coupled, nonlinear, partial differential equations to be solved for ρ, u, v, and T. However, by rewriting the streamwise pressure gradient in the form of equation (2.12), an additional unknown, p'_ξ, has been introduced. The standard procedure for computing p'_ξ during a matching step is as follows (Refs. 9, 20):

1. Guess p'_ξ.

2. Solve some form of the streamwise momentum equation for the u velocity distribution at the new station (after uncoupling and linearizing the equation by lagging quantities one step).

3. Compute the mass flow rate through the duct at the new station (which, in general, will be incorrect) using

$$\int_A \rho u \, dA = \dot{m} \tag{2.35}$$

where A is the duct area and $\dot{m}$ is the total mass flow rate.

4. Correct p'_ξ to give the proper mass flow rate.

In this analysis, however, the differential continuity equation is to be solved simultaneously with the momentum and energy equations. The mass flow rate through the duct is automatically conserved during a marching step no matter what value of p'_ξ is used, at least within the truncation error of the numerical method. Conservation of total mass flow rate, therefore, cannot be used to compute p'_ξ after equations (2.13)-(2.16) are simultaneously marched one step. It can still be used, however, if p'_ξ is computed before each main marching step. Then, once p'_ξ is known, equations (2.13)-(2.16) can be solved simultaneously with p'_ξ treated as a source term.

In this analysis, in other words, a preliminary marching step is taken using a modified form of the procedure outlined above to compute p'_ξ. The streamwise momentum equation is uncoupled from the continuity, cross-flow momentum, and energy equations and linearized by lagging certain quantities one step, just as above. The total mass flow rate equation is written as

$$\int_A \frac{P(\xi,n) + p'(\xi)}{RT} u^* \, dA = \dot{m} \tag{2.36}$$

The superscript * is used on u to distinguish it from the streamwise velocity computed during the main marching step. Better results were obtained using the equation in this form rather than equation (2.35). Then, instead of iterating to find the value of p'_ξ that satisfies total continuity, the streamwise momentum equation and equation (2.36) are solved simultaneously as a coupled set to get p'_ξ.

This procedure for computing p'_ξ is not completely rigorous, at least not as rigorous as the rest of the solution, since an uncoupled form of the streamwise momentum equation must be used. However, p'

ORIGINAL PAGE IS
OF POOR QUALITY

is only a correction to P, the imposed pressure field, to account for viscous blockage. Thus, small percentage errors in p' will give much smaller errors in P + p'. In addition, in deriving a set of equations that can be solved by forward marching, it was assumed that the flow is primarily in the ξ direction. The errors in computing the increase (or decrease) in viscous blockage over one marching step by using the uncoupled streamwise momentum equation should be small.

2.3.2 Imposed Pressure Field

In this analysis, the computational mesh for a general case is computed using a planar potential flow solution, as described in Section 2.1. Thus, for planar two-dimensional flows a potential flow velocity can be directly related to the mesh through

$$V_p = \frac{1}{h_1} = \frac{1}{h_2} \tag{2.37}$$

For axisymmetric flows a separate potential flow solution is required. Using the method of Reference 36, the axisymmetric potential equation,

$$\left(\frac{h_2 h_3}{h_1} \varphi_{AX_\xi}\right)_\xi + \left(\frac{h_1 h_3}{h_2} \varphi_{AX_n}\right)_n = 0 \tag{2.38}$$

is solved using an iterative alternating-direction implicit method. An axisymmetric potential flow velocity is then computed from

$$V_p = \left[\left(\frac{1}{h_1} \varphi_{AX_\xi}\right)^2 + \left(\frac{1}{h_2} \varphi_{AX_n}\right)^2\right]^{1/2} \tag{2.39}$$

The "real" incompressible inviscid velocity is found from

ORIGINAL PAGE IS
OF POOR QUALITY

$$V_i = V_r V_p \tag{2.40}$$

where

$$V_r = \frac{V_{i_{AVE}}}{V_{P_{AVE}}}$$

The subscript AVE here denotes the average value at the initial station. The average incompressible velocity $V_{i_{AVE}}$ comes from

$$V_{i_{AVE}} = \frac{\dot{m}}{\rho_i A_1}$$

where $\dot{m}$ is the mass flow rate, A_1 is the duct area at the initial station, and ρ_i is the incompressible, or total, density. For compressible flows, the velocity given by equation (2.40) is modified using the Lieblein-Stockman compressibility correction, which was developed specifically for internal flows (Ref. 37). This compressibility correction has been shown to yield very good agreement with data over a wide range of flow conditions, including high Mach number subsonic and even transonic flow (Refs. 38-42). Good agreement with data was obtained in Reference 39 for local Mach numbers as high as 1.3 in small regions of supersonic flow. The details of this compressibility correction are given in Appendix C.

The inviscid pressure itself, then, is computed from

$$\frac{p}{p_0} = \left[1 - \frac{\gamma - 1}{2}\left(\frac{V_C}{a_0}\right)^2\right]^{\gamma/(\gamma-1)} \tag{2.41}$$

where p_0 is the total pressure, a_0 is the total speed of sound, V_C is the compressible velocity, and γ is the ratio of specific heats.

It should be noted that, for a given geometry, the potential flow needs to be computed only once. The velocity field given by equation (2.37) or (2.39) can be saved on a mass storage device. A pressure field can then be computed for any initial flow conditions from equations (2.40) and (2.41).

2.4 TURBULENCE MODEL

The Reynolds stresses and the turbulent heat flux are modeled using an eddy viscosity approach to relate these terms to the mean flow (see Appendix A). A two-layer model is used. In the outer or wake region, the turbulence model of Cebeci and Smith (Ref. 43) is used. In the inner or near-wall region, either the model of Cebeci and Smith or of McDonald and Camarata (Ref. 44) can be used. The computer code includes subroutines for both of these models, which are known as algebraic, or zero-equation, turbulence models. A more complex multi-equation turbulence model (i.e., one that solves partial differential equations for the turbulence length and/or velocity scales) could be incorporated into the code at a later date. However, given the current status of multi-equation models and the past success of algebraic models, this probably is not warrented at the present time (Refs. 29, 45).

ORIGINAL PAGE IS
OF POOR QUALITY

2.4.1 Outer Region Model

In the outer region, the eddy viscosity is given by

$$\epsilon_o = \alpha u_e \delta_k^* \tag{2.42}$$

Here, for internal flows, the subscript e implies a value at the point of the first maximum streamwise velocity away from a wall. For most applications, this is simply the maximum velocity in the duct. Also, δ_k^* is the kinematic displacement thickness,

$$\delta_k^* = \int_0^{y_e} \left(1 - \frac{u}{u_e}\right) dy$$

where y is distance from the wall. The parameter α is given by

$$\alpha = \alpha_0 \frac{1 + \Pi_0}{1 + \Pi}$$

where $\alpha_0 = 0.0168$ and $\Pi_0 = 0.55$. The parameter Π is Coles' profile parameter, defined as

$$\Pi = \Pi_0 \left[1 - \exp\left(-0.243 \sqrt{z_1} - 0.298 z_1\right)\right]$$

where

$$z_1 = \frac{1}{425} Re_{\theta_k} - 1$$

$$Re_{\theta_k} = \frac{u_e \theta_k}{\nu_w}$$

$$\theta_k = \int_0^{y_e} \frac{u}{u_e}\left(1 - \frac{u}{u_e}\right)dy$$

Here ν is the kinematic viscosity and the subscript W denotes a wall value. The factor $(1 + \Pi_0)/(1 + \Pi)$ is essentially a low Reynolds number correction to α_0.

In conventional boundary layer analyses, the eddy viscosity given by equation (2.42) is often multiplied by an intermittency factor. This accounts for the experimentally observed fact that, as the free stream is approached, the fraction of time the flow is turbulent decreases. For internal flows, however, this is not necessarily true. In fully-developed pipe flow, for example, the eddy viscosity in the outer region is essentially constant (Ref. 46). Also, in their calculation of developing turbulent pipe flow, Richman and Azad (Ref. 47) used both a constant outer-region eddy viscosity and a variable eddy viscosity that decreased as the centerline was approached. They found that the computed mean velocity profiles were insensitive to the outer-region eddy viscosity distribution. It was therefore decided not to use an intermittency factor in this internal flow analysis.

2.4.2 Cebeci-Smith Inner Region Model

In the Cebeci-Smith model, the inner-region eddy viscosity is given by

$$\epsilon_i = \ell^2\left|\frac{\partial u}{\partial y}\right| \qquad (2.43)$$

where ℓ, the mixing length, is given by

ORIGINAL PAGE IS
OF POOR QUALITY

$$\ell = \kappa y(1 - e^{-y/A}) \tag{2.44}$$

Here κ is the von Karman constant, set equal to 0.40, and y is distance from the wall. The parameter A is the well-known Van Driest damping parameter. As modified by Cebeci for flows with pressure gradient, heat transfer, and mass transfer (Refs. 48-49), A is given by

$$A = A^+ \frac{\nu}{N} \frac{1}{u_\tau} \left(\frac{\rho}{\rho_W}\right)^{1/2}$$

where

$$A^+ = 26$$

$$u_\tau = \sqrt{\frac{\tau_W}{\rho_W}}$$

$$\tau_W = \mu_W \left(\frac{\partial u}{\partial y}\right)_W$$

$$N^2 = \frac{\mu_L}{\mu_{L_e}} \frac{p^+}{v_W^+}\left[1 - \exp\left(11.8 \frac{\mu_W}{\mu_L} v_W^+\right)\right] + \exp\left(11.8 \frac{\mu_W}{\mu_L} v_W^+\right)$$

$$v_W^+ = \frac{v_W}{u_\tau}$$

$$p^+ = -\frac{\mu_{L_e}}{\rho_W^2 u_\tau^3} \frac{1}{h_1} \left(\frac{\partial p}{\partial \xi}\right)_W$$

For flows without bleed ($v_W^+ = 0$),

$$N^2 = 1 - 11.8 \frac{\mu_W}{\mu_{L_e}} p^+$$

ORIGINAL PAGE IS
OF POOR QUALITY

2.4.3 McDonald-Camarata Inner Region Model

The inner-region eddy viscosity in the McDonald-Camarata model is still given by equation (2.43), but the form of the mixing length is different. They use

$$\ell = \ell_\infty \, \delta \tanh\left(\frac{\kappa y}{\ell_\infty \delta}\right) \mathcal{D} \tag{2.45}$$

where $\ell_\infty = 0.09$, $\kappa = 0.43$, and $\delta = y$ at the point where $u = 0.99\, u_e$. The damping factor $\mathcal{D}$ is given by

$$\mathcal{D} = \mathcal{P}^{1/2}\left(\frac{y^+ - \bar{y}^+}{\sigma_1}\right) \tag{2.46}$$

where $\mathcal{P}$ is the normal probability function, $\bar{y}^+ = 23$, and $\sigma_1 = 8$. The parameter y^+ is found from

$$y^+ = \frac{y u_\tau}{\nu}$$

where

$$u_\tau = \sqrt{\frac{\tau_{E_{12}}}{\rho}}$$

Note that in this model, the friction velocity u_τ is computed from local values of density and shear stress, not wall values.

The boundary between the inner and outer regions is determined by requiring that the eddy viscosity be a continuous function of distance from the wall. In other words, starting at the wall, $\epsilon = \epsilon_i$ until $\epsilon_i > \epsilon_o$, then $\epsilon = \epsilon_o$.

For axisymmetric flows with a centerbody and for nonsymmetric planar flows, the eddy viscosity is computed separately for each wall. In general this leads to a discontinuity in the two outer-region values. In this case, the eddy viscosity is made continuous by linearly interpolating between the two values over the outer 50 percent of each outer region. If ϵ_i never reaches ϵ_o for either boundary layer, the point of maximum ϵ_i is used. In addition, the interpolation region is forced to include at least the outer 50 percent of each boundary layer.

An example of a typical eddy viscosity profile is presented in Figures 2-2a and b. This particular profile is for developing turbulent flow in a pipe. Figure 2-2a shows the entire inner region, with ϵ_i increasing from zero at the wall to the constant outer region value ϵ_o. In Figure 2-2b, the profile very near the wall is presented, showing the damping effect in the viscous sublayer.

ORIGINAL PAGE IS
OF POOR QUALITY

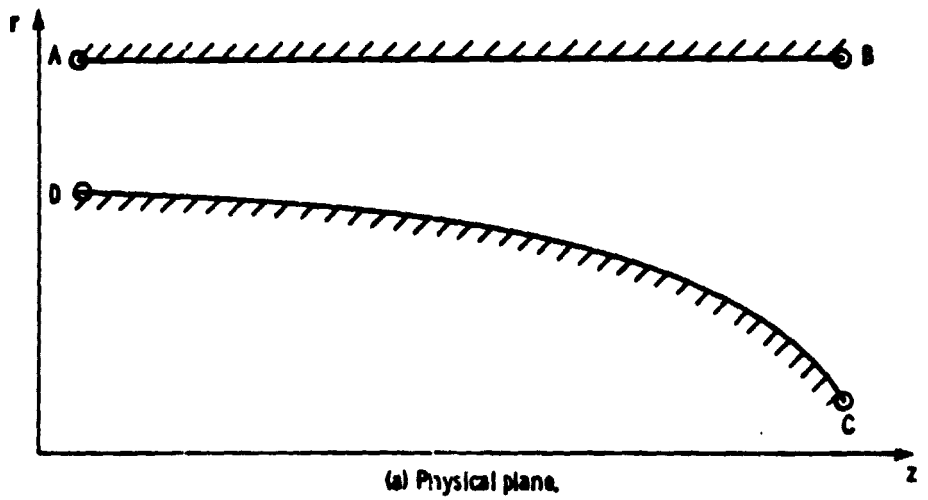

(a) Physical plane.

Figure 2-1. - Flow domain in physical and computational planes.

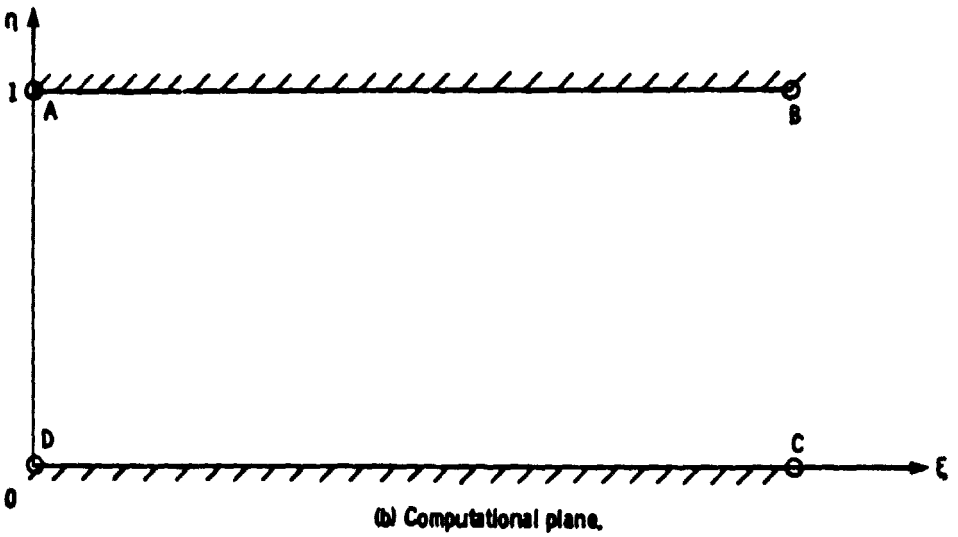

(b) Computational plane.

Figure 2-1. - Concluded.

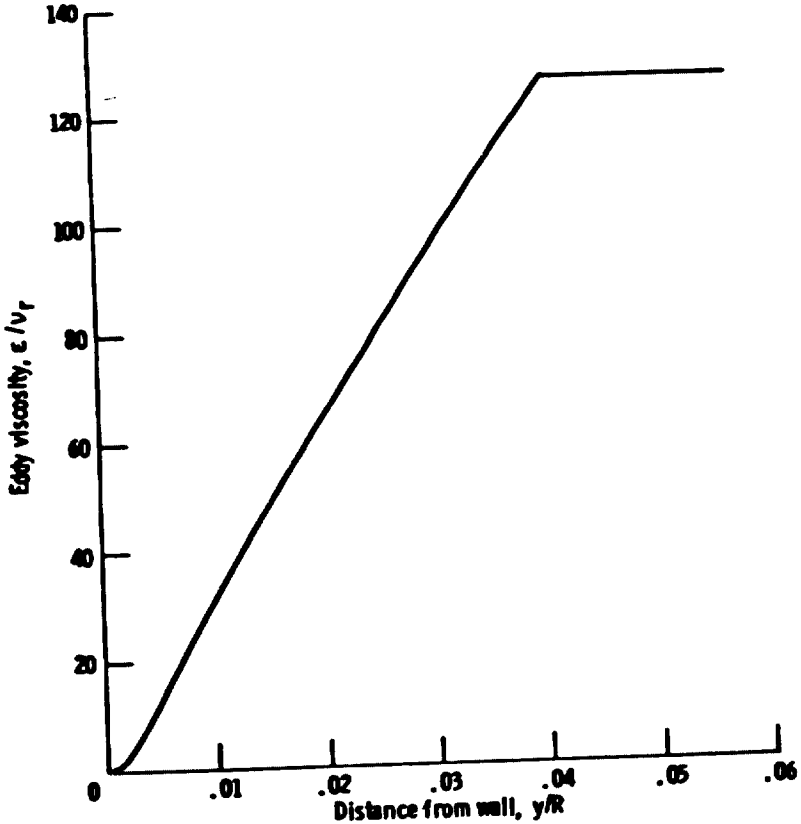

(a) Inner region.

Figure 2-2. - Eddy viscosity in developing turbulent pipe flow.

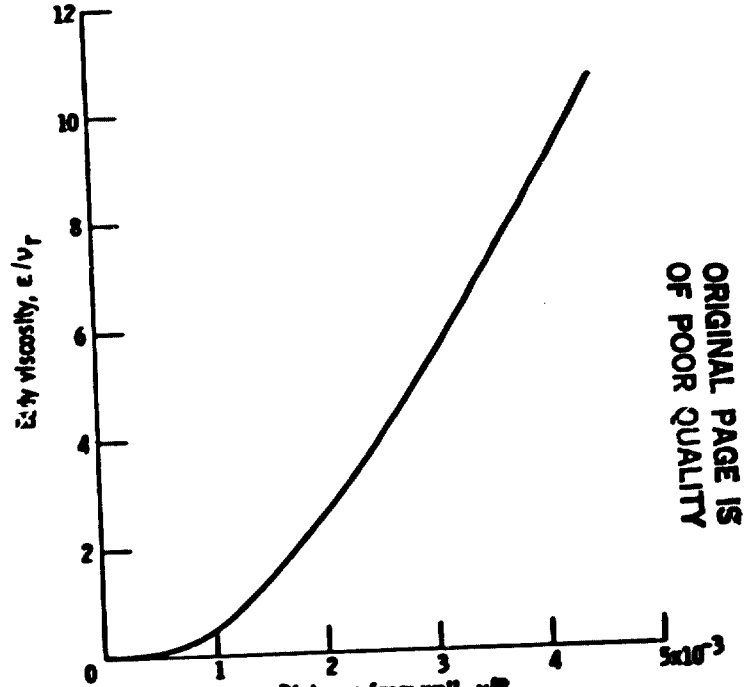

(b) Near-wall region.

Figure 2-2. - Concluded.

ORIGINAL PAGE IS
OF POOR QUALITY

ORIGINAL PAGE IS
OF POOR QUALITY

SECTION 3

NUMERICAL METHOD

3.1 BASIC DIFFERENCING PROCEDURE

3.1.1 Computational Mesh

The governing equations presented in Section 2 are solved using a finite-difference method. A computational grid, or mesh, is thus required in the (ξ,η) coordinate system. Since the method is to be applied to viscous flow problems, grid points should be closely spaced near the walls, where the velocity gradients in the η direction are expected to be largest. For convenience when applying difference formulas, however, a uniformly spaced mesh is desired normal to the walls. The desired grid is obtained by employing the following transformation (Ref. 2):

$$\eta = \frac{\left(C + \frac{1}{2}\right)\exp\left[2\left(Y - \frac{1}{2}\right)\ln\frac{C + \frac{1}{2}}{C - \frac{1}{2}}\right] - \left(C - \frac{1}{2}\right)}{1 + \exp\left[2\left(Y - \frac{1}{2}\right)\ln\frac{C + \frac{1}{2}}{C - \frac{1}{2}}\right]} \tag{3.1}$$

where

$$C = \frac{1}{2}\,(1 - 2D)^{-1/2}$$

and D is given by

$$\frac{1}{D_S} = -D \ln \frac{D}{2}$$

In equation (3.1), Y is the equally spaced, or transformed, coordinate normal to the walls and η is the packed, or untransformed, coordinate. Note that Y is a function of η only. The transformation is implemented by using chain rule differentiation in the form

$$\frac{\partial}{\partial \eta} = \frac{dY}{d\eta} \frac{\partial}{\partial Y}$$

where $dY/d\eta$ can be derived from equation (3.1) as

$$\frac{dY}{d\eta} = \frac{1}{2}\left(\frac{1}{C + \frac{1}{2} - \eta} + \frac{1}{C - \frac{1}{2} + \eta}\right) \ln \frac{C + \frac{1}{2}}{C - \frac{1}{2}} \qquad (3.2)$$

For geometries with two walls (e.g., an axisymmetric flow with a centerbody or a nonsymmetric planar flow), both Y and η in equation (3.1) vary from 0 to 1. Then, for uniform spacing in Y, the transformed coordinate, equation (3.1) will pack the η points close to both walls. For cases with only one wall, Y, and thus η, are allowed to vary only from 0.5 to 1. The η points are then packed only at the outer wall. This mesh is then expanded down to the centerline, where $Y = \eta = 0$. The degree of grid packing is controlled by the parameter D_S, which would typically be between 5 and 500. Increasing D_S packs more points near the walls.

It should be noted that no transformation is used in the streamwise direction, since the locations of high gradients in that direction will vary from case to case. However, the marching step size $\Delta\xi$ is not assumed constant. The user can therefore tailor the distribution of

grid points in the ξ direction to the particular case being studied.

The relationship between the (ξ,η) and (ξ,Y) coordinate systems is shown in Figure 3-1. Also shown in the figure are the indices used in the finite-difference grid. An "i" is used as the index for the ξ, or marching, direction, with $i = 1$ at the initial station. A "j" is used in the cross-stream direction, with $j = 1$ at the lower wall or symmetry line and $j = J$ at the upper wall.

3.1.2 Difference Formulas

Standard difference formulas can be derived using Taylor series expansions. The derivations can be found in any basic reference on finite-difference methods (e.g., Refs. 50-52). Therefore, only the resulting formulas are presented here.

First derivatives in the marching direction are represented by

$$\left(\frac{\partial F}{\partial \xi}\right)_{i+w} \cong \frac{F_{i+1} - F_i}{\Delta \xi} \tag{3.3}$$

This expression is either first or second order in ξ, depending on the value of the implicit weighting factor w. This will become clearer in Section 3.2.

Derivatives in the Y direction at interior points ($2 \leq j \leq J-1$) are all represented by standard second-order centered differencing formulas. For first derivatives the formula is

$$\left(\frac{\partial F}{\partial Y}\right)_j \cong \delta_Y F_j = \frac{F_{j+1} - F_{j-1}}{2\,\Delta Y} \tag{3.4}$$

ORIGINAL PAGE IS
OF POOR QUALITY

and for second derivatives it is

$$\left(\frac{\partial^2 F}{\partial Y^2}\right)_j \approx \delta_Y^2 F_j = \frac{F_{j+1} - 2F_j + F_{j-1}}{(\Delta Y)^2} \tag{3.5}$$

Mixed second derivatives are simply given by a combination of equations (3.3) and (3.4). That is,

$$\left(\frac{\partial^2 F}{\partial \xi \, \partial Y}\right)_{i+w,j} \approx \frac{1}{\Delta \xi} \left(\delta_Y F_{i+1,j} - \delta_Y F_{i,j}\right) \tag{3.6}$$

Difference formulas for Y-derivatives are also needed at boundary points ($j = 1$ and $j = J$) in order to apply some of the boundary conditions described in Section 2.2.2. These formulas are presented in Section 3.4.

With the above difference formulas, the resulting set of coupled algebraic equations will have a block tri-diagonal coefficient matrix with 4x4 submatrices.

3.2 LINEARIZATION PROCEDURE

When a marching step is taken from station i, where the solution is known, to station i+1, where it is unknown, the finite-difference equations are written at the intermediate station i+w. Here w is the implicit weighting factor, $0 < w \leq 1$. For $w = 1$ the difference formulation is therefore fully implicit, while for $w = 1/2$ it is of Crank-Nicholson type. This explains why the difference formula for ξ-derivatives (eq. (3.3)) can be either first or second-order. For $w = 1/2$ it is a second-order centered difference formula, while for

$w = 1$ it is a first-order backward difference formula. Different values of w can be used in each of the four governing equations. When this type of implicit weighting is used on a simple linear model equation, stability analyses show the method to be unconditionally stable for $1/2 \leq w \leq 1$, but only conditionally stable for $0 < w < 1/2$ (Ref. 52). For the complex system of nonlinear equations considered in this analysis, however, these stability conditions can only be used as guidelines (Ref. 51). The results to be presented in Section 4, therefore, were computed using $w = 1$ throughout because of its greater margin of stability.

When the governing equations are written at $i+w$, the unknown terms are, in general, nonlinear functions of the unknown dependent variables ρ, u, v, and T. For example, in the streamwise momentum equation the terms $\rho u \frac{\partial u}{\partial \xi}$ and $\rho v \frac{\partial u}{\partial Y}$ appear. These nonlinear terms must be linearized in order to solve the final set of algebraic equations by matrix inversion.

One method of linearization would be to simply evaluate the coefficients at the known station i and only evaluate the derivatives at $i+w$. However, this is only a first-order method, unless iteration is applied. In the present analysis, a second-order linearization procedure is desired, but without requiring iteration.

This is accomplished by expanding each unknown nonlinear term in a Taylor series in ξ about the known station at ξ_i. This same procedure has been used in other finite-difference marching analyses (Refs. 2, 53-54). Let $G = G(\rho,u,v,T)$ represent a general nonlinear term. Expanding in a Taylor series gives

ORIGINAL PAGE IS
OF POOR QUALITY

$$G_{i+1} = G_i + \left(\frac{\partial G}{\partial \xi}\right)_i \Delta\xi + \mathcal{O}(\Delta\xi)^2 \tag{3.7}$$

where $\Delta\xi = \xi_{i+1} - \xi_i$ and

$$\frac{\partial G}{\partial \xi} = \frac{\partial G}{\partial \rho}\frac{\partial \rho}{\partial \xi} + \frac{\partial G}{\partial u}\frac{\partial u}{\partial \xi} + \frac{\partial G}{\partial v}\frac{\partial v}{\partial \xi} + \frac{\partial G}{\partial T}\frac{\partial T}{\partial \xi} \tag{3.8}$$

Note that for G_{i+1} to be second-order accurate, $\left(\frac{\partial G}{\partial \xi}\right)_i$ and therefore $\left(\frac{\partial \rho}{\partial \xi}\right)_i$, etc., need only be first-order accurate. Note also that a general term G will include metric scale coefficients and the grid stretching parameter $dY/d\eta$. However, these are known a priori and can be evaluated at $i+w$ directly.

In the governing equations, there are six basic forms of nonlinear terms, as follows:

$$f,\ f\frac{\partial Q}{\partial Y},\ \frac{\partial}{\partial Y}\left(f\frac{\partial Q}{\partial Y}\right),\ f\frac{\partial Q}{\partial \xi},\ \frac{\partial}{\partial Y}\left(f\frac{\partial Q}{\partial \xi}\right),\ \frac{\partial}{\partial \xi}\left(f\frac{\partial Q}{\partial Y}\right)$$

Here f is a function of ρ, u, v, and T. In the second and third basic forms, Q is also a general function of ρ, u, v, and T. In the last three, however, it is identically equal to ρ, u, v, or T. The first three forms, which do not include ξ-derivatives, are written at station $i+w$ as

$$G_{i+w} = wG_{i+1} + (1 - w)G_i \tag{3.9}$$

(For all equations in Section 3, terms without an "i" or "j" subscript are understood to be at grid location i or j, unless stated otherwise).

Applying equations (3.7) and (3.8) to the first basic expression, simply f, gives

ORIGINAL PAGE IS
OF POOR QUALITY

$$f_{i+1} = f_i + \left(\frac{\partial f}{\partial \xi}\right)_i \Delta\xi$$

$$f_{i+1} = f_i + \left(\frac{\partial f}{\partial \rho}\frac{\partial \rho}{\partial \xi} + \frac{\partial f}{\partial u}\frac{\partial u}{\partial \xi} + \frac{\partial f}{\partial v}\frac{\partial v}{\partial \xi} + \frac{\partial f}{\partial T}\frac{\partial T}{\partial \xi}\right)_i \Delta\xi$$

Then, using forward difference formulas for the ξ-derivatives and applying equation (3.9) gives

$$f_{i+w} = f_i + w\left(\frac{\partial f}{\partial \rho}\Delta\rho + \frac{\partial f}{\partial u}\Delta u + \frac{\partial f}{\partial v}\Delta v + \frac{\partial f}{\partial T}\Delta T\right)_i \qquad (3.10)$$

where $(\Delta\rho)_i = \rho_{i+1} - \rho_i$, etc. The nonlinear term f_{i+w} is thus represented as a linear combination of the dependent variables at the unknown $i+1$ station. As an example, using a term from the streamwise momentum equation, let

$$f = \frac{h_{1_n}}{h_1 h_2}\rho u v$$

The subscript n denotes partial differentiation. Writing the metrics at $i + w$ directly, and using equation (3.10),

$$f_{i+w} = \left(\frac{h_{1_n}}{h_1 h_2}\right)_{i+w}\Big\{\rho_i u_i v_i + w\big[u_i v_i(\rho_{i+1} - \rho_i) + \rho_i v_i(u_{i+1} - u_i) + \rho_i u_i(v_{i+1} - v_i)\big]\Big\}$$

The second basic expression is $f\frac{\partial Q}{\partial Y}$, where both f and Q can be functions of ρ, u, v, and T. Equation (3.7) gives

$$\left(f\frac{\partial Q}{\partial Y}\right)_{i+1} = \left(f\frac{\partial Q}{\partial Y}\right)_i + \frac{\partial}{\partial \xi}\left(f\frac{\partial Q}{\partial Y}\right)_i \Delta\xi$$

Now

ORIGINAL PAGE IS
OF POOR QUALITY

$$\frac{\partial}{\partial \xi}\left(f \frac{\partial Q}{\partial Y}\right) = \frac{\partial f}{\partial \xi} \frac{\partial Q}{\partial Y} + f \frac{\partial}{\partial Y}\left(\frac{\partial Q}{\partial \xi}\right)$$

Combining, and using equation (3.8), gives

$$\left(f \frac{\partial Q}{\partial Y}\right)_{i+1} = \left(f \frac{\partial Q}{\partial Y}\right)_i + \left(\frac{\partial f}{\partial \rho} \frac{\partial \rho}{\partial \xi} + \frac{\partial f}{\partial u} \frac{\partial u}{\partial \xi} + \frac{\partial f}{\partial v} \frac{\partial v}{\partial \xi} + \frac{\partial f}{\partial T} \frac{\partial T}{\partial \xi}\right)_i \left(\frac{\partial Q}{\partial Y}\right)_i \Delta \xi$$

$$+ f_i \frac{\partial}{\partial Y}\left(\frac{\partial Q}{\partial \rho} \frac{\partial \rho}{\partial \xi} + \frac{\partial Q}{\partial u} \frac{\partial u}{\partial \xi} + \frac{\partial Q}{\partial v} \frac{\partial v}{\partial \xi} + \frac{\partial Q}{\partial T} \frac{\partial T}{\partial \xi}\right)_i \Delta \xi$$

Finally, using forward differences for the ξ-derivatives and applying equations (3.9) and (3.4),

$$\left(f \frac{\partial Q}{\partial Y}\right)_{i+w} = (f \delta_Y Q)_i + w\left(\frac{\partial f}{\partial \rho} \Delta \rho + \frac{\partial f}{\partial u} \Delta u + \frac{\partial f}{\partial v} \Delta v + \frac{\partial f}{\partial T} \Delta T\right)_i \delta_Y Q_i$$

$$+ w f_i \delta_Y \left(\frac{\partial Q}{\partial \rho} \Delta \rho + \frac{\partial Q}{\partial u} \Delta u + \frac{\partial Q}{\partial v} \Delta v + \frac{\partial Q}{\partial T} \Delta T\right)_i \qquad (3.11)$$

The third basic expression is $\frac{\partial}{\partial Y}\left(f \frac{\partial Q}{\partial Y}\right)$. Its linearized and differenced form can be written directly using equation (3.11).

$$\left[\frac{\partial}{\partial Y}\left(f \frac{\partial Q}{\partial Y}\right)\right]_{i+w} = \delta_Y\left[(f \delta_Y Q)_i + w\left(\frac{\partial f}{\partial \rho} \Delta \rho + \frac{\partial f}{\partial u} \Delta u + \frac{\partial f}{\partial v} \Delta v + \frac{\partial f}{\partial T} \Delta T\right)_i \delta_Y Q_i\right]$$

$$+ w f_i \delta_Y^2 \left(\frac{\partial Q}{\partial \rho} \Delta \rho + \frac{\partial Q}{\partial u} \Delta u + \frac{\partial Q}{\partial v} \Delta v + \frac{\partial Q}{\partial T} \Delta T\right)_i + w(\delta_Y f)_i \delta_Y \left(\frac{\partial Q}{\partial \rho} \Delta \rho\right.$$

$$\left. + \frac{\partial Q}{\partial u} \Delta u + \frac{\partial Q}{\partial v} \Delta v + \frac{\partial Q}{\partial T} \Delta T\right)_i \qquad (3.12)$$

The fourth expression to be linearized is $f \frac{\partial Q}{\partial \xi}$. This is written at $i+w$ as

$$\left(f \frac{\partial Q}{\partial \xi}\right)_{i+w} = f_{i+w} \frac{Q_{i+1} - Q_i}{\Delta \xi}$$

ORIGINAL PAGE IS
OF POOR QUALITY

Recall that for the last three basic expressions to be linearized, Q is identically ρ, u, v, or T. To evaluate f_{i+w}, equations (3.7)-(3.9) are used. That is,

$$f_{i+w} = wf_{i+1} + (1 - w)f_i$$

where

$$f_{i+1} = f_i + \left(\frac{\partial f}{\partial \xi}\right)_i \Delta\xi$$

However, to maintain linearity of the difference equations, $\left(\frac{\partial f}{\partial \xi}\right)_i$ must not contain terms at i+1. Therefore, backward differencing is used in this case. Thus,

$$\left(\frac{\partial f}{\partial \xi}\right)_i = \frac{f_i - f_{i-1}}{\Delta\xi_B}$$

where $\Delta\xi_B = \xi_i - \xi_{i-1}$. Then

$$f_{i+w} = f_i + w\lambda(f_i - f_{i-1})$$

where $\lambda = \frac{\Delta\xi}{\Delta\xi_B}$. Finally, the original expression becomes

$$\left(f\,\frac{\partial Q}{\partial \xi}\right)_{i+w} = \left[f_i + w\lambda(f_i - f_{i-1})\right]\frac{Q_{i+1} - Q_i}{\Delta\xi} \qquad (3.13)$$

The fifth expression to be linearized is $\frac{\partial}{\partial Y}\left(f\,\frac{\partial Q}{\partial \xi}\right)$. Its linearized and differenced form can be easily written using equation (3.13).

$$\left[\frac{\partial}{\partial Y}\left(f\,\frac{\partial Q}{\partial \xi}\right)\right]_{i+w} = \left[f_i + w\lambda(f_i - f_{i-1})\right]\delta_Y\left(\frac{Q_{i+1} - Q_i}{\Delta\xi}\right)$$

$$+ \frac{Q_{i+1} - Q_i}{\Delta\xi}\,\delta_Y\left[f_i + w\lambda(f_i - f_{i-1})\right] \qquad (3.14)$$

ORIGINAL PAGE IS
OF POOR QUALITY

Finally, the sixth expression is $\frac{\partial}{\partial \xi}\left(f \frac{\partial Q}{\partial Y}\right)$. This is written, using equations (3.13) and (3.8), as

$$\left[\frac{\partial}{\partial \xi}\left(f \frac{\partial Q}{\partial Y}\right)\right]_{i+w} \cong \left[f_i + w\lambda(f_i - f_{i-1})\right]\delta_Y\left(\frac{Q_{i+1} - Q_i}{\Delta \xi}\right)$$

$$+ (\delta_Y Q)_{i+w}\left[\left(\frac{\partial f}{\partial \rho}\right)_{i+w} \frac{\rho_{i+1} - \rho_i}{\Delta \xi} + \left(\frac{\partial f}{\partial u}\right)_{i+w} \frac{u_{i+1} - u_i}{\Delta \xi}\right.$$

$$\left. + \left(\frac{\partial f}{\partial v}\right)_{i+w} \frac{v_{i+1} - v_i}{\Delta \xi} + \left(\frac{\partial f}{\partial T}\right)_{i+w} \frac{T_{i+1} - T_i}{\Delta \xi}\right] \qquad (3.15)$$

where the combination $(\delta_Y Q)_{i+w}\left(\frac{\partial f}{\partial \rho}\right)_{i+w}$ is given by

$$(\delta_Y Q)_{i+w}\left(\frac{\partial f}{\partial \rho}\right)_{i+w} \cong \left(\frac{\partial f}{\partial \rho}\delta_Y Q\right)_i + w\lambda\left[\left(\frac{\partial f}{\partial \rho}\delta_Y Q\right)_i - \left(\frac{\partial f}{\partial \rho}\delta_Y Q\right)_{i-1}\right]$$

etc.

Every term in the governing equations was linearized and differenced using equations (3.10)-(3.15), with two exceptions. The first is the effective viscous dissipation in the energy equation, given by equation (2.10). While this term could also be linearized to second-order in ξ, the resulting difference form would be quite complex. It was therefore decided during the initial code development to use a first-order linearization, evaluating the viscous dissipation at the known station i. For the cases computed to date, this has proved to be sufficient.

The second exception is the turbulent viscosity μ_T (and therefore the turbulent thermal conductivity k_T, also). The turbulent viscosity is too complex a function of the dependent variables to linearize using the formal procedure presented in this section. It is

therefore computed using the turbulence model equations of Section 2.4 with the dependent variables evaluated at the known station. The laminar viscosity μ_L, however, is treated formally as a function of temperature during the linearization procedure.

The difference equations resulting from the application of this linearization procedure are quite long, even when the difference operators δ_Y and δ_Y^2 are used. Therefore, they are not written here, but instead are presented in Appendix D.

3.3 BOUNDARY CONDITIONS

3.3.1 Derivatives at Boundaries

In order to solve the difference equations, difference forms of the boundary conditions presented in Section 2.2.2 are needed. In particular, a difference formulation for $\frac{\partial Q}{\partial Y}$, where Q is one of the dependent variables, is needed at $j = 1$ and $j = J$. A three-point, second-order, one-sided difference formula can be derived using Taylor series. Thus,

$$\left(\frac{\partial Q}{\partial Y}\right)_j \approx (\delta_Y Q)_j = \frac{\mp 3Q_j \pm 4Q_{j\pm1} \mp Q_{j\pm2}}{2\Delta Y} \tag{3.16}$$

where the top sign is used for the $j = 1$ boundary and the bottom sign is used for the $j = J$ boundary. Solving for Q_j gives

$$Q_j = \frac{1}{3}\left[\mp(2\Delta Y)\left(\frac{\partial Q}{\partial Y}\right)_j + 4Q_{j\pm1} - Q_{j\pm2}\right] \tag{3.17}$$

ORIGINAL PAGE IS
OF POOR QUALITY

With this formula, the tri-diagonality of the coefficient matrix is retained.

When the cross-flow momentum equation is evaluated at a wall to derive the density boundary condition, a one-sided difference formula is also needed for $\frac{\partial^2 v}{\partial Y^2}$. Unfortunately, a second-order one-sided difference formula would require more than three points and thus destroy the tri-diagonality of the coefficient matrix. Thus, a first-order formula was employed, given by

$$\left(\frac{\partial^2 v}{\partial Y^2}\right)_j \approx \left(\delta_Y^2 v\right)_j = \frac{v_j - 2v_{j\pm1} + v_{j\pm2}}{(\Delta Y)^2} \tag{3.18}$$

where, again, $j = 1$ or J. Note that this first-order formula at the wall is the same as the second-order formula one point away from the wall.

3.3.2 Symmetry Line

At a symmetry line, the boundary conditions are given by equations (2.17). Using equation (3.17) with $j = 1$, these are expressed in difference form as

$$\left.\begin{aligned} \rho_1 &= \tfrac{1}{3}(4\rho_2 - \rho_3) \\ u_1 &= \tfrac{1}{3}(4u_2 - u_3) \\ T_1 &= \tfrac{1}{3}(4T_2 - T_3) \\ v_1 &= 0 \end{aligned}\right\} \tag{3.19}$$

where the subscripts refer to j-locations in the grid.

3.3.3 Solid Surfaces

ORIGINAL PAGE IS
OF POOR QUALITY

At a solid surface, the usual boundary conditions for u, v, and T are given by equations (2.18). The conditions for u and v in difference form are simply

$$u_j = u_w \tag{3.20}$$

$$v_j = v_w \tag{3.21}$$

where $j = 1$ or J, and u_w and v_w are known functions of ξ. For no slip and no bleed, $u_w = v_w = 0$. The condition for specified wall temperature is

$$T_j = T_w \tag{3.22a}$$

For a specified temperature gradient at the wall, equation (3.17) gives

$$T_j = \frac{1}{3}\left[\mp(2\Delta Y)\left(\frac{\partial T}{\partial Y}\right)_j + 4T_{j\pm1} - T_{j\pm2}\right] \tag{3.22b}$$

For an adiabatic wall, of course, $\left(\frac{\partial T}{\partial Y}\right)_w = 0$.

The density at a solid surface is found by evaluating the cross-flow momentum equation at the surface. The difference equation at the wall is the same as the difference equation at interior points, and is presented in Appendix D as equation (D.3). At the wall, however, the δ_Y and δ_Y^2 operators in equation (D.3) are given by equations (3.16) and (3.18). When the resulting algebraic equation is solved for ρ_j, the result has the form

ORIGINAL PAGE IS
OF POOR QUALITY

$$\rho_j = \frac{1}{C_{W_1}} \left(C_{W_2}\rho_{j\pm1} + C_{W_3}\rho_{j\pm2} + C_{W_4}u_j + C_{W_5}u_{j\pm1} + C_{W_6}u_{j\pm2} + C_{W_7}v_j \right.$$

$$\left. + C_{W_8}v_{j\pm1} + C_{W_9}v_{j\pm2} + C_{W_{10}}T_j + C_{W_{11}}T_{j\pm1} + C_{W_{12}}T_{j\pm2} + S_j \right) \quad (3.23)$$

where, again, $j = 1$ or J. Details on the derivation of this equation are presented in Appendix E.

The boundary conditions on ρ, u, v, and T that are normally used at a solid surface are thus given by equations (3.23), (3.20), (3.21), and either (3.22a) or (3.22b).

3.3.4 Wall Functions

In turbulent flow, if it is assumed that the streamwise velocity near the wall obeys the logarithmic law-of-the-wall, a slip velocity (or wall function) boundary condition can be derived. The velocity gradient normal to the wall in the law-of-the-wall region is given by equation (2.20). Applying this equation, in difference form, at the first point away from the wall gives

$$\frac{u_{j\pm2} - u_j}{2\Delta Y} \left(\frac{dY}{dn}\right)_{j\pm1} = h_{2_{j\pm1}} \frac{u_{\tau_j}}{\kappa} \frac{1}{y_{j\pm1}}$$

Solving for u_j gives

$$u_j = u_{j\pm2} - (2\Delta Y) \left(\frac{h_2}{dY/dn}\right)_{j\pm1} \frac{u_{\tau_j}}{\kappa} \frac{1}{y_{j\pm1}} \quad (3.24)$$

where $j = 1$ or J, and $y_{j\pm1}$ is the distance from the appropriate wall. The friction velocity u_{τ_j} is computed from the results at the previous station by a secant iteration procedure.

ORIGINAL PAGE IS
OF POOR QUALITY

If a wall function boundary condition is used for u, it must also be used for T if the wall temperature T_W is specified. Applying equation (2.23), in difference form, at the first point away from the wall gives

$$\frac{T_{j\pm2} - T_j}{2\Delta Y}\left(\frac{dY}{dn}\right)_{j\pm1} = h_{2_{j\pm1}} \frac{T_{j\pm1} - T_W}{\kappa y_{j\pm1}\left(Pr_T \frac{1}{\kappa} \ln y^+_{j\pm1} + c_1\right)}$$

Solving for T_j gives

$$T_j = T_{j\pm2} - (2\Delta Y)\left(\frac{h_2}{dY/dn}\right)_{j\pm1} \frac{T_{j\pm1} - T_W}{\kappa y_{j\pm1}\left(Pr_T \frac{1}{\kappa} \ln y^+_{j\pm1} + c_1\right)} \tag{3.25}$$

where again $j = 1$ or J, $y_{j\pm1}$ is the distance from the appropriate wall, and $y^+ = \frac{u_\tau y}{\nu_W}$.

The other conditions are the same as those given in Section 3.3.3. Thus, when wall functions are used at a solid surface, the boundary conditions on ρ, u, v, and T are given by equations (3.23), (3.24), (3.21), and either (3.25) or (3.22b).

3.4 TRI-DIAGONAL MATRIX INVERSION ALGORITHM

When the boundary conditions are applied to equations (D.5)-(D.8), the resulting equations can be written as

$$\left.\begin{aligned} \tilde{\tilde{B}}_2\tilde{X}_2 + \tilde{\tilde{C}}_2\tilde{X}_3 &= \tilde{S}_2 \\ \tilde{\tilde{A}}_j\tilde{X}_{j-1} + \tilde{\tilde{B}}_j\tilde{X}_j + \tilde{\tilde{C}}_j\tilde{X}_{j+1} &= \tilde{S}_j \qquad (3 \le j \le J-2) \\ \tilde{\tilde{A}}_{J-1}\tilde{X}_{J-2} + \tilde{\tilde{B}}_{J-1}\tilde{X}_{J-1} &= \tilde{S}_{J-1} \end{aligned}\right\} \tag{3.26}$$

ORIGINAL PAGE IS
OF POOR QUALITY

where the $\tilde{\tilde{A}}$'s, $\tilde{\tilde{B}}$'s, and $\tilde{\tilde{C}}$'s are known 4x4 matrices whose elements are the coefficients of equations (D.5)-(D.8), the $\tilde{S}$'s are 4-element vectors made up of the source terms in equations (D.5)-(D.8),

$$\tilde{S} = \begin{bmatrix} S_C \\ S_X \\ S_Y \\ S_E \end{bmatrix}$$

and the $\tilde{X}$'s are the 4-element solution vectors,

$$\tilde{X} = \begin{bmatrix} \rho \\ u \\ v \\ T \end{bmatrix}$$

The $\tilde{\tilde{A}}$'s, $\tilde{\tilde{B}}$'s, $\tilde{\tilde{C}}$'s, and $\tilde{S}$'s are presented in Appendix F. Equations (3.26) can be written in matrix form as

$$\begin{bmatrix} \tilde{\tilde{B}}_2 & \tilde{\tilde{C}}_2 & & & & \\ \tilde{\tilde{A}}_3 & \tilde{\tilde{B}}_3 & \tilde{\tilde{C}}_3 & & & \\ & \ddots & \ddots & \ddots & & \\ & & \tilde{\tilde{A}}_{J-2} & \tilde{\tilde{B}}_{J-2} & \tilde{\tilde{C}}_{J-2} & \\ & & & \tilde{\tilde{A}}_{J-1} & \tilde{\tilde{B}}_{J-1} & \end{bmatrix} \begin{bmatrix} \tilde{X}_2 \\ \tilde{X}_3 \\ \vdots \\ \tilde{X}_{J-2} \\ \tilde{X}_{J-1} \end{bmatrix} = \begin{bmatrix} \tilde{S}_2 \\ \tilde{S}_3 \\ \vdots \\ \tilde{S}_{J-2} \\ \tilde{S}_{J-1} \end{bmatrix} \qquad (3.27)$$

ORIGINAL PAGE IS
OF POOR QUALITY

The equations thus have a block tri-diagonal coefficient matrix whose elements are 4x4 sub-matrices, and can therefore be solved using a standard tri-diagonal inversion algorithm (Refs. 51, 55). The algorithm for a block tri-diagonal matrix is the same as for a scalar matrix, but with scalar divisions changed to multiplications by matrix inverses.

With the indexing as used in equation (3.26) and (3.27), the algorithm is as follows. First let

$$\tilde{\tilde{F}}_1 = \tilde{\tilde{B}}_2^{-1}\tilde{\tilde{C}}_2 \tag{3.28}$$

$$\tilde{G}_1 = \tilde{\tilde{B}}_2^{-1}\tilde{S}_2 \tag{3.29}$$

Then, for j increasing from 3 to J-1, compute and store

$$\tilde{\tilde{F}}_{j-1} = \left(\tilde{\tilde{B}}_j - \tilde{\tilde{A}}_j\tilde{\tilde{F}}_{j-2}\right)^{-1}\tilde{\tilde{C}}_j \tag{3.30}$$

$$\tilde{G}_{j-1} = \left(\tilde{\tilde{B}}_j - \tilde{\tilde{A}}_j\tilde{\tilde{F}}_{j-2}\right)^{-1}\left(\tilde{S}_j - \tilde{\tilde{A}}_j\tilde{G}_{j-2}\right) \tag{3.31}$$

The $\tilde{X}$'s themselves are computed by back substitution. First

$$\tilde{X}_{J-1} = \tilde{G}_{J-2} \tag{3.32}$$

Then, for j decreasing from J-2 to 2,

$$\tilde{X}_j = \tilde{G}_{j-1} - \tilde{\tilde{F}}_{j-1}\tilde{X}_{j+1} \tag{3.33}$$

Finally, $\tilde{X}_1$ and $\tilde{X}_J$ are found by using the boundary conditions.

ORIGINAL PAGE IS
OF POOR QUALITY

3.5 VISCOUS PRESSURE CORRECTION

3.5.1 Streamwise Momentum Equation

The viscous pressure correction is computed by solving the streamwise momentum equation, equation (2.14), and the total mass flow rate equation, equation (2.36), during a preliminary marching step, as described in Section 2.3.1. In order to do this, the streamwise momentum equation must be uncoupled from the differential continuity, crossflow momentum, and energy equations. The uncoupling is done by treating u and p'_ξ as the only unknowns, evaluating ρ, v, and T at the previous station. The equation is differenced using the difference formulas of Section 3.1.2, and the unknown terms are written at $i+w$ using equation (3.9). The resulting difference equation is fairly long. It is presented in Appendix G as equation (G.1).

After collecting terms, equation (G.1) can be written as

$$b_2 u_2^* + c_2 u_3^* + d_2 p'_\xi = s_{x_2}$$

$$a_j u_{j-1}^* + b_j u_j^* + c_j u_{j+1}^* + d_j p'_\xi = s_{x_j} \qquad (3 \le j \le J-2) \qquad (3.34)$$

$$a_{J-1} u_{J-2}^* + b_{J-1} u_{J-1}^* + d_{J-1} p'_\xi = s_{x_{J-1}}$$

The "i+1" and "i+w" subscripts have been omitted from the unknowns u^* and p'_ξ, respectively. Here the a's, b's, c's, and d's are the known coefficients and the s_x's the known source terms that come from

ORIGINAL PAGE IS
OF POOR QUALITY

collecting terms in equation (G.1). They are written out in full in Appendix G. The superscript * is used on u^* to distinguish it from the streamwise velocity computed during the main marching step.

3.5.2 Total Mass Flow Rate Equation

The total mass flow rate equation, equation (2.36), is written at station i+1 as

$$\int_{A_{i+1}} \frac{P_{i+1}(\xi,\eta) + p'_{i+1}(\xi)}{RT_i} u^*_{i+1} \, dA_{i+1} = \dot{m} \qquad (3.35)$$

Note that the temperature has been lagged one step, just as in the streamwise momentum equation. The differential area is given by

$$dA = \frac{h_2 h_3}{dY/d\eta} (2\pi)^{\omega} \, dY \qquad (3.36)$$

where $\omega = 0$ for planar flow and 1 for axisymmetric flow. The pressure correction p' is related to the gradient p'_ξ by

$$p'_{\xi_{i+w}} = \frac{p'_{i+1} - p'_i}{\Delta\xi}$$

Substituting the above expression into equation (3.35) gives

$$\int_{A_{i+1}} \frac{P_{i+1} + p'_i + p'_{\xi_{i+w}} \Delta\xi}{RT_i} u^*_{i+1} \, dA_{i+1} = \dot{m} \qquad (3.37)$$

ORIGINAL PAGE IS
OF POOR QUALITY

The nonlinear term $p'_{\xi_{i+w}} u^*_{i+1}$ has thus been introduced. This term is linearized following the procedure described in Section 3.2, but for a general function of p'_ξ and u^*, instead of ρ, u, v, and T. The result is

$$p'_{\xi_{i+w}} u^*_{i+1} = p'_{\xi_{i-1+w}} u_i + u_i \left(p'_{\xi_{i+w}} - p'_{\xi_{i-1+w}} \right) + p'_{\xi_{i-1+w}} \left(u^*_{i+1} - u_i \right)$$

$$= u_i p'_{\xi_{i+w}} + p'_{\xi_{i-1+w}} u^*_{i+1} - p'_{\xi_{i-1+w}} u_i$$

Note, in this equation, that the streamwise velocities at the known station i are those from the previous completely-coupled main marching step. Substituting into equation (3.37) and using equation (3.36),

$$\int_0^1 \frac{1}{RT_i} \left[-p'_{\xi_{i-1+w}} u_i \, \Delta\xi + \left(P_{i+1} + p'_i + p'_{\xi_{i-1+w}} \Delta\xi \right) u^*_{i+1} \right.$$

$$\left. + u_i p'_{\xi_{i+w}} \Delta\xi \right] \left(\frac{h_2 h_3}{dY/d\eta} \right)_{i+1} (2\pi)^\omega \, dY = \dot{m} \qquad (3.38)$$

The unknowns in this equation are u^*_{i+1} and $p'_{\xi_{i+w}}$.

When equation (3.38) is integrated numerically using Simpson's rule, and the boundary conditions on u^* are applied, the resulting equation can be written as

$$e_2 u^*_2 + e_3 u^*_3 + \ldots + e_{J-2} u^*_{J-2} + e_{J-1} u^*_{J-1} + f p'_\xi = s_M \qquad (3.39)$$

where again the "i+1" and "i+w" subscripts have been omitted. Details on the derivation of this equation are presented in Appendix G. Equations (3.34) and (3.39) represent a system of J-1 equations in J-1 unknowns (J-2 u_j's and p'_ξ).

ORIGINAL PAGE IS
OF POOR QUALITY

3.5.3 Solution Algorithm

In matrix form, equations (3.34) and (3.39) are written as

$$\begin{bmatrix} b_2 & c_2 & & & & & d_2 \\ a_3 & b_3 & c_3 & & & & d_3 \\ & \ddots & \ddots & \ddots & & & \vdots \\ & & a_{J-2} & b_{J-2} & c_{J-2} & & d_{J-2} \\ & & & a_{J-1} & b_{J-1} & & d_{J-1} \\ e_2 & e_3 & \cdots & \cdots & e_{J-2} & J-1 & f \end{bmatrix} \begin{bmatrix} u_2^* \\ u_3^* \\ \vdots \\ u_{J-2}^* \\ u_{J-1}^* \\ p'_\zeta \end{bmatrix} = \begin{bmatrix} s_{x_2} \\ s_{x_3} \\ \vdots \\ s_{x_{J-2}} \\ s_{x_{J-1}} \\ s_M \end{bmatrix} \tag{3.40}$$

The system thus has a scalar coefficient matrix that is "almost tri-diagonal". An efficient solution algorithm can be derived using Gaussian elimination, in the same way the standard tri-diagonal inversion algorithm is derived. With the indexing as used in equation (3.40), the resulting algorithm is as follows. First let

$$F_1 = c_2/b_2 \tag{3.41}$$

$$G_1 = s_{x_2}/b_2 \tag{3.42}$$

$$H_1 = d_2/b_2 \tag{3.43}$$

Then, for j increasing from 3 to $J-1$, compute and store

ORIGINAL PAGE IS
OF POOR QUALITY

$$F_{j-1} = c_j/(b_j - a_j F_{j-2}) \tag{3.44}$$

$$G_{j-1} = \left(s_{X_j} - a_j G_{j-2}\right)\Big/\left(b_j - a_j F_{j-2}\right) \tag{3.45}$$

$$H_{j-1} = \left(d_j - a_j H_{j-2}\right)\Big/\left(b_j - a_j F_{j-2}\right) \tag{3.46}$$

$$e_j = e_j - F_{j-2} e_{j-1} \tag{3.47}$$

$$f = f - H_{j-2} e_{j-1} \tag{3.48}$$

$$s_M = s_M - G_{j-2} e_{j-1} \tag{3.49}$$

In equations (3.47)-(3.49), and in equations (3.50) and (3.51) below, the "equals" sign is used in the FORTRAN sense to mean "is replaced by". Next, compute

$$f = f - H_{J-2} e_{J-1} \tag{3.50}$$

$$s_M = s_M - G_{J-2} e_{J-1} \tag{3.51}$$

Then

$$p'_\xi = s_M/f \tag{3.52}$$

$$u^*_{J-1} = G_{J-2} H_{J-2} p'_\xi \tag{3.53}$$

Continuing the back substitution for j decreasing from $J-2$ to 2,

$$u^*_j \quad G_{j-1} - \ ,_{-1} u^*_{j+1} - H_{j-1} p'_\xi \tag{3.54}$$

Finally, u^*_1 and u^*_J are found by using the boundary conditions. Note that, for this application, the algorithm can be stopped after equation (3.52) since only p'_ξ is needed for the main marching step.

The viscous pressure gradient correction p'_ξ computed by this procedure tends to oscillate for the first few marching steps. This is probably due to starting the calculation with the physically unrealistic value of $p'_\xi = 0$. Under many flow conditions, these oscillations tend to damp out as the calculation proceeds. In some cases, however, they can become severe enough to stop the calculation. To prevent this from happening, the value of p'_ξ was "underrelaxed" using

$$(p'_\xi)_{i+w} = (1 - f_R)(p'_\xi)_{i-1+w} + f_R(p'_\xi)^*_{i+w} \qquad (3.55)$$

where $(p'_\xi)^*_{i+w}$ is the value computed using equation (3.52), and f_R is the relaxation factor. It was found that with $f_R = 0.1$ the oscillations in p'_ξ damped out within the first several marching steps. In addition, the computed results with and without underrelaxation were essentially the same for cases in which the oscillations would have damped out naturally. The value of f_R was therefore set equal to 0.1 for all the test cases presented in Section 4.

ORIGINAL PAGE IS
OF POOR QUALITY

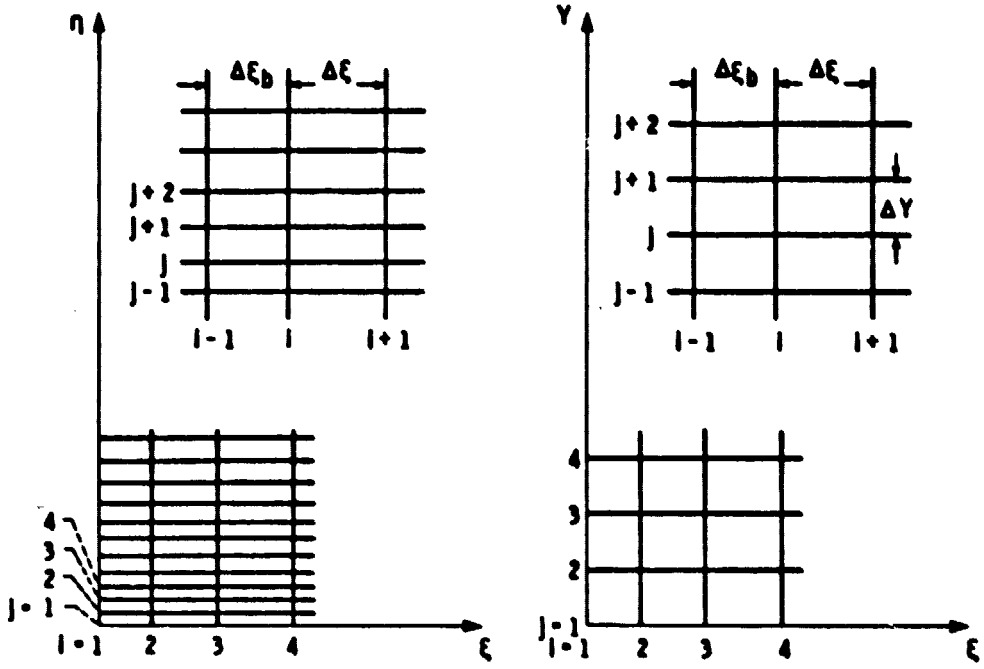

Figure 3-1. - Relationship between untransformed (ξ, η) and transformed (ξ, Y) computational coordinates.

SECTION 4

RESULTS

To validate the marching analysis described in Sections 2 and 3, several test cases were run. In this section, computed results are presented and discussed for five cases: (1) developing laminar flow in a circular pipe; (2) laminar flow in a two-dimensional converging channel (Jeffery-Hamel flow); (3) developing turbulent flow in a circular pipe; (4) turbulent flow in a two-dimensional S-duct; and (5) turbulent flow in a typical subsonic diffuser for a supersonic inlet. For all cases, the results are compared with experimental data and/or exact solutions.

4.1 LAMINAR DEVELOPING PIPE FLOW

A basic test case for a subsonic viscous internal flow analysis is laminar developing flow in a circular pipe. Experimental data suitable for comparison with analysis are plentiful (Refs. 56-58). Other numerical results are also available (Ref. 55). In addition, the computed results should approach the exact Poiseuille solution far downstream of the pipe entrance.

4.1.1 Grid and Initial Conditions

The obvious orthogonal coordinate system for a straight pipe is a cylindrical coordinate system. Therefore the metric scale coefficients used were simply

$$h_1 = h_2 = 1$$

$$h_3 = r$$

For this coordinate system, the computational (ξ,η) and physical (z,r) coordinates coincide so that $\xi = z$ and $\eta = r$. The configuration is illustrated in Figure 4-1.

The imposed pressure $P(\xi,\eta)$ was set equal to a constant everywhere in the duct, since for this case there are no elliptic effects due to geometry. The streamwise pressure gradient is then completely determined by the viscous correction $p'_\xi(\xi)$. This case is thus an important test of the method used to compute p'_ξ during the marching solution.

The entrance length L_e for developing pipe flow (i.e., the distance from the entrance at which the flow can be considered fully developed) is given by (Ref. 59)

$$\frac{L_e}{D} = 0.08\ Re_D$$

where D is the the pipe diameter and Re_D is the Reynolds number based on D and u_0, the average velocity in the pipe. The pipe diameter and flow conditions were chosen to give a Reynolds number low enough to allow the computation of the entire entrance length within a

reasonable number of pipe diameters. A pipe radius of 0.061 cm (0.002 ft) was used as the reference length L_r. The reference velocity U_r was 6.10 m/sec (20 ft/sec). This corresponds to the centerline velocity for fully-developed flow, which is twice the average velocity in the pipe. Standard atmosphere values of 288 K (519° R) and 1.2246 kg/m^3 (0.07645 lb$_m$/ft^3) were used for the reference temperature T_r and density ρ_r, respectively. The reference Reynolds number Re_r was thus 254.151, which corresponds to an entrance length of 40.66 radii.

The calculation could not be started exactly at the pipe entrance because the u and v velocity profiles would be singular at the wall. It was therefore started slightly downstream of the actual entrance, at $z/R = 0.254$. The initial streamwise velocity, nondimensionalized by the average velocity u_0, is presented in Figure 4-2. This profile was given by the tabulated finite-difference results of Hornbeck (Ref. 55), with weighted average quadratic interpolation used to get values between the tabulated points. The interpolation resulted in a slight kink in the profile near the edge of the boundary layer. This kink was quickly eliminated, however, through viscous effects and had no appreciable effect on the computed results. The initial cross-flow velocity v was set equal to zero. It should be noted that this is not physically realistic. In fact, the v-velocity should be largest near the pipe entrance. However, it should still be small compared to the u-velocity. In addition, it was felt that setting v equal to zero was representative of the way this analysis would be used in a practical situation, where the initial v-velocity profile is usually unknown. Finally, since the flow in this case is essentially

incompressible, the initial dimensionless density and temperature were both set equal to one.

No-slip and no-bleed boundary conditions were used for u and v at the wall. An adiabatic wall boundary condition was used for the temperature. Fifty-one grid points were used between the centerline and the wall. The points were lightly packed near the wall using the transformation given by equation (3.1) with $D_S = 5$. The marching step size $\Delta\xi$ was 0.05. This grid is plotted in Figure 4-3. Since the same grid was used through the entire pipe, only a short section near the entrance is shown. To reach the end of the estimated entrance length at $\xi = 40.66$, 809 marching steps were required. The calculation took 3.5 minutes of CPU time on an IBM 370/3033. It should be stated, however, that a mesh size study was not done for this case. Based on the results to be shown in the following section, it is felt that $\Delta\xi$ could be increased considerably, especially downstream of the region very near the entrance. The number of transverse grid points could probably also be reduced.

4.1.2 Results

The computed axial velocity profiles are presented in Figure 4-4. Profiles are plotted every ten marching stations, with the abscissa displaced by 1/4 of the interval width for each successive profile. The boundary layer thickness increases rapidly near the entrance and soon reaches the duct centerline. It takes much longer, however, for the centerline velocity to reach its fully-developed value.

The computed cross-flow velocity profiles are presented in Figure 4-5. Although the initial v-velocity was set equal to zero, the analysis quickly generates a realistic profile. The computed v-velocity is negative, with the flow moving away from the wall, and its magnitude is a maximum near the edge of the boundary layer. As the boundary layer thickness increases, the point of maximum v-velocity moves out from the wall. Further downstream, where the flow in the duct is completely viscous, the v-velocity is essentially zero.

The computed u-velocities are compared with the numerical results of Hornbeck (Ref. 55) in Figure 4-6. Note that the abscissa in Figure 4-6 is $z/(R\ Re_R)$, where $Re_R = \rho u_0 R/\mu_L$. This removes the Reynolds number dependence from the problem, allowing the present results to be compared directly with other results or data. Hornbeck solved the incompressible streamwise momentum equation, minus the diffusion terms involving v, along with the total mass flow equation, for the streamwise velocity distribution and the pressure. The agreement between the present results and those of Hornbeck is excellent. The velocity near the centerline increases continuously until the flow becomes fully-developed. Near the wall the velocity decreases continuously. In-between (at $r/R = 0.6$ and 0.7) the velocity first increases to compensate for the increasing boundary layer blockage. Then, as the boundary layer thickens further, including these points, the velocity decreases gradually to its fully-developed value.

The present results are compared with the experimental data of Pfenninger (Ref. 56), Reshotko (Ref. 57), and Nikuradse (Ref. 58) in Figures 4-7 to 4-9, respectively. In these figures the streamwise velocity ratio u/u_0 is plotted as a function of $z/(R\ Re_R)$ at six

radial locations. Note that Pfenninger's data are all near the duct entrance and thus an expanded abscissa is used in Figure 4-7. The agreement with Pfenninger's data is excellent. The agreement with Reshotko's data, presented in Figure 4-8, is also excellent, except at $r/R = 0.8$ and 0.9. However, the accuracy of the data at these radial locations, as plotted in the figure, is questionable. The data in Reference 57 are presented as velocity profile plots at various axial stations. The disagreement in Figure 4-8 can be explained by assuming that the data near the wall were actually taken at slightly lower values of r/R than 0.8 and 0.9, either intentionally or because of a systematic error in determining the probe location near the wall. (The radial locations are not explicitly stated in Reference 57, and the plots can only be read to an accuracy of about 0.02 in r/R). As an indication that this may be the case, note that the experimental velocity near the wall does not approach the Poiseuille profile value. (The computed velocity does, as will be shown in a later figure). The agreement between the analysis and Nikuradse's data is excellent in the downstream half of the pipe, but not as good near the entrance. However, these data may also be questioned, since they do not agree with the results of Reference 55, or the data of References 51 and 52. The present results are also compared with the data of References 56-58, in the form of velocity profiles at various axial stations, in Figures 4-10 to 4-12, respectively.

In Figure 4-13, the computed axial pressure gradient, in the form of $\frac{d(p'/\rho u_0^2)}{d(z/R\ Re_R)}$, is plotted as a function of $z/(R\ Re_R)$. Also shown are the results of Hornbeck (Ref. 55), the data of Reshotko (Ref. 57), and

the fully-developed Poiseuille value. Recall that since the imposed pressure is a constant for this case, the axial pressure gradient is determined completely by the viscous correction p'_ξ. The starting transient near the entrance is a result of starting with the physically unrealistic (but, as with the cross-flow velocity, realistic in practice) value of $p'_\xi = 0$. The pressure gradient rapidly reaches the correct value, however, and slowly approaches the fully-developed value far downstream. The agreement with the results of Reference 55 and the data of Reference 57 is excellent, indicating that the method used to compute the viscous pressure correction p'_ξ is valid.

In Figure 4-14 the computed skin friction coefficient is plotted as a function of axial distance. The shear stress at the wall was found by second-order one-sided numerical differentiation of the computed axial velocity. Also shown in the figure is the value for fully-developed Poiseuille flow. As one would expect, the skin friction starts out high, where the boundary layer is thin, decreases rapidly as the boundary layer thickens, and then slowly approaches the fully-developed Poiseuille value.

Finally, in Figure 4-15 the computed streamwise velocity profile at the last station is compared with the exact Poiseuille profile. The agreement is excellent, indicating that a fully-develped state has been reached.

ORIGINAL PAGE IS
OF POOR QUALITY

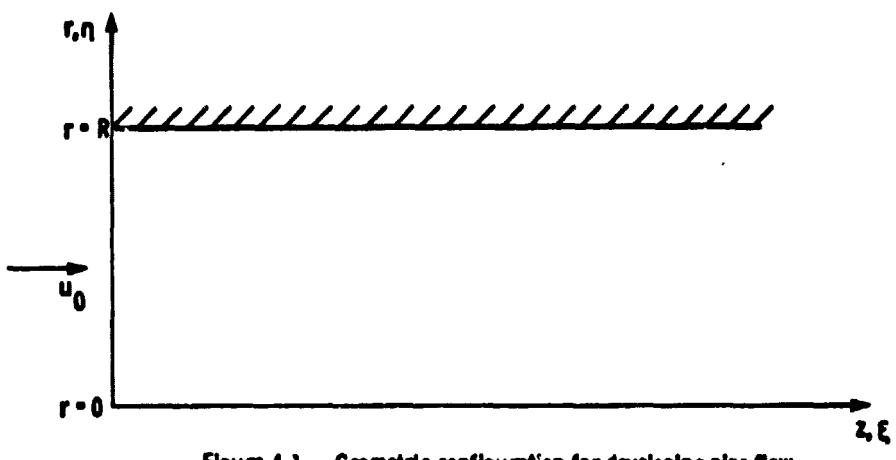

Figure 4-1. - Geometric configuration for developing pipe flow.

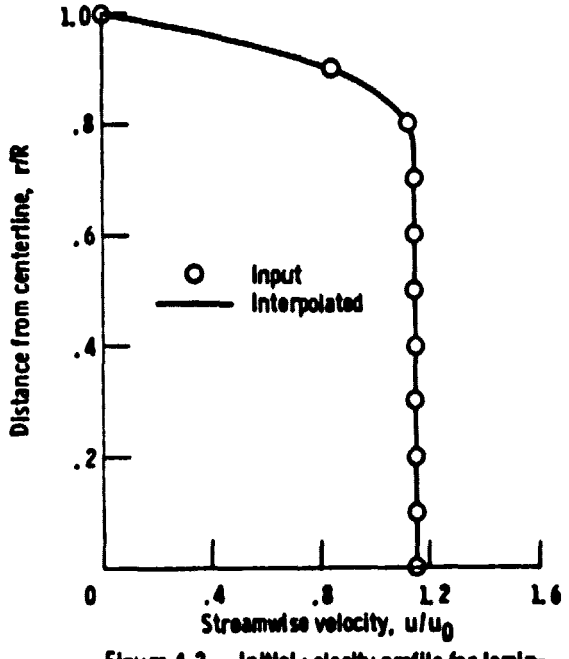

Figure 4-2. - Initial velocity profile for laminar developing pipe flow, z/R = 0.254.

ORIGINAL PAGE IS
OF POOR QUALITY

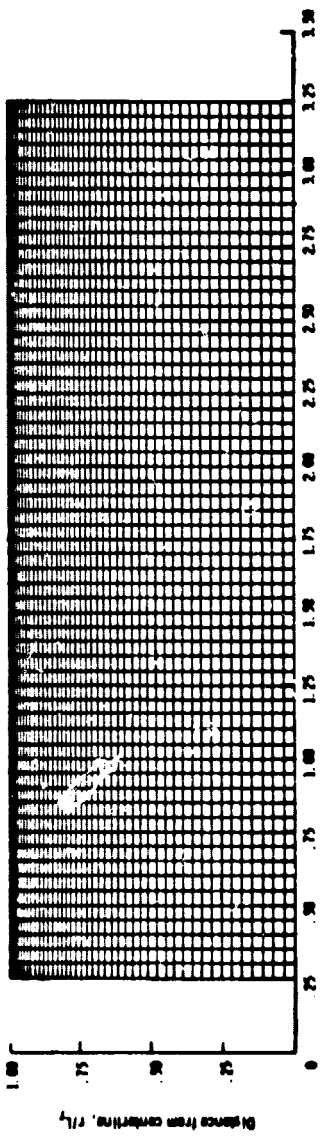

Figure 4-3. - Computational grid used in calculation of laminar developing pipe flow.

ORIGINAL PAGE IS
OF POOR QUALITY

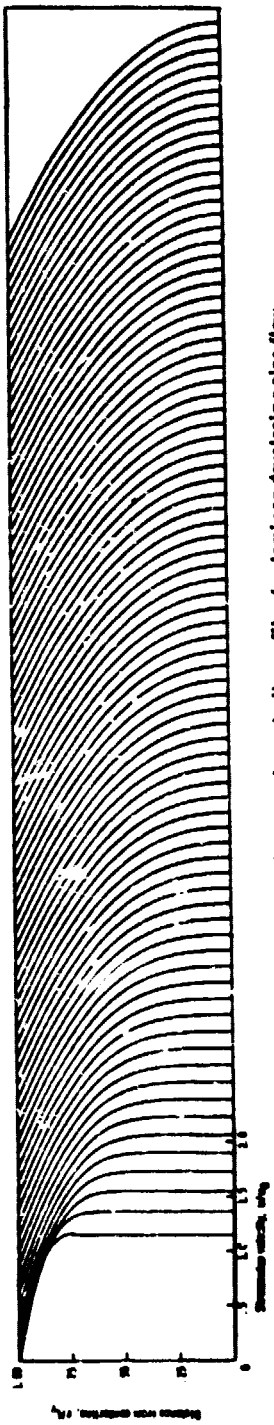

Figure 4-4. - Computed streamwise velocity profiles for laminar developing pipe flow.

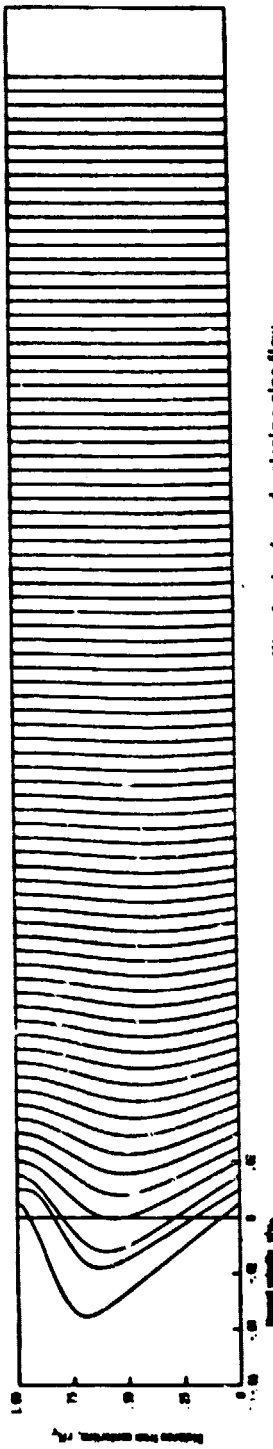

Figure 4-5. - Computed cross-flow velocity profiles for laminar developing pipe flow.

ORIGINAL PAGE IS
OF POOR QUALITY

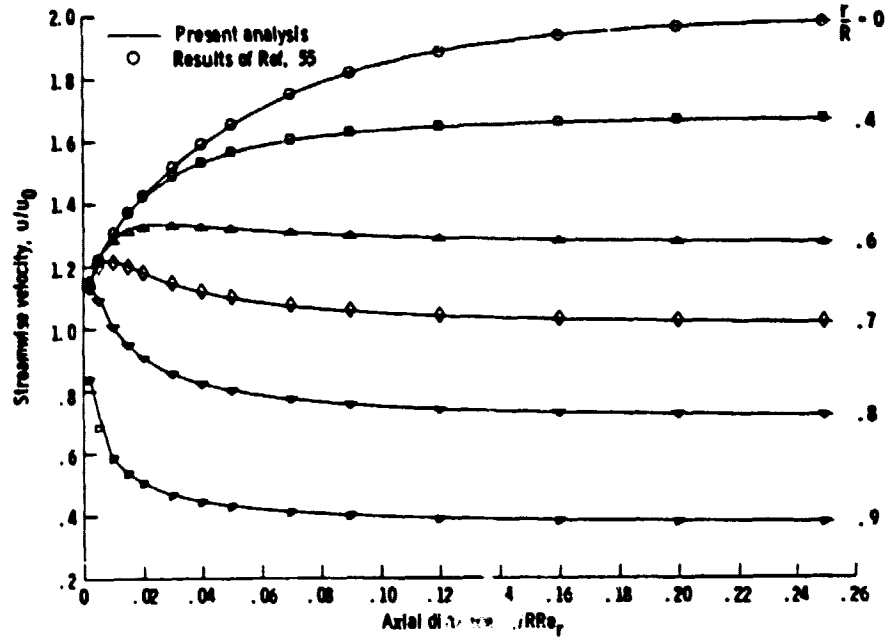

Figure 4-6. - Comparison of computed streamwise velocity with results of Hornbeck for laminar developing pipe flow.

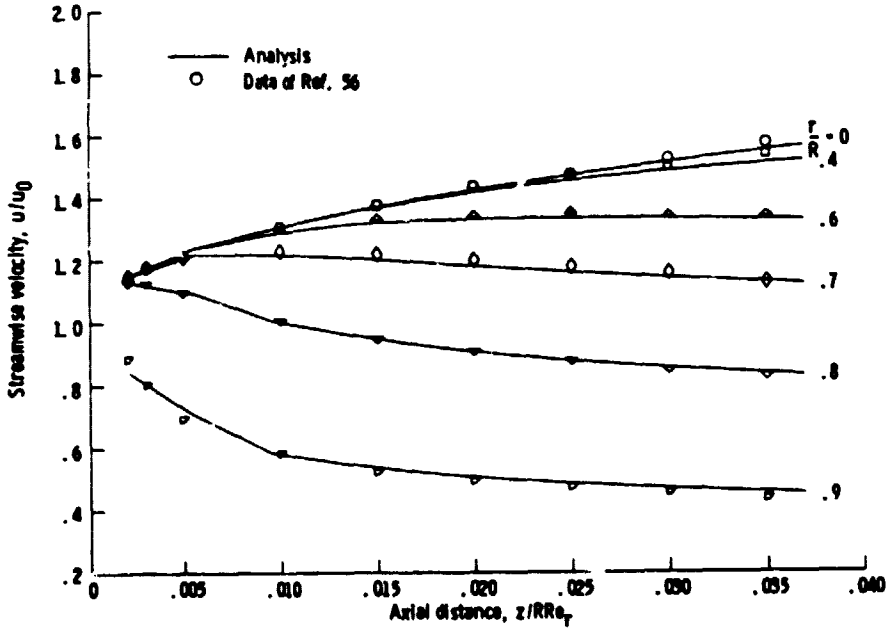

Figure 4-7. - Comparison of computed streamwise velocity with data of Pfenninger for laminar developing pipe flow.

ORIGINAL PAGE IS
OF POOR QUALITY

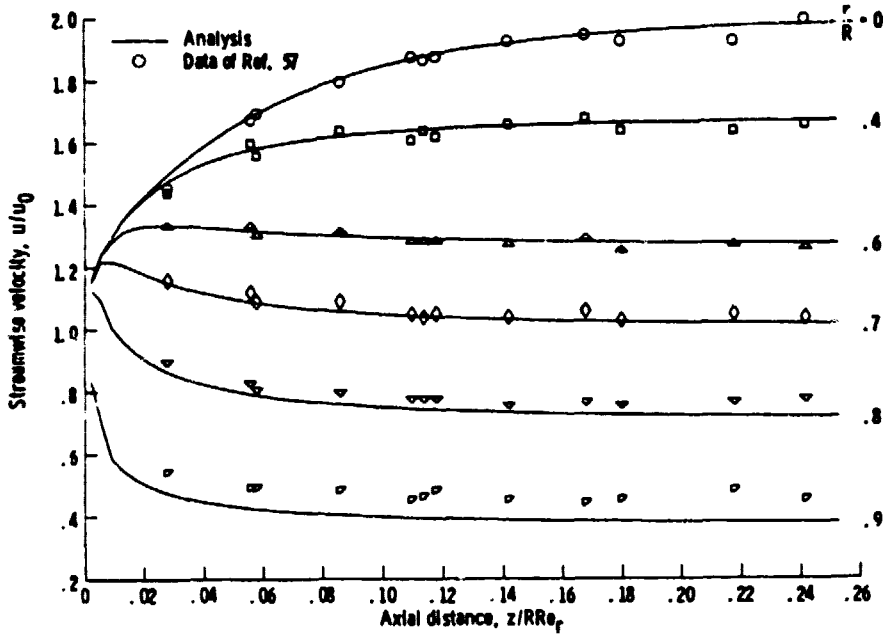

Figure 4-8. - Comparison of computed streamwise velocity with data of Reshotko for laminar developing pipe flow.

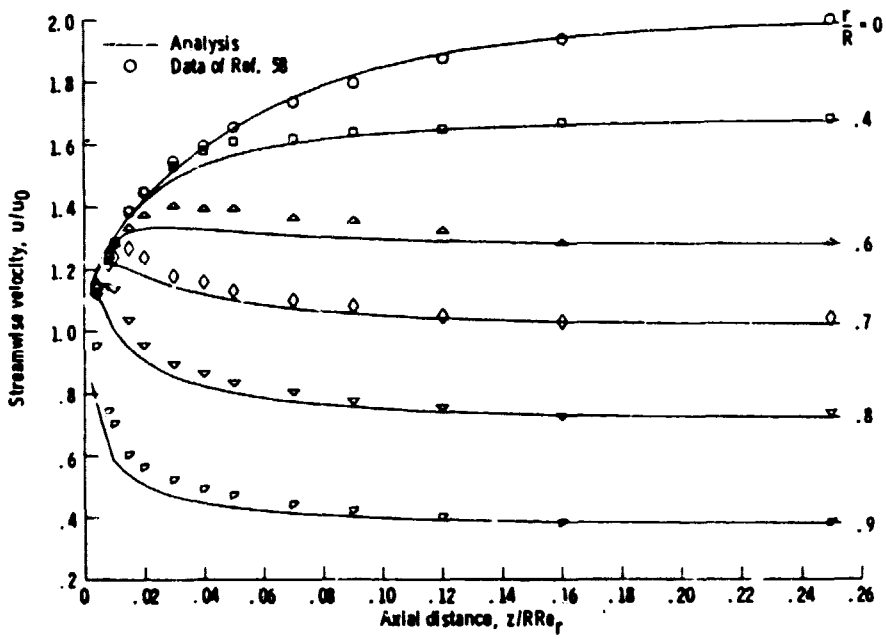

Figure 4-9. - Comparison of computed streamwise velocity with data of Nikuradse for laminar developing pipe flow.

ORIGINAL PAGE IS
OF POOR QUALITY

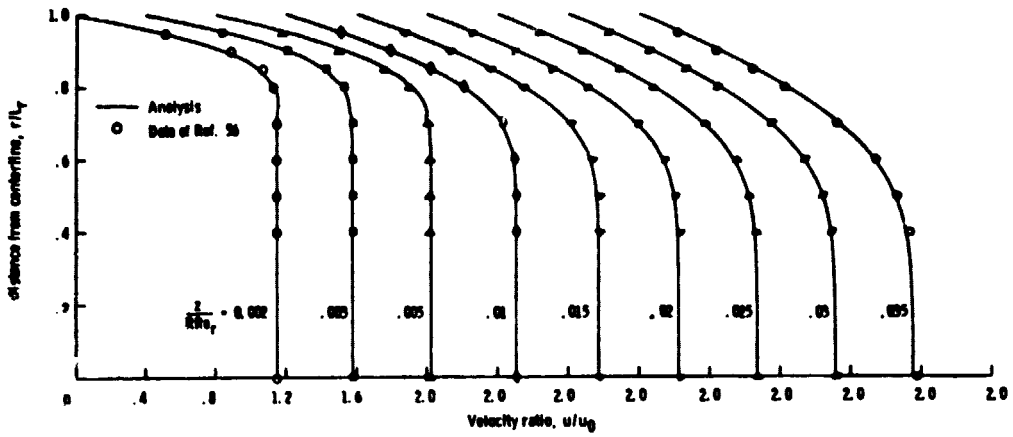

Figure 4-10. - Comparison of computed velocity profiles with data of Pfenninger for laminar developing pipe flow.

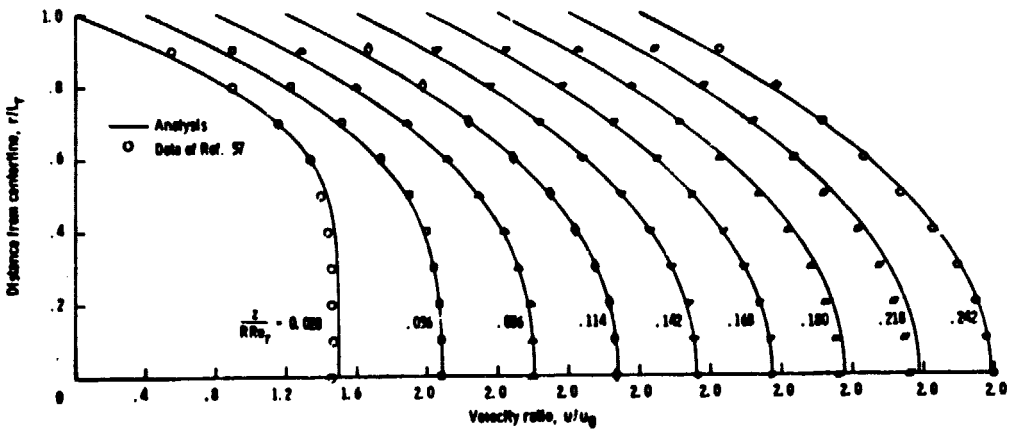

Figure 4-11. - Comparison of computed velocity profiles with data of Reshotko for laminar developing pipe flow.

ORIGINAL PAGE IS
OF POOR QUALITY

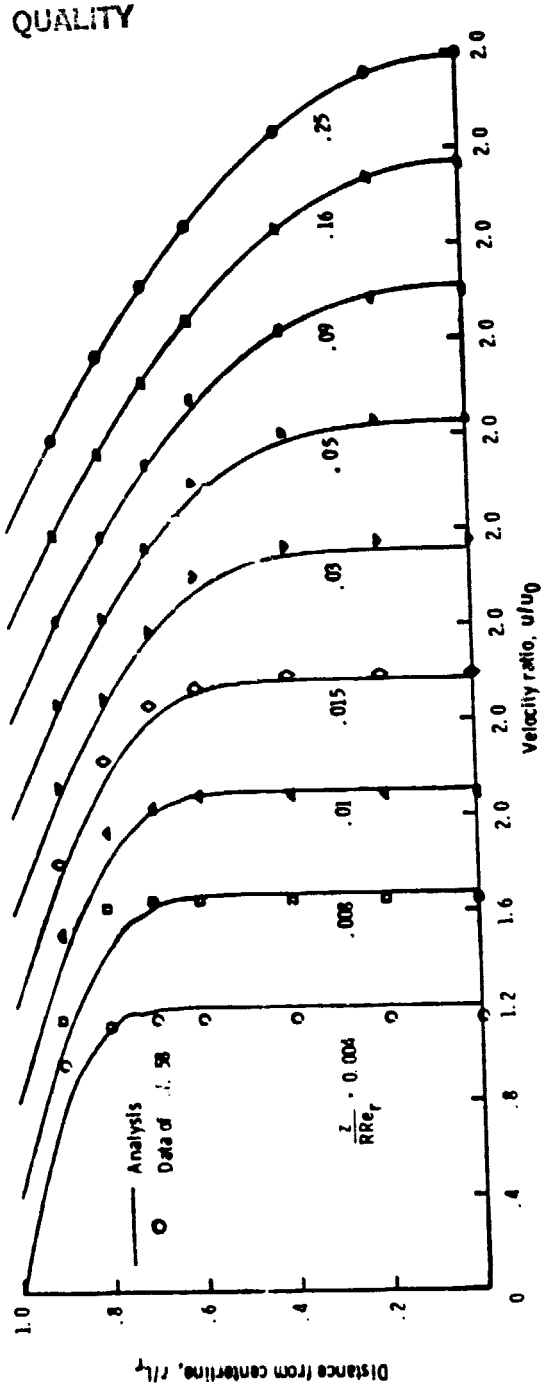

Figure 4-12. - Comparison of computed velocity profiles with data of Nikuradse for laminar developing pipe flow.

ORIGINAL PAGE IS
OF POOR QUALITY

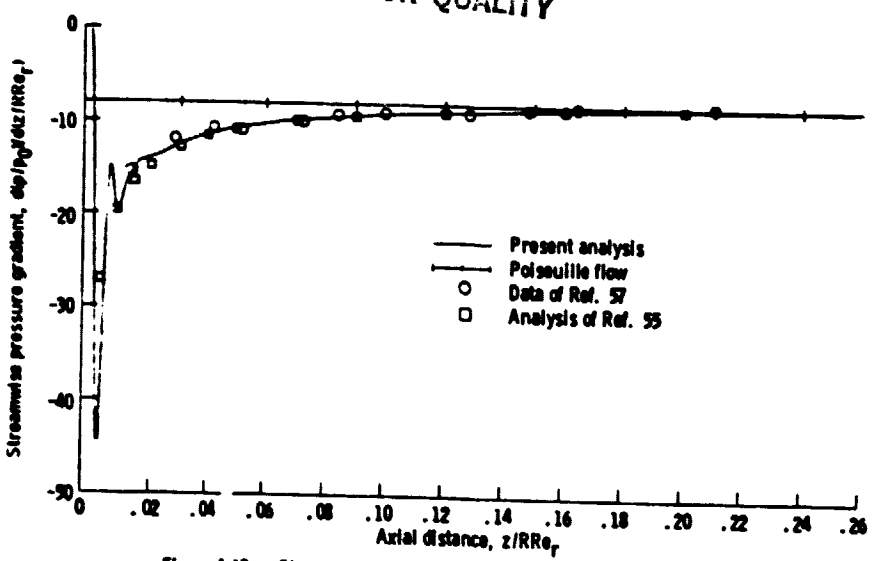

Figure 4-13. - Streamwise pressure gradient in laminar developing pipe flow.

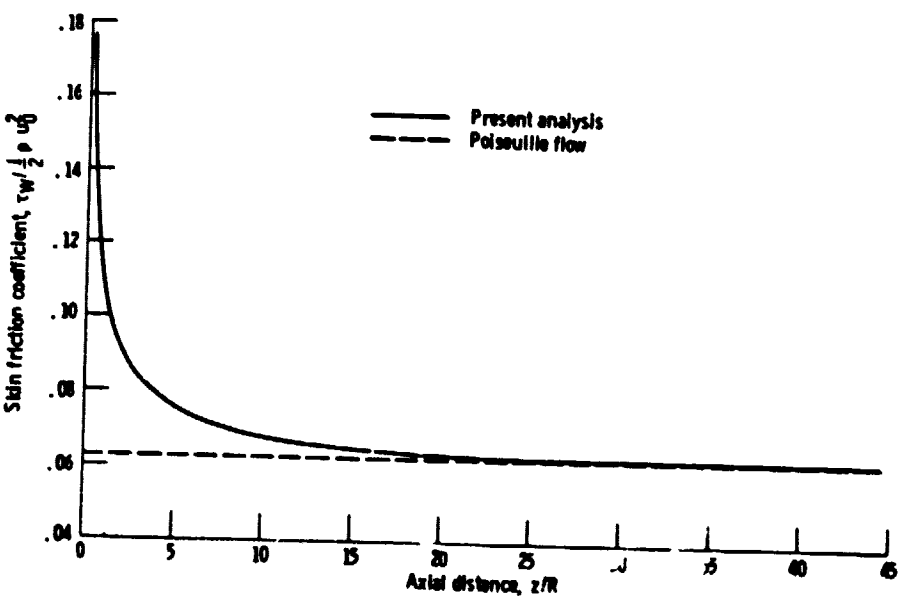

Figure 4-14. - Skin friction coefficient in laminar developing pipe flow.

ORIGINAL PAGE IS
OF POOR QUALITY

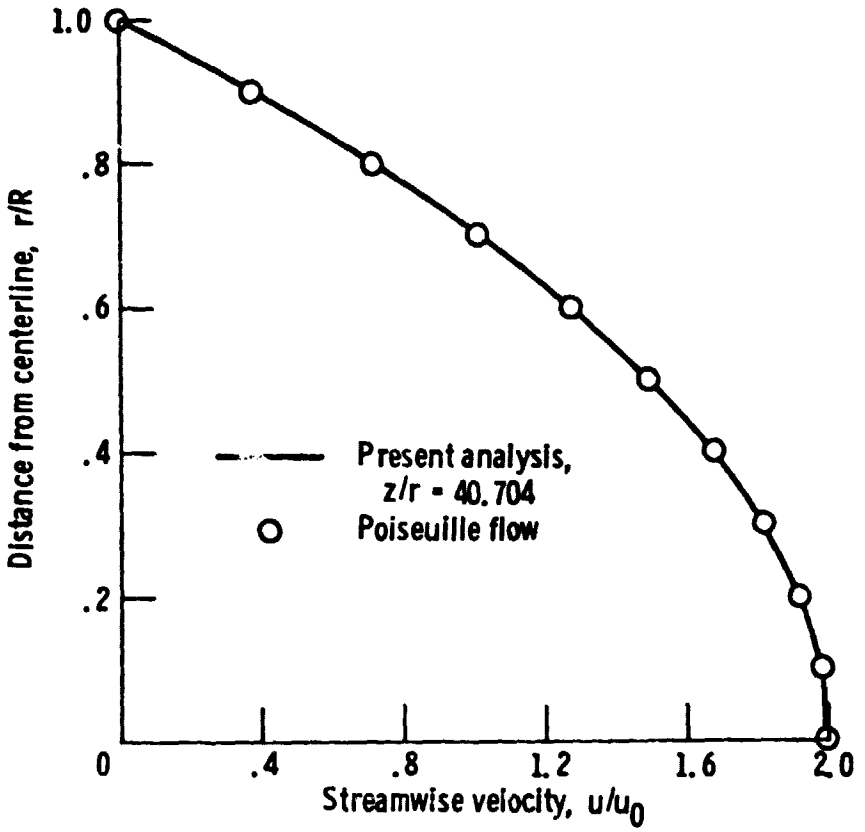

Figure 4-15. - Comparison of computed velocity profile at z/R = 40.7 with Poiseuille flow value.

4.2 JEFFERY-HAMEL FLOW

Another useful test case is laminar incompressible flow in a two-dimensional wedge-shaped channel, known as Jeffery-Hamel flow. When self-similarity is assumed, an exact solution to the Navier-Stokes equations exists for this flow. The streamlines are radial, intersecting at a line source (for diverging flow) or sink (for converging flow). The solution for the velocity, derived in terms of Jacobian elliptic functions, is given by Millsaps and Pohlhausen (Ref. 60).

4.2.1 Grid and Initial Conditions

The configuration and coordinate system for converging Jeffery-Hamel flow is illustrated in Figure 4-16. The particular geometry used in this study was a converging channel with a half-angle α of 5 degrees. A polar coordinate system, centered at the intersection of the wall and symmetry plane, was used as the orthogonal coordinate system for the analysis. In Figure 4-16, R_S is the radial coordinate measured from the center of the polar system, and φ is the angular coordinate measured in the clockwise direction from the symmetry plane. Since the flow is in the $-R_S$ direction, the computational streamwise coordinate is

$$\xi = R_{S_1} - R_S$$

where R_{S_1} is the radial coordinate at the initial station. The computational cross-stream coordinate is simply

$$\eta = \varphi/\alpha$$

The metric scale coefficients are then

$$h_1 = h_3 = 1$$

$$h_2 = R_S\alpha$$

This flow, unfortunately, violates one of the basic assumptions made in formulating a set of equations that can be solved by spatial marching. The streamwise pressure gradient cannot be represented by an inviscid pressure gradient plus a one-dimensional viscous correction if self-similarity is to be maintained. For this reason the exact solution was used to compute the imposed pressure gradient $P_\xi(\xi,\eta)$. The derivation of the equation for P_ξ from the exact solution for u is presented in Appendix H. Under these conditions, the computed viscous pressure correction p'_ξ should be essentially zero throughout the duct.

The Reynolds number used in Reference 60 was defined as

$$Re_0 = \frac{u_{CL}R_S}{\nu}$$

where u_{CL} is the centerline velocity at a given R_S. For this case, a value of $Re_0 = -5000$ was used. (The value is negative because u_{CL} is in the negative R_S direction.) An initial channel half-width of 0.061 cm (0.002 ft) was used as the reference length L_r. The value of R_{S_1} was thus 0.6995 cm (0.02295 ft). Standard atmosphere values of 288 K (519° R) and 1.2246 kg/m^3 (0.07645 lb$_m$/ft^3) were used for the reference temperature and density, respectively. The centerline velocity at the initial station, which for $Re_0 = -5000$ was 10.45 m/sec

(34.29 ft/sec), was used for the reference velocity. The reference Reynolds number was thus 435.8.

The exact solution was used for the initial streamwise velocity profile. (See Appendix H for the equation). The initial dimensionless values of cross-flow velocity, density, and temperature were zero, one, and one, respectively. No-slip and no-bleed boundary conditions were used for u and v at the wall. An adiabatic wall boundary condition was used for the temperature. Fifty-one grid points were used between the symmetry plane and the wall. The points were lightly packed near the wall with $D_S = 10$ in equation (3.1). One hundred marching steps were taken with a step size $\Delta\xi$ of 0.05. The final area was thus 0.56 times the initial area. The computational grid is shown in Figure 4-17 with every other streamwise station plotted. The inset in the figure shows the grid near the wall magnified by a factor of five. A circle is centered at corresponding locations in the full grid and the inset. This calculation required 28.9 seconds of CPU time on an IBM 370/3033.

4.2.2 Results

The computed streamwise velocity profiles are presented in Figure 4-18. Profiles are plotted every other marching station. The flow accelerates through the duct and the boundary layer thins somewhat. Self-similarity is maintained in the calculation, as shown in Figure 4-19, where the computed solution after 100 marching steps is compared with the exact solution. The two solutions are the same to within the resolution of the plot.

The cross-flow velocity profiles are presented in Figure 4-20. Except for a slight starting transient, where it reaches a dimensionless value of about 0.0005, the cross-flow velocity is essentially zero everywhere in the duct.

The viscous pressure correction also remains essentially zero. It reaches a maximum at the last station of about 0.0018 (nondimensionally), compared to an overall level of about 757. The viscous correction to the pressure gradient at this station is -0.0017, compared to the exact values of -0.49 at the centerline and 0.73 at the wall.

ORIGINAL PAGE IS
OF POOR QUALITY

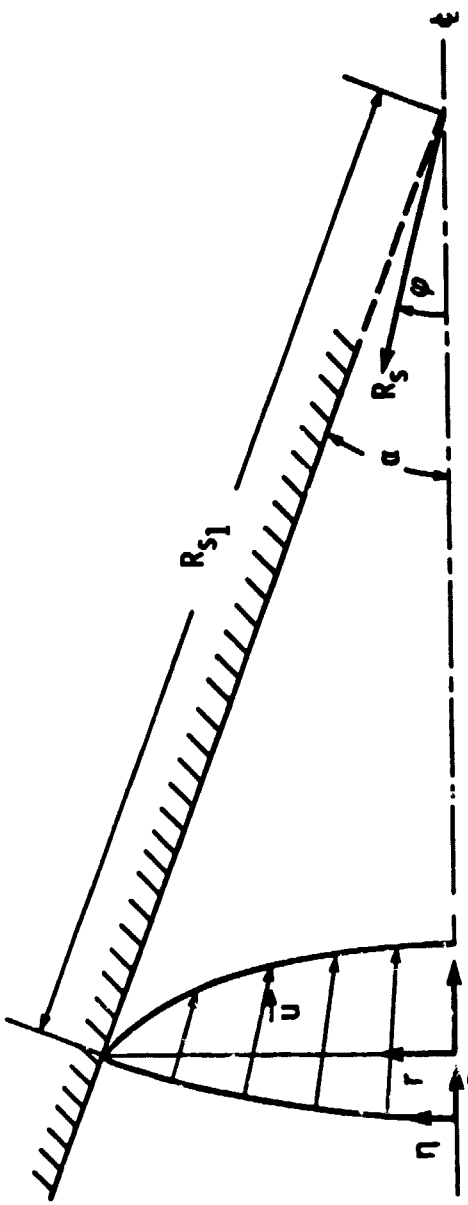

Figure 4-16. - Geometric configuration for converging Jeffery-Hamel flow (not to scale).

ORIGINAL PAGE IS
OF POOR QUALITY

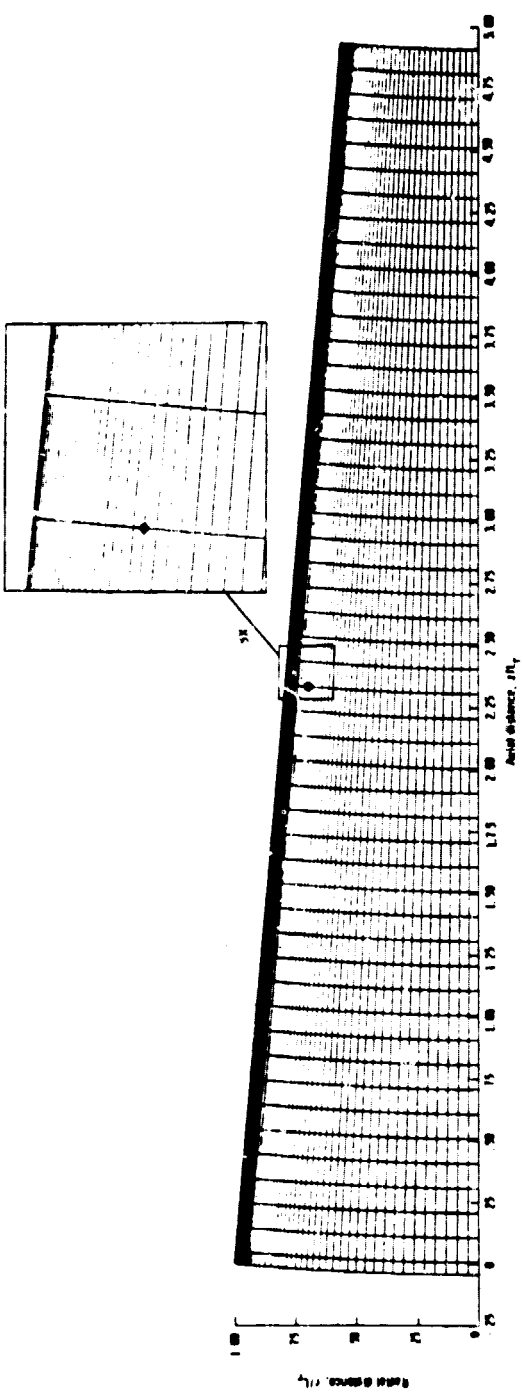

Figure 4-17. - Computational grid used for viscous calculation, converging Jeffery-Hamel flow.

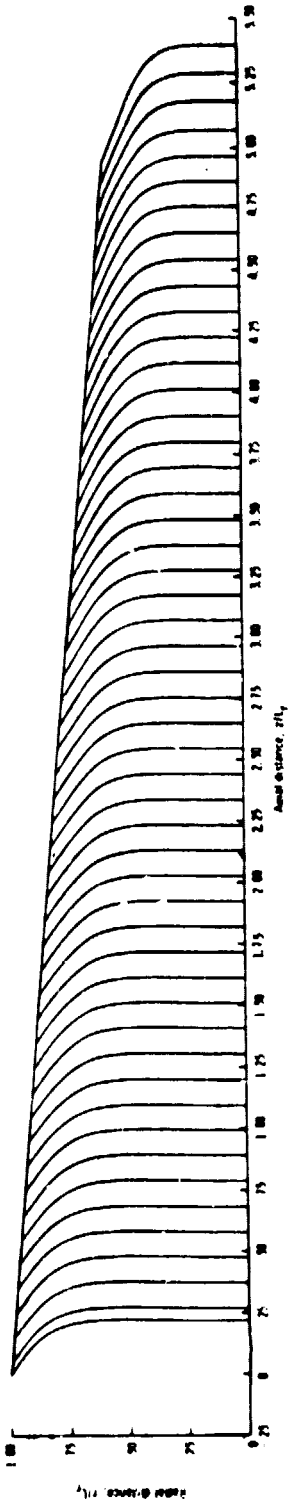

Figure 4-18. - Computed streamwise velocity profiles for converging Jeffery-Hamel flow.

ORIGINAL PAGE IS
OF POOR QUALITY

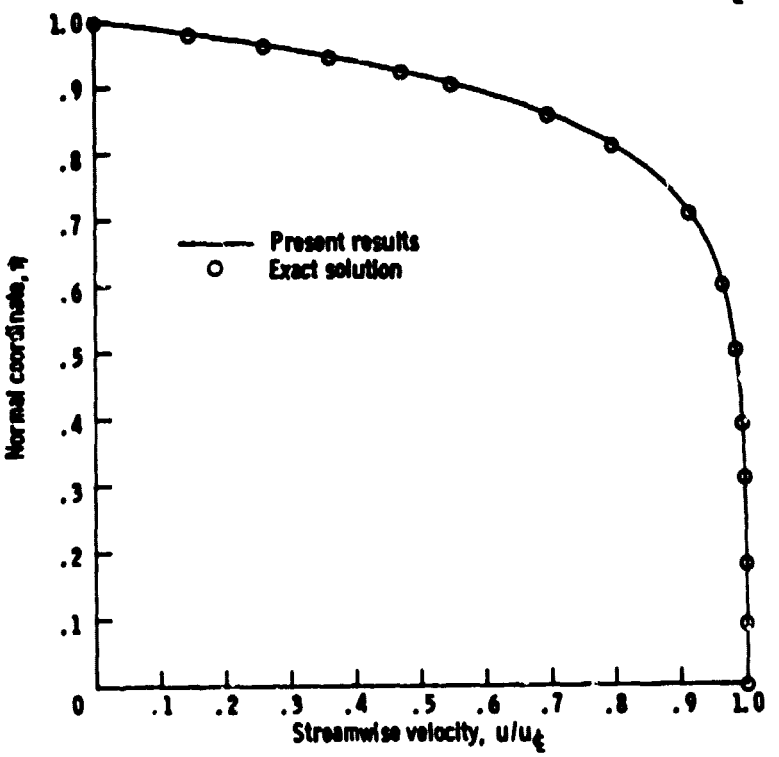

Figure 4-19. - Comparison of final computed velocity profile with exact solution for converging Jeffery-Hamel flow.

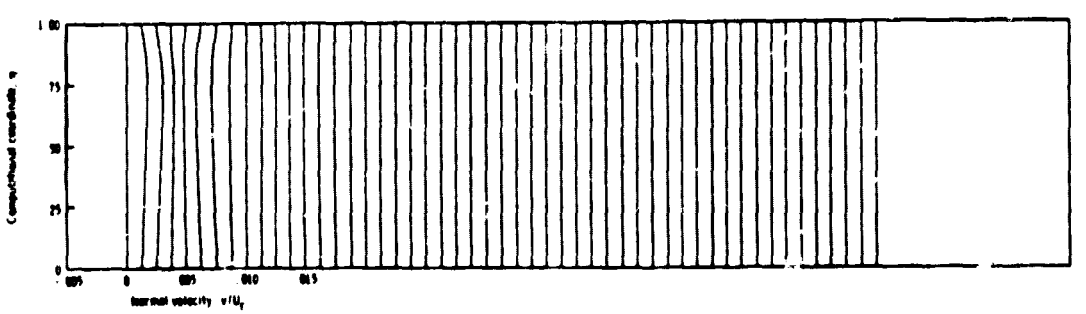

Figure 4-20. - Computed cross-flow velocity profiles for converging Jeffery-Hamel flow.

4.3 TURBULENT DEVELOPING PIPE FLOW

One of the most basic test cases for turbulent flow is developing flow in a circular pipe. Although no exact solution exists, the problem has been studied experimentally by several investigators (Refs. 47, 61-64). The data of Barbin (Ref. 62) were chosen for comparison with the present analysis.

4.3.1 Grid and Initial Conditions

As in the laminar developing pipe flow case, a cylindrical coordinate system was used, as illustrated in Figure 4-1. Again, the computational (ξ,η) and physical (z,r) coordinates coincide, so that $\xi = z$ and $\eta = r$. Also, as in the laminar case, the imposed pressure $P(\xi,\eta)$ is equal to a constant everywhere in the duct. The streamwise pressure gradient is completely determined by the viscous correction $p'_\xi(\xi)$.

The pipe radius in Reference 62 was 10.16 cm (4.0 in). This was used as the reference length L_r in the analysis. The reference velocity U_r was 29.9 m/sec (98.1 ft/sec), the average velocity in the pipe. The reference temperature T_r that was used was the standard atmosphere value of 288 K (519° R). The Reynolds number in Reference 62, based on pipe diameter and average velocity, was 388,000. In order to match this, the reference density was set equal to 1.143 kg/m^3 (0.07138 lb$_m$/ft^3). The reference Reynolds number was thus 194,000.

The measured velocity profile at the first experimental station, 1.5 diameters downstream of the pipe entrance, was used as the initial

streamwise velocity profile for the analysis. Weighted average quadratic interpolation was used to obtain values between the tabulated experimental data points. In addition, the method outlined in Section 2.2.3 was used to obtain realistic velocity values between the wall and the first experimental point away from the wall. The initial cross-flow velocity v was set equal to zero. The initial dimensionless density and temperature were both set equal to one. This case was run using both the Cebeci-Smith and McDonald-Camarata turbulence models in the inner region.

No-slip and no-bleed boundary conditions were used for u and v at the wall. An adiabatic wall boundary condition was used for the temperature. Fifty-one grid points were used between the centerline and the wall, with the points packed near the wall using equation (3.1) with $D_S = 100$. A constant marching step size $\Delta\xi$ of 0.1 was used. The grid near the pipe entrance is plotted in Figure 4-21a. The grid was the same through the entire pipe. The boxed region near the wall in Figure 4-21a is shown magnified 20 times in Figure 4-21b. A circle is centered at corresponding locations in the two figures.

In the experiment of Reference 62, the last data station was 8.84 m (29.0 ft), or 87 radii, from the pipe entrance. The data indicate that the flow, although close, was not quite fully developed at this point. The calculations, therefore, were extended to 120 radii downstream of the entrance. Thus, 1170 marching steps were needed between $\xi = 3$ and $\xi = 120$. The value of $\Delta\xi$ could probably be greatly increased, especially downstream of the near-entrance region, to cut down the number of steps, and therefore computer time, required

for this case. The case as run took 4.1 minutes of CPU time on an IBM 370/3033.

4.3.2 Results

The computed streamwise velocity profiles are shown in Figure 4-22. Profiles are plotted every 20 marching steps, with the abscissa displaced by 1/4 of the interval width for each successive profile. These results were computed using the Cebeci-Smith turbulence model in the inner region. The differences between these results and those obtained using the McDonald-Camarata turbulence model were too small to be distinguished in this type of plot. The boundary layer growth along the wall can be clearly seen in Figure 4-22. The edge of the boundary layer reaches the pipe centerline about halfway through the pipe. From this point through to the end of the pipe the velocity profile changes shape very gradually. The dimensionless centerline velocity, for example, only increases from 1.210 at $\xi = 70$ to 1.215 at $\xi = 120$.

The computed cross-flow velocity profiles are presented in Figure 4-23. As in the laminar developing pipe flow case, the analysis quickly generates a realistic profile even though the initial v-velocity was set equal to zero. The point of maximum v-velocity moves away from the wall as the boundary layer thickness increases. Once the flow becomes completely viscous, the v-velocity quickly decreases and remains essentially zero. Although no experimental values for the cross-flow velocity are given in Reference 62, these profiles are qualitatively the same as those obtained experimentally and analytically by Richman and Azad (Ref. 47).

The u-velocities computed using both the Cebeci-Smith and McDonald-Camarata turbulence models are compared with the data of Reference 62 in Figures 4-24 and 4-25, respectively. Streamwise velocity is plotted as a function of axial distance at five radial locations. The agreement between theory and experiment is generally very good. The two turbulence models give essentially the same results, except very near the wall where the McDonald-Camarata model is in slightly better agreement with the data. These results are also compared with the data of Reference 62, in the form of velocity profiles at five axial locations, in Figures 4-26 and 4-27.

It should be noted that in the present analysis the centerline velocity continually increases and approaches its fully-developed value asymptotically from below. Several authors (Refs. 64-67) have reported that the centerline velocity in developing turbulent pipe and channel flow typically overshoots its fully-developed value slightly, and then approaches it from above. This overshoot phenomenon is not apparent in the data of Reference 62, perhaps because measurements were not made far enough downstream. The exact cause of this behavior is not clear, but it apparently cannot be predicted with an algebraic turbulence model, at least without some strictly empirical problem-dependent modifications (Refs. 65, 68).

The computed and experimental pressure coefficients are plotted as a function of axial distance in Figure 4-28. Recall that since the imposed pressure in this case is a constant, this pressure coefficient is determined by the viscous correction p'. The agreement between theory and experiment is fairly good, with the experimental results falling about halfway between the computed results from the two turbulence

models. This again indicates that the method used to compute the viscous pressure correction is valid, and that the slight disagreement in Figure 4-28 is an effect of the turbulence model.

In Figure 4-29, the computed skin friction coefficient is plotted as a function of axial distance for both turbulence models. The shear stress at the wall was found by second-order one-sided numerical differentiation of the computed streamwise velocity. Also shown in the figure is the expected fully-developed value computed from Prandtl's formula for wall friction (Ref. 28). This formula is

$$\frac{1}{\sqrt{\Lambda}} = 2 \log \left(Re_D \sqrt{\Lambda} \right) - 0.8 \qquad (4.1)$$

where

$$\Lambda = \frac{8\tau_{W_{F-D}}}{\rho u_{AVE}^2} = 4c_f$$

$$Re_D = \frac{u_{AVE} D}{\nu}$$

A curve fit to equation (4.1), accurate to ±3 percent, is given by White (Ref. 28) as

$$\Lambda = 1.02 \, (\log Re_D)^{-2.5} \qquad (4.2)$$

Equation (4.2) is the one actually used to get the fully-developed skin friction value presented in Figure 4-29.

With both turbulence models, the skin friction decreases rapidly near the pipe entrance, where the boundary layer thickness is increasing rapidly. Unlike the results in laminar developing flow, however, it dips below the final fully-developed value and then gradually increases. Although no direct skin friction measurements were

made in the experiment of Reference 62, and the data are not detailed enough to compute reliable values, these results are qualitatively similar to those obtained in other experiments (Refs. 66-67). Of the two turbulence models, the results obtained using the Cebeci-Smith model are in better agreement with equation (4.2).

Finally, the predicted Reynolds stress profiles are compared with data at four axial stations in Figure 4-30. The Reynolds stress, in the form $\overline{u'v'}/(u_{\tau_{F-D}})^2$, is plotted as a function of normalized distance from the wall. Here $u_{\tau_{F-D}}$ is the friction velocity for fully-developed flow, given by

$$u_{\tau_{F-D}} = \sqrt{\frac{\tau_{W_{F-D}}}{\rho}}$$

For the predicted values of Reynolds stress, equation (4.2) was used to compute $\tau_{W_{F-D}}$. The experimental values were taken directly from Reference 62, where the value of $\tau_{W_{F-D}}$ is not given. The experimental and theoretical values presented in Figure 4-30 may therefore be normalized by slightly different values. It's interesting to note that the Reynolds stress curves for the two turbulence models would essentially coincide if each were normalized using its own predicted value of $u_{\tau_{F-D}}$.

The agreement between theory and experiment is qualitative, at best, at $z/R = 9$ and 33, but is fairly good at $z/R = 57$ and 81. In the experiment, transition from laminar to turbulent flow was artificially promoted using a strip of sand grain roughness near the pipe entrance. This could be the cause of the disagreement at the first two stations in Figure 4-30. Of course, the disagreement could also be due simply to inadequacies in the turbulence models.

ORIGINAL PAGE IS
OF POOR QUALITY

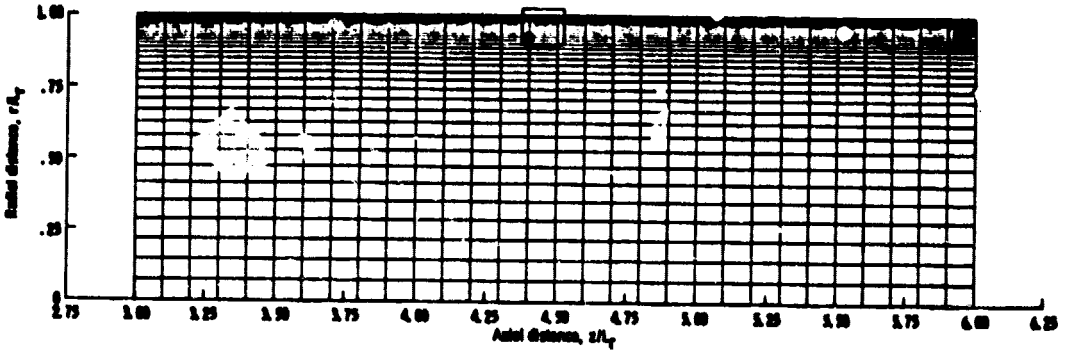

(a) Complete cross-section.

Figure 4-21. - Computational grid used in calculation of turbulent developing pipe flow.

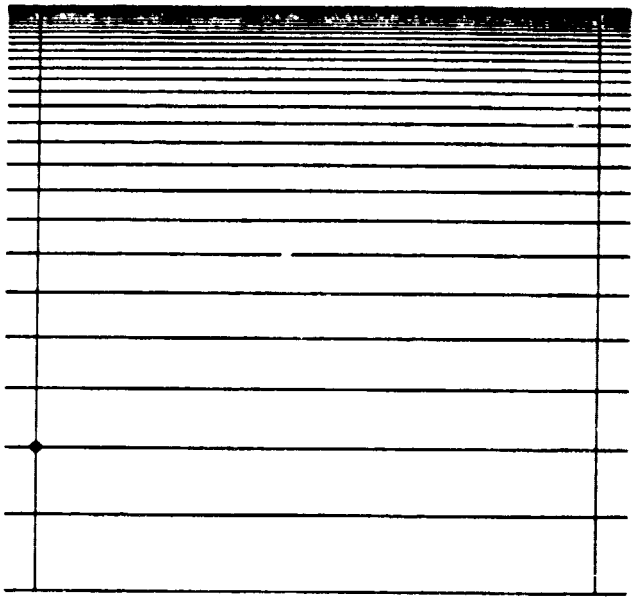

(b) Region near wall magnified 20 times.

Figure 4-21. - Concluded.

ORIGINAL PAGE IS
OF POOR QUALITY

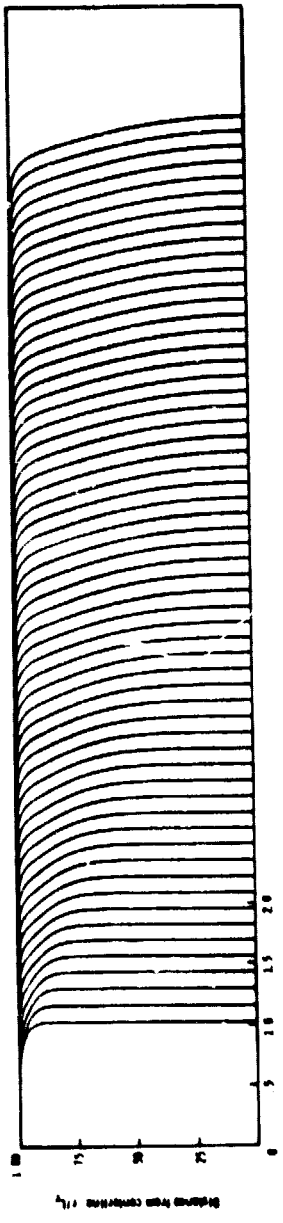

Figure 4-22. - Computed streamwise velocity profiles for turbulent developing pipe flow.

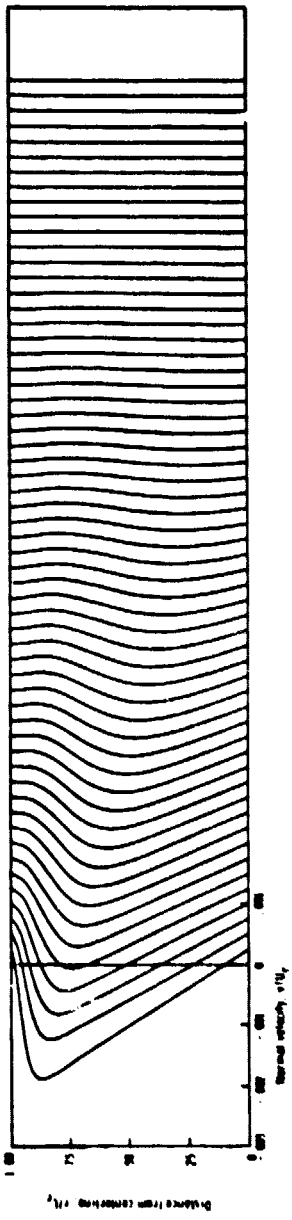

Figure 4-23. - Computed cross-flow velocity profiles for turbulent developing pipe flow.

ORIGINAL PAGE IS
OF POOR QUALITY

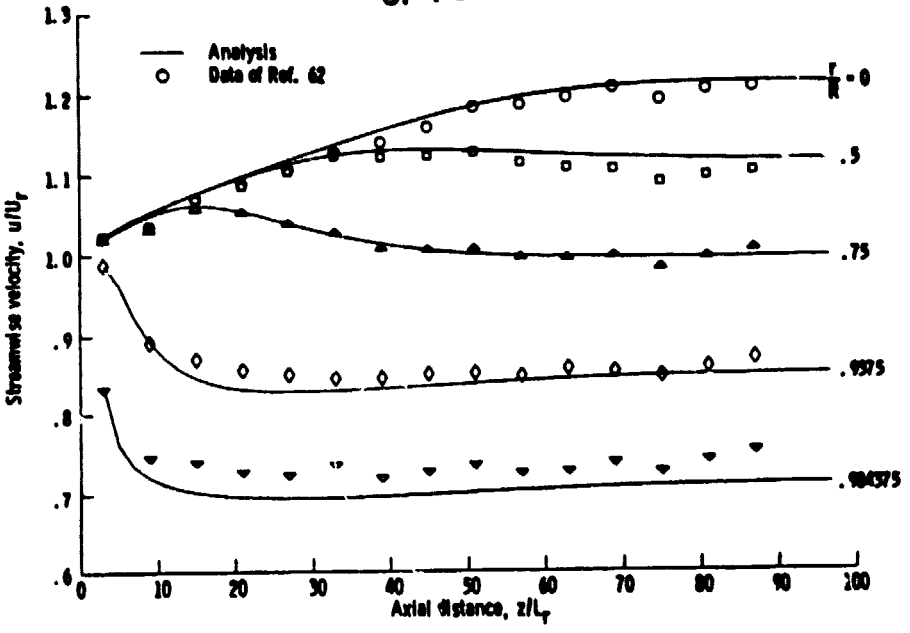

Figure 4-24. - Computed and experimental streamwise velocities in turbulent developing pipe flow, Cebeci-Smith turbulence model.

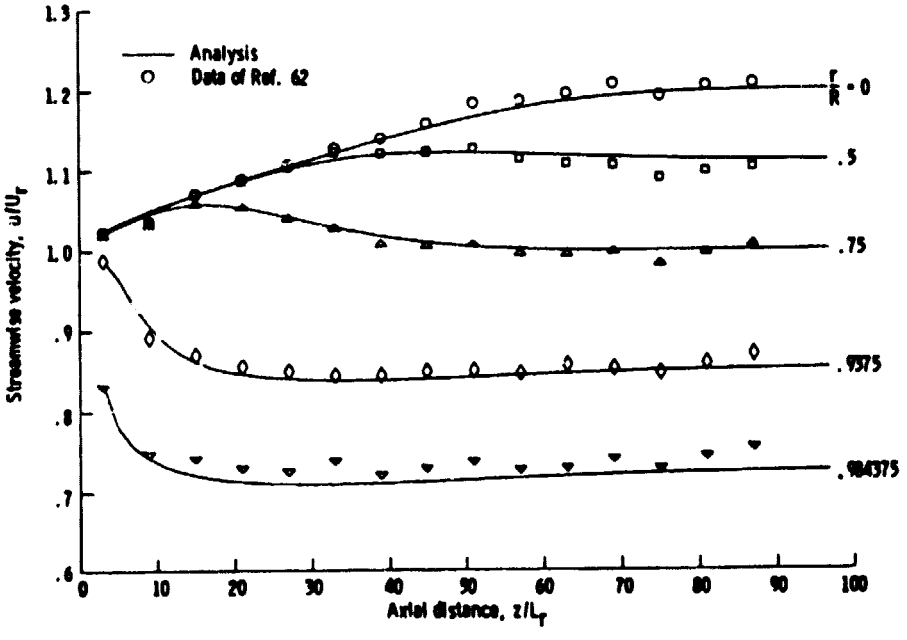

Figure 4-25. - Computed and experimental streamwise velocities in turbulent developing pipe flow, McDonald-Camarata turbulence model.

ORIGINAL PAGE IS
OF POOR QUALITY

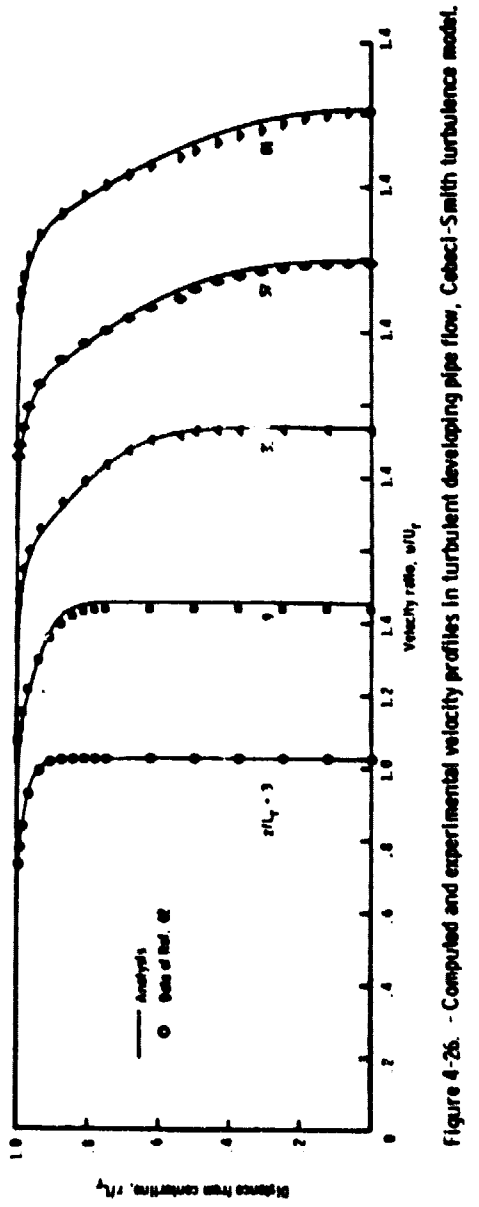

Figure 4-26. - Computed and experimental velocity profiles in turbulent developing pipe flow, Cebeci-Smith turbulence model.

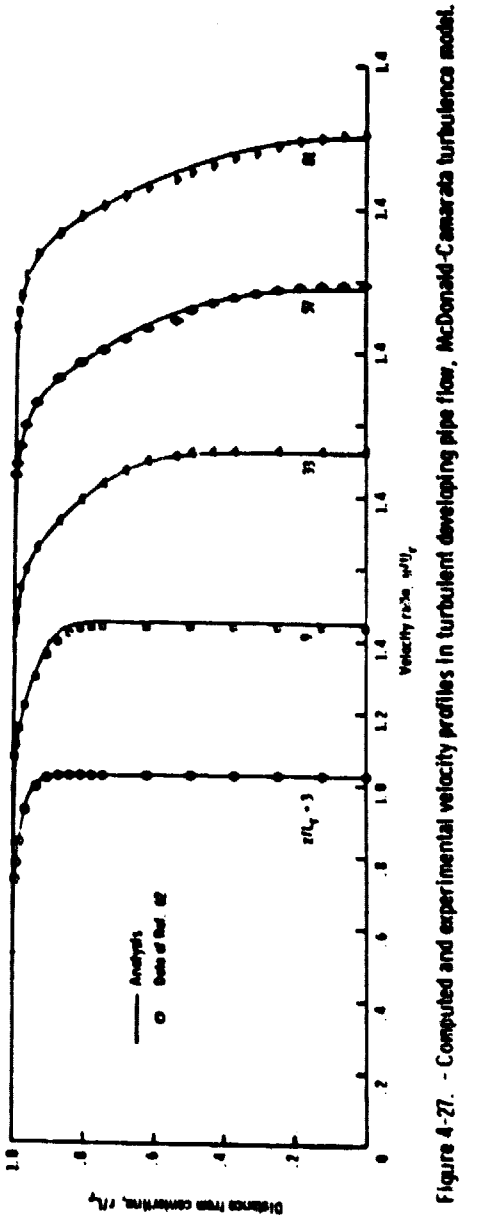

Figure 4-27. - Computed and experimental velocity profiles in turbulent developing pipe flow, McDonald-Camarata turbulence model.

ORIGINAL PAGE IS
OF POOR QUALITY

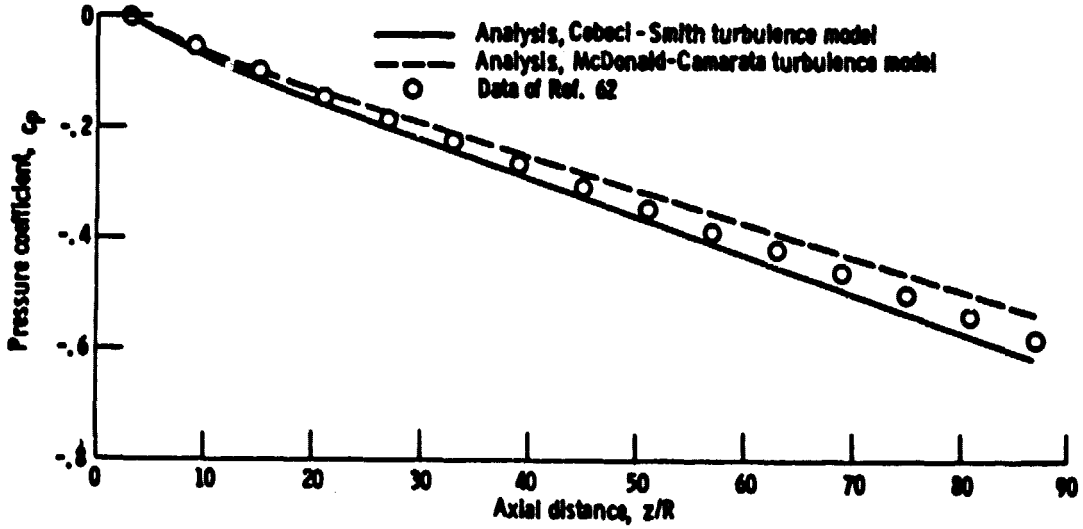

Figure 4-28. - Computed and experimental pressure coefficients in turbulent developing pipe flow.

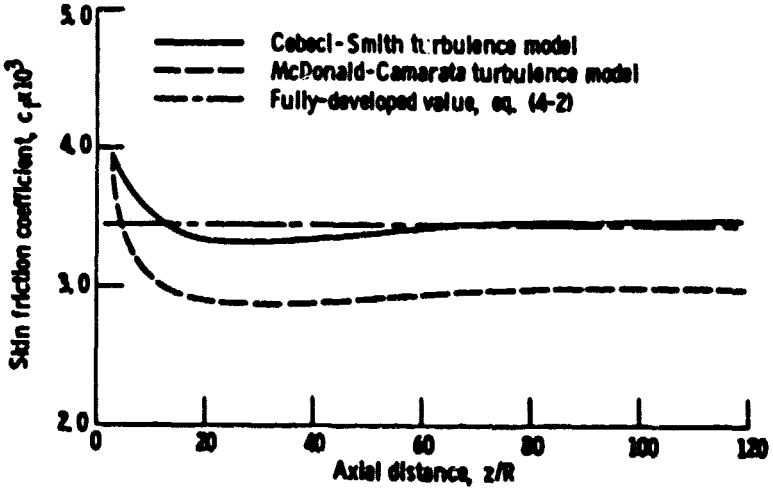

Figure 4-29. - Computed skin friction coefficient in turbulent developing pipe flow and expected fully-developed value.

ORIGINAL PAGE IS
OF POOR QUALITY

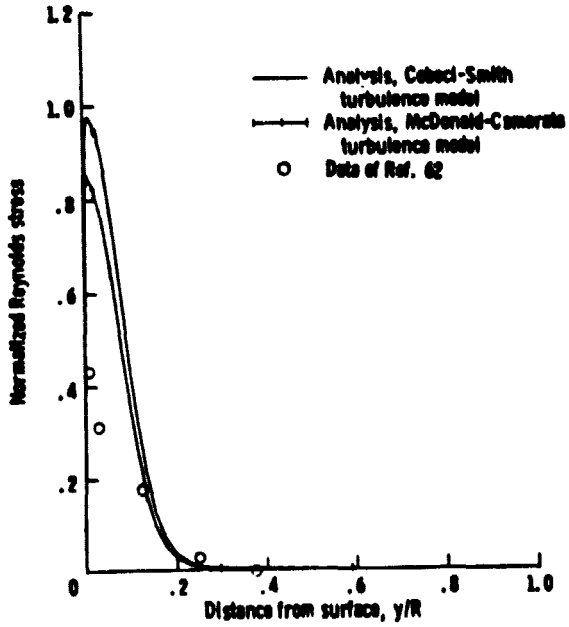

(a) z/R = 9.

Figure 4-30. - Predicted and experimental Reynolds stress profiles in turbulent developing pipe flow.

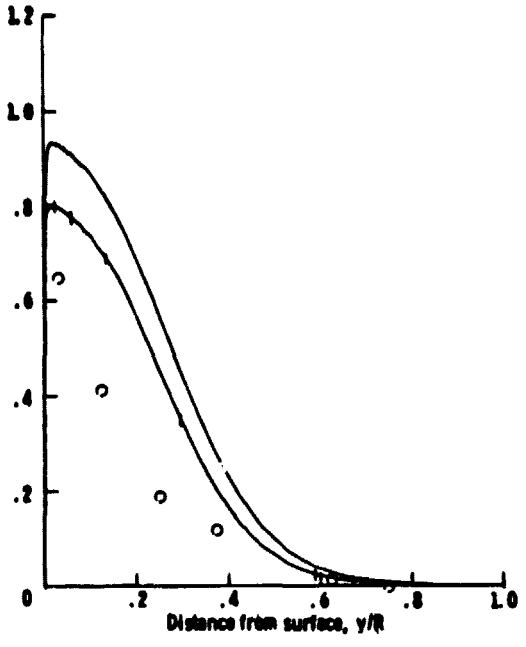

(b) z/R = 33.

Figure 4-30. - Continued.

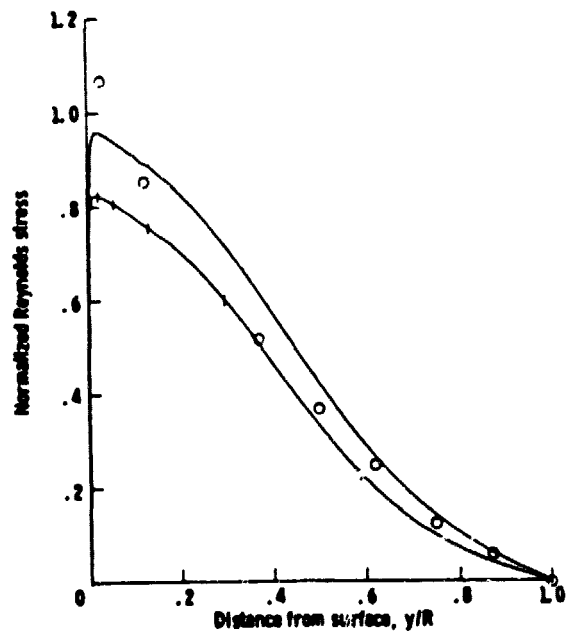

(c) z/R = 57.

Figure 4-30. - Continued.

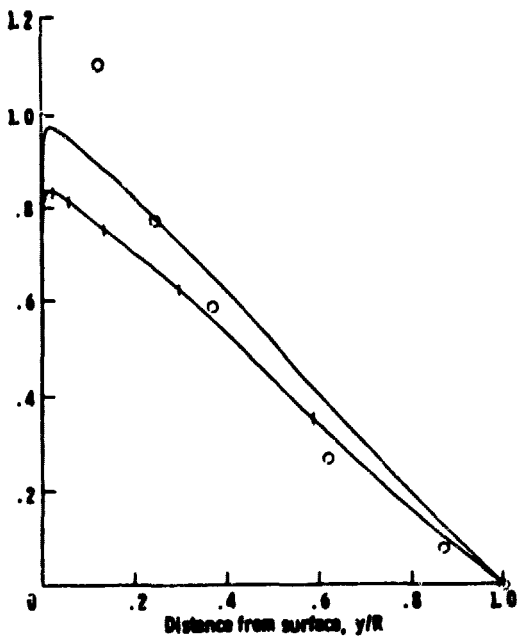

(d) z/R = 81.

Figure 4-30. - Concluded.

4.4 S-SHAPED DUCT FLOW

The next test case studied was turbulent flow in a two-dimensional S-shaped duct. This is a fairly complex flow, with the boundary layer on each wall seeing both favorable and adverse pressure gradients. In addition, the curvature terms in the equations become important since the metric scale coefficients vary in both coordinate directions. The particular geometry used for this case was the 30°-45° S-duct studied experimentally by Butz (Ref. 69).

4.4.1 Geometry and Computational Coordinates

The geometric configuration is presented in Figure 4-31. Two circular arc bends, both with a centerline radius of 0.508 m (20.0 in), were used to make up the S-duct. The first bend covered an arc of 30°, and the second an arc of 45°. The duct width was 0.1016 m (4.0 in).

The computational coordinate system for this configuration was computed using the method of References 2 and 3, as described in Section 2.1. In order to satisfy the uniform inflow and outflow boundary conditions that are used with this method, straight sections four inches, or one duct width, long were added upstream and downstream of the S-duct. The resulting coordinate system is shown in Figure 4-32. Distances have been nondimensionalized by the outer wall radius. (As a check, a coordinate system was later constructed using straight sections that were two duct widths long. The metric parameters for the two cases were essentially identical). The coordinates were generated with 51 cross-stream points and 100 streamwise points, evenly spaced

(in the computational coordinates ξ and η) in both directions. During the viscous marching solution, the metric parameters at each point in the viscous grid were found by interpolation over this evenly spaced grid.

The metric coefficients generated by the method of References 2 and 3 are, unfortunately, not smooth. In Figure 4-33 the metric scale coefficient h (recall $h_1 = h_2$ with this method) is plotted along both walls as a function of axial distance. It was found that the computed streamwise velocities were not affected by the oscillations shown in Figure 4-33a. These oscillations were, however, reflected in the computed cross-flow velocities, although the calculation did not go unstable. To eliminate the sharp oscillations in the metric coefficients, they were smoothed by splitting the $h = h(\xi)$ curve at each constant η-line into several sections, separated by "knots," and using a cubic spline smoothing within each section. The knot locations were chosen to yield the best overall fit, in the least squares sense, to the original $h = h(\xi)$ curve at $\eta = 0$. The same knot locations were then used for all the η-lines. (New knot locations could not be used for each η-line because this led to sharp changes in h in the η-direction at a given ξ). The smoothed metric coefficients, using 10 knots, are plotted in Figure 4-33b. The smoothing removed the sharp oscillations, although a couple of stretched out "bumps" remain. These caused no difficulties in the viscous calculation, however.

4.4.2 Imposed Pressure Field

Since the computational mesh consists of the streamlines and potential lines from a planar potential flow solution, the imposed pressure was computed directly from the metric scale coefficients, as described in Section 2.3.2. The imposed, or inviscid, pressure coefficient on each wall is compared with the experimental data in Figure 4-34. Here c_p is defined as

$$c_p = \frac{p - p_{ref}}{\frac{1}{2} \rho_r U_r^2}$$

where ρ_r is the density, U_r is the average velocity at the duct entrance, and p_{ref} is the static pressure at the first measurement location on the upper wall.

The gradients given by the inviscid pressure distribution match the experimental pressure gradients very well. In particular, the elliptic effects of the geometry on the pressure field are correctly reproduced. The pressure along the top wall starts to decrease ahead of the inflection station, at 30 degrees, and increases ahead of the exit, at 75 degrees. The pressure along the bottom wall, of course, does just the opposite. This imposed pressure field, therefore, correctly introduces the elliptic effects of the geometry into the viscous marching solution.

One additional point should be mentioned here. In the experiment of Reference 69, the S-duct was constructed from two separate circular arc sections. Flow surveys were made by inserting a 3.81 cm (1.5 in) long survey section, containing a translating probe, at either end of a circular arc section. Since straight sections were added upstream

and downstream of the S-duct when generating the computational mesh (and therefore the pressure field), the effect of this survey section on the flow is properly accounted for when comparing with the data at the entrance and exit of the S-duct. Putting the survey section at the inflection station, however, changes the geometry slightly. This change turns out to be important, as will be shown later, because the inflection station is where the streamwise pressure gradients are the largest. A second computational mesh and imposed pressure field were therefore generated, with the survey section between the two circular arc sections, for use when comparing with the data at the inflection station.

4.4.3 Initial Conditions

The reference conditions used in the analysis were chosen to match the flow conditions in the experiment of Reference 69. The average inlet velocity of 19.2 m/sec (63 ft/sec) was used as the reference velocity U_r. The reference length L_r was 0.5588 m (1.83333 ft), the outer wall radius at the inlet. To match the experimental conditions, a reference Reynolds number Re_r of 7.216×10^5 was then required. The reference temperature was assumed to be 288 K (519° R), and the reference density was computed to be 1.2042 kg/m^3 (0.075173 lb$_m$/ft^3).

The measured streamwise velocity profile at the entrance station was used to start the marching procedure. This profile is shown in Figure 4-35. Interpolation was used to get values between the data points. The initial cross-flow velocity was set equal to zero, and

the initial dimensionless density and temperature were both set equal to one. The marching calculation was started 3.33 cm (1.3125 in) upstream of the start of the first bend. This is the actual measurement location for the entrance station, accounting for the presence of the survey section and the 1.429 cm (0.5625 in) upstream extension of the probe itself (Ref. 70).

No-slip and no-bleed boundary conditions were used for the velocities at the walls. An adiabatic wall boundary condition was used for the temperature. Fifty-one grid points were used between the two walls. Because the boundary layers were thin, the points were tightly packed near both walls, with $D_S = 200$ in equation (3.1). The streamwise step size $\Delta\xi$ was 0.05. The actual mesh used in the viscous calculation, for the case without the survey section in the middle, is shown in Figure 4-36. For clarity, only every other streamwise station is shown. The inset in the figure shows the grid near the wall magnified by a factor of 25. A circle is centered at corresponding locations in the full grid and the inset. For this case 163 marching steps were needed to reach the end of the duct, requiring 48.5 seconds of CPU time on an IBM 370/3033. For the case with the survey section, 170 marching steps were needed and 50.6 seconds of CPU time were required.

4.4.4 Results

This case was run using both the Cebeci-Smith and McDonald-Camarata turbulence models. The results were virtually identical, so only the results obtained for the Cebeci-Smith turbulence model will be shown in this section.

The computed streamwise velocity profiles are shown in Figure 4-37a. The boundary layer growth through the duct can be clearly seen, although it's still relatively thin at the exit station. The slope of the velocity profile in the essentially inviscid core region is consistent with a potential vortex flow, with the velocity inversely proportional to the distance from the center of curvature of the duct section. This can be seen more clearly in Figures 4-37b and 4-37c, where the predicted profiles midway through the first and second bends are plotted to a larger scale. The velocity near the bottom wall (i.e., the inner wall in the first bend and the outer wall in the second bend) increases as the flow enters the first bend, decreases around the inflection station, and increases again leaving the second bend. Near the top wall, of course, the opposite occurs.

The computed streamwise velocity profiles at the inflection and exit stations are compared with the experimental profiles in Figure 4-38. The computed values at the inflection station are for a configuration with the survey section between the two circular sections, as described in Section 4.4.2. The actual locations of the inflection and exit stations, taking into account the survey section and the upstream extension of the probe, are 0.476 cm (0.1875 in) downstream of the ends of the first and second bends. In general the agreement between theory and experiment is very good.

It is interesting to note how important it is to include the effects of the survey section and probe, especially when comparing with the data at the inflection station. The velocity profile changes shape rapidly in this region because of the steep favorable and adverse pressure gradients on the top and bottom walls, respectively.

In Figure 4-39, the theoretical results exactly at the inflection plane, ignoring the effects of the survey section, are compared with the data. The agreement is not nearly as good as that shown in Figure 4-38a.

In Figure 4-40 the pressure coefficient for the viscous flow along each wall is compared with the experimental data. The pressure coefficient is determined by the imposed, or inviscid, pressure plus the viscous pressure correction. By comparing with Figure 4-34, it can be seen that the viscous correction in the first bend yields slightly worse agreement with the data along the top wall and about the same level of agreement along the bottom wall. In the second bend the agreement is improved along the top wall and is slightly worse along the bottom wall. It should be noted, however, that because of the scatter in the data, it is difficult to determine exactly how well the theory matches the experiment. In defining the pressure coefficient, the pressure at the first measurement location on the top wall was used as the reference pressure. If this particular measured pressure were too high or low, all of the experimental values would be too low or high relative to the predicted values.

ORIGINAL PAGE IS
OF POOR QUALITY

ORIGINAL PAGE IS
OF POOR QUALITY

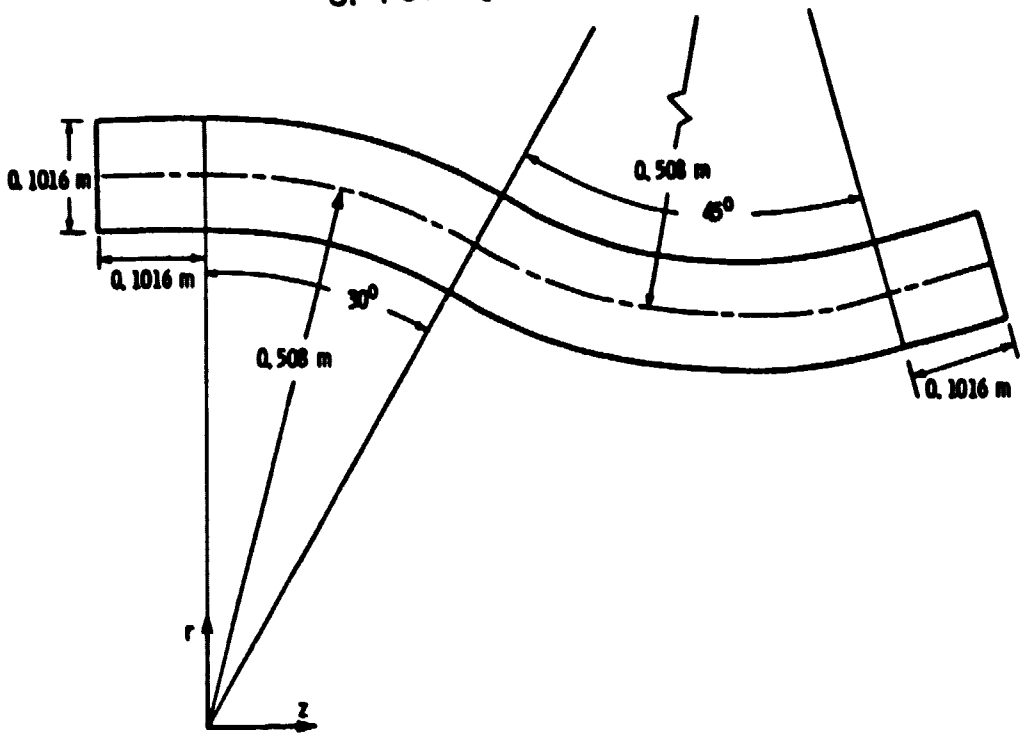

Figure 4-31. - Geometric configuration for S-shaped duct flow.

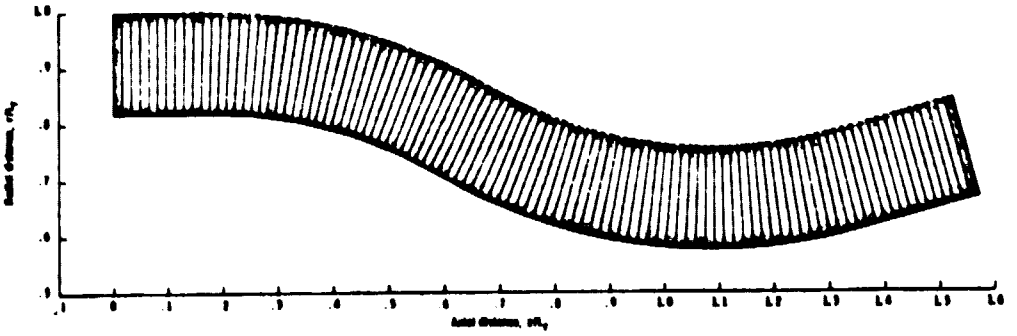

Figure 4-32. - Computational coordinate system for S-shaped duct flow.

ORIGINAL PAGE IS
OF POOR QUALITY

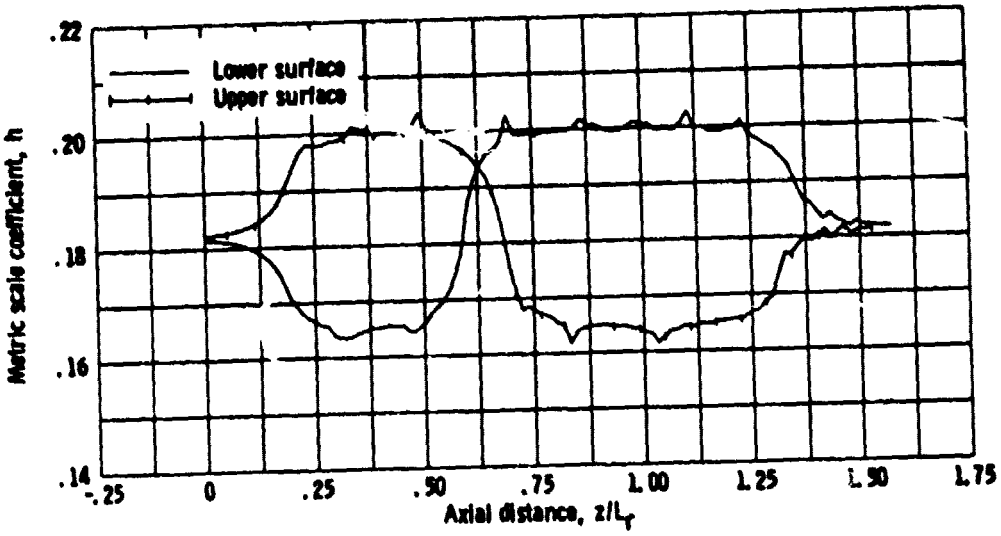

(a) Unsmoothed.

Figure 4-33. - Metric scale coefficients for S-shaped duct flow.

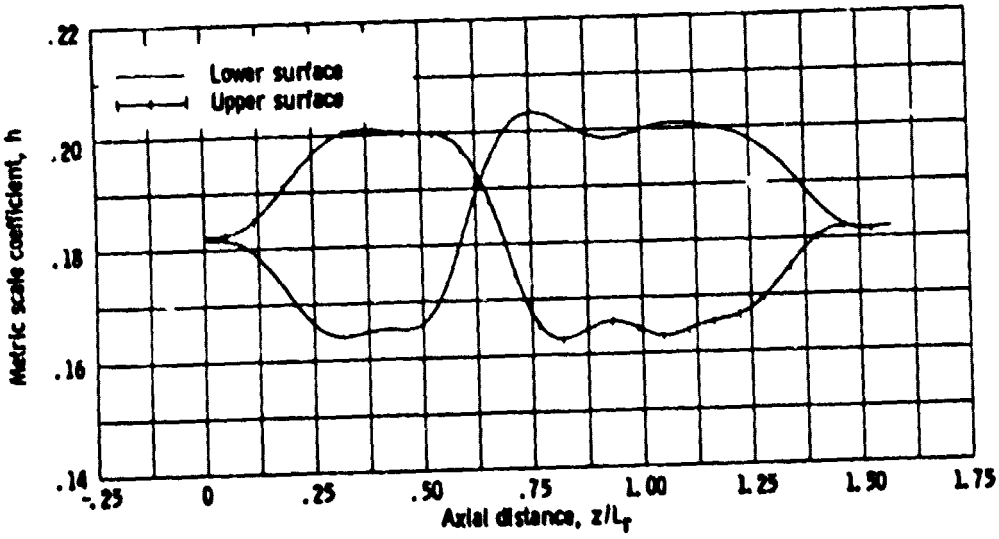

(b) Smoothed.

Figure 4-33. - Concluded.

ORIGINAL PAGE IS
OF POOR QUALITY

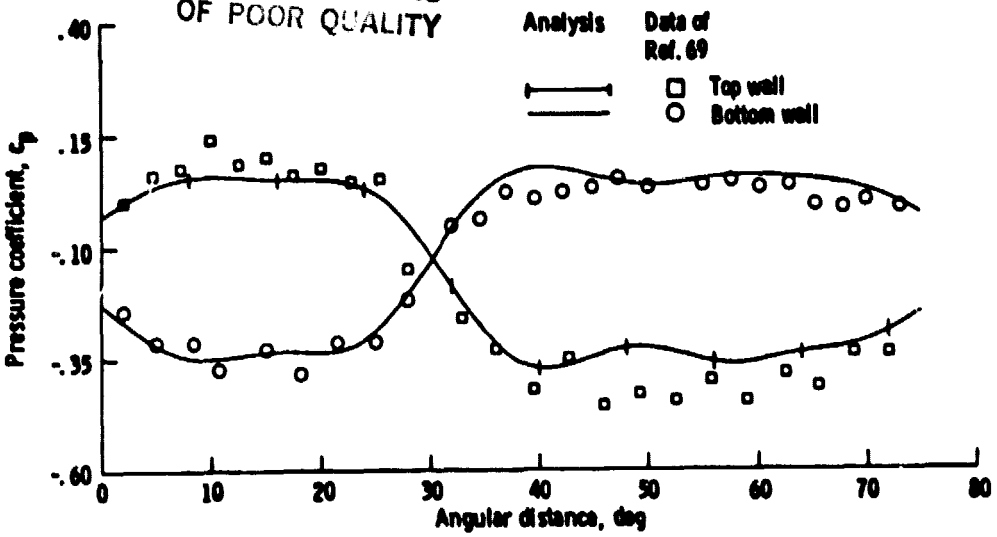

Figure 4-34. Imposed pressure coefficients compared with data for S-shaped duct flow.

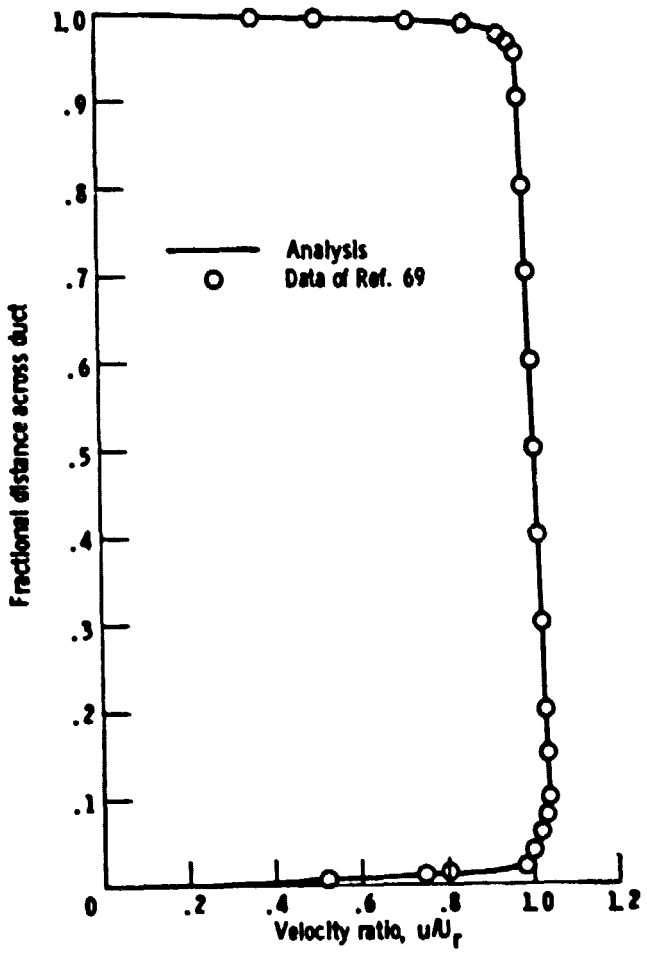

Figure 4-35. - Initial streamwise velocity profile for S-shaped duct flow.

ORIGINAL PAGE IS
OF POOR QUALITY

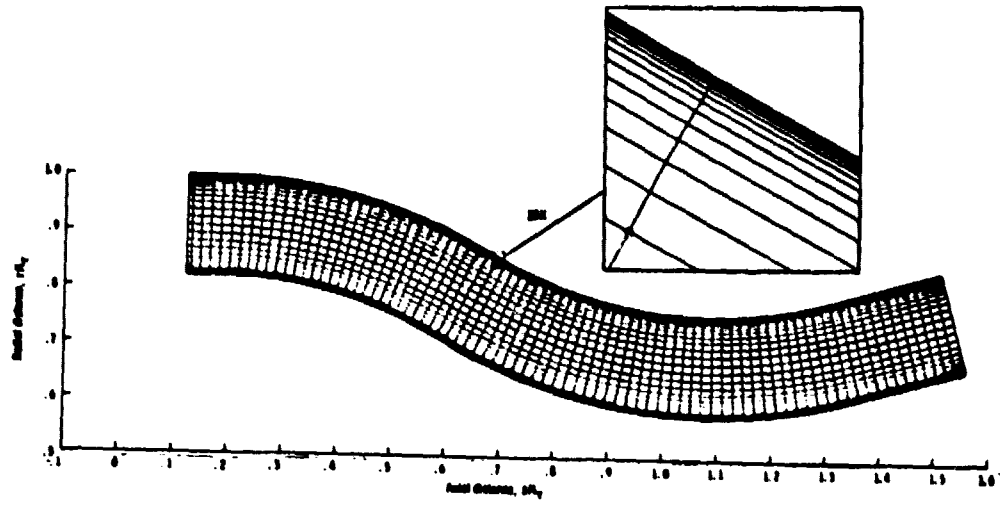

Figure 4-36. - Computational grid used for viscous calculation, S-shaped duct flow.

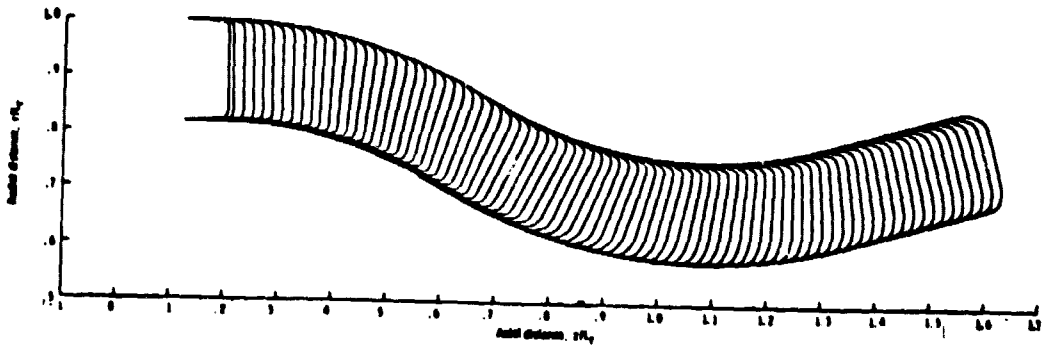

(a) Complete flowfield.

Figure 4-37. - Computed streamwise velocity profiles for S-shaped duct flow.

ORIGINAL PAGE IS
OF POOR QUALITY

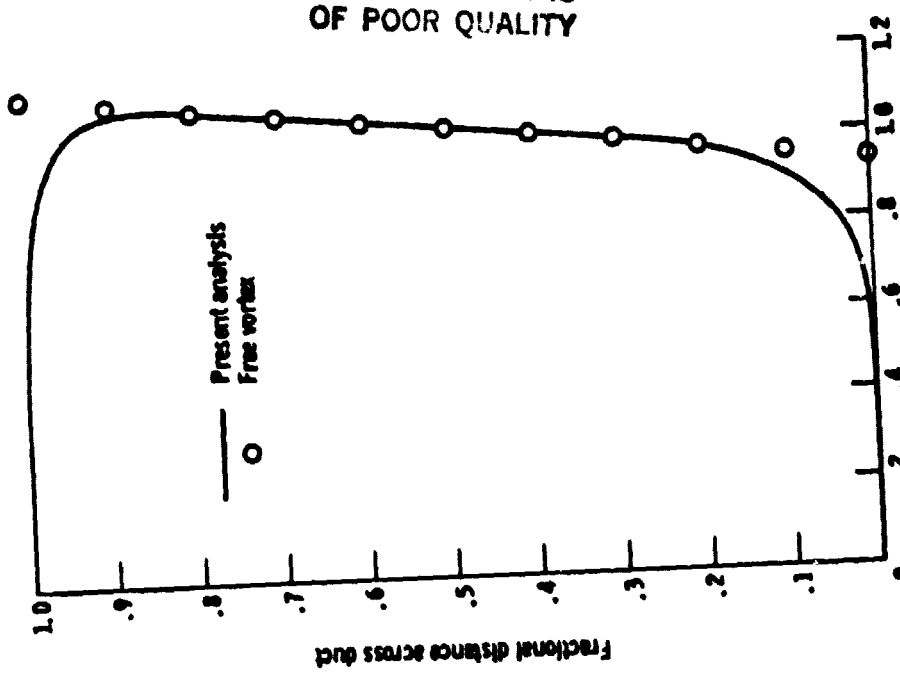

(c) Midway through second bend.

Figure 4-37. - Concluded.

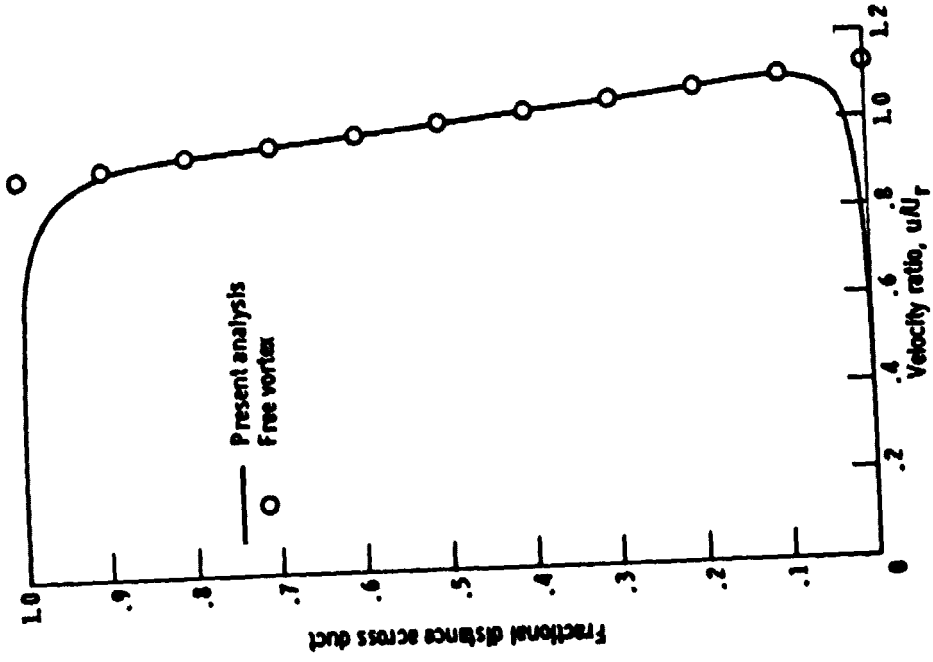

(b) Midway through first bend.

Figure 4-37. - Continued.

ORIGINAL PAGE IS
OF POOR QUALITY

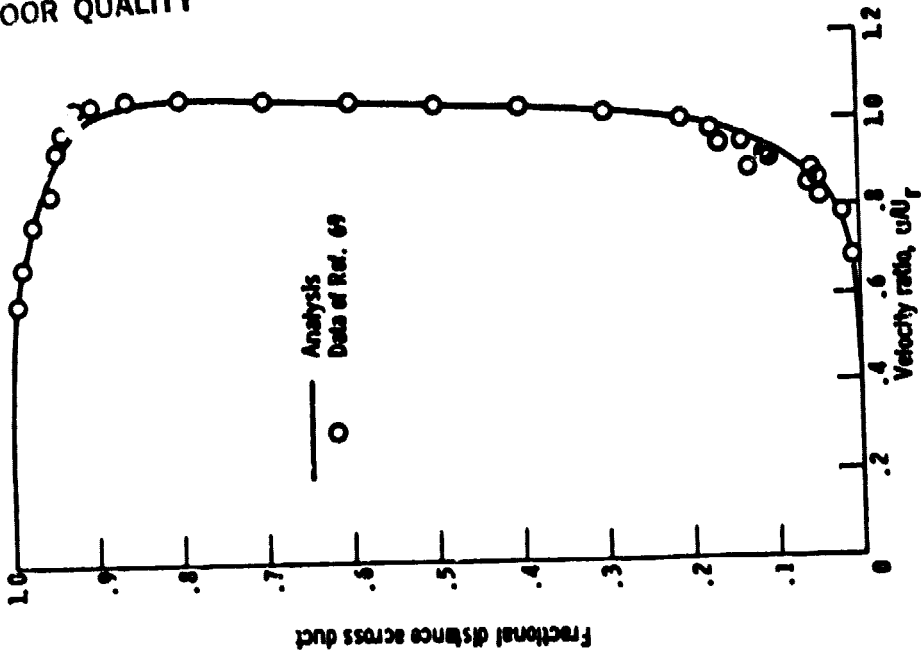

(b) Exit station.

Figure 4-38. - Concluded.

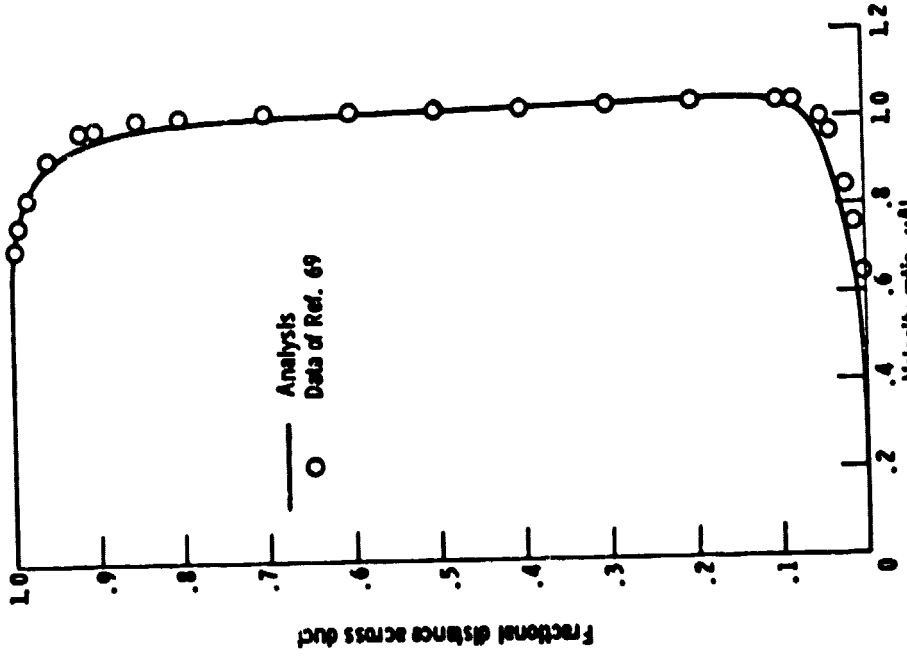

(a) Inflection station.

Figure 4-38. - Computed and experimental velocity profiles for S-shaped duct flow.

ORIGINAL PAGE IS
OF POOR QUALITY

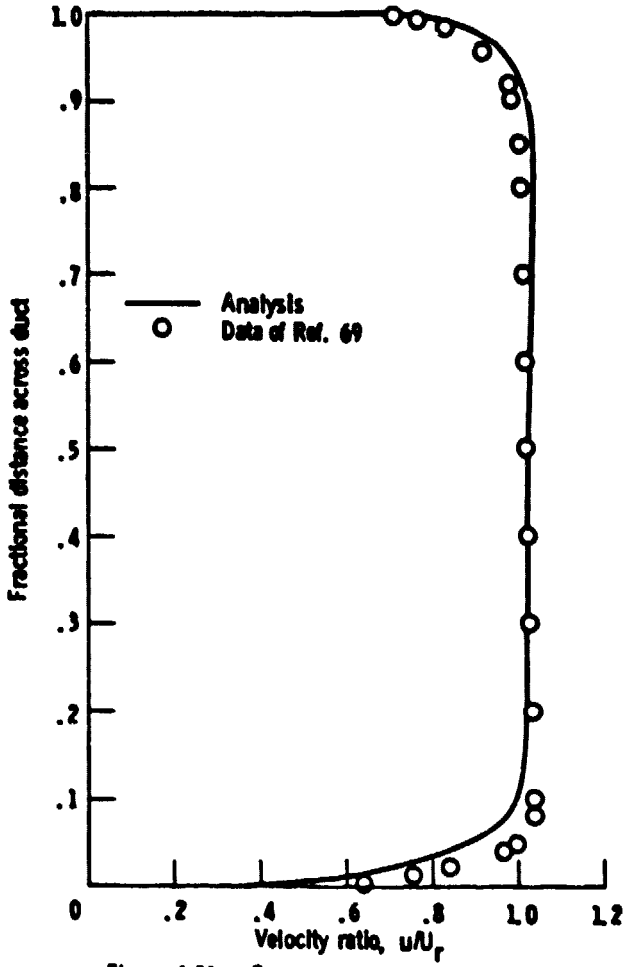

Figure 4-39. - Computed and experimental velocity profiles at inflection station for S-shaped duct flow, ignoring effect of survey section on flow.

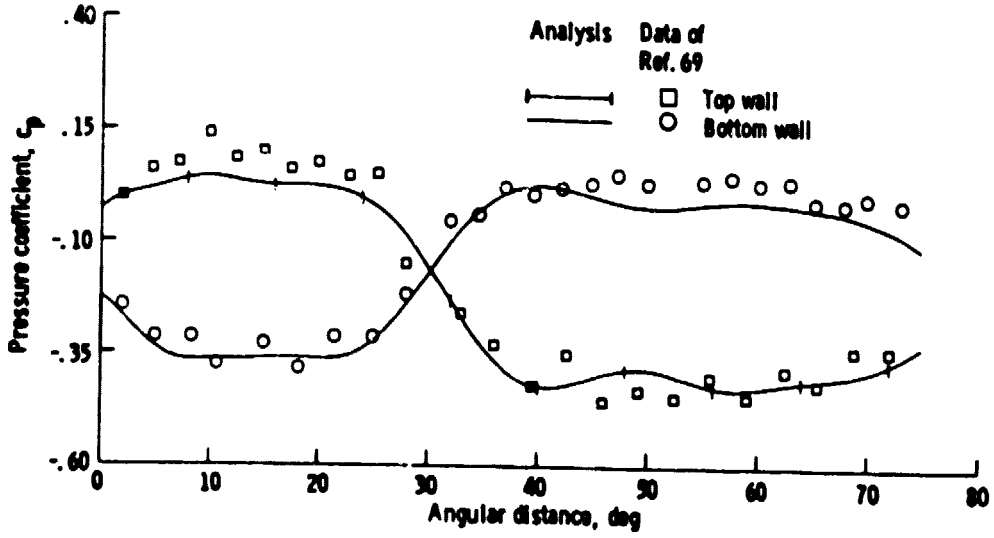

Figure 4-40. - Viscous pressure coefficients compared with data for S-shaped duct flow.

4.5 SUBSONIC DIFFUSER FLOW

As a final test case, compressible turbulent flow in an axisymmetric subsonic diffuser typical of those used in supersonic propulsion systems was studied. The diffuser chosen is called a dM/dz diffuser because the area distribution is such that the one-dimensional Mach number distribution through the diffuser is linear. This type of diffuser has been tested as a component of a supersonic inlet system (Ref. 71), as part of an investigation of various diffuser types (Ref. 6), and as part of a vortex generator study (Ref. 72). Because of their greater detail, the data of Shaw (Ref. 72) were chosen for comparison with the present analysis. Two cases were run, both with the Cebeci-Smith turbulence model, with average inlet Mach numbers of 0.29 and 0.75.

4.5.1 Geometry and Computational Coordinates

The geometric configuration is presented in Figure 4-41. The cowl radius was constant at 15.24 cm (6.0 in), while the centerbody radius varied from 11.43 cm (4.5 in) at the diffuser inlet station, where z = 0.0, to 5.387 cm (2.121 in) at the exit station, where z = 22.9 cm (9.0 in). Upstream of the diffuser itself was a slightly diverging throat section, with a centerbody wall angle of 3 degrees. The diffuser area ratio was 2.0. In this type of diffuser the area change, and thus the rate of diffusion, is fairly small near the entrance, but increases rapidly in the downstream half of the diffuser. Also shown in Figure 4-41 are the locations of the five total pressure rakes,

designated A to E, that were used in the experiment of Reference 72. These rakes were vertical, and were located at z = 0.0, 6.98, 11.4, 17.8, and 22.9 cm (0.0, 2.75, 4.5, 7.0, and 9.0 in).

The computational coordinate system was again computed using the method described in Section 2.1. A cubic fairing was added along the centerbody in the region of the diffuser exit to eliminate the sharp change in wall curvature at that point, which would have caused numerical problems in generating the coordinate system. Straight sections were again added upstream and downstream of the duct to satisfy the uniform inflow and outflow boundary conditions assumed by the coordinate generation method. A longer straight section was used at the downstream end than at the upstream end because of the larger annular width and the larger centerbody curvature at that point. The resulting coordinate system is shown in Figure 4-42. Distances have been nondimensionalized by the cowl radius. Near the diffuser exit plane, the actual centerbody contour is drawn as a dashed line, showing the extent of the cubic fairing used in this region. The coordinates were generated using 51 cross-stream points and 100 streamwise points, evenly spaced (in the computational coordinates ξ and η) in both directions. During the viscous marching solution, the metric parameters at each point in the viscous grid were found by interpolation over this evenly spaced grid.

The metric scale coefficients along each wall are shown in Figure 4-43. Along the straight outer cowl the distribution is smooth. Along the curved centerbody, however, there are oscillations. It was again found, as in the S-duct case of Section 4.4, that the computed streamwise velocities were not affected by these oscillations. Therefore,

for the results presented in this section, no smoothing of the metric coefficients was performed.

4.5.2 Imposed Pressure Field

The imposed, or inviscid, pressure field was computed using the method described in Section 2.3.2. Since this is an axisymmetric case, this involved solving the axisymmetric potential equation, equation (2.38), to get an incompressible inviscid velocity. The Lieblein-Stockman correction was used to include the effects of compressibility on the imposed pressure field. The resulting pressure coefficients along each wall are compared with the experimental data, for both the $M_1 = 0.29$ and $M_1 = 0.75$ cases, in Figures 4-44 and 4-45, respectively. Here c_p is defined as $(p-p_{ref})/Q_1$, where Q_1 is the nominal inlet dynamic pressure and p_{ref} for each wall is the measured static pressure closest to the diffuser inlet station. For the cowl this was exactly at the inlet station and for the centerbody it was 2.54 cm (1.0 in) upstream.

In general the agreement between the inviscid pressure coefficients and the data is fairly good. The bumpiness in the pressure distribution along the centerbody is a result of the bumpiness in the metric scale coefficient. The viscous pressure correction computed during the marching solution will tend to shift the theoretical values down as axial distance increases. Note the flattening of the experimental pressures along the centerbody at the downstream end for both Mach numbers. This indicates the presence of boundary layer separation

on the centerbody near $z/L_r = 1.1$. No separation is indicated along the cowl.

4.5.3 Initial Conditions

The reference conditions used in the analysis were chosen to match the flow conditions in the experiment of Reference 72. The cowl radius was used for the reference length L_r. The average inlet values of velocity, temperature, and density were used for the reference values. These reference conditions are summarized in Table 4-1 for the two cases.

The marching calculation was started at the diffuser inlet, the location of rake A in the experiment. The initial boundary layer profile could not be determined in detail from the data, however. Therefore the initial streamwise velocity profile was constructed by specifying the free-stream velocity plus boundary layer thickness parameters on both the cowl and centerbody. The velocity in the boundary layers was then found using the procedure for turbulent flow described in Section 2.2.3. The boundary layer parameters were adjusted by judicious trial-and-error to give a good fit to the experimental profile. The values used are presented in Table 4-2.

The initial cross-flow velocity was set equal to zero. The initial dimensionless density and temperature were both set equal to one in the free-stream. The values of density and temperature in the boundary layer were found using the procedure of Section 2.2.3.

No-slip and no-bleed boundary conditions were used for the velocities at the walls. An adiabatic wall boundary condition was used for

the temperature. Fifty-one grid points were used in the cross-stream direction, packed at both walls with $D_S = 50$ in equation (3.1). The streamwise step size $\Delta\xi$ was 0.05. The actual mesh used in the viscous calculation is shown in Figure 4-46. The inset in the figure shows the grid near the wall magnified by a factor of 25. A circle is centered at corresponding locations in the full grid and the inset. For both Mach numbers the analysis predicted flow separation before the end of the diffuser was reached. For the $M_1 = 0.29$ case, 87 marching steps were taken, requiring 27.0 seconds of CPU time on an IBM 370/3033. For the $M_1 = 0.75$ case, 78 marching steps and 24.2 seconds of CPU time were used.

4.5.4 Results

The computed streamwise velocity profiles are shown in Figures 4-47a and b. For both inlet Mach numbers, the boundary layers on the cowl and centerbody grow rapidly in the downstream half of the diffuser until the flow finally separates along the centerbody. The predicted separation location, taken as the point where negative streamwise velocities first occur, was $z/L_r = 1.26$ for the $M_1 = 0.29$ case and $z/L_r = 1.10$ for the $M_1 = 0.75$ case. Both of these locations are in good agreement with those indicated by the experimental pressure distributions shown in Figures 4-44a and 4-45a. The marching procedure was able to continue past separation, but it quickly became unstable, giving physically unrealistic results. The results shown in Figure 4-47, therefore, include profiles only up to the separation point. It should be noted that by modifying the streamwise convective terms in

the governing equations a marching procedure can be made stable in separated flow regions (Ref. 73). However, the resulting equations are approximate and can be used only if the separation region is small (i.e., the flow quickly reattaches) and does not appreciably affect the rest of the flow field. This is clearly not the case for the flows considered here.

The computed streamwise velocity profiles for the $M_1 = 0.29$ case are compared with the experimental results in Figure 4-48. The velocity ratio is plotted as a function of fractional distance across the duct. Comparisons can only be made at the first four rakes since the flow separates before the last rake is reached in both the analysis and the experiment. The agreement between the predicted and experimental results is generally very good.

The analytical results for the $M_1 = 0.75$ case are compared with the data in Figure 4-49. Since the analysis predicted separation slightly upstream of the rake D location for this case, the predicted results can only be shown for the first three rakes. The agreement with the data at these rakes is again very good. The experimental velocity profile at rake D, which is also shown in Figure 4-49, does not indicate separated flow. However, the experimental static pressure distribution along the centerbody (see Figure 4-45a) indicates separation close to the rake D location. It's possible that the flow actually was separated at rake D, but that the first tube in the rake was too far from the wall to detect it.

The pressure coefficient for the viscous flow along each surface is compared with the experimental data in Figure 4-50 for the $M_1 = 0.29$ case and in Figure 4-51 for the $M_1 = 0.75$ case. By

comparing with Figure 4-44, it can be seen that the viscous blockage correction shifts the pressure downward only slightly for the $M_1 = 0.29$ case. There is a larger shift in the $M_1 = 0.75$ case (compare Figures 4-51 and 4-45) because of the thicker boundary layer along the centerbody. The analytical and experimental pressure gradients along the centerbody match closely, but the absolute pressure levels themselves are slightly off. This could be due to not having exactly the right reference pressure when computing the pressure coefficients. Along the cowl, the predicted and experimental pressures agree well near the beginning of the diffuser, but disagree further downstream. This is probably due to the upstream influence of the separated flow region in the experiment. The large separation region reduces the effective flow area, causing the flow along the cowl to accelerate. This effect cannot be predicted, of course, by a marching procedure.

Finally, the theoretical and experimental Reynolds stresses at rakes B, C, and D for the $M_1 = 0.29$ case are shown in Figure 4-52. (The Reynolds stresses were not measured for the $M_1 = 0.75$ case, or at rake A for the $M_1 = 0.29$ case). From the figure, it can be seen that the Cebeci-Smith turbulence model yields at least qualitatively correct Reynolds stresses at rakes B and C. The agreement is much poorer at rake D, which is very near the point of boundary layer separation.

Table 4-1. Reference Conditions for Diffuser Flow Test Cases

	$M_1 = 0.29$	$M_1 = 0.75$
L_r	0.152 m (0.5 ft)	0.152 m (0.5 ft)
U_r	99.40 m/sec (326.1 ft/sec)	247.0 m/sec (810.3 ft/sec)
ρ_r	2.0055 kg/m^3 (0.12520 lb$_m$/ft^3)	1.6087 kg/m^3 (0.10043 lb$_m$/ft^3)
T_r	292.4 K (526.3° R)	269.9 K (485.8° R)
Re_r	1.68×10^6	3.56×10^6

Table 4-2. Initial Profile Parameters for Diffuser Flow Test Cases

	$M_1 = 0.29$	$M_1 = 0.75$
$(u/U_r)_e$	1.05	1.03
$(\delta/L_r)_{COWL}$	0.03	0.03
$(\delta^*/L_r)_{COWL}$	0.00333	0.00429
$(\theta/L_r)_{COWL}$	0.00267	0.00321
$(\delta/L_r)_{C-BODY}$	0.0433	0.0433
$(\delta^*/L_r)_{C-BODY}$	0.00394	0.00867
$(\theta/L_r)_{C-BODY}$	0.00328	0.00578

ORIGINAL PAGE IS
OF POOR QUALITY

ORIGINAL PAGE IS
OF POOR QUALITY

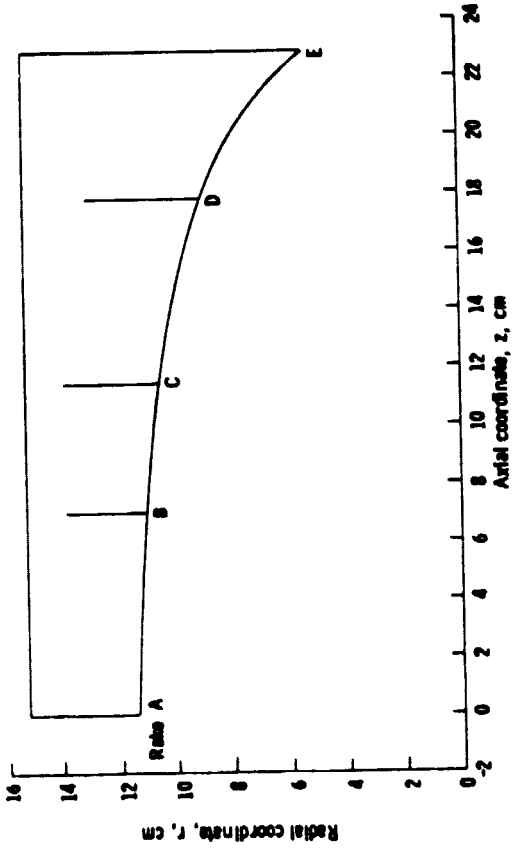

Figure 4-41. - Geometric configuration for diffuser flow.

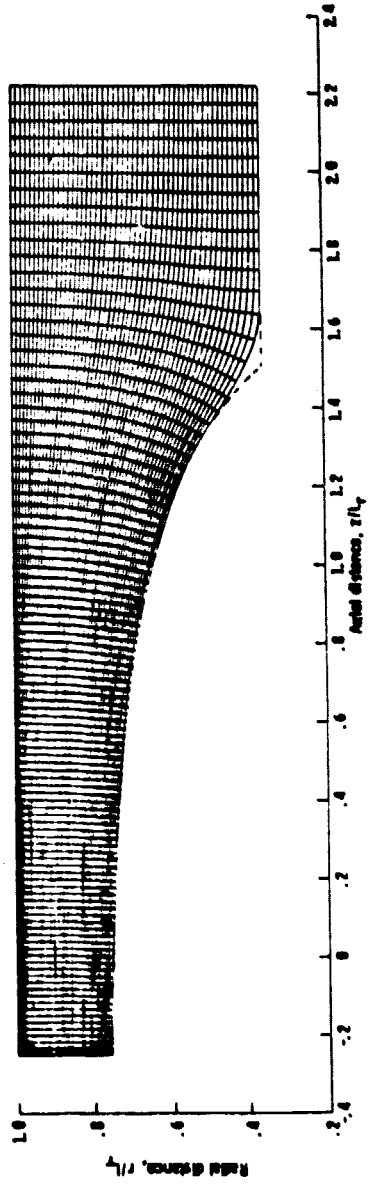

Figure 4-42. - Computational coordinate system for diffuser flow.

ORIGINAL PAGE IS
OF POOR QUALITY

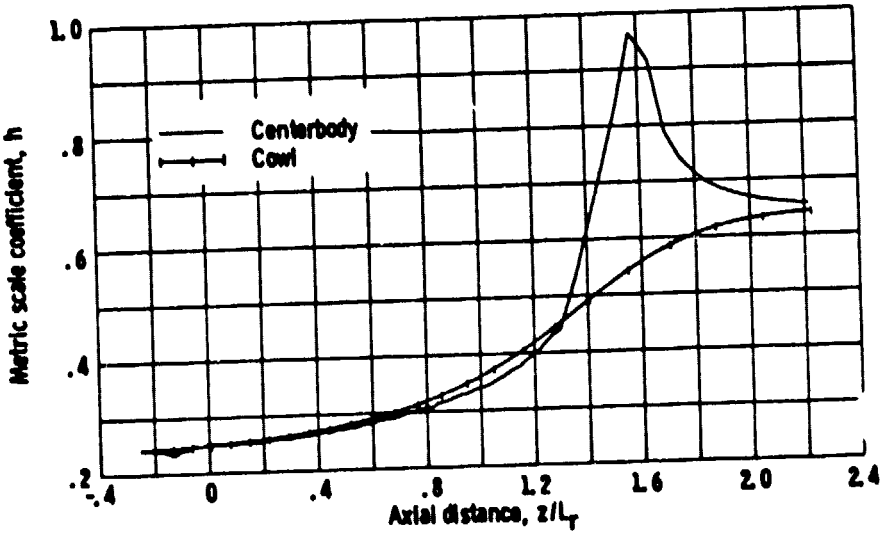

Figure 4-43. - Metric scale coefficients for diffuser flow.

ORIGINAL PAGE IS
OF POOR QUALITY

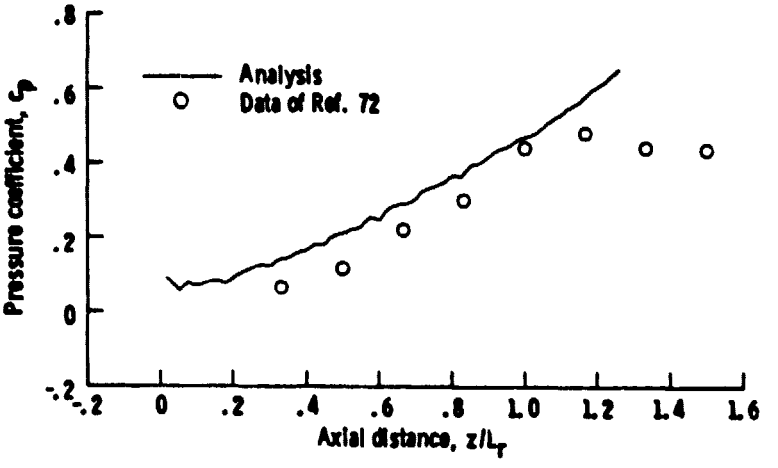

(a) Centerbody.

Figure 4-44. - Imposed pressure coefficients compared with data for diffuser flow, $M_1 = 0.29$.

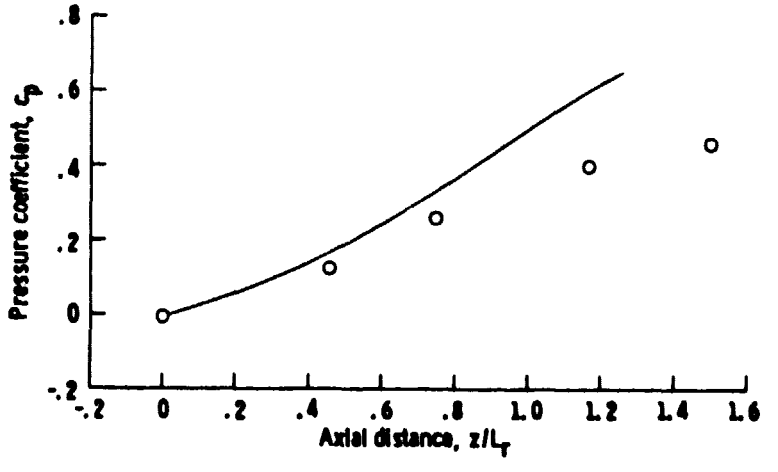

(b) Cowl.

Figure 4-44. - Concluded.

ORIGINAL PAGE IS
OF POOR QUALITY

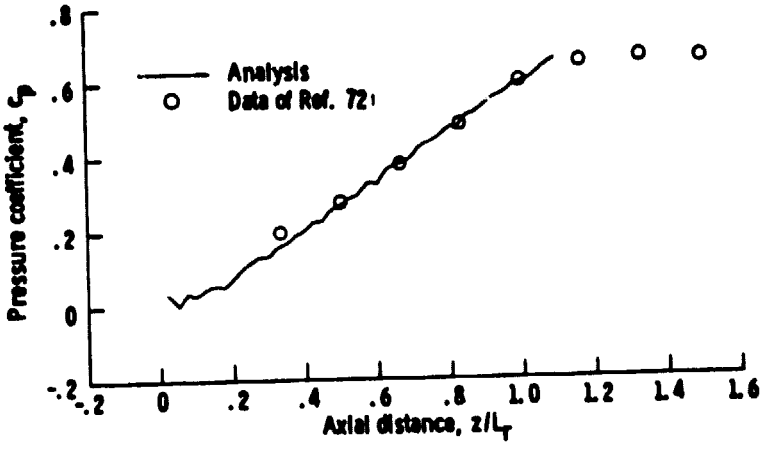

(a) Centerbody.

Figure 4-45. - Imposed pressure coefficients compared with data for diffuser flow, $M_1 = 0.75$.

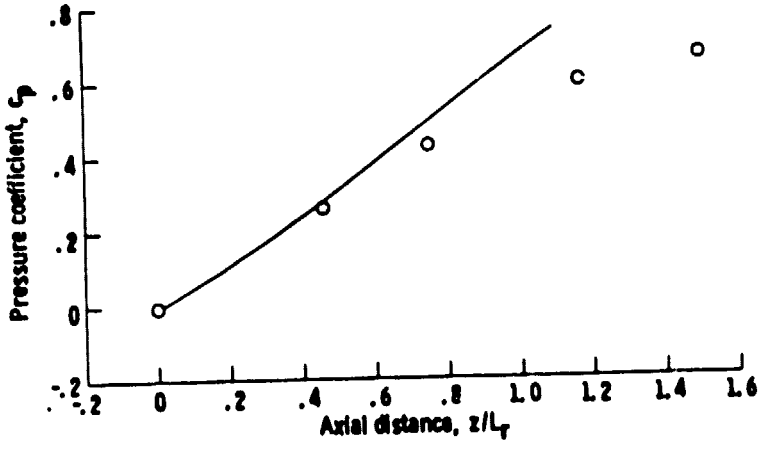

(b) Cowl.

Figure 4-45. - Concluded.

ORIGINAL PAGE IS
OF POOR QUALITY

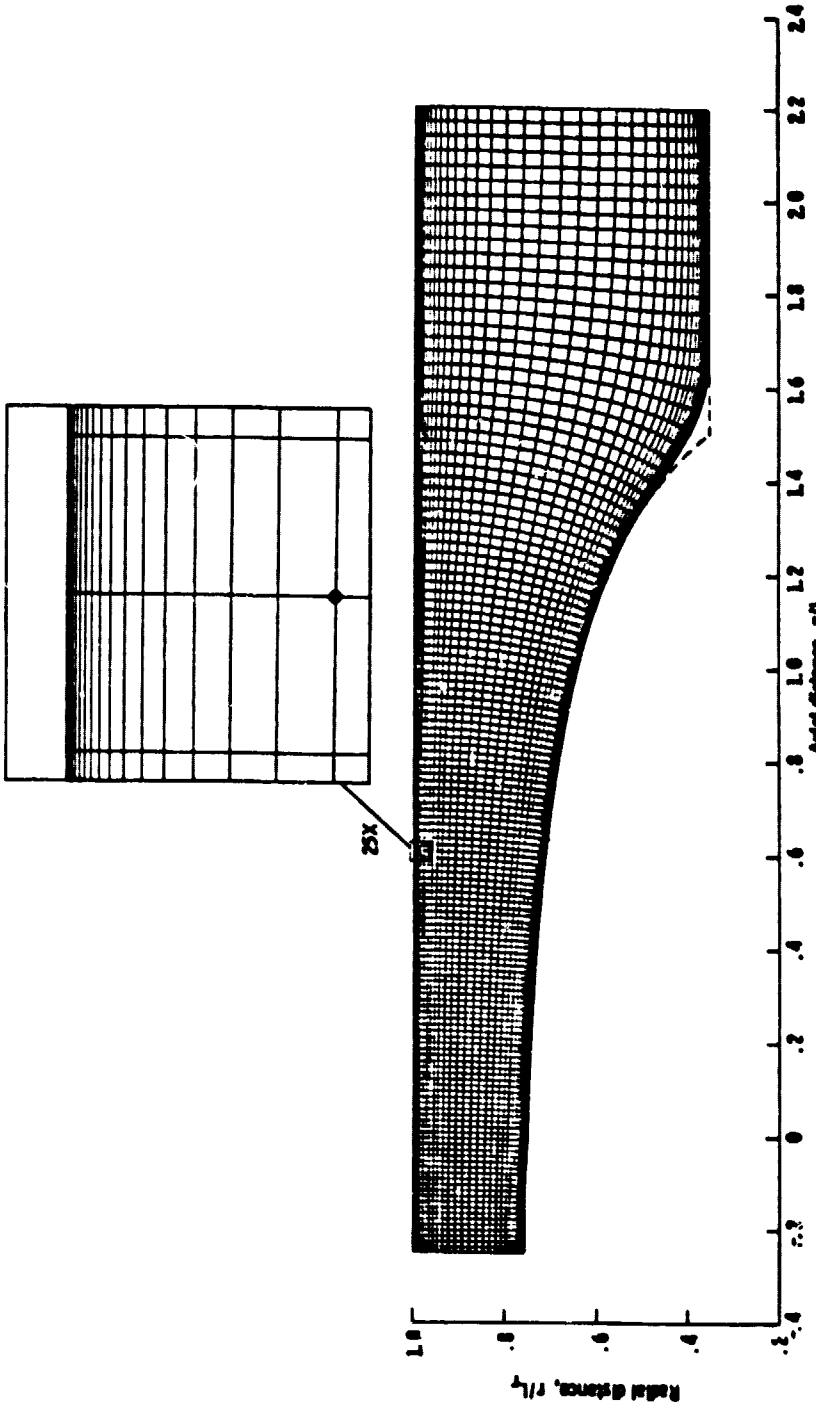

Figure 4-46. - Computational grid used for viscous calculation, diffuser flow.

ORIGINAL PAGE IS
OF POOR QUALITY

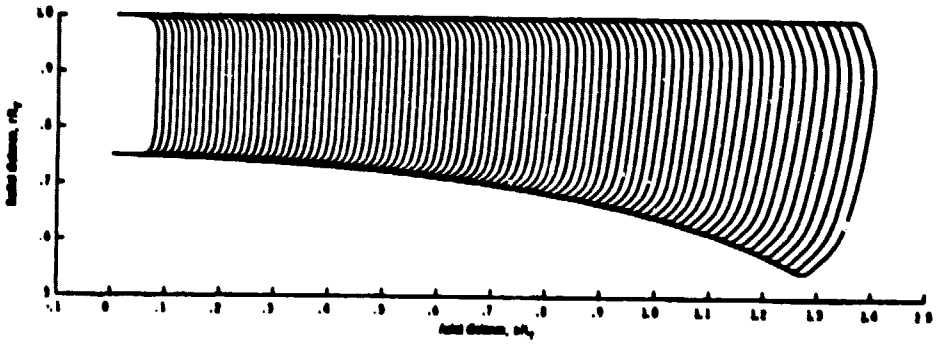

(a) $M_1 = 0.29$.

Figure 4-47. - Computed streamwise velocity profiles for diffuser flow.

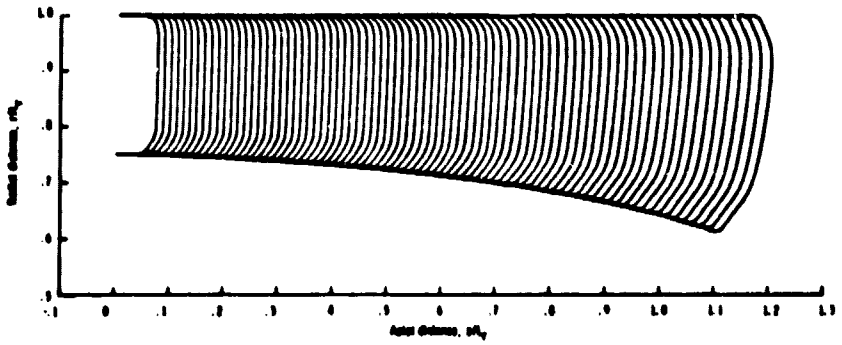

(b) $M_1 = 0.75$.

Figure 4-47. - Concluded.

ORIGINAL PAGE IS
OF POOR QUALITY

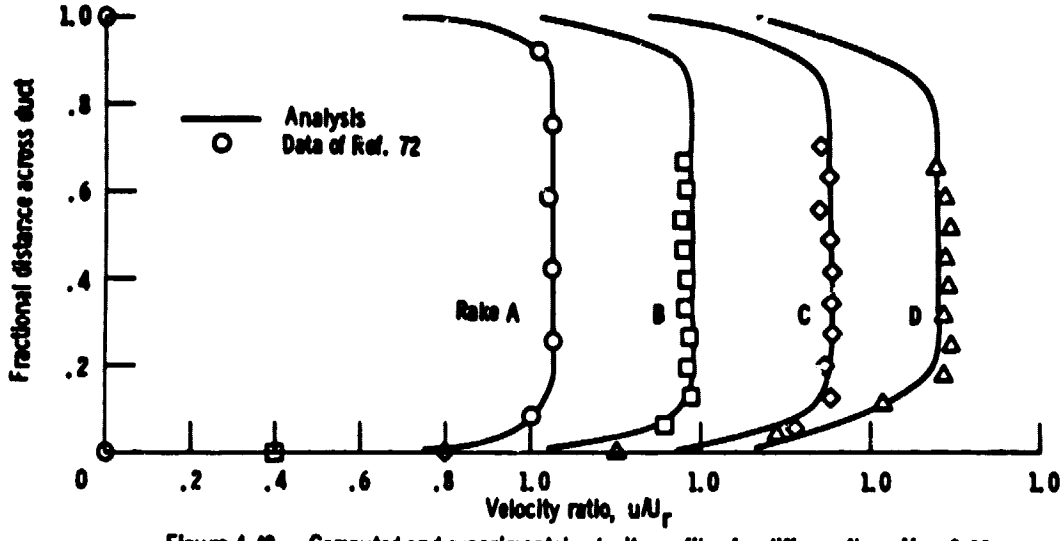

Figure 4-48. - Computed and experimental velocity profiles for diffuser flow, $M_1 = 0.29$.

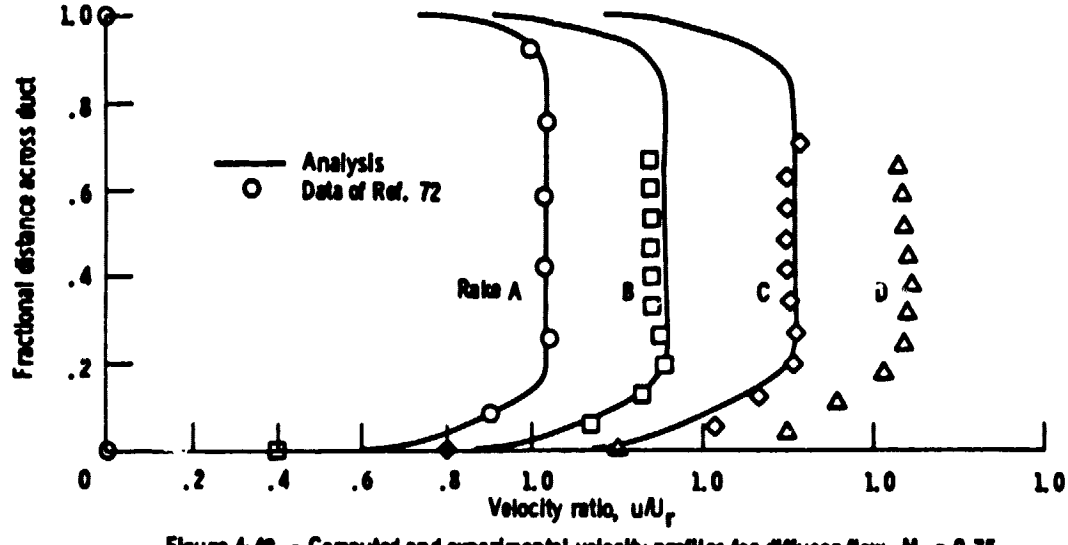

Figure 4-49. - Computed and experimental velocity profiles for diffuser flow, $M_1 = 0.75$.

ORIGINAL PAGE IS
OF POOR QUALITY

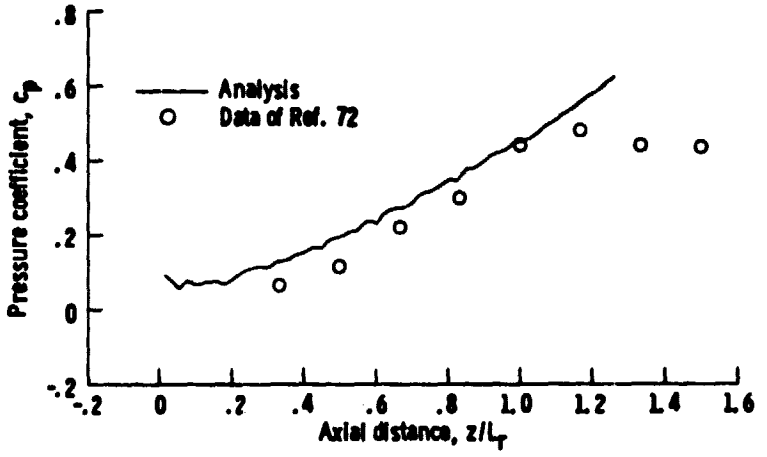

(a) Centerbody.

Figure 4-50. - Viscous pressure coefficients compared with data for diffuser flow, $M_1 = 0.29$.

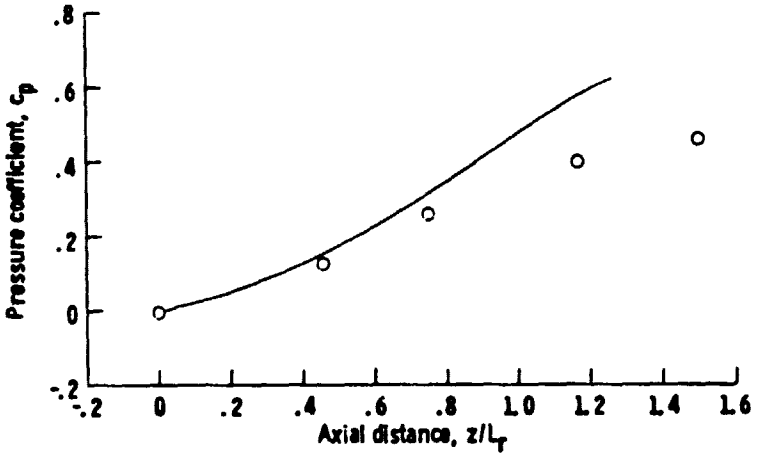

(b) Cowl.

Figure 4-50. - Concluded.

ORIGINAL PAGE IS
OF POOR QUALITY

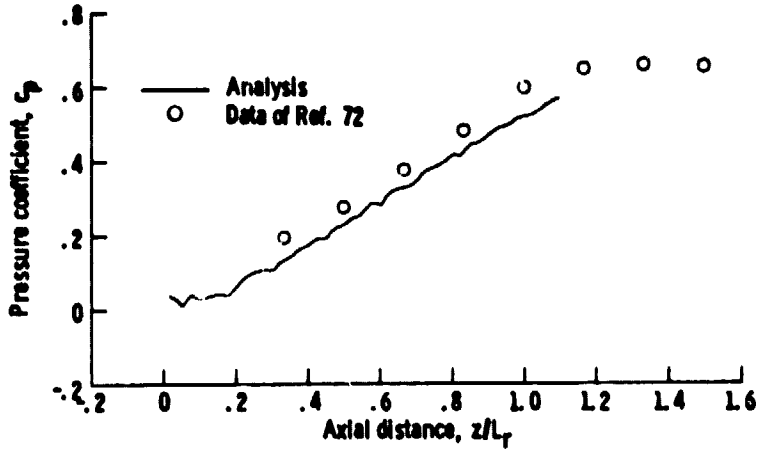

(a) Centerbody.

Figure 4-51. - Viscous pressure coefficients compared with data for diffuser flow, $M_1 = 0.75$.

(b) Cowl.

Figure 4-51. - Concluded.

ORIGINAL PAGE IS
OF POOR QUALITY

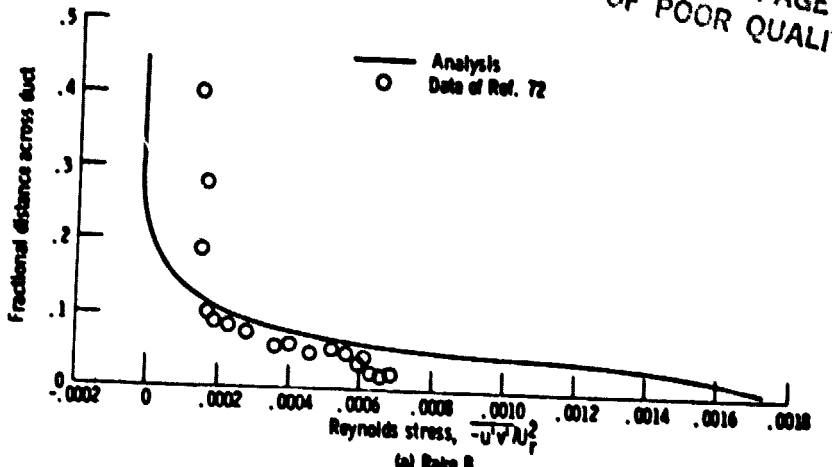

(a) Rake B.

Figure 4-52. - Predicted and experimental Reynolds stress profiles for diffuser flow, $M_1 = 0.29$.

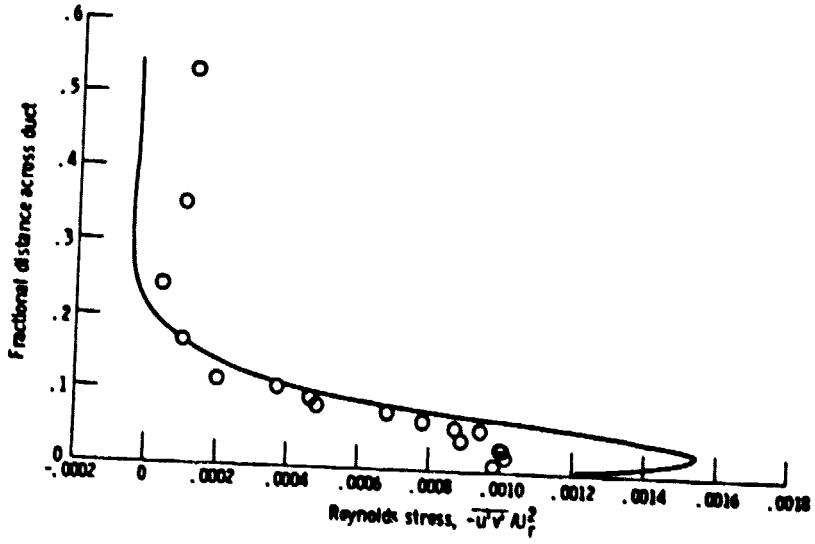

(b) Rake C.

Figure 4-52. - Continued.

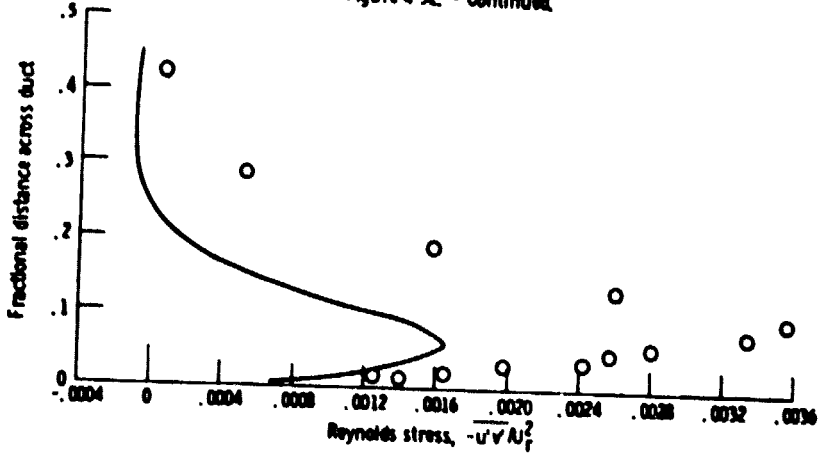

(c) Rake D.

Figure 4-52. - Concluded.

SECTION 5

CONCLUSIONS

A new solution procedure has been developed and used to compute compressible viscous subsonic flow in both planar and axisymmetric ducts. A set of equations that can be solved by forward marching was derived by neglecting second derivatives in the streamwise direction and by uncoupling the streamwise and cross-flow pressure gradients. The streamwise pressure gradient was written as the sum of a known two-dimensional imposed pressure gradient and an unknown one-dimensional viscous correction computed as part of the marching procedure. The governing equations were solved simultaneously using an implicit finite-difference method. Based on the results of the test cases presented in Section 4, a number of specific conclusions can be made about the analysis.

1. The analytical results agree extremely well with experimental data and/or exact solutions for the laminar flow cases studied. This indicates that the basic solution procedure is valid since the turbulence model, of course, has no effect in these cases.

2. The analytical results for turbulent flow also agree well with data, although not quite as well as for laminar flow. Both turbulence models that were used give equally good results for the cases studied.

3. The method used to compute the viscous pressure gradient correction is valid. This was demonstrated by the laminar and turbulent pipe flow cases, where the streamwise gradient is given solely by the viscous correction, and by the Jeffery-Hamel flow case, where the viscous correction is essentially zero.

4. When the imposed pressure field is a good approximation to the actual pressure field, the computed results will be accurate. This was demonstrated by the Jeffery-Hamel flow case.

5. The analysis can be used for flows with both favorable and adverse pressure gradients. It can also be used to accurately predict the location of flow separation, as shown by the diffuser flow test cases.

6. The predicted streamwise velocities are not especially sensitive to any oscillations present in the metric scale coefficients and imposed pressure field. These oscillations are reflected in the predicted cross-flow velocities, but not to the point of numerical instability.

7. The marching procedure can be started with the initial cross-flow velocity set equal to zero when the actual profile is unknown, as is often the case in engineering practice. The analysis will then generate a realistic profile in the first few marching steps.

8. The analysis is fast enough for use in parametric studies and design work. A typical turbulent flow case with a 51x100 mesh will run in about 30 seconds on an IBM 370/3033.

LIST OF REFERENCES

1. Anderson, O. L., "Finite-Difference Solution for Turbulent Swirling Compressible Flow in Axisymmetric Ducts with Struts," NASA CR-2365, Feb. 1974.

2. Anderson, O. L., "User's Manual for a Finite-Difference Calculation of Turbulent Swirling Compressible Flow in Axisymmetric Ducts with Struts and Slot Cooled Walls," Vol. 1, USAAMRDL-TR-74-50, 1974.

3. Anderson, O. L., "Extensions to an Analysis of Turbulent Swirling Compressible Flow in Axisymmetric Ducts," Report R81-914720, United Technologies Research Center, Feb. 1981.

4. Bowditch, D. N., "Some Design Considerations for Supersonic Cruise Mixed Compression Inlets," AIAA Paper 73-1269, Nov. 1973.

5. Anderson, O. L., "A Method of Predicting the Aerodynamic Performance of Centerbody-Plug IR Suppressors," Report N911630-13, United Aircraft Research Laboratory, June 1974.

6. Povinelli, L. A., "An Experimental and Analytical Investigation of Axisymmetric Diffusers," AIAA Journal, Vol. 14, No. 9, Sept. 1976.

7. Neumann, H. E., Povinelli, L. A., and Coltrin, R. E., "An Analytical and Experimental Study of a Short S-Shaped Subsonic Diffuser of a Supersonic Inlet," AIAA Paper 80-0386, Jan. 1980.

8. Rubin, S. G., and Lin, T. C., "Numerical Methods for Two- and Three-Dimensional Viscous Flow Problems: Application to Hypersonic Leading Edge Equations," AFOSR-TR-71-0778, Apr. 1971.

9. Patankar, S. V., and Spalding, D. B., "A Calculation Procedure for Heat, Mass, and Momentum Transfer in Three-Dimensional Parabolic Flows," International Journal of Heat and Mass Transfer, Vol. 15, 1972, pp. 1787-1806.

10. Caretto, L. S., Curr, R. M., and Spalding, D. B., "Two Numerical Methods for Three-Dimensional Boundary Layers," Computer Methods in Applied Mechanics and Engineering, Vol. 1, 1972, pp. 39-57.

11. Ghia, U., Ghia, K. N., and Studerus, C. J., "Three-Dimensional Laminar Incompressible Flow in Straight Polar Ducts," Computers and Fluids, Vol. 5, 1977, pp. 205-218.

12. Pratap, V. S., and Spalding, D. B., "Numerical Computations of the Flow in Curved Ducts," Aeronautical Quarterly, Vol. 26, Aug. 1975, pp. 219-228.

13. Pratap, V. S., and Spalding, D. B., "Fluid Flow and Heat Transfer in Three-Dimensional Duct Flows," International Journal of Heat and Mass Transfer, Vol. 19, 1976, pp. 1183-1188.

14. Singhal, A. K., and Spalding, D. B., "A 2D Partially-Parabolic Procedure for Axial-Flow Turbomachinery Cascades," ARC R&M 3807, Oct. 1976.

15. Roberts, D. W., and Forester, C. K., "A Parabolic Computational Procedure for Three-Dimensional Flows in Ducts with Arbitrary Cross-Sections," AIAA Paper 78-143, Jan. 1978.

16. Emery, A. F., Neighbors, P. K., and Gessner, F. B., "Computational Procedure for Developing Turbulent Flow and Heat Transfer in a Square Duct," Numerical Heat Transfer, Vol. 2, 1979, pp. 399-416.

17. Patankar, S. V., Pratap, V. S., and Spalding, D. B., "Prediction of Laminar Flow and Heat Transfer in Helically Coiled Pipes," Journal of Fluid Mechanics, Vol. 62, Part 3, 1974, pp. 539-551.

18. Patankar, S. V., Pratap, V. S., and Spalding, D. B., "Prediction of Turbulent Flow in Curved Pipes," Journal of Fluid Mechanics, Vol. 67, Part 3, 1975, pp. 583-595.

19. Rushmore, W. L., and Taulbee, D. B., "Numerical Investigation of Developing Pipe Flows of Arbitrary Curvature," Computers and Fluids, Vol. 6, 1978, pp. 125-140.

20. Briley, W. R., "Numerical Method for Predicting Three-Dimensional Steady Viscous Flow in Ducts," Journal of Computational Physics, Vol. 14, No. 1, Jan. 1974, pp. 8-28.

21. Briley, W. R., and McDonald, H., "Analysis and Computation of Viscous Subsonic Primary and Secondary Flows," AIAA Paper 79-1453, July 1979.

22. Levy, R., McDonald, H., Briley, W. R., and Kreskovsky, J. P., "A Three-Dimensional Turbulent Compressible Subsonic Duct Flow Analysis for Use with Constructed Coordinate Systems," AIAA Paper 80-1398, July 1980.

23. Kreskovsky, J. P., Briley, W. R., and McDonald, H., "Prediction of Laminar and Turbulent Primary and Secondary Flows in Strongly Curved Ducts," NASA CR-3388, Feb. 1981.

24. Povinelli, L. A., Anderson, B. H., and Gerstenmaier, W., "Computation of Three-Dimensional Flow in Turbofan Mixers and Comparison with Experimental Data," AIAA Paper 80-0227, Jan. 1980.

25. Anderson, B., Povinelli, L., and Gerstenmaier, W., "Influence of Pressure Driven Secondary Flows on the Behavior of Turbofan Forced Mixers," AIAA Paper 80-1198, June 1980.

26. Anderson, B. H., and Povinelli, L. A., "Factors Which Influence the Behavior of Turbofan Forced Mixer Nozzles," AIAA Paper 81-0274, Jan. 1981.

27. Dodge, P. R., "Numerical Method for 2D and 3D Viscous Flows," AIAA Journal, Vol. 15, No. 7, July 1977, pp. 961-965.

28. White, F. M., Viscous Fluid Flow, McGraw-Hill, 1974.

29. Bushnell, D. M., Cary, A. M., Jr., and Harris, J. E., "Calculation Methods for Compressible Turbulent Boundary Layers - 1976," NASA SP-422, 1977.

30. Maise, G., and McDonald, H., "Mixing Length and Kinematic Eddy Viscosity in a Compressible Boundary Layer," AIAA Journal, Vol. 6, No. 1, Jan. 1968, pp. 73-80.

31. Walz, A., Boundary Layers of Flow and Temperature, M. I. T. Press, 1969.

32. Coles, D., "The Law of the Wake in the Turbulent Boundary Layer," Journal of Fluid Mechanics, Vol. 1, 1956, pp. 191-226.

33. Sasman, P. K., and Cresci, R. J., "Compressible Turbulent Boundary Layer with Pressure Gradient and Heat Transfer," AIAA Journal, Vol. 4, No. 1, Jan. 1966, pp. 19-25.

34. Hesse, W. J., and Mumford, N. V. S , Jr., Jet Propulsion for Aerospace Applications, Second Edition, Pitman Publishing Corp., 1964, p. 220.

35. Hilsenruth, J., et. al., Tables of Thermal Properties of Gases, National Bureau of Standards Circular 564, Nov. 1955, p. 11.

36. Kreskovsky, J. P., Briley, W. R., and McDonald, H., "Turbofan Forced Mixer-Nozzle Internal Flowfield. III - A Computer Code for 3-D Mixing in Axisymmetric Nozzles," NASA CR-3494, April 1982.

37. Lieblein, S., and Stockman, N. O., "Compressibility Correction for Internal Flow Solutions," Journal of Aircraft, Vol. 9, No. 4, Apr. 1972, pp. 312-313.

38. Albers, James A., "Application of Compressibility Correction to Calculation of Flow in Inlets," Journal of Aircraft, Vol. 10, No. 7, July 1973, pp. 441-442.

39. Albers, James A., "Theoretical and Experimental Internal Flow Characteristics of a 13.97-Centimeter-Diameter Inlet at STOL Take-off and Approach Conditions," NASA TN D-7185, March 1973.

40. Stockman, Norbert O., "Potential and Viscous Flow in VTOL, STOL or CTOL Propulsion System Inlets," AIAA Paper 75-1186, Sept. 1975.

41. Kao, H. C., "Some Aspects of Calculating Flows About Three-Dimensional Subsonic Inlets," AIAA Paper 81-1361, July 1981.

42. Bober, Lawrence J., "Use of Potential Flow Theory to Evaluate Subsonic Inlet Data from a Simulator-Powered Nacelle at Cruise Conditions," NASA TND-7850, Dec. 1974.

43. Cebeci, T., and Smith, A. M. O., Analysis of Turbulent Boundary Layers, Academic Press, 1974.

44. McDonald, H., and Camarata, F. J., "An Extended Mixing Length Approach for Computing the Turbulent Boundary Layer Development," Computation of Turbulent Boundary Layers - 1968 AFOSR-IFP-Stanford Conference, S. J. Kline, et. al., eds., Stanford University, 1969, pp. 83-98.

45. Coakley, T. J., and Bergmann, M. Y., "Effects of Turbulence Model Selection on the Prediction of Complex Aerodynamic Flows," AIAA Paper 79-0070, Jan. 1979.

46. Laufer, J., "The Structure of Turbulence in Fully Developed Pipe Flow," NACA Report 1174, 1954.

47. Richman, J. W., and Azad, R. S., "Developing Turbulent Flow in Smooth Pipes," Applied Scientific Research, Vol. 28, Dec. 1973, pp. 419-441.

48. Cebeci, T., "Behavior of Turbulent Flow near a Porous Wall with Pressure Gradient," AIAA Journal, Vol. 8, No. 12, Dec. 1970, pp. 2152-2156.

49. Cebeci, T., "Calculation of Compressible Turbulent Boundary Layers with Heat and Mass Transfer," AIAA Journal, Vol. 9, No. 6, June 1971, pp. 1091-1097.

50. Carnahan, B., Luther, H. A., and Wilkes, J. O., Applied Numerical Methods, Wiley, 1969.

51. Roache, P. J., Computational Fluid Dynamics, Hermosa, 1972.

52. Smith, G. D., Numerical Solution of Partial Differential Equations, Oxford University Press, 1965.

53. McDonald, H., and Briley, W. R., "Three-Dimensional Supersonic Flow of a Viscous or Inviscid Gas," Journal of Computational Physics, Vol. 19, 1975, pp. 150-178.

54. Beam, R. M., and Warming, R. F., "An Implicit Finite-Difference Algorithm for Hyperbolic Systems in Conservation-Law Form," Journal of Computational Physics, Vol. 22, 1976, pp. 87-110.

55. Hornbeck, R. W., "Numerical Marching Techniques for Fluid Flows with Heat Transfer," NASA SP-297, 1973.

56. Pfenninger, W., "Boundary Layer Suction Experiments with Laminar Flow at High Reynolds Numbers in the Inlet Length of a Tube by Various Suction Methods," Boundary Layer and Flow Control. Its Principles and Application, Vol. 2, G. V. Lachmann, ed., Pergamon Press, 1961.

57. Reshotko, E., "Experimental Study of the Stability of Pipe Flow. Establishment of an Axially Symmetric Poiseuille Flow," Progress Report Number 20-364, Jet Propulsion Laboratory, Oct. 1958.

58. Prandtl, L., and Tietjens, O. G. (J. P. Den Hartog, transl.), Applied Hydro- and Aeromechanics, McGraw-Hill, 1934.

59. Schlichting, H. (J. Kestin, transl.), Boundary-Layer Theory, McGraw-Hill, 1968.

60. Millsaps, K., and Pohlhausen, K., "Thermal Distributions in Jeffery-Hamel Flows Between Nonparallel Plane Walls," Journal of the Aeronautical Sciences, Vol. 20, March 1953, pp. 187-196.

61. Deissler, R. G., "Turbulent Heat Transfer and Friction in the Entrance Region of Smooth Passages," Transactions of the ASME, Vol. 77, No. 8, Nov. 1955, pp. 1221-1233.

62. Barbin, A. R., "Development of Turbulence in the Inlet of a Smooth Pipe," Ph. D. Thesis, Purdue University, Aug. 1961.

63. Barbin, A. R., and Jones, J. B., "Turbulent Flow in the Inlet Region of a Smooth Pipe," Journal of Basic Engineering, Transactions of the ASME, Vol. 85, March 1963, pp. 29-34.

64. Laws, E. M., Lim, E. H., and Livesey, J. L., "Turbulent Pipe Flows in Development and Decay," Second Symposium on Turbulent Shear Flows, Imperial College, London, July 1979.

65. Johnston, J. P., "Internal Flows," Topics in Applied Physics, Vol. 12. Turbulence, P. Bradshaw, ed., Springer-Verlag, 1978.

66. Byrne, J., Hatton, A. P., and Marriott, P. G., "Turbulent Flow and Heat Transfer in the Entrance Region of a Parallel Wall Passage," Proceedings of the Institution of Mechanical Engineers, Vol. 184, Part 1, No. 39, 1969-70, pp. 697-712.

67. Bradshaw, P., Dean, R. B., and McEligot, D. M., "Calculation of Interacting Turbulent Shear Layers: Duct Flow," Journal of Fluids Engineering, Transactions of the ASME, Vol. 95, June 1973, pp. 214-220.

68. Cebeci, T., and Chang, K. C., "A General Method for Calculating Momentum and Heat Transfer in Laminar and Turbulent Duct Flows," Numerical Heat Transfer, Vol. 1, 1978, pp. 39-68.

69. Butz, L. A., "Turbulent Flow in S-Shaped Ducts," M. S. Thesis, Purdue University, Dec. 1979.

70. Sullivan, J. P., Private Communication, Aug. 1980.

71. Neumann, H. E., Wasserbauer, J. F., and Shaw, R. J., "Performance of Vortex Generators in a Mach 2.5 Low-Bleed Full Scale 45-Percent-Internal-Contraction Axisymmetric Inlet," NASA TM X-3195, Apr. 1975.

72. Shaw, R. J., "An Experimental Investigation of Forced Mixing of a Turbulent Boundary Layer in an Annular Diffuser," Ph. D. Thesis, Ohio State University, June 1979.

73. Reyhner, T. A., and Flugge-Lotz, I., "The Interaction of a Shock Wave with a Laminar Boundary Layer," International Journal of Non-Linear Mechanics, Vol. 3, 1968, pp. 173-199.

74. Hughes, W. F., and Gaylord, E. W., Basic Equations of Engineering Science, Schaum's Outline Series, McGraw-Hill, 1964.

75. Sislian, J. P., "Equations of Motion and Two-Equation Turbulence Model for Plane or Axisymmetric Turbulent Flows in Body-Oriented Orthogonal Curvilinear Coordinates and Mass-Averaged Dependent Variables," NASA CR 3025, Aug. 1978.

76. Van Driest, E. R., "Turbulent Boundary Layer in Compressible Fluids," Journal of the Aeronautical Sciences, Vol. 18, No. 3, March 1951, pp. 145-160, 216.

77. Abramowitz, M., and Stegun, I. A., eds., Handbook of Mathematical Functions, Dover, 1965.

ORIGINAL PAGE IS
OF POOR QUALITY

APPENDIX A

DERIVATION OF GOVERNING EQUATIONS

The general equations for compressible, viscous fluid flow, in orthogonal curvilinear coordinates, can be found in one form or another in several references (e.g., References 74-75). Here they are written as:

CONTINUITY

$$\rho_t + \frac{1}{h_1 h_2 h_3}\left[(h_2 h_3 \rho u)_\xi + (h_1 h_3 \rho v)_\eta + (h_1 h_2 \rho w)_\theta\right] = 0 \qquad (A.1)$$

ξ-MOMENTUM

$$(\rho u)_t + \frac{1}{h_1 h_2 h_3}\left[(h_2 h_3 \rho u^2)_\xi + (h_1 h_3 \rho uv)_\eta + (h_1 h_2 \rho uw)_\theta\right] - \frac{h_{2_\xi}}{h_1 h_2}\rho v^2$$

$$+ \frac{h_{1_\eta}}{h_1 h_2}\rho uv + \frac{h_{1_\theta}}{h_1 h_3}\rho uw - \frac{h_{3_\xi}}{h_1 h_3}\rho w^2 = -\frac{1}{h_1} p_\xi$$

$$+ \frac{1}{h_1 h_2 h_3}\left[(h_2 h_3 \tau_{11})_\xi + (h_1 h_3 \tau_{21})_\eta + (h_1 h_2 \tau_{31})_\theta\right]$$

$$+ \frac{h_{1_\eta}}{h_1 h_2}\tau_{12} + \frac{h_{1_\theta}}{h_1 h_3}\tau_{31} - \frac{h_{2_\xi}}{h_1 h_2}\tau_{22} - \frac{h_{3_\xi}}{h_1 h_3}\tau_{33} \qquad (A.2)$$

η–MOMENTUM

ORIGINAL PAGE IS
OF POOR QUALITY

$$(\rho v)_t + \frac{1}{h_1 h_2 h_3}\left[(h_2 h_3 \rho uv)_\xi + (h_1 h_3 \rho v^2)_\eta + (h_1 h_2 \rho vw)_\theta\right] - \frac{h_{3_\eta}}{h_2 h_3}\rho w^2$$

$$+ \frac{h_{2_\theta}}{h_2 h_3}\rho vw + \frac{h_{2_\xi}}{h_1 h_2}\rho uv - \frac{h_{1_\eta}}{h_1 h_2}\rho u^2 = -\frac{1}{h_2}p_\eta$$

$$+ \frac{1}{h_1 h_2 h_3}\left[(h_2 h_3 \tau_{12})_\xi + (h_1 h_3 \tau_{22})_\eta + (h_1 h_2 \tau_{32})_\theta\right]$$

$$+ \frac{h_{2_\theta}}{h_2 h_3}\tau_{23} + \frac{h_{2_\xi}}{h_1 h_2}\tau_{12} - \frac{h_{3_\eta}}{h_2 h_3}\tau_{33} - \frac{h_{1_\eta}}{h_1 h_2}\tau_{11} \qquad (A.3)$$

θ–MOMENTUM

$$(\rho w)_t + \frac{1}{h_1 h_2 h_3}\left[(h_2 h_3 \rho uw)_\xi + (h_1 h_3 \rho vw)_\eta + (h_1 h_2 \rho w^2)_\theta\right] - \frac{h_{1_\theta}}{h_1 h_3}\rho u^2$$

$$+ \frac{h_{3_\xi}}{h_1 h_3}\rho uw + \frac{h_{3_\eta}}{h_2 h_3}\rho vw - \frac{h_{2_\theta}}{h_2 h_3}\rho v^2 = -\frac{1}{h_3}p_\theta$$

$$+ \frac{1}{h_1 h_2 h_3}\left[(h_2 h_3 \tau_{13})_\xi + (h_1 h_3 \tau_{23})_\eta + (h_1 h_2 \tau_{33})_\theta\right]$$

$$+ \frac{h_{3_\xi}}{h_1 h_3}\tau_{31} + \frac{h_{3_\eta}}{h_2 h_3}\tau_{23} - \frac{h_{1_\theta}}{h_1 h_3}\tau_{11} - \frac{h_{2_\theta}}{h_2 h_3}\tau_{22} \qquad (A.4)$$

ENERGY

$$(\rho h)_t + \frac{1}{h_1 h_2 h_3}\left[(h_2 h_3 \rho uh)_\xi + (h_1 h_3 \rho vh)_\eta + (h_1 h_2 \rho wh)_\theta\right] = \frac{1}{h_1}up_\xi + \frac{1}{h_2}vp_\eta$$

$$+ \frac{1}{h_3}wp_\theta - \frac{1}{h_1 h_2 h_3}\left[(h_2 h_3 q_1)_\xi + (h_1 h_3 q_2)_\eta + (h_1 h_2 q_3)_\theta\right] + \Phi_L \qquad (A.5)$$

ORIGINAL PAGE IS
OF POOR QUALITY

In these equations, h_1, h_2, and h_3 are the metric scale coefficients for the orthogonal curvilinear coordinate system; ξ, η, and θ are the three coordinate directions; u, v, and w are the velocities in the ξ, η, and θ directions, respectively; ρ is the static density; p is the static pressure; and h is the static enthalpy. The subscripts ξ, η, θ, and t denote partial differentiation.

The shear stresses are given by

$$\left.\begin{aligned}
\tau_{11} &= 2\mu_L\left(\frac{1}{h_1}u_\xi + \frac{h_{1_\eta}}{h_1h_2}v + \frac{h_{1_\theta}}{h_1h_3}w\right) + \lambda\,\nabla\cdot\vec{V}\\
\tau_{22} &= 2\mu_L\left(\frac{1}{h_2}v_\eta + \frac{h_{2_\theta}}{h_2h_3}w + \frac{h_{2_\xi}}{h_1h_2}u\right) + \lambda\,\nabla\cdot\vec{V}\\
\tau_{33} &= 2\mu_L\left(\frac{1}{h_3}w_\theta + \frac{h_{3_\xi}}{h_1h_3}u + \frac{h_{3_\eta}}{h_2h_3}v\right) + \lambda\,\nabla\cdot\vec{V}\\
\tau_{12} &= \tau_{21} = \mu_L\left[\frac{h_2}{h_1}\left(\frac{v}{h_2}\right)_\xi + \frac{h_1}{h_2}\left(\frac{u}{h_1}\right)_\eta\right]\\
\tau_{13} &= \tau_{31} = \mu_L\left[\frac{h_1}{h_3}\left(\frac{u}{h_1}\right)_\theta + \frac{h_3}{h_1}\left(\frac{w}{h_3}\right)_\xi\right]\\
\tau_{23} &= \tau_{32} = \mu_L\left[\frac{h_3}{h_2}\left(\frac{w}{h_3}\right)_\eta + \frac{h_2}{h_3}\left(\frac{v}{h_2}\right)_\theta\right]
\end{aligned}\right\} \quad (A.6)$$

where

$$\nabla\cdot\vec{V} = \frac{1}{h_1h_2h_3}\left[(h_2h_3u)_\xi + (h_1h_3v)_\eta + (h_1h_2w)_\theta\right]$$

and μ_L is the molecular viscosity. The second coefficient of viscosity, λ, is assumed equal to $-2\mu_L/3$.

ORIGINAL PAGE IS
OF POOR QUALITY

The heat fluxes are given by

$$\left.\begin{aligned} q_1 &= -\frac{1}{h_1} k_L T_\xi \\ q_2 &= -\frac{1}{h_2} k_L T_\eta \\ q_3 &= -\frac{1}{h_3} k_L T_\theta \end{aligned}\right\} \qquad (A.7)$$

where T is static temperature and k_L is the molecular thermal conductivity.

Finally, the viscous dissipation, Φ_L, is given by

$$\Phi_L = \mu_L\left[2\left(e_{11}^2 + e_{22}^2 + e_{33}^2\right) + (2e_{23})^2 + (2e_{31})^2 + (2e_{12})^2\right] - \frac{2}{3}\mu_L(e_{11} + e_{22} + e_{33})^2 \qquad (A.8)$$

where

$$e_{mn} = \frac{1}{2\mu_L}\left(\tau_{mn} + \delta_{mn}\frac{2}{3}\mu_L \nabla \cdot \vec{V}\right)$$

Equations (A.1)-(A.5) are, in theory, valid for turbulent as well as laminar flow. In practice, however, solving them directly for turbulent flow would be a hopeless task. The extremely fine resolution that would be required in both space and time is simply beyond the capacity of current and foreseeable computers.

The way around this problem is to replace the instantaneous quantities in the equations with the sum of their average and fluctuating values. This can be done using either conventional time averaged values or mass averaged values. The conventional time average of a quantity f is defined by

ORIGINAL PAGE IS
OF POOR QUALITY

$$\overline{f} = \frac{1}{\beta} \int_{t_0}^{t_0+\beta} f \, dt \tag{A.9}$$

where β is some time period that is long compared to the characteristic time scale of the turbulent fluctuations. The mass averaged value of a quantity f is defined by

$$\tilde{f} = \frac{\overline{\rho f}}{\overline{\rho}} \tag{A.10}$$

Here, following the procedure of Cebeci and Smith (Ref. 43), mass averaged values are used for the velocities and enthalpy, and conventional time averages are used for the remaining variables. Therefore,

$$\left.\begin{aligned} u &= \tilde{u} + u' \\ v &= \tilde{v} + v' \\ w &= \tilde{w} + w' \\ h &= \tilde{h} + h' \\ T &= \overline{T} + T' \\ p &= \overline{p} + p'' \\ \rho &= \overline{\rho} + \rho'' \end{aligned}\right\} \tag{A.11}$$

Note that an overbar and double prime have been used for conventional time averaging and a tilde and single prime for mass weighted averaging. With mass weighted averaging, as shown in Reference 43,

$$\left.\begin{aligned} \overline{\rho f} &= \overline{\rho}\tilde{f} \\ \overline{\rho f'} &= 0 \\ \overline{f''} &= \overline{f} - \tilde{f} \end{aligned}\right\} \tag{A.12}$$

ORIGINAL PAGE IS
OF POOR QUALITY

The expressions for u, v, w, h, ρ, and p are substituted into equations (A.1)-(A.5), and the resulting equations are then time averaged. At this point, the equations are restricted to steady, two-dimensional, mean flow. The results are as follows:

CONTINUITY

$$\frac{1}{h_1 h_2 h_3}\left[(h_2 h_3 \bar{\rho}\tilde{u})_\xi + (h_1 h_3 \bar{\rho}\tilde{v})_\eta\right] = 0 \qquad \text{(A.13)}$$

ξ-MOMENTUM

$$\frac{1}{h_1 h_2 h_3}\left[\left(h_2 h_3 \bar{\rho}\tilde{u}^2\right)_\xi + (h_1 h_3 \bar{\rho}\tilde{u}\tilde{v})_\eta\right] - \frac{h_{2_\xi}}{h_1 h_2}\bar{\rho}\tilde{v}^2 + \frac{h_{1_\eta}}{h_1 h_2}\bar{\rho}\tilde{u}\tilde{v} = -\frac{1}{h_1}\bar{p}_\xi$$

$$+ \frac{1}{h_1 h_2 h_3}\left\{\left[h_2 h_3\left(\bar{\tau}_{11} - \overline{\rho u'^2}\right)\right]_\xi + \left[h_1 h_3\left(\bar{\tau}_{21} - \overline{\rho u'v'}\right)\right]_\eta\right\} + \frac{h_{1_\eta}}{h_1 h_2}$$

$$\times\left(\bar{\tau}_{12} - \overline{\rho u'v'}\right) - \frac{h_{2_\xi}}{h_1 h_2}\left(\bar{\tau}_{22} - \overline{\rho v'^2}\right) - \frac{h_{3_\xi}}{h_1 h_3}\left(\bar{\tau}_{33} - \overline{\rho w'^2}\right) \qquad \text{(A.14)}$$

η-MOMENTUM

$$\frac{1}{h_1 h_2 h_3}\left[(h_2 h_3 \bar{\rho}\tilde{u}\tilde{v})_\xi + (h_1 h_3 \bar{\rho}\tilde{v}^2)_\eta\right] + \frac{h_{2_\xi}}{h_1 h_2}\bar{\rho}\tilde{u}\tilde{v} - \frac{h_{1_\eta}}{h_1 h_2}\bar{\rho}\tilde{u}^2 = -\frac{1}{h_2}\bar{p}_\eta$$

$$+ \frac{1}{h_1 h_2 h_3}\left\{\left[h_2 h_3\left(\bar{\tau}_{12} - \overline{\rho u'v'}\right)\right]_\xi + \left[h_1 h_3\left(\bar{\tau}_{22} - \overline{\rho v'^2}\right)\right]_\eta\right\} + \frac{h_{2_\xi}}{h_1 h_2}$$

$$\times\left(\bar{\tau}_{12} - \overline{\rho u'v'}\right) - \frac{h_{3_\eta}}{h_2 h_3}\left(\bar{\tau}_{33} - \overline{\rho w'^2}\right) - \frac{h_{1_\eta}}{h_1 h_2}\left(\bar{\tau}_{11} - \overline{\rho u'^2}\right) \qquad \text{(A.15)}$$

ORIGINAL PAGE IS
OF POOR QUALITY

θ-MOMENTUM

$$0 = \frac{1}{h_1 h_2 h_3}\left\{\left[h_2 h_3\left(\bar{\tau}_{13} - \overline{\rho u' w'}\right)\right]_\xi + \left[h_1 h_3\left(\bar{\tau}_{23} - \overline{\rho v' w'}\right)\right]_\eta\right\}$$

$$+ \frac{h_{3_\xi}}{h_1 h_3}\left(\bar{\tau}_{31} - \overline{\rho u' w'}\right) + \frac{h_{3_\eta}}{h_2 h_3}\left(\bar{\tau}_{23} - \overline{\rho v' w'}\right) \qquad (A.16)$$

ENERGY

$$\frac{1}{h_1 h_2 h_3}\left[(h_2 h_3 \widetilde{\rho u h})_\xi + (h_1 h_3 \widetilde{\rho v h})_\eta\right] = \frac{1}{h_1}\left(\widetilde{u}\bar{p}_\xi + \overline{u' p}_\xi\right) + \frac{1}{h_2}\left(\widetilde{v}\bar{p}_\eta + \overline{v' p}_\eta\right)$$

$$+ \frac{1}{h_3}\overline{w' p}_\theta - \frac{1}{h_1 h_2 h_3}\left\{\left[h_2 h_3\left(\bar{q}_1 + \overline{\rho u' h'}\right)\right]_\xi\right.$$

$$\left. + \left[h_1 h_3\left(\bar{q}_2 + \overline{\rho v' h'}\right)\right]_\eta\right\} + \varphi_L \qquad (A.17)$$

Because of the inherently three-dimensional nature of turbulence, there are correlation terms involving w' appearing in these two-dimensional mean flow equations. In fact, at this point, the θ-momentum equation has not been completely eliminated.

Following the experimental and order-of-magnitude arguments of Reference 43, several assumptions are now made.

1. Fluctuations in pressure, viscosity, thermal conductivity, and specific heat are neglected.

2. Triple correlations are neglected. This gives

$$\overline{\rho u'^2} = \bar{\rho}\,\overline{u'^2}$$

$$\overline{\rho u' v'} = \bar{\rho}\,\overline{u' v'}$$

etc.

ORIGINAL PAGE IS
OF POOR QUALITY

3. Tildes can be replaced by overbars on u, h, and T, but not on v. Thus,

$$\tilde{u} = \bar{u}$$

$$\tilde{h} = \bar{h}$$

$$\tilde{T} = \bar{T}$$

$$\tilde{v} = \bar{v} + \frac{\overline{\rho'' v''}}{\bar{\rho}}$$

Assuming $\tilde{T} = \bar{T}$ also means that the time averaged equation of state for a perfect gas, given by

$$\bar{p} = R\,\overline{\rho T}$$

can be written as

$$\bar{p} = R\,\bar{\rho}\,\bar{T} \tag{A.18}$$

The energy equation can be modified by using the definition of enthalpy,

$$\bar{h} = \bar{e} + \frac{\bar{p}}{\bar{\rho}} \tag{A.19}$$

where $\bar{e}$ is specific internal energy, and then replacing $\frac{\partial \bar{e}}{\partial \zeta}$ and $\frac{\partial \bar{e}}{\partial \eta}$ with $c_v \frac{\partial \bar{T}}{\partial \zeta}$ and $c_v \frac{\partial \bar{T}}{\partial \eta}$. Note that this does not imply constant c_v, only a perfect gas.

The $\overline{u'p_\zeta}$ and $\overline{v'p_\eta}$ terms can be eliminated using the momentum equations. When this is done, several turbulence terms appear that are analagous to the terms in the viscous dissipation, φ_L (Ref. 76). Together, these terms are called the apparent dissipation, φ_T.

ORIGINAL PAGE IS
OF POOR QUALITY

The continuity equation can be used to eliminate the ρ derivatives in the energy equation and to write the momentum and energy equations in nonconservative form. When all of this is done, equations (A.13)-(A.17) become:

CONTINUITY

$$\frac{1}{h_1 h_2 h_3}\left[(h_2 h_3 \bar{\rho}\,\tilde{u})_\xi + (h_1 h_3 \bar{\rho}\tilde{v})_n\right] = 0 \qquad \text{(A.20)}$$

ξ-MOMENTUM

$$\frac{1}{h_1}\bar{\rho}\,\tilde{u}\,\tilde{u}_\xi + \frac{1}{h_2}\bar{\rho}\,\tilde{v}\,\tilde{u}_n - \frac{h_{2_\xi}}{h_1 h_2}\bar{\rho}\tilde{v}^2 + \frac{h_{1_n}}{h_1 h_2}\bar{\rho}\,\widetilde{uv} = -\frac{1}{h_1}\bar{p}_\xi + \frac{1}{h_1 h_2 h_3}$$

$$\times\left\{\left[h_2 h_3\left(\bar{\tau}_{11} - \bar{\rho}\,\overline{u''^2}\right)\right]_\xi + \left[h_1 h_3\left(\bar{\tau}_{21} - \bar{\rho}\,\overline{u''v''}\right)\right]_n\right\} + \frac{h_{1_n}}{h_1 h_2}$$

$$\times\left(\bar{\tau}_{12} - \bar{\rho}\,\overline{u''v''}\right) - \frac{h_{2_\xi}}{h_1 h_2}\left(\bar{\tau}_{22} - \bar{\rho}\,\overline{v''^2}\right) - \frac{h_{3_\xi}}{h_1 h_3}\left(\bar{\tau}_{33} - \bar{\rho}\,\overline{w''^2}\right) \qquad \text{(A.21)}$$

n-MOMENTUM

$$\frac{1}{h_1}\bar{\rho}\,\widetilde{uv}_\xi + \frac{1}{h_2}\bar{\rho}\tilde{v}\tilde{v}_n + \frac{h_{2_\xi}}{h_1 h_2}\bar{\rho}\,\widetilde{uv} - \frac{h_{1_n}}{h_1 h_2}\bar{\rho}\,\tilde{u}^2 = -\frac{1}{h_2}\bar{p}_n + \frac{1}{h_1 h_2 h_3}$$

$$\times\left\{\left[h_2 h_3\left(\bar{\tau}_{12} - \bar{\rho}\,\overline{u''v''}\right)\right]_\xi + \left[h_1 h_3\left(\bar{\tau}_{22} - \bar{\rho}\,\overline{v''^2}\right)\right]_n\right\}$$

$$+ \frac{h_{2_\xi}}{h_1 h_2}\left(\bar{\tau}_{12} - \bar{\rho}\,\overline{u''v''}\right) - \frac{h_{3_n}}{h_2 h_3}\left(\bar{\tau}_{33} - \bar{\rho}\,\overline{w''^2}\right)$$

$$- \frac{h_{1_n}}{h_1 h_2}\left(\bar{\tau}_{11} - \bar{\rho}\,\overline{u''^2}\right) \qquad \text{(A.22)}$$

ORIGINAL PAGE IS
OF POOR QUALITY

θ-MOMENTUM

$$0 = \frac{1}{h_1 h_2 h_3}\left\{\left[h_2 h_3\left(\bar{\tau}_{13} - \bar{\rho}\,\overline{u'w'}\right)\right]_\xi + \left[h_1 h_3\left(\bar{\tau}_{23} - \bar{\rho}\,\overline{v'w'}\right)\right]_\eta\right\}$$

$$+ \frac{h_{3_\xi}}{h_1 h_3}\left(\bar{\tau}_{31} - \bar{\rho}\,\overline{u'w'}\right) + \frac{h_{3_\eta}}{h_2 h_3}\left(\bar{\tau}_{23} - \bar{\rho}\,\overline{v'w'}\right) \qquad \text{(A.23)}$$

ENERGY

$$\frac{1}{h_1}\bar{\rho}\,\bar{u}c_v\bar{T}_\xi + \frac{1}{h_2}\bar{\rho}\tilde{v}c_v\bar{T}_\eta = -\frac{1}{h_1 h_2 h_3}\bar{p}\left[(h_2 h_3\bar{u})_\xi + (h_1 h_3\tilde{v})_\eta\right]$$

$$- \frac{1}{h_1 h_2 h_3}\left\{\left[h_2 h_3\left(\bar{q}_1 + \bar{\rho}\,\overline{u'h'}\right)\right]_\xi\right.$$

$$\left. + \left[h_1 h_3\left(\bar{q}_2 + \bar{\rho}\,\overline{v'h'}\right)\right]_\eta\right\} + \overline{\varphi_L} + \varphi_T \qquad \text{(A.24)}$$

It is now assumed that the Reynolds stresses ($\bar{\rho}\,\overline{u'v'}$, etc.) can be modeled in exactly the same form as the viscous stresses (τ_{12}, etc.) in equation (A.6), by using a turbulent viscosity μ_T. Thus,

$$\left.\begin{aligned} -\bar{\rho}\,\overline{u'^2} &= 2\mu_T\left(\frac{1}{h_1}\bar{u}_\xi + \frac{h_{1_\eta}}{h_1 h_2}\tilde{v}\right) - \frac{2}{3}\mu_T\,\nabla\cdot\vec{V} \\ -\bar{\rho}\,\overline{u'v'} &= \mu_T\left[\frac{h_2}{h_1}\left(\frac{\tilde{v}}{h_2}\right)_\xi + \frac{h_1}{h_2}\left(\frac{\bar{u}}{h_1}\right)_\eta\right] \end{aligned}\right\} \qquad \text{(A.25)}$$

etc. The turbulent viscosity is defined by

$$\mu_T = \bar{\rho}\,\varepsilon \qquad \text{(A.26)}$$

where ε is an eddy viscosity which comes from some appropriate turbulence model. Note that this formulation assumes the eddy viscosity

ORIGINAL PAGE IS
OF POOR QUALITY

is an isotropic scalar. At this point, the θ-momentum equation drops out for two-dimensional flow. It is also assumed that the turbulent heat fluxes ($\bar{\rho}\,\overline{u'h'}$ and $\bar{\rho}\,\overline{v'h'}$) in the energy equation can be modeled in the same form as the molecular heat fluxes (q_1 and q_2) in equation (A.7) by using a turbulent thermal conductivity, k_T. Thus,

$$\left.\begin{aligned} -\bar{\rho}\,\overline{u'h'} &= -\frac{1}{h_1}\,k_T\,\frac{\partial T}{\partial \xi} \\ -\bar{\rho}\,\overline{v'h'} &= -\frac{1}{h_2}\,k_T\,\frac{\partial T}{\partial n} \end{aligned}\right\} \qquad (A.27)$$

where

$$k_T = \frac{c_p \mu_T}{Pr_T} \qquad (A.28)$$

When these modeling assumptions are incorporated into equations (A.20)-(A.22) and (A.24), and the overbars and tildes dropped for simplicity, the results are as follows:

CONTINUITY

$$\frac{1}{h_1 h_2 h_3}\left[(h_2 h_3 \rho u)_\xi + (h_1 h_3 \rho v)_n\right] = 0 \qquad (A.29)$$

STREAMWISE MOMENTUM

$$\frac{1}{h_1}\,\rho u u_\xi + \frac{1}{h_2}\,\rho v u_n - \frac{h_{2_\xi}}{h_1 h_2}\,\rho v^2 + \frac{h_{1_n}}{h_1 h_2}\,\rho u v = -\frac{1}{h_1}\,p_\xi + \frac{1}{h_1 h_2 h_3}$$

$$\times\left[\left(h_2 h_3 \tau E_{11}\right)_\xi + \left(h_1 h_3 \tau E_{12}\right)_n\right] + \frac{h_{1_n}}{h_1 h_2}\,\tau E_{12}$$

$$-\frac{h_{2_\xi}}{h_1 h_2}\,\tau E_{22} - \frac{h_{3_\xi}}{h_1 h_3}\,\tau E_{33} \qquad (A.30)$$

ORIGINAL PAGE IS
OF POOR QUALITY

CROSS-FLOW MOMENTUM

$$\frac{1}{h_1}\rho u v_\xi + \frac{1}{h_2}\rho v v_\eta + \frac{h_{2_\xi}}{h_1 h_2}\rho u v - \frac{h_{1_\eta}}{h_1 h_2}\rho u^2 = -\frac{1}{h_2}p_\eta + \frac{1}{h_1 h_2 h_3}$$

$$\times \left[\left(h_2 h_3 \tau_{E_{12}}\right)_\xi + \left(h_1 h_3 \tau_{E_{22}}\right)_\eta\right] + \frac{h_{2_\xi}}{h_1 h_2}\tau_{E_{12}}$$

$$- \frac{h_{3_\eta}}{h_2 h_3}\tau_{E_{33}} - \frac{h_{1_\eta}}{h_1 h_2}\tau_{E_{11}} \qquad \text{(A.31)}$$

ENERGY

$$\frac{1}{h_1}\rho u c_v T_\xi + \frac{1}{h_2}\rho v c_v T_\eta = -\frac{1}{h_1 h_2 h_3}p\left[(h_2 h_3 u)_\xi + (h_1 h_3 v)_\eta\right]$$

$$- \frac{1}{h_1 h_2 h_3}\left[\left(h_2 h_3 q_{E_1}\right)_\xi + \left(h_1 h_3 q_{E_2}\right)_\eta\right] + \varphi_E \qquad \text{(A.32)}$$

APPENDIX B

ORDER-OF-MAGNITUDE ANALYSIS

In order to use a forward marching solution procedure, second derivatives in the ξ direction, which appear in the shear stress terms, must be eliminated. An order-of-magnitude analysis is used to show that this is justified. First, it is assumed that the flow is primarily in the ξ direction. Thus v, the velocity in the η direction, is assumed to be of order δ. (Here δ is taken to be a small number representing the order-of-magnitude difference between the streamwise and cross-flow velocities. It is not necessarily a boundary layer thickness, since, in this internal flow analysis, viscous terms are included throughout the flowfield and the boundary layers can grow to fill the duct.) It is expected that gradients normal to the walls will be greater than gradients in the streamwise direction. Therefore, derivatives in the η direction are assumed to be of order $1/\delta$. In order to make the largest viscous term the same order as the convective terms, the effective viscosity μ_E is set equal to order δ^2. (Equivalently, the Reynolds number is assumed to be of order $1/\delta^2$.) Similarly, k_E is also set equal to order δ^2. All other terms, including the metric coefficients and their derivatives, are set equal to order 1.

ORIGINAL PAGE IS
OF POOR QUALITY

With these assumptions, the magnitude of the effective shear stresses can be estimated as shown below. The order of magnitude is written below each term.

$$\left.\begin{aligned}
\tau_{E_{11}} &= \underbrace{2\mu_E}_{\delta^2}\left(\underbrace{\frac{1}{h_1}\frac{\partial u}{\partial \xi}}_{1} + \underbrace{\frac{h_{1_\eta}}{h_1 h_2} v}_{\delta}\right) - \frac{2}{3}\mu_E \nabla \cdot \vec{V} \\
\tau_{E_{22}} &= \underbrace{2\mu_E}_{\delta^2}\left(\underbrace{\frac{1}{h_2}\frac{\partial v}{\partial \eta}}_{1} + \underbrace{\frac{h_{2_\xi}}{h_1 h_2} u}_{1}\right) - \frac{2}{3}\mu_E \nabla \cdot \vec{V} \\
\tau_{E_{33}} &= \underbrace{2\mu_E}_{\delta^2}\left(\underbrace{\frac{h_{3_\xi}}{h_1 h_3} u}_{1} + \underbrace{\frac{h_{3_\eta}}{h_2 h_3} v}_{\delta}\right) - \frac{2}{3}\mu_E \nabla \cdot \vec{V} \\
\tau_{E_{12}} &= \tau_{E_{21}} = \underbrace{\mu_E}_{\delta^2}\left[\underbrace{\frac{h_2}{h_1}\frac{\partial}{\partial \xi}\left(\frac{v}{h_2}\right)}_{\delta} + \underbrace{\frac{h_1}{h_2}\frac{\partial}{\partial \eta}\left(\frac{u}{h_1}\right)}_{1/\delta}\right]
\end{aligned}\right\} \quad (B.1)$$

where

$$-\frac{2}{3}\mu_E \nabla \cdot \vec{V} = -\frac{2}{3}\underbrace{\mu_E}_{\delta^2}\frac{1}{h_1 h_2 h_3}\left[\underbrace{\frac{\partial}{\partial \xi}(h_2 h_3 u)}_{1} + \underbrace{\frac{\partial}{\partial \eta}(h_1 h_3 v)}_{1/\delta \quad \delta}\right]$$

Therefore

ORIGINAL PAGE IS
OF POOR QUALITY

$$\left.\begin{aligned} \tau_{E_{11}} &= O(\delta^2) + O(\delta^3) \\ \tau_{E_{22}} &= O(\delta^2) \\ \tau_{E_{33}} &= O(\delta^2) + O(\delta^3) \\ \tau_{E_{12}} = \tau_{E_{21}} &= O(\delta) + O(\delta^3) \end{aligned}\right\} \qquad (B.2)$$

Then, in the streamwise momentum equation,

$$\left.\begin{aligned} \frac{\partial}{\partial \xi}\left(h_2 h_3 \tau_{E_{11}}\right) &= O(\delta^2) + O(\delta^3) \\ \frac{\partial}{\partial \eta}\left(h_1 h_3 \tau_{E_{12}}\right) &= O(1) + O(\delta^2) \end{aligned}\right\} \qquad (B.3)$$

In the cross-flow momentum equation,

$$\left.\begin{aligned} \frac{\partial}{\partial \xi}\left(h_2 h_3 \tau_{E_{12}}\right) &= O(\delta) + O(\sigma^3) \\ \frac{\partial}{\partial \eta}\left(h_1 h_3 \tau_{E_{22}}\right) &= O(\delta) + O(\delta^2) \end{aligned}\right\} \qquad (B.4)$$

And in the energy equation,

$$\left.\begin{aligned} -\frac{\partial}{\partial \xi}\left(h_2 h_3 q_{E_1}\right) &= \underbrace{\frac{\partial}{\partial \xi}}_{1}\left(\frac{h_2 h_3}{h_1}\underbrace{k_E}_{\delta^2}\underbrace{\frac{\partial T}{\partial \xi}}_{1}\right) = O(\delta^2) \\ -\frac{\partial}{\partial \eta}\left(h_1 h_3 q_{E_2}\right) &= \underbrace{\frac{\partial}{\partial \eta}}_{1/\delta}\left(\frac{h_1 h_3}{h_2}\underbrace{k_E}_{\delta^2}\underbrace{\frac{\partial T}{\partial \eta}}_{1/\delta}\right) = O(1) \end{aligned}\right\} \qquad (B.5)$$

All terms of order 1 and order δ, at least, are to be retained. Therefore, in the streamwise momentum equation, the term $\frac{\partial}{\partial \xi}\left(h_2 h_3 \tau E_{11}\right)$ can be eliminated. In the cross-flow momentum equation, the $\mathcal{O}(\delta^3)$ part of the term $\frac{\partial}{\partial \xi}\left(h_2 h_3 \tau E_{12}\right)$ can also be eliminated. This is enough to eliminate all second derivatives with respect to ξ, and thus allow the use of a marching solution procedure. Many of the other terms are high order and could also be eliminated, but it is not necessary since they can be handled within the framework of a numerical marching procedure.

ORIGINAL PAGE IS
OF POOR QUALITY

APPENDIX C

POTENTIAL FLOW COMPRESSIBILITY CORRECTION

For compressible flow, the incompressible velocity given by equation (2.40) is modified using the Lieblein-Stockman compressibility correction (Ref. 37). This correction was developed specifically for internal flows. The compressible velocity is given by

$$V_C = \left(\frac{\rho_i}{\rho_{C_{AVE}}}\right)^{V_i/V_{i_{AVE}}} V_i \qquad (C.1)$$

where $V_{i_{AVE}}$ is the average incompressible velocity at a given station, ρ_i is the incompressible (or total) density, and $\rho_{C_{AVE}}$ is the average compressible density at a station. One-dimensional isentropic relations are used to get $\rho_i/\rho_{C_{AVE}}$. Thus,

$$\frac{\rho_{C_{AVE}}}{\rho_i} = \left[1 - \frac{\gamma - 1}{2}\left(\frac{V_{C_{AVE}}}{a_0}\right)^2\right]^{1/(\gamma-1)} \qquad (C.2)$$

where a_0 is the total speed of sound. The value of $V_{C_{AVE}}/a_0$ is found from

$$\frac{A^*}{A} = \left(\frac{\gamma + 1}{2}\right)^{(\gamma+1)/[2(\gamma-1)]} \frac{V_{C_{AVE}}}{a_0}\left[1 - \frac{\gamma - 1}{2}\left(\frac{V_{C_{AVE}}}{a_0}\right)^2\right]^{1/(\gamma-1)} \qquad (C.3)$$

ORIGINAL PAGE IS
OF POOR QUALITY

where

$$A^* = \frac{\dot{m}\sqrt{T_0}}{\left[\frac{\gamma}{R}\left(\frac{2}{\gamma+1}\right)^{(\gamma+1)/(\gamma-1)}\right]^{1/2} p_0}$$

Equation (C.3) is solved for $V_{C_{AVE}}/a_0$ by Newton iteration.

APPENDIX D

COUPLED DIFFERENCE EQUATIONS

In this appendix, the governing equations are written in finite-difference form. These equations are the result of the differencing and linearization procedures presented in Sections 3.1 and 3.2. The equations correspond to the differential equations (2.13)-(2.16), with the shear stress and heat flux terms written out in full. Since the equations in this appendix are valid at any j-location in the grid, the "j" subscript has been omitted. In addition, the metric scale coefficients are understood to be at the $(i+w,j)$ grid location, so these subscripts are also omitted. The Δ notation from Section 3.2 is used, so that $\Delta\rho = \rho_{i+1} - \rho_i$, etc. The variable μ_{i+w} in the equations is given by

$$\mu_{i+w} = \mu_i + w\lambda(\mu_i - \mu_{i-1})$$

The subscripts ξ and η denote partial differentiation.

ORIGINAL PAGE IS
OF POOR QUALITY

CONTINUITY

$$\frac{1}{h_1}\left[u_i + w\lambda(u_i - u_{i-1})\right]\frac{\rho_{i+1} - \rho_i}{\Delta\xi} + \frac{1}{h_1}\left[\rho_i + w\lambda(\rho_i - \rho_{i-1})\right]\frac{u_{i+1} - u_i}{\Delta\xi}$$

$$+ \frac{1}{h_2}\frac{d\gamma}{d\eta}\left[\delta_\gamma(\rho v)_i + w\delta_\gamma(v_i\,\Delta\rho + \rho_i\,\Delta v)\right]$$

$$+ \frac{1}{h_1 h_2 h_3}\left\{(h_2 h_3)_\xi\left[\rho_i u_i + w(\rho_i\,\Delta u + u_i\,\Delta\rho)\right]\right.$$

$$\left. + (h_1 h_3)_\eta\left[\rho_i v_i + w(\rho_i\,\Delta v + v_i\,\Delta\rho)\right]\right\} = 0 \qquad (D.1)$$

STREAMWISE MOMENTUM

$$\frac{1}{h_1}\left[\rho_i u_i + w\lambda(\rho_i u_i - \rho_{i-1}u_{i-1})\right]\frac{u_{i+1} - u_i}{\Delta\xi} + \frac{1}{h_2}\frac{d\gamma}{d\eta}\left[\rho_i v_i\,\delta_\gamma u_i + w\right.$$

$$\left. \times (v_i\,\Delta\rho + \rho_i\,\Delta v)\delta_\gamma u_i + w\rho_i v_i\,\delta_\gamma(\Delta u)\right] - \frac{h_{2_\xi}}{h_1 h_2}\left[\rho_i v_i^2 + w\left(v_i^2\,\Delta\rho\right.\right.$$

$$\left.\left. + 2\rho_i v_i\,\Delta v\right)\right] + \frac{h_{1_\eta}}{h_1 h_2}\left[\rho_i u_i v_i + w(u_i v_i\,\Delta\rho + \rho_i v_i\,\Delta u + \rho_i u_i\,\Delta v)\right]$$

$$= -\frac{1}{h_1}(p_\xi + p'_\xi)_{i+w} + \frac{1}{Re_r}\frac{1}{h_1 h_2 h_3}\left[h_3\frac{d\gamma}{d\eta}\left[\mu_{i+w}\,\delta_\gamma\left(\frac{v_{i+1} - v_i}{\Delta\xi}\right)\right.\right.$$

$$\left.\left. + (\delta_\gamma\mu_{i+w})\frac{v_{i+1} - v_i}{\Delta\xi}\right] + h_{3_\eta}\mu_{i+1}\frac{v_{i+1} - v_i}{\Delta\xi} - \frac{h_3 h_{2_\xi}}{h_2}\frac{d\gamma}{d\eta}\right.$$

$$\left.\times\left\{\delta_\gamma(\mu v)_i + w\left[\mu_i\,\delta_\gamma(\Delta v) + (\delta_\gamma\mu_i)\Delta v + \left(\frac{d\mu}{dT}\right)_1 v_i\,\delta_\gamma(\Delta T)\right.\right.\right.$$

Continued on next page

ORIGINAL PAGE IS
OF POOR QUALITY

$$+ \delta_\gamma \left(\frac{d\mu}{dT} v\right)_i \Delta T \Big]\Big\} - \left(\frac{h_3 h_{2\xi}}{h_2}\right)_n \left\{\mu_i v_i + w\left[\mu_i \Delta v + \left(\frac{d\mu}{dT}\right)_i v_i \Delta T\right]\right\}$$

$$+ \frac{h_1 h_3}{h_2} \frac{d\gamma}{dn} \left\{\delta_\gamma \left(\frac{d\gamma}{dn} \mu_i \delta_\gamma u_i\right) + w \frac{d\gamma}{dn} \left(\frac{d\mu}{dT}\right)_i (\delta_\gamma u_i) \delta_\gamma(\Delta T) + w \delta_\gamma \right.$$

$$\left. \times \left[\frac{d\gamma}{dn} \left(\frac{d\mu}{dT}\right)_i \delta_\gamma u_i\right] \Delta T + w \frac{d\gamma}{dn} \mu_i \delta_\gamma^2(\Delta u) + w \delta_\gamma \left(\frac{d\gamma}{dn} \mu_i\right) \delta_\gamma(\Delta u)\right\}$$

$$+ \left(\frac{h_1 h_3}{h_2}\right)_n \frac{d\gamma}{dn}\left[\mu_i \delta_\gamma u_i + w \left(\frac{d\mu}{dT}\right)_i (\delta_\gamma u)_i \Delta T + w \mu_i \delta_\gamma(\Delta u)\right]$$

$$- \frac{h_3 h_{1n}}{h_2} \frac{d\gamma}{dn} \left\{\delta_\gamma(\mu u)_i + w\left[\mu_i \delta_\gamma(\Delta u) + (\delta_\gamma \mu_i)\Delta u + \left(\frac{d\mu}{dT}\right)_i u_i \delta_\gamma(\Delta T)\right.\right.$$

$$\left.\left. + \delta_\gamma \left(\frac{d\mu}{dT} u\right)_i \Delta T\right]\right\} - \left(\frac{h_3 h_{1n}}{h_2}\right)_n \left\{\mu_i u_i + w\left[\mu_i \Delta u + \left(\frac{d\mu}{dT}\right)_i u_i \Delta T\right]\right\} \Bigg]$$

$$+ \frac{1}{Re_r} \frac{h_{1n}}{h_1 h_2} \Bigg[\frac{1}{h_1} \mu_{i+w} \frac{v_{i+1} - v_i}{\Delta\xi} - \frac{h_{2\xi}}{h_1 h_2} \left\{\mu_i v_i + w\left[\mu_i \Delta v\right.\right.$$

$$\left.\left. + \left(\frac{d\mu}{dT}\right)_i v_i \Delta T\right]\right\} + \frac{1}{h_2} \frac{d\gamma}{dn}\left[\mu_i \delta_\gamma u_i + w \left(\frac{d\mu}{dT}\right)_i (\delta_\gamma u_i)\Delta T\right.$$

$$\left. + w\mu_i \delta_\gamma(\Delta u)\right] - \frac{h_{1n}}{h_1 h_2} \left\{\mu_i u_i + w\left[\mu_i \Delta u + \left(\frac{d\mu}{dT}\right)_i u_i \Delta T\right]\right\}\Bigg]$$

$$- \frac{1}{Re_r} \frac{h_{2\xi}}{h_1 h_2} \Bigg[\frac{4}{3} \frac{1}{h_2} \frac{d\gamma}{dn}\left[\mu_i \delta_\gamma v_i + w \left(\frac{d\mu}{dT}\right)_i (\delta_\gamma v)_i \Delta T + w\mu_i \delta_\gamma(\Delta v)\right]$$

Continued on next page

ORIGINAL PAGE IS
OF POOR QUALITY

$$- \frac{2}{3}\frac{1}{h_2}\left(\frac{h_{1_\eta}}{h_1} + \frac{h_{3_\eta}}{h_3}\right)\left\{\mu_i v_i + w\left[\mu_i\,\Delta v + \left(\frac{d\mu}{dT}\right)_i v_i\,\Delta T\right]\right\} - \frac{2}{3}\frac{1}{h_1}\mu_{i+w}$$

$$\times \frac{u_{i+1} - u_i}{\Delta\xi} + \frac{2}{3}\frac{1}{h_1}\left(2\frac{h_{2_\xi}}{h_2} - \frac{h_{3_\xi}}{h_3}\right)\left\{\mu_i u_i + w\left[\mu_i\,\Delta u\right.\right.$$

$$\left.\left. + \left(\frac{d\mu}{dT}\right)_i u_i\,\Delta T\right]\right\}\Bigg] - \frac{1}{Re_r}\frac{h_{3_\xi}}{h_1 h_3}\Bigg[-\frac{2}{3}\frac{1}{h_1}\mu_{i+w}\frac{u_{i+1} - u_i}{\Delta\xi} + \frac{2}{3}\frac{1}{h_1}$$

$$\times \left(2\frac{h_{3_\xi}}{h_3} - \frac{h_{2_\xi}}{h_2}\right)\left\{\mu_i u_i + w\left[\mu_i\,\Delta u + \left(\frac{d\mu}{dT}\right)_i u_i\,\Delta T\right]\right\} - \frac{2}{3}\frac{1}{h_2}\frac{dY}{d\eta}$$

$$\times \left[\mu_i\,\delta_Y v_i + w\left(\frac{d\mu}{dT}\right)_i(\delta_Y v_i)\Delta T + w\mu_i\,\delta_Y(\Delta v)\right] + \frac{2}{3}\frac{1}{h_2}\left(2\frac{h_{3_\eta}}{h_3}\right.$$

$$\left. - \frac{h_{1_\eta}}{h_1}\right)\left\{\mu_i v_i + w\left[\mu_i\,\Delta v + \left(\frac{d\mu}{dT}\right)_i v_i\,\Delta T\right]\right\}\Bigg] \qquad (D.2)$$

CROSS-FLOW MOMENTUM

$$\frac{1}{h_1}\left[\rho_i u_i + w\lambda(\rho_i u_i - \rho_{i-1}u_{i-1})\right]\frac{v_{i+1} - v_i}{\Delta\xi} + \frac{1}{h_2}\frac{dY}{d\eta}\left[\rho_i v_i\,\delta_Y v_i + w\right.$$

$$\times (v_i\,\Delta\rho + \rho_i\,\Delta v)\delta_Y v_i + w\rho_i v_i\,\delta_Y(\Delta v)\Big] + \frac{h_{2_\xi}}{h_1 h_2}\left[\rho_i u_i v_i + w\right.$$

$$\times (u_i v_i\,\Delta\rho + \rho_i v_i\,\Delta u + u_i\,\Delta v)\Big] - \frac{h_{1_\eta}}{h_1 h_2}\left[\rho_i u_i^2 + w\left(u_i^2\,\Delta\rho\right.\right.$$

Continued on next page

ORIGINAL PAGE IS OF POOR QUALITY

$$+ 2\rho_i u_i\,\Delta u)\Big] = -\frac{1}{h_2}\frac{dY}{d\eta} R\left[\delta_Y(\rho T)_i + w\,\delta_Y(\rho_i \Delta T + T_i \Delta\rho)\right]$$

$$+ \frac{1}{Re_r}\frac{1}{h_1 h_2 h_3}\Bigg[h_3\frac{dY}{d\eta}\left\{\left[\left(\frac{d\mu}{dT}\,\delta_Y u\right)_i + w\lambda\left(\left(\frac{d\mu}{dT}\right)_i \delta_Y u_i - \left(\frac{d\mu}{dT}\right)_{i-1}\right.\right.\right.$$

$$\left.\left.\left.\times\,\delta_Y u_{i-1}\right)\right]\frac{T_{i+1} - T_i}{\Delta\xi} + \mu_{i+w}\,\delta_Y\left(\frac{u_{i+1} - u_i}{\Delta\xi}\right)\right\} + h_{3_\xi}\frac{dY}{d\eta}$$

$$\times\left[(\mu\,\delta_Y u)_i + w\left(\frac{d\mu}{dT}\right)_i (\delta_Y u)_i\,\Delta T + w\mu_i\,\delta_Y(\Delta u)\right] - \frac{h_3 h_{1_\eta}}{h_1}$$

$$\times\left\{\mu_{i+w}\frac{u_{i+1} - u_i}{\Delta\xi} + \left[\left(\frac{d\mu}{dT}\right)_i u_i + w\lambda\left(\left(\frac{d\mu}{dT}\right)_i u_i - \left(\frac{d\mu}{dT}\right)_{i-1} u_{i-1}\right)\right]\right.$$

$$\left.\times\,\frac{T_{i+1} - T_i}{\Delta\xi}\right\} - \left(\frac{h_3 h_1}{h_1}\right)_\xi\left\{\mu_i u_i + w\left[\mu_i\,\Delta u + \left(\frac{d\mu}{dT}\right)_i u_i\,\Delta T\right]\right\}\Bigg]$$

$$+ \frac{1}{Re_r}\frac{1}{h_1 h_2 h_3}\Bigg[\frac{4}{3}\frac{h_1 h_3}{h_2}\frac{dY}{d\eta}\left\{\delta_Y\left(\frac{dY}{d\eta}\,\mu_i\,\delta_Y v_i\right) + w\frac{dY}{d\eta}\left(\frac{d\mu}{dT}\right)_i\right.$$

$$\times\,(\delta_Y v_i)\delta_Y(\Delta T) + w\,\delta_Y\left[\frac{dY}{d\eta}\left(\frac{d\mu}{dT}\right)_i\,\delta_Y v_i\right]\Delta T + w\frac{dY}{d\eta}\,\mu_i\,\delta_Y^2(\Delta v)$$

$$\left.+ w\,\delta_Y\left(\frac{dY}{d\eta}\,\mu_i\right)\delta_Y(\Delta v)\right\} + \frac{4}{3}\left(\frac{h_1 h_3}{h_2}\right)_\eta\frac{dY}{d\eta}\left[\mu_i\,\delta_Y v_i + w\left(\frac{d\mu}{dT}\right)_i\right.$$

$$\left.\times\,(\delta_Y v)_i\,\Delta T + w\mu_i\,\delta_Y(\Delta v)\right] - \frac{2}{3}\frac{h_1 h_3}{h_2}\left(\frac{h_{1_\eta}}{h_1} + \frac{h_{3_\eta}}{h_3}\right)\frac{dY}{d\eta}$$

Continued on next page

ORIGINAL PAGE IS
OF POOR QUALITY

$$x\left\{\delta_\gamma(\mu v)_i + w\left[\mu_i\,\delta_\gamma(\Delta v) + (\delta_\gamma\mu_i)\Delta v + \left(\frac{d\mu}{dT}\right)_i v_i\,\delta_\gamma(\Delta T)\right.\right.$$

$$\left.\left. + \delta_\gamma\left(\frac{d\mu}{dT}\,v\right)_i \Delta T\right]\right\} - \frac{2}{3}\left[\frac{h_1 h_3}{h_2}\left(\frac{h_{1_\eta}}{h_1} + \frac{h_{3_\eta}}{h_3}\right)\right]_\eta \left\{\mu_i v_i + w\right.$$

$$\left.\times\left[\mu_i\,\Delta v + \left(\frac{d\mu}{dT}\right)_i v_i\,\Delta T\right]\right\} - \frac{2}{3}\,h_3\,\frac{d\gamma}{d\eta}\left[\mu_{i+w}\,\delta_\gamma\left(\frac{u_{i+1} - u_i}{\Delta\xi}\right)\right.$$

$$\left. + (\delta_\gamma\mu_{i+w})\,\frac{u_{i+1} - u_i}{\Delta\xi}\right] - \frac{2}{3}\,h_{3_\eta}\,\mu_{i+w}\,\frac{u_{i+1} - u_i}{\Delta\xi} + \frac{2}{3}\,h_3$$

$$\times\left(2\,\frac{h_{2_\xi}}{h_2} - \frac{h_{3_\xi}}{h_3}\right)\frac{d\gamma}{d\eta}\left\{\delta_\gamma(\mu u)_i + w\left[\mu_i\,\delta_\gamma(\Delta u) + (\delta_\gamma\mu_i)\Delta u\right.\right.$$

$$\left.\left. + \left(\frac{d\mu}{dT}\right)_i u_i\,\delta_\gamma(\Delta T) + \delta_\gamma\left(\frac{d\mu}{dT}\,u\right)_i \Delta T\right]\right\} + \frac{2}{3}\left[h_3\left(2\,\frac{h_{2_\xi}}{h_2} - \frac{h_{3_\xi}}{h_3}\right)\right]_\eta$$

$$\times\left\{\mu_i u_i + w\left[\mu_i\,\Delta u + \left(\frac{d\mu}{dT}\right)_i u_i\,\Delta T\right]\right\}\Bigg] + \frac{1}{Re_r}\,\frac{h_{2_\xi}}{h_1 h_2}\left[\frac{1}{h_1}\,\mu_{i+w}\,\frac{v_{i+1} - v_i}{\Delta\xi}\right.$$

$$\left. - \frac{h_{2_\xi}}{h_1 h_2}\left\{\mu_i v_i + w\left[\mu_i\,\Delta v + \left(\frac{d\mu}{dT}\right)_i v_i\,\Delta T\right]\right\} + \frac{1}{h_2}\,\frac{d\gamma}{d\eta}\left[\mu_i\,\delta_\gamma u_i\right.\right.$$

$$\left.\left. + w\left(\frac{d\mu}{dT}\right)_i(\delta_\gamma u_i)\Delta T + w\mu_i\,\delta_\gamma(\Delta u)\right] - \frac{h_{1_\eta}}{h_1 h_2}\left\{\mu_i u_i + w\left[\mu_i\,\Delta u\right.\right.\right.$$

Continued on next page

ORIGINAL PAGE IS
OF POOR QUALITY

$$+\left(\frac{d\mu}{dT}\right)_i u_i\ \Delta T\Big]\Big\}\Big] - \frac{1}{Re_r}\frac{h_{3_\eta}}{h_2 h_3}\Big[-\frac{2}{3}\frac{1}{h_1}\mu_{i+w}\frac{u_{i+1}-u_i}{\Delta\xi}+\frac{2}{3}\frac{1}{h_1}$$

$$\times\left(2\frac{h_{3_\xi}}{h_3}-\frac{h_{2_\xi}}{h_2}\right)\Big\{\mu_i u_i + w\Big[\mu_i\ \Delta u+\left(\frac{d\mu}{dT}\right)_i u_i\ \Delta T\Big]\Big\} - \frac{2}{3}\frac{1}{h_2}\frac{dY}{d\eta}$$

$$\times\Big[\mu_i\ \delta_Y v_i + w\left(\frac{d\mu}{dT}\right)_i(\delta_Y v_i)\Delta T + w\mu_i\ \delta_Y(\Delta v)\Big] + \frac{2}{3}\frac{1}{h_2}\left(2\frac{h_{3_\eta}}{h_3}\right.$$

$$\left.-\frac{h_{1_\eta}}{h_1}\right)\Big\{\mu_i v_i + w\Big[\mu_i\ \Delta v+\left(\frac{d\mu}{dT}\right)_i v_i\ \Delta T\Big]\Big\}\Big] \qquad (D.3)$$

ENERGY

$$\frac{1}{h_1}\Big[\rho_i u_i c_{v_i} + w\lambda\left(\rho_i u_i c_{v_i} - \rho_{i-1}u_{i-1}c_{v_{i-1}}\right)\Big]\frac{T_{i+1}-T_i}{\Delta\xi}+\frac{1}{h_2}\frac{dY}{d\eta}$$

$$\times\Big\{\rho_i v_i c_{v_i}\ \delta_Y T_i + w\Big[v_i c_{v_i}\ \Delta\rho + \rho_i c_{v_i}\ \Delta v + \rho_i v_i\left(\frac{dc_v}{dT}\right)_i\ \Delta T\Big]$$

$$\times\ \delta_Y T_i + w\rho_i v_i c_{v_i}\ \delta_Y(\Delta T)\Big\} = -\frac{1}{h_1 h_2 h_3}R\Big\{h_2 h_3\Big[\rho_i T_i + w\lambda(\rho_i T_i$$

$$-\rho_{i-1}T_{i-1})\Big]\frac{u_{i+1}-u_i}{\Delta\xi} + h_1 h_3\frac{dY}{d\eta}\Big[\rho_i T_i\ \delta_Y v_i + w(T_i\ \Delta\rho + \rho_i\ \Delta T)$$

$$\times\ \delta_Y v_i + w\rho_i T_i\ \delta_Y(\Delta v)\Big] + (h_2 h_3)_\xi\Big[\rho_i T_i u_i + w(T_i u_i\ \Delta\rho + \rho_i T_i\ \Delta u$$

$$+\rho_i u_i\ \Delta T)\Big] + (h_1 h_3)_\eta\Big[\rho_i T_i v_i + w(T_i v_i\ \Delta\rho + \rho_i T_i\ \Delta v + \rho_i v_i\ \Delta T)\Big]\Big\}$$

Continued on next page

ORIGINAL PAGE IS
OF POOR QUALITY

$$+ \frac{1}{Re_r Pr_r} \frac{1}{h_1 h_2 h_3}\left[\frac{h_1 h_3}{h_2}\frac{dY}{d\eta}\left\{\delta_Y\left(\frac{dY}{d\eta}\, k_i \delta_Y T_i\right) + w\frac{dY}{d\eta}\left(\frac{dk}{dT}\right)_i (\delta_Y T_i)\delta_Y(\Delta T)\right.\right.$$

$$+ w\,\delta_Y\left[\frac{dY}{d\eta}\left(\frac{dk}{dT}\right)_i \delta_Y T_i\right]\Delta T + w\frac{dY}{d\eta}\, k_i\, \delta_Y^2(\Delta T) + w\,\delta_Y\left(\frac{dY}{d\eta}\, k_i\right)\delta_Y(\Delta T)\Big\}$$

$$\left.+\left(\frac{h_1 h_3}{h_2}\right)_\eta \frac{dY}{d\eta}\left[k_i\,\delta_Y T_i + w\left(\frac{dk}{dT}\right)_i (\delta_Y T_i)\Delta T + wk_i\,\delta_Y(\Delta T)\right]\right] + \frac{1}{Re_r}\varphi_E \qquad (D.4)$$

By expanding the Δ and δ_y operators, and after much collecting of terms, these equations can be written in the following forms. The dependent variables in equations (D.5)-(D.8) are at the unknown i+1 station, and the "i+1" subscript has been omitted.

CONTINUITY

$$C_{C_1}\rho_{j-1} + C_{C_2}\rho_j + C_{C_3}\rho_{j+1} + C_{C_4}u_{j-1} + C_{C_5}u_j + C_{C_6}u_{j+1} + C_{C_7}v_{j-1}$$

$$+ C_{C_8}v_j + C_{C_9}v_{j+1} + C_{C_{10}}T_{j-1} + C_{C_{11}}T_j + C_{C_{12}}T_{j+1} = S_C \qquad (D.5)$$

where

$$C_{C_1} = -\frac{1}{h_2}\frac{dY}{d\eta}\, wv_i\, \frac{\Delta\xi}{2\Delta Y}$$

$$C_{C_2} = \frac{1}{h_1}\left[u_i + w\lambda(u_i - u_{i-1})\right] + \frac{1}{h_2}\frac{dY}{d\eta}\, w(\delta_Y v_i)\Delta\xi + \frac{1}{h_1 h_2 h_3}\left[(h_2 h_3)_\xi wu_i\right.$$

$$\left. + (h_1 h_3)_\eta wv_i\right]\Delta\xi$$

$$C_{C_3} = -C_{C_1}$$

$$C_{C_4} = 0$$

ORIGINAL PAGE IS
OF POOR QUALITY

$$C_{C_5} = \frac{1}{h_1}\left[\rho_i + w\lambda(\rho_i - \rho_{i-1})\right] + \frac{1}{h_1 h_2 h_3}(h_2 h_3)_\xi w\rho_i \,\Delta\xi$$

$$C_{C_6} = 0$$

$$C_{C_7} = -\frac{1}{h_2}\frac{dY}{d\eta} w\rho_i \frac{\Delta\xi}{2\Delta Y}$$

$$C_{C_8} = \frac{1}{h_2}\frac{dY}{d\eta} w(\delta_Y \rho_i)\Delta\xi + \frac{1}{h_1 h_2 h_3}(h_1 h_3)_\eta w\rho_i \,\Delta\xi$$

$$C_{C_9} = -C_{C_7}$$

$$C_{C_{10}} = C_{C_{11}} = C_{C_{12}} = 0$$

$$S_C = \frac{1}{h_1}\left[u_i + w\lambda(u_i - u_{i-1})\right]\rho_i + \frac{1}{h_1}\left[\rho_i + w\lambda(\rho_i - \rho_{i-1})\right]u_i - \frac{1}{h_2}\frac{dY}{d\eta}$$

$$\times (1 - 2w)\delta_Y(\rho v)_i \,\Delta\xi - \frac{1}{h_1 h_2 h_3}\left[(h_2 h_3)_\xi (1 - 2w)\rho_i u_i + (h_2 h_3)_\eta\right.$$

$$\left.\times (1 - 2w)\rho_i v_i\right]\Delta\xi$$

STREAMWISE MOMENTUM

$$C_{X_1}\rho_{j-1} + C_{X_2}\rho_j + C_{X_3}\rho_{j+1} + C_{X_4}u_{j-1} + C_{X_5}u_j + C_{X_6}u_{j+1} + C_{X_7}v_{j-1}$$

$$+ C_{X_8}v_j + C_{X_9}v_{j+1} + C_{X_{10}}T_{j-1} + C_{X_{11}}T_j + C_{X_{12}}T_{j+1} = S_X \qquad (D.6)$$

where

$$C_{X_1} = 0$$

$$C_{X_2} = \frac{1}{h_2}\frac{dY}{d\eta} wv_i(\delta_Y u_i)\Delta\xi - \frac{h_{2_\xi}}{h_1 h_2} wv_i^2 \,\Delta\xi + \frac{h_{1_\eta}}{h_1 h_2} wu_i v_i \,\Delta\xi$$

$$C_{X_3} = 0$$

ORIGINAL PAGE IS
OF POOR QUALITY

$$C_{X_4} = -\frac{1}{h_2}\frac{dY}{d\eta} w\rho_i v_i \frac{\Delta\xi}{2\Delta Y} + \frac{1}{Re_r}\frac{1}{h_1 h_2 h_3}\frac{dY}{d\eta} w\left[\frac{h_1 h_3}{h_2}\delta_Y\left(\frac{dY}{d\eta}\mu_i\right)\right.$$

$$\left. + \left(\frac{h_1 h_3}{h_2}\right)_\eta \mu_i - \frac{h_3 h_{1_\eta}}{h_2}\mu_i\right]\frac{\Delta\xi}{2\Delta Y} + \frac{1}{Re_r}\frac{h_{1_\eta}}{h_1 h_2^2}\frac{dY}{d\eta} w\mu_i \frac{\Delta\xi}{2\Delta Y}$$

$$- \frac{1}{Re_r}\frac{1}{h_2^2}\left(\frac{dY}{d\eta}\right)^2 w\mu_i \frac{\Delta\xi}{(\Delta Y)^2}$$

$$C_{X_5} = \frac{1}{h_1}\left[\rho_i u_i + w\lambda(\rho_i u_i - \rho_{i-1}u_{i-1})\right] - \frac{1}{Re_r}\left(\frac{h_{2_\xi}}{h_1 h_2} + \frac{h_{3_\xi}}{h_1 h_3}\right)\frac{2}{3}\frac{1}{h_1}\mu_i + w$$

$$+ \frac{h_{1_\eta}}{h_1 h_2} w\rho_i v_i \Delta\xi + \frac{1}{Re_r}\frac{1}{h_1 h_2 h_3} w\left[\frac{h_3 h_{1_\eta}}{h_2}\frac{dY}{d\eta}\delta_Y\mu_i + \left(\frac{h_3 h_{1_\eta}}{h_2}\right)_\eta \mu_i\right]\Delta\xi$$

$$+ \frac{1}{Re_r}\left[\left(\frac{h_{1_\eta}}{h_1 h_2}\right)^2 + \frac{2}{3}\frac{h_{2_\xi}}{h_1^2 h_2}\left(2\frac{h_{2_\xi}}{h_2} - \frac{h_{3_\xi}}{h_3}\right) + \frac{2}{3}\frac{h_{3_\xi}}{h_1^2 h_3}\left(2\frac{h_{3_\xi}}{h_3}\right.\right.$$

$$\left.\left. - \frac{h_{2_\xi}}{h_2}\right)\right] w\mu_i \Delta\xi + \frac{2}{Re_r}\frac{1}{h_2^2}\left(\frac{dY}{d\eta}\right)^2 w\mu_i \frac{\Delta\xi}{(\Delta Y)^2}$$

$$C_{X_6} = -C_{X_4} - \frac{2}{Re_r}\frac{1}{h_2^2}\left(\frac{dY}{d\eta}\right)^2 w\mu_i \frac{\Delta\xi}{(\Delta Y)^2}$$

ORIGINAL PAGE IS
OF POOR QUALITY

$$C_{X_7} = \frac{1}{Re_r}\frac{1}{h_1h_2}\frac{dY}{d\eta}\left(\frac{\mu_{i+w}}{\Delta\xi} - \frac{h_{2_\xi}}{h_2}w\mu_i\right)\frac{\Delta\xi}{2\Delta Y} - \frac{1}{Re_r}\frac{dY}{d\eta}\frac{1}{h_1h_2}$$

$$\times\left(\frac{4}{3}\frac{h_{2_\xi}}{h_2} - \frac{2}{3}\frac{h_{3_\xi}}{h_3}\right)w\mu_i\frac{\Delta\xi}{2\Delta Y}$$

$$C_{X_8} = -\frac{1}{Re_r}\frac{1}{h_1h_2h_3}\left(h_3\frac{dY}{d\eta}\delta_Y\mu_{i+w} + h_{3_\eta}\mu_{i+w}\right) - \frac{1}{Re_r}\frac{h_{1_\eta}}{h_1^2h_2}\mu_{i+w}$$

$$+\left(\frac{1}{h_2}\frac{dY}{d\eta}\delta_Y u_i - 2\frac{h_{2_\xi}}{h_1h_2}v_i + \frac{h_{1_\eta}}{h_1h_2}u_i\right)w\rho_i\Delta\xi + \frac{1}{Re_r}\frac{1}{h_1h_2h_3}w$$

$$\times\left[\frac{h_3h_{2_\xi}}{h_2}\frac{dY}{d\eta}\delta_Y\mu_i + \left(\frac{h_3h_{2_\xi}}{h_2}\right)_\eta\mu_i\right]\Delta\xi + \frac{1}{Re_r}\frac{h_{1_\eta}h_{2_\xi}}{h_1^2h_2^2} - \frac{2}{3}\frac{h_{2_\xi}}{h_1h_2^2}$$

$$\times\left(\frac{h_{1_\eta}}{h_1} + \frac{h_{3_\eta}}{h_3}\right) + \frac{2}{3}\frac{h_{3_\xi}}{h_1h_2h_3}\left(2\frac{h_{3_\eta}}{h_3} - \frac{h_{1_\eta}}{h_1}\right)w\mu_i\Delta\xi$$

$$C_{X_9} = -C_{X_7}$$

$$C_{X_{10}} = -\frac{1}{Re_r}\frac{1}{h_1h_2^2}\frac{dY}{d\eta}\left(\frac{d\mu}{dT}\right)_i w\left(h_{2_\xi}v_i - h_1\frac{dY}{d\eta}\delta_Y u_i + h_{1_\eta}\frac{dY}{d\eta}u_i\right)\frac{\Delta\xi}{2\Delta Y}$$

$$C_{X_{11}} = \frac{1}{Re_r}\frac{1}{h_1h_2h_3}w\left\{\frac{h_3h_{2_\xi}}{h_2}\frac{dY}{d\eta}\delta_Y\left(\frac{d\mu}{dT}v\right)_i + \left(\frac{h_3h_{2_\xi}}{h_2}\right)_\eta\left(\frac{d\mu}{dT}v\right)_i\right.$$

$$\left. - \frac{h_1h_3}{h_2}\frac{dY}{d\eta}\delta_Y\left[\frac{dY}{d\eta}\left(\frac{d\mu}{dT}\right)_i\delta_Y u_i\right] - \left(\frac{h_1h_3}{h_2}\right)_\eta\frac{dY}{d\eta}\left(\frac{d\mu}{dT}\right)_i\delta_Y u_i\right.$$

Continued on next page

ORIGINAL PAGE IS
OF POOR QUALITY

$$+ \frac{h_3 h_{1_n}}{h_2} \frac{dY}{d\eta} \delta_Y \left(\frac{d\mu}{dT} u\right)_i + \left(\frac{h_3 h_{1_n}}{h_2}\right)_n \left(\frac{d\mu}{dT} u\right)_i \Bigg\} \Delta\xi + \frac{1}{Re_r} \frac{1}{h_1} w \left(\frac{d\mu}{dT}\right)_i$$

$$\times \Bigg\{ \frac{h_{1_n} h_{2_\xi}}{h_1 h_2^2} v_i - \frac{h_{1_n}}{h_2^2} \frac{dY}{d\eta} \delta_Y u_i + \frac{h_{1_n}^2}{h_1 h_2^2} u_i + \frac{4}{3} \frac{h_{2_\xi}}{h_2^2} \frac{dY}{d\eta} \delta_Y v_i - \frac{2}{3} \frac{h_{2_\xi}}{h_2^2}$$

$$\times \left(\frac{h_{1_n}}{h_1} + \frac{h_{3_n}}{h_3}\right) v_i + \frac{2}{3} \frac{h_{2_\xi}}{h_1 h_2} \left(2 \frac{h_{2_\xi}}{h_2} - \frac{h_{3_\xi}}{h_3}\right) u_i + \frac{2}{3} \frac{h_{3_\xi}}{h_1 h_3}$$

$$\times \left(2 \frac{h_{3_\xi}}{h_3} - \frac{h_{2_\xi}}{h_2}\right) u_i - \frac{2}{3} \frac{h_{3_\xi}}{h_2 h_3} \frac{dY}{d\eta} \delta_Y v_i + \frac{2}{3} \frac{h_{3_\xi}}{h_1 h_3}$$

$$\times \left(2 \frac{h_{3_n}}{h_3} - \frac{h_{1_n}}{h_1}\right) v_i \Bigg\} \Delta\xi$$

$$C_{X_{12}} = -C_{X_{10}}$$

$$S_X = \frac{1}{h_1} [\rho_i u_i + w\lambda (\rho_i u_i - \rho_{i-1} u_{i-1})] u_i - \frac{1}{h_2} \frac{dY}{d\eta} (1 - 3w)$$

$$\times \rho_i v_i (\delta_Y u_i) \Delta\xi + \frac{h_{2_\xi}}{h_1 h_2} (1 - 3w) \rho_i v_i^2 \Delta\xi - \frac{h_{1_\eta}}{h_1 h_2} (1 - 3w) \rho_i u_i v_i \Delta\xi$$

$$+ \frac{1}{h_1} \left(P_\xi + p'_\xi\right)_{i+w} \Delta\xi + \frac{1}{Re_r} \frac{1}{h_1 h_2 h_3} \Bigg\{ h_3 \frac{dY}{d\eta} \left[- \mu_{i+w} \frac{\delta_Y v_i}{\Delta\xi} \right.$$

$$\left. - (\delta_Y \mu_{i+w}) \frac{v_i}{\Delta\xi} \right] - h_{3_\eta} \mu_{i+w} \frac{v_i}{\Delta\xi} - \frac{h_3 h_{2_\xi}}{h_2} \frac{dY}{d\eta} \left[(1 - w) \delta_Y (\mu v)_i \right.$$

$$\left. - w \left(\frac{d\mu}{dT}\right)_i v_i \delta_Y T_i - w \delta_Y \left(\frac{d\mu}{dT} v\right)_i T_i \right] - \left(\frac{h_3 h_{2_\xi}}{h_2}\right)_\eta \left[(1 - w) \mu_i v_i \right.$$

ORIGINAL PAGE IS
OF POOR QUALITY

$$- w \left(\frac{d\mu}{dT}\right)_i v_i T_i \Big] + \frac{h_1 h_3}{h_2} \frac{dY}{d\eta} \Big[\delta_Y \left(\frac{dY}{d\eta} \mu_i \delta_Y u_i\right) - w \frac{dY}{d\eta} \left(\frac{d\mu}{dT}\right)_i (\delta_Y u_i)$$

$$\times \delta_Y T_i - w \delta_Y \left(\frac{dY}{d\eta} \frac{d\mu}{dT} \delta_Y u\right)_i T_i - w \frac{dY}{d\eta} \mu_i \delta_Y^2 u_i - w \delta_Y \left(\frac{dY}{d\eta} \mu_i\right) \delta_Y u_i \Big]$$

$$+ \left(\frac{h_1 h_3}{h_2}\right)_\eta \frac{dY}{d\eta} \Big[(1 - w) \mu_i \delta_Y u_i - w \left(\frac{d\mu}{dT} \delta_Y u\right)_i T_i \Big] - \frac{h_3 h_{1_\eta}}{h_2} \frac{dY}{d\eta}$$

$$\times \Big[(1 - w) \delta_Y (\mu u)_i - w \left(\frac{d\mu}{dT}\right)_i u_i \delta_Y T_i - \delta_Y \left(\frac{d\mu}{dT} u\right)_i T_i \Big]$$

$$- \left(\frac{h_3 h_{1_\eta}}{h_2}\right)_\eta \Big[(1 - w) \mu_i u_i - w \left(\frac{d\mu}{dT}\right)_i u_i T_i \Big] \Big\} \Delta\xi + \frac{1}{Re_r} \frac{h_{1_\eta}}{h_1 h_2}$$

$$\times \Big\{ - \frac{1}{h_1} \mu_{i+w} \frac{v_i}{\Delta\xi} + \frac{h_{2_\xi}}{h_1 h_2} \Big[(1 - w) \mu_i v_i - w \left(\frac{d\mu}{dT}\right)_i v_i T_i \Big] + \frac{1}{h_2} \frac{dY}{d\eta}$$

$$\times \Big[(1 - w) \mu_i \delta_Y u_i - w \left(\frac{d\mu}{dT} \delta_Y u\right)_i T_i \Big] - \frac{h_{1_\eta}}{h_1 h_2} \Big[(1 - w) \mu_i u_i$$

$$- w \left(\frac{d\mu}{dT}\right)_i u_i T_i \Big] \Big\} \Delta\xi - \frac{1}{Re_r} \frac{h_{2_\xi}}{h_1 h_2} \Big\{ \frac{4}{3} \frac{1}{h_2} \frac{dY}{d\eta} \Big[(1 - w) \mu_i \delta_Y v_i$$

$$- w \left(\frac{d\mu}{dT} \delta_Y v\right)_i T_i \Big] - \frac{2}{3} \frac{1}{h_2} \left(\frac{h_{1_\eta}}{h_1} + \frac{h_{3_\eta}}{h_3}\right) \Big[(1 - w) \mu_i v_i - w \left(\frac{d\mu}{dT}\right)_i v_i T_i \Big]$$

$$+ \frac{2}{3} \frac{1}{h_1} \mu_{i+w} \frac{u_i}{\Delta\xi} + \frac{2}{3} \frac{1}{h_1} \left(2 \frac{h_{2_\xi}}{h_2} - \frac{h_{3_\xi}}{h_3}\right) \Big[(1 - w) \mu_i u_i - w \left(\frac{d\mu}{dT}\right)_i u_i T_i \Big] \Big\}$$

$$\times \Delta\xi - \frac{1}{Re_r} \frac{h_{3_\xi}}{h_1 h_3} \Big\{ \frac{2}{3} \frac{1}{h_1} \mu_{i+w} \frac{u_i}{\Delta\xi} + \frac{2}{3} \frac{1}{h_1} \left(2 \frac{h_{3_\xi}}{h_3} - \frac{h_{2_\xi}}{h_2}\right) \Big[(1 - w) \mu_i u_i$$

Continued on next page

ORIGINAL PAGE IS
OF POOR QUALITY

$$- w\left(\frac{d\mu}{dT}\right)_i u_i T_i\Big] - \frac{2}{3}\frac{1}{h_2}\frac{dY}{d\eta}\Big[(1-w)\mu_i\,\delta_Y v_i - w\left(\frac{d\mu}{dT}\,\delta_Y v\right)_i T_i\Big]$$

$$+ \frac{2}{3}\frac{1}{h_2}\left(2\frac{h_{3_\eta}}{h_3} - \frac{h_{1_\eta}}{h_1}\right)\Big[(1-w)\mu_i v_i - w\left(\frac{d\mu}{dT}\right)_i v_i T_i\Big]\Big\}\,\Delta\xi$$

CROSS-FLOW MOMENTUM

$$C_{Y_1}\rho_{j-1} + C_{Y_2}\rho_j + C_{Y_3}\rho_{j+1} + C_{Y_4}u_{j-1} + C_{Y_5}u_j + C_{Y_6}u_{j+1} + C_{Y_7}v_{j-1}$$

$$+ C_{Y_8}v_j + C_{Y_9}v_{j+1} + C_{Y_{10}}T_{j-1} + C_{Y_{11}}T_j + C_{Y_{12}}T_{j+1} = S_Y \qquad (D.7)$$

where

$$C_{Y_1} = -\frac{1}{h_2}\frac{dY}{d\eta}\,w\,RT_i\,\frac{\Delta\xi}{2\,\Delta Y}$$

$$C_{Y_2} = \frac{1}{h_2}\frac{dY}{d\eta}\,wv_i(\delta_Y v_i)\,\Delta\xi + \frac{h_{2_\xi}}{h_1h_2}\,wu_iv_i\,\Delta\xi - \frac{h_{1_\eta}}{h_1h_2}\,wu_i^2\,\Delta\xi + \frac{1}{h_2}\frac{dY}{d\eta}$$

$$\times\, wR(\delta_Y T_i)\,\Delta\xi$$

$$C_{Y_3} = -C_{Y_1}$$

$$C_{Y_4} = \frac{1}{Re_r}\frac{1}{h_1h_2h_3}\frac{dY}{d\eta}\left(h_3\frac{\mu_{i+w}}{\Delta\xi} + h_{3_\xi}w\mu_i\right)\frac{\Delta\xi}{2\,\Delta Y} - \frac{1}{Re_r}\frac{1}{h_1h_2}\frac{2}{3}\frac{dY}{d\eta}$$

$$\times\left[\frac{\mu_{i+w}}{\Delta\xi} - \left(2\frac{h_{2_\xi}}{h_2} - \frac{h_{3_\xi}}{h_3}\right)w\mu_i\right]\frac{\Delta\xi}{2\,\Delta Y} + \frac{1}{Re_r}\frac{h_{2_\xi}}{h_1h_2^2}\frac{dY}{d\eta}\,w\mu_i\,\frac{\Delta\xi}{2\,\Delta Y}$$

$$C_{Y_5} = \frac{1}{Re_r}\frac{h_{1_\eta}}{h_1^2h_2}\mu_{i+w} + \frac{1}{Re_r}\frac{2}{3}\frac{1}{h_1h_2h_3}\left(h_3\frac{dY}{d\eta}\,\delta_Y\mu_{i+w} + h_{3_\eta}\mu_{i+w}\right)$$

Continued on next page

ORIGINAL PAGE IS
OF POOR QUALITY

$$- \frac{1}{Re_r}\frac{2}{3}\frac{h_{3_n}}{h_1h_2h_3}\mu_{i+w} + \frac{1}{h_1h_2}\left(1.2_\xi v_i - 2h_{1_n}u_i\right)w\rho_i\,\Delta\xi$$

$$+ \frac{1}{Re_r}\frac{1}{h_1h_2h_3}\left(\frac{h_3h_{1_n}}{h_1}\right)_\xi w\mu_i\,\Delta\xi - \frac{1}{Re_r}\frac{2}{3}\frac{1}{h_1h_2h_3}w\left\{h_3\frac{dY}{dn}\right.$$

$$\times\left(2\frac{h_{2_\xi}}{h_2} - \frac{h_{3_\xi}}{h_3}\right)\delta_Y\mu_i + \left.\left[h_3\left(2\frac{h_{2_\xi}}{h_2} - \frac{h_{3_\xi}}{h_3}\right)\right]_n\mu_i\right\}\Delta\xi$$

$$+ \frac{1}{Re_r}\frac{1}{h_1h_2}\left[\frac{h_{1_n}h_{2_\xi}}{h_1h_2} + \frac{2}{3}\frac{h_{3_n}}{h_3}\left(2\frac{h_{3_\xi}}{h_3} - \frac{h_{2_\xi}}{h_2}\right)\right]w\mu_i\,\Delta\xi$$

$$C_{Y_6} = -C_{Y_4}$$

$$C_{Y_7} = -\frac{1}{h_2}\frac{dY}{dn}w\rho_iv_i\frac{\Delta\xi}{2\,\Delta Y} + \frac{1}{Re_r}\frac{1}{h_1h_2h_3}\frac{2}{3}\frac{dY}{dn}w\left[2\,\delta_Y\left(\frac{dY}{dn}\mu_i\right)\right.$$

$$\left. + 2\left(\frac{h_1h_3}{h_2}\right)_n\mu_i - \frac{h_1h_3}{h_2}\left(\frac{h_{1_n}}{h_1} + \frac{h_{3_n}}{h_3}\right)\mu_i\right]\frac{\Delta\xi}{2\,\Delta Y} + \frac{1}{Re_r}\frac{2}{3}\frac{h_{3_n}}{h_2^2h_3}\frac{dY}{dn}$$

$$\times w\mu_i\frac{\Delta\xi}{2\,\Delta Y} - \frac{1}{Re_r}\frac{4}{3}\frac{1}{h_2^2}\left(\frac{dY}{dn}\right)^2 w\mu_i\frac{\Delta\xi}{(\Delta Y)^2}$$

$$C_{Y_8} = \frac{1}{h_i}\left[\rho_iu_i + w\lambda(\rho_iu_i - \rho_{i-1}u_{i-1})\right] - \frac{1}{Re_r}\frac{h_{2_\xi}}{h_1^2h_2}\mu_{i+w} + \left(\frac{1}{h_2}\frac{dY}{dn}\delta_Yv_i\right.$$

$$\left. + \frac{h_{2_\xi}}{h_1h_2}u_i\right)w\rho_i\,\Delta\xi + \frac{1}{Re_r}\frac{2}{3}\frac{1}{h_1h_2h_3}w\left\{\frac{h_1h_3}{h_2}\left(\frac{h_{1_n}}{h_1} + \frac{h_{3_n}}{h_3}\right)\right.$$

Continued on next page

ORIGINAL PAGE IS
OF POOR QUALITY

$$\times \frac{dY}{dn}\,\delta_Y u_i + \left[\frac{h_1 h_3}{h_2}\left(\frac{h_1}{h_1}_n + \frac{h_3}{h_3}_n\right)\right]_n u_i \Bigg\}\,\Delta\xi + \frac{1}{Re_r}\left[\left(\frac{h_{2_\xi}}{h_1 h_2}\right)^2\right.$$

$$\left. + \frac{2}{3}\frac{h_3}{h_2^2 h_3}_n\left(2\,\frac{h_3}{n_3}_n - \frac{h_1}{h_1}_n\right)\right] w u_i\,\Delta\xi + \frac{2}{Re_r}\frac{4}{3}\frac{1}{h_2^2}\left(\frac{dY}{dn}\right)^2 w u_i\,\frac{\Delta\xi}{(\Delta Y)^2}$$

$$C_{Y_9} = -C_{Y_7} - \frac{2}{Re_r}\frac{4}{3}\frac{1}{h_2^2}\left(\frac{dY}{dn}\right)^2 w u_i\,\frac{\Delta\xi}{(\Delta Y)^2}$$

$$C_{Y_{10}} = -\frac{1}{h_2}\frac{dY}{dn}\,wR\rho_i\,\frac{\Delta\xi}{2\,\Delta Y} + \frac{1}{Re_r}\frac{2}{3}\frac{1}{h_1 h_2}\frac{dY}{dn}\,w\left(\frac{d\mu}{dT}\right)_i\left[2\,\frac{h_1}{h_2}\frac{dY}{dn}\,\delta_Y v_i\right.$$

$$\left. - \frac{h_1}{h_2}\left(\frac{h_1}{h_1}_n + \frac{h_3}{h_3}_n\right) v_i + \left(2\,\frac{h_{2_\xi}}{h_2} - \frac{h_{3_\xi}}{h_3}\right) u_i\right]\frac{\Delta\xi}{2\,\Delta Y}$$

$$C_{Y_{11}} = -\frac{1}{Re_r}\frac{1}{h_1 h_2}\left\{\frac{dY}{dn}\left[\left(\frac{d\mu}{dT}\right)_i \delta_Y u_i + w\lambda\left(\left(\frac{d\mu}{dT}\right)_i \delta_Y u_i\right.\right.\right.$$

$$\left. - \left(\frac{d\mu}{dT}\right)_{i-1}\delta_Y u_{i-1}\right)\Big] - \frac{h_1}{h_1}_n\left[\left(\frac{d\mu}{dT}\right)_i u_i + w\lambda\left(\left(\frac{d\mu}{dT}\right)_i u_i\right.\right.$$

$$\left.\left. - \left(\frac{d\mu}{dT}\right)_{i-1} u_{i-1}\right)\Big]\right\} + \frac{1}{h_2}\frac{dY}{dn}\,wR(\delta_Y\rho_i)\,\Delta\xi - \frac{1}{Re_r}\frac{1}{h_1 h_2 h_3}$$

$$\times w\left(\frac{d\mu}{dT}\right)_i\left[h_{3_\xi}\frac{dY}{dn}\,\delta_Y u_i - \left(\frac{h_3 h_1}{h_1}_n\right)_\xi u_i\right]\Delta\xi - \frac{1}{Re_r}\frac{1}{h_1 h_2 h_3}\frac{2}{3}\,w$$

$$\times\left\{2\,\frac{h_1 h_3}{h_2}\frac{dY}{dn}\,\delta_Y\left[\frac{dY}{dn}\left(\frac{d\mu}{dT}\right)_i \delta_Y v_i\right] + 2\left(\frac{h_1 h_3}{h_2}\right)_n\frac{dY}{dn}\left(\frac{d\mu}{dT}\right)_i \delta_Y v_i\right.$$

Continued on next page

ORIGINAL PAGE IS
OF POOR QUALITY

$$- \frac{h_1 h_3}{h_2}\left(\frac{h_{1_\eta}}{h_1} + \frac{h_{3_\eta}}{h_3}\right)\frac{dY}{d\eta}\,\delta_Y\left(\frac{d\mu}{dT}\,v\right)_i - \left[\frac{h_1 h_3}{h_2}\left(\frac{h_{1_\eta}}{h_1} + \frac{h_{3_\eta}}{h_3}\right)\right]_\eta$$

$$\times \left(\frac{d\mu}{dT}\right)_i v_i + h_3\left(2\,\frac{h_{2_\xi}}{h_2} - \frac{h_{3_\xi}}{h_3}\right)\frac{dY}{d\eta}\,\delta_Y\left(\frac{d\mu}{dT}\,u\right)_i + \left[h_3\left(2\,\frac{h_{2_\xi}}{h_2}\right.\right.$$

$$\left.\left. - \frac{h_{3_\xi}}{h_3}\right)\right]_\eta \left(\frac{d\mu}{dT}\right)_i u_i \Bigg\}\,\Delta\xi - \frac{1}{Re_r}\,\frac{h_{2_\xi}}{h_1 h_2}\,w\left(\frac{d\mu}{dT}\right)_i \left[-\frac{h_{2_\xi}}{h_1 h_2}\,v_i\right.$$

$$\left. + \frac{1}{h_2}\frac{dY}{d\eta}\,\delta_Y u_i - \frac{h_{1_\eta}}{h_1 h_2}\,u_i\right]\Delta\xi - \frac{1}{Re_r}\,\frac{2}{3}\,\frac{h_{3_\eta}}{h_2 h_3}\,w\left(\frac{d\mu}{dT}\right)_i \left[-\frac{1}{h_1}\right.$$

$$\left. \times \left(2\,\frac{h_{3_\xi}}{h_3} - \frac{h_{2_\xi}}{h_2}\right)u_i + \frac{1}{h_2}\frac{dY}{d\eta}\,\delta_Y v_i - \frac{1}{h_2}\left(2\,\frac{h_{3_\eta}}{h_3} - \frac{h_{1_\eta}}{h_1}\right)v_i\right]\Delta\xi$$

$$C_{Y_{12}} = - C_{Y_{10}}$$

$$S_Y = \frac{1}{h_1}\left[\rho_i u_i + w\lambda(\rho_i u_i - \rho_{i-1}u_{i-1})\right]v_i - \frac{1}{h_2}\frac{dY}{d\eta}\,(1 - 3w)\rho_i v_i(\delta_Y v_i)\,\Delta\xi$$

$$- \frac{h_{2_\xi}}{h_1 h_2}\,(1 - 3w)\rho_i u_i v_i\,\Delta\xi - \frac{h_{1_\eta}}{h_1 h_2}\,(1 - 3w)\rho_i u_i^2\,\Delta\xi$$

$$- \frac{1}{h_2}\frac{dY}{d\eta}\,(1 - 2w)R\,\delta_Y(\rho T)_i\,\Delta\xi + \frac{1}{Re_r}\,\frac{1}{h_1 h_2 h_3}\left[-h_3\,\frac{dY}{d\eta}\left\{\left[\left(\frac{d\mu}{dT}\right)_i \delta_Y u_i\right.\right.\right.$$

$$\left.\left.\left. + w\lambda\left(\left(\frac{d\mu}{dT}\right)_i \delta_Y u_i - \left(\frac{d\mu}{dT}\right)_{i-1}\delta_Y u_{i-1}\right)\right]\frac{T_i}{\Delta\xi} - \mu_{i+w}\,\frac{\delta_Y u_i}{\Delta\xi}\right\}\right.$$

$$\left. + h_{3_\xi}\,\frac{dY}{d\eta}\left[(1 - w)\mu_i\,\delta_Y u_i - w\left(\frac{d\mu}{dT}\,\delta_Y u\right)_i T_i\right] - \frac{h_3 h_{1_\eta}}{h_1}\right.$$

Continued on next page

ORIGINAL PAGE IS
OF POOR QUALITY

$$\times \left\{ - \mu_{i+w} \frac{u_i}{\Delta\xi} - \left[\left(\frac{d\mu}{dT}\right)_i u_i + w\lambda \left(\left(\frac{d\mu}{dT}\right)_i u_i - \left(\frac{d\mu}{dT}\right)_{i-1} u_{i-1} \right) \right] \right.$$

$$\left. \times \frac{T_i}{\Delta\xi} \right\} - \left(\frac{h_3 h_1}{h_1}\right)_\xi \left[(1 - w)\mu_i u_i - w \left(\frac{d\mu}{dT}\right)_i u_i T_i \right] \Bigg] \Delta\xi$$

$$+ \frac{1}{Re_r} \frac{1}{h_1 h_2 h_3} \left[\frac{4}{3} \frac{h_1 h_3}{h_2} \frac{d\gamma}{d\eta} \left\{ \delta_\gamma \left(\frac{d\gamma}{d\eta} \mu_i \delta_\gamma v_i \right) - w \frac{d\gamma}{d\eta} \left(\frac{d\mu}{dT} \delta_\gamma v \right)_i \delta_\gamma T_i \right. \right.$$

$$\left. - w \delta_\gamma \left[\frac{d\gamma}{d\eta} \left(\frac{d\mu}{dT}\right)_i \delta_\gamma v_i \right] T_i - w \frac{d\gamma}{d\eta} \mu_i \delta_\gamma^2 v_i - w \delta_\gamma \left(\frac{d\gamma}{d\eta} \mu_i \right) \delta_\gamma v_i \right\}$$

$$+ \frac{4}{3} \left(\frac{h_1 h_3}{h_2}\right)_\eta \frac{d\gamma}{d\eta} \left[(1 - w)\mu_i \delta_\gamma v_i - w \left(\frac{d\mu}{dT} \delta_\gamma v\right)_i T_i \right] - \frac{2}{3} \frac{h_1 h_3}{h_2}$$

$$\times \left(\frac{h_1}{h_1}_\eta + \frac{h_3}{h_3}_\eta \right) \frac{d\gamma}{d\eta} \left[(1 - w)\delta_\gamma (\mu v)_i - \left(\frac{d\mu}{dT}\right)_i v_i \delta_\gamma T_i - \delta_\gamma \left(\frac{d\mu}{dT} v\right)_i T_i \right]$$

$$- \frac{2}{3} \left[\frac{h_1 h_3}{h_2} \left(\frac{h_1}{h_1}_\eta + \frac{h_3}{h_3}_\eta \right) \right]_\eta \left[(1 - w)\mu_i v_i - \left(\frac{d\mu}{dT}\right)_i v_i T_i \right]$$

$$- \frac{2}{3} h_3 \frac{d\gamma}{d\eta} \left[- \mu_{i+w} \frac{\delta_\gamma u_i}{\Delta\xi} - (\delta_\gamma \mu_{i+w}) \frac{u_i}{\Delta\xi} \right] + \frac{2}{3} h_{3_\eta} \mu_{i+w} \frac{u_i}{\Delta\xi}$$

$$+ \frac{2}{3} h_3 \left(2 \frac{h_{2_\xi}}{h_2} - \frac{h_{3_\xi}}{h_3} \right) \frac{d\gamma}{d\eta} \left[(1 - w)\varepsilon_\gamma (\mu u)_i - \left(\frac{d\mu}{dT}\right)_i u_i \delta_\gamma T_i \right.$$

$$\left. - \delta_\gamma \left(\frac{d\mu}{dT} u\right)_i T_i \right] + \frac{2}{3} \left[h_3 \left(2 \frac{h_{2_\xi}}{h_2} - \frac{h_{3_\xi}}{h_3} \right) \right]_\eta \left[(1 - w)\mu_i u_i \right.$$

Continued on next page

ORIGINAL PAGE IS
OF POOR QUALITY

$$- \left(\frac{d\mu}{dT}\right)_i u_i T_i \Bigg] \Bigg] \Delta\xi + \frac{1}{Re_r} \frac{h_{2_\xi}}{h_1 h_2} \Bigg\{ - \frac{1}{h_1} \mu_{i+w} \frac{v_i}{\Delta\xi}$$

$$- \frac{h_{2_\xi}}{h_1 h_2} \left[(1-w)\mu_i v_i - w \left(\frac{d\mu}{dT}\right)_i v_i T_i \right] + \frac{1}{h_2} \frac{d\gamma}{d\eta} \left[(1-w)\mu_i \, \delta_\gamma u_i \right.$$

$$\left. - w \left(\frac{d\mu}{dT}\right)_i (\delta_\gamma u_i) T_i \right] - \frac{h_{1_\eta}}{h_1 h_2} \left[(1-w)\mu_i u_i - w \left(\frac{d\mu}{dT}\right)_i u_i T_i \right] \Bigg\} \Delta\xi$$

$$- \frac{1}{Re_r} \frac{h_{3_\eta}}{h_2 h_3} \Bigg\{ \frac{2}{3} \frac{1}{h_1} \mu_{i+w} \frac{u_i}{\Delta\xi} + \frac{2}{3} \frac{1}{h_1} \left(2 \frac{h_{3_\xi}}{h_3} - \frac{h_{2_\xi}}{h_2} \right) \left[(1-w)\mu_i u_i \right.$$

$$\left. - w \left(\frac{d\mu}{dT}\right)_i u_i T_i \right] - \frac{2}{3} \frac{1}{h_2} \frac{d\gamma}{d\eta} \left[(1-w)\mu_i \, \delta_\gamma v_i - w \left(\frac{d\mu}{dT}\right)_i (\delta_\gamma v_i) T_i \right]$$

$$+ \frac{2}{3} \frac{1}{h_2} \left(2 \frac{h_{3_\eta}}{h_3} - \frac{h_{1_\eta}}{h_1} \right) \left[(1-w)\mu_i v_i - w \left(\frac{d\mu}{dT}\right)_i v_i T_i \right] \Bigg\} \Delta\xi$$

ENERGY

$$C_{E_1} \rho_{j-1} + C_{E_2} \rho_j + C_{E_3} \rho_{j+1} + C_{E_4} u_{j-1} + C_{E_5} u_j + C_{E_6} u_{j+1} + C_{E_7} v_{j-1}$$

$$+ C_{E_8} v_j + C_{E_9} v_{j+1} + C_{E_{10}} T_{j-1} + C_{E_{11}} T_j + C_{E_{12}} T_{j+1} = S_E \qquad (D.8)$$

where

$$C_{E_1} = 0$$

$$C_{E_2} = \frac{1}{h_2} \frac{d\gamma}{d\eta} w \, c_{v_i} v_i (\delta_\gamma T_i) \, \Delta\xi + \frac{1}{h_1 h_2 h_3} R T_i w \left[h_1 h_3 \frac{d\gamma}{d\eta} \delta_\gamma v_i + \left(h_2 h_3\right)_\xi u_i \right.$$

$$\left. + \left(h_1 h_3\right)_\eta v_i \right] \Delta\xi$$

ORIGINAL PAGE IS
OF POOR QUALITY

$$C_{E_3} = C_{E_4} = 0$$

$$C_{E_5} = \frac{1}{h_1} R\,[\rho_i T_i + w\lambda(\rho_i T_i - \rho_{i-1} T_{i-1})] + \frac{1}{h_1 h_2 h_3}\,(h_2 h_3)_\xi\, wR\rho_i T_i\, \Delta\xi$$

$$C_{E_6} = 0$$

$$C_{E_7} = -\frac{1}{h_2}\frac{dY}{d\eta}\, wR\rho_i T_i\, \frac{\Delta\xi}{2\,\Delta Y}$$

$$C_{E_8} = \frac{1}{h_2}\frac{dY}{d\eta}\, wc_{v_i}\rho_i v_i\, \Delta\xi + \frac{1}{h_1 h_2 h_3}\,(h_1 h_3)_\eta\, wR\rho_i T_i\, \Delta\xi$$

$$C_{E_9} = -C_{E_7}$$

$$C_{E_{10}} = -\frac{1}{h_2}\frac{dY}{d\eta}\, wc_{v_i}\rho_i v_i\, \frac{\Delta\xi}{2\,\Delta Y} + \frac{1}{Re_r Pr_r}\frac{1}{h_1 h_2 h_3}\frac{dY}{d\eta}\, w\left[\frac{h_1 h_3}{h_2}\frac{dY}{d\eta}\left(\frac{dk}{dT}\right)_i \delta_Y T_i\right.$$

$$\left. + \frac{h_1 h_3}{h_2}\frac{dY}{d\eta}\,\delta_Y\left(\frac{dY}{d\eta}\,k_i\right) + \left(\frac{h_1 h_3}{h_2}\right)_\eta k_i\right]\frac{\Delta\xi}{2\,\Delta Y}$$

$$- \frac{1}{Re_r Pr_r}\frac{1}{h_2^2}\left(\frac{dY}{d\eta}\right)^2 wk_i\,\frac{\Delta\xi}{(\Delta Y)^2}$$

$$C_{E_{11}} = \frac{1}{h_1}\left[\rho_i u_i c_v + w\lambda\left(\rho_i u_i c_{v_i} - \rho_{i-1} u_{i-1} c_{v_{i-1}}\right)\right] + \frac{1}{h_2}\frac{dY}{d\eta}\, w\left(\frac{dc_v}{dT}\right)_i$$

$$\times\ \rho_i v_i(\delta_Y T_i)\,\Delta\xi + \frac{1}{h_1 h_2 h_3} R\rho_i w\left[h_1 h_3\frac{dY}{d\eta}\,\delta_Y v_i + (h_2 h_3)_\xi\, u_i\right.$$

$$\left. + (h_1 h_3)_\eta\, v_i\right]\,\Delta\xi - \frac{1}{Re_r Pr_r}\frac{1}{h_1 h_2 h_3}\frac{dY}{d\eta}\, w\left[\frac{h_1 h_3}{h_2}\,\delta_Y\left(\frac{dY}{d\eta}\frac{dk}{dT}\,\delta_Y T\right)_i\right.$$

Continued on next page

ORIGINAL PAGE IS
OF POOR QUALITY

$$+ \left(\frac{h_1 h_3}{h_2}\right)_n \left(\frac{dk}{dT}\right)_i \delta_Y T_i \Bigg] \Delta\xi + \frac{2}{Re_r Pr_r} \frac{1}{h_2^2} \left(\frac{dY}{d\eta}\right)^2 wk_i \frac{\Delta\xi}{(\Delta Y)^2}$$

$$C_{E_{12}} = - C_{E_{10}} - \frac{2}{Re_r Pr_r} \frac{1}{h_2^2} \left(\frac{dY}{d\eta}\right)^2 wk_i \frac{\Delta\xi}{(\Delta Y)^2}$$

$$S_E = \frac{1}{h_1}\left[\rho_i u_i c_{v_i} + w\lambda\left(\rho_i u_i c_{v_i} - \rho_{i-1} u_{i-1} c_{v_{i-1}}\right)\right] T_i$$

$$- \frac{1}{h_2}\frac{dY}{d\eta}\left[(1 - 3w)\rho_i v_i c_{v_i} - w\left(\frac{dc_v}{dT}\right)_i \rho_i v_i T_i\right](\delta_Y T_i)\,\Delta\xi$$

$$- \frac{1}{h_1 h_2 h_3} R \Bigg\{ - h_2 h_3 \left[\rho_i T_i + w\lambda\left(\rho_i T_i - \rho_{i-1} T_{i-1}\right)\right]\frac{u_i}{\Delta\xi}$$

$$+ h_1 h_3 \frac{dY}{d\eta}(1 - 3w)\rho_i T_i\, \delta_Y v_i + \left(h_2 h_3\right)_\xi (1 - 3w)\rho_i u_i T_i$$

$$+ \left(h_1 h_3\right)_\eta (1 - 3w)\rho_i v_i T_i \Bigg\}\Delta\xi + \frac{1}{Re_r Pr_r}\frac{1}{h_1 h_2 h_3}\Bigg\{\frac{h_1 h_3}{h_2}\frac{dY}{d\eta}$$

$$\times \Bigg[\delta_Y\left(\frac{dY}{d\eta} k_i\, \delta_Y T_i\right) - w\frac{dY}{d\eta}\left(\frac{dk}{dT}\delta_Y T\right)_i \delta_Y T_i - w\,\delta_Y\left(\frac{dY}{d\eta}\frac{dk}{dT}\delta_Y T\right)_i T_i$$

$$- w\frac{dY}{d\eta} k_i\, \delta_Y^2 T_i - w\,\delta_Y\left(\frac{dY}{d\eta} k_i\right)\delta_Y T_i\Bigg] + \left(\frac{h_1 h_3}{h_2}\right)_\eta \frac{dY}{d\eta}\Bigg[(1 - w)k_i\,\delta_Y T_i$$

$$- w\left(\frac{dk}{dT}\delta_Y T\right)_i T_i\Bigg]\Bigg\}\Delta\xi + \frac{1}{Re_r}\varphi_e\,\Delta\xi$$

$$\varphi_E = 2\mu_E\left[\left(\frac{1}{h_1}\frac{u_i - u_{i-1}}{\Delta\xi_B} + \frac{h_{1_\eta}}{h_1 h_2} v_i\right)^2 + \left(\frac{1}{h_2}\frac{dY}{d\eta}\delta_Y v_i + \frac{h_{2_\xi}}{h_1 h_2} u_i\right)^2\right.$$

Continued on next page

ORIGINAL PAGE IS
OF POOR QUALITY

$$+\left(\frac{h_{3_\xi}}{h_1 h_3}u_i+\frac{h_{3_\eta}}{h_2 h_3}v_i\right)^2+\frac{1}{2}\left(\frac{1}{h_1}\frac{v_i-v_{i-1}}{\Delta\xi_B}-\frac{h_{2_\xi}}{h_1 h_2}v_i\right.$$

$$\left.+\frac{1}{h_2}\frac{dY}{d\eta}\delta_Y u_i-\frac{h_{1_\eta}}{h_1 h_2}u\right)^2\Bigg]-\frac{2}{3}\mu_E\left(\frac{1}{h_1}\frac{u_i-u_{i-1}}{\Delta\xi_B}+\frac{h_{1_\eta}}{h_1 h_2}v_i\right.$$

$$\left.+\frac{1}{h_2}\frac{dY}{d\eta}\delta_Y v_i+\frac{h_{2_\xi}}{h_1 h_2}u_i+\frac{h_{3_\xi}}{h_1 h_3}u_i+\frac{h_{3_\eta}}{h_2 h_3}v_i\right)^2$$

As described in Section 3.2, the effective viscous dissipation is evaluated at station i and thus appears in the source term S_E in the energy equation. Note also that the source term S_x in the streamwise momentum equation contains the viscous pressure correction computed during the preliminary marching step described in Sections 2.3.1 and 3.5. Although the "j" subscript has been omitted from the coefficients and source terms, they will be different at each j-location in the grid.

Equations (D.5)-(D.8) are written for $j = 2$ to $j = J-1$. The values of the dependent variables at $j = 1$ and $j = J$ are either known functions of ξ or expressible in terms of the dependent variables at other j-locations (see Section 3.3). These equations thus represent a system of $4(J-2)$ coupled linear algebraic equations in $4(J-2)$ unknowns. They can also be written as a matrix equation with a block tri-diagonal coefficient matrix.

ORIGINAL PAGE IS
OF POOR QUALITY

APPENDIX E

DENSITY BOUNDARY CONDITION AT A WALL

The density at a solid surface is found by evaluating the cross-flow momentum equation at the surface. The difference equation at the wall is the same as at interior points, and is presented in Appendix D as equation (D.3). At the wall, however, the δ_Y and δ_Y^2 operators in equation (D.3) are given by equations (3.16) and (3.18). When the resulting algebraic equation is solved for ρ_j, it has the form

$$\rho_j = \frac{1}{C_{W_1}} \left(C_{W_2}\rho_{j\pm1} + C_{W_3}\rho_{j\pm2} + C_{W_4}u_j + C_{W_5}u_{j\pm1} + C_{W_6}u_{j\pm2} + C_{W_7}v_j \right.$$

$$\left. + C_{W_8}v_{j\pm1} + C_{W_9}v_{j\pm2} + C_{W_{10}}T_j + C_{W_{11}}T_{j\pm1} + C_{W_{12}}T_{j\pm2} + S_W \right) \qquad (E.1)$$

where $j = 1$ or J.

The C_W's and S_W can be expressed in terms of the C_Y's and S_Y presented in Appendix D. Their exact form depends on the type of temperature boundary condition used. For a specified wall temperature,

ORIGINAL PAGE IS
OF POOR QUALITY

$$C_{W_1} = C_{Y_2} \pm 3C_{Y_1}$$

$$C_{W_2} = \pm 4C_{Y_1}$$

$$C_{W_3} = \mp C_{Y_1}$$

$$C_{W_4} = - C_{Y_5} \mp 3C_{Y_4}$$

$$C_{W_5} = \pm 4C_{Y_4}$$

$$C_{W_6} = \mp C_{Y_4}$$

$$C_{W_7} = - C_{Y_8} \mp 3C'_{Y_7} + \frac{1}{Re_r}\frac{4}{3}\frac{1}{h_2^2}\left(\frac{dY}{d\eta}\right)^2 w\mu_i \frac{\Delta\xi}{(\Delta Y)^2} \qquad \text{(E2.a)}$$

$$C_{W_8} = \pm 4C'_{Y_7} - \frac{2}{Re_r}\frac{4}{3}\frac{1}{h_2^2}\left(\frac{dY}{d\eta}\right)^2 w\mu_i \frac{\Delta\xi}{(\Delta Y)^2}$$

$$C_{W_9} = \mp C'_{Y_7} + \frac{1}{Re_r}\frac{4}{3}\frac{1}{h_2^2}\left(\frac{dY}{d\eta}\right)^2 w\mu_i \frac{\Delta\xi}{(\Delta Y)^2}$$

$$C_{W_{10}} = - C_{Y_{11}} \mp 3C_{Y_9}$$

$$C_{W_{11}} = \pm 4C_{Y_9}$$

$$C_{W_{12}} = \mp C_{Y_9}$$

$$S_W = S_Y$$

ORIGINAL PAGE IS
OF POOR QUALITY

where

$$C'_{Y_7} = C_{Y_7} + \frac{1}{Re_r}\frac{4}{3}\frac{1}{h_2^2}\left(\frac{dY}{dn}\right)^2 w\mu_i \frac{\Delta\xi}{(\Delta Y)^2}$$

In these equations the top sign is used for the $j = 1$ boundary and the bottom sign is used for the $j = J$ boundary.

For a specified temperature gradient normal to the wall, C_{W_1}, $C_{W_{10}}$-$C_{W_{12}}$, and S_W change. They become

$$C_{W_1} = C_{Y_2} - \frac{1}{h_2}\frac{dY}{dn} wR(\delta_Y T_i)\,\Delta\xi + \frac{1}{h_2}\frac{dY}{dn} wR \left\{\left(\frac{\partial T}{\partial Y}\right)_{W_i} + w\left[\left(\frac{\partial T}{\partial Y}\right)_{W_{i+1}} - \left(\frac{\partial T}{\partial Y}\right)_{W_i}\right]\right\}\Delta\xi \pm 3C_{Y_1}$$

$$C_{W_{10}} = 0$$

$$C_{W_{11}} = -\frac{4}{3} C_{Y_{11}} \qquad \text{(E.2b)}$$

$$C_{W_{12}} = \frac{1}{3} C_{Y_{11}}$$

$$S_W = S_Y \mp \frac{1}{2}\left(\frac{\partial T}{\partial Y}\right)_{W_{i+1}} (\Delta Y) C_{W_{11}}$$

ORIGINAL PAGE IS
OF POOR QUALITY

APPENDIX F

COEFFICIENT MATRICES AND SOURCE TERMS

When the boundary conditions presented in Section 3.3 are applied to equations (D.5)-(D.8), the resulting equations can be written as

$$\tilde{\tilde{B}}_2 \tilde{X}_2 + \tilde{\tilde{C}}_2 \tilde{X}_3 = \tilde{S}_2 \qquad \text{(F.1a)}$$

$$\tilde{\tilde{A}}_j \tilde{X}_{j-1} + \tilde{\tilde{B}}_j \tilde{X}_j + \tilde{\tilde{C}}_j \tilde{X}_{j+1} = \tilde{S}_j \qquad (3 \leq j \leq J-2) \qquad \text{(F.1b)}$$

$$\tilde{\tilde{A}}_{J-1} \tilde{X}_{J-2} + \tilde{\tilde{B}}_{J-1} \tilde{X}_{J-1} = \tilde{S}_{J-1} \qquad \text{(F.1c)}$$

where the $\tilde{\tilde{A}}$'s, $\tilde{\tilde{B}}$'s, and $\tilde{\tilde{C}}$'s are the known 4x4 coefficient matrices, the $\tilde{S}$'s are the known 4-element source term vectors, and the $\tilde{X}$'s are the 4-element solution vectors given by

$$\tilde{X} = \begin{bmatrix} \rho \\ u \\ v \\ T \end{bmatrix} \qquad \text{(F.2)}$$

For $3 \leq j \leq J-2$, the coefficient matrices and source term vectors are given by

$$\tilde{\tilde{A}}_j = \begin{bmatrix} C_{C_1} & C_{C_4} & C_{C_7} & C_{C_{10}} \\ C_{X_1} & C_{X_4} & C_{X_7} & C_{X_{10}} \\ C_{Y_1} & C_{Y_4} & C_{Y_7} & C_{Y_{10}} \\ C_{E_1} & C_{E_4} & C_{E_7} & C_{E_{10}} \end{bmatrix} \qquad \text{(F.3a)}$$

ORIGINAL PAGE IS
OF POOR QUALITY

$$\tilde{\tilde{B}}_j = \begin{bmatrix} C_{C_2} & C_{C_5} & C_{C_8} & C_{C_{11}} \\ C_{X_2} & C_{X_5} & C_{X_8} & C_{X_{11}} \\ C_{Y_2} & C_{Y_5} & C_{Y_8} & C_{Y_{11}} \\ C_{E_2} & C_{E_5} & C_{E_8} & C_{E_{11}} \end{bmatrix} \qquad \text{(F.3b)}$$

$$\tilde{\tilde{C}}_j = \begin{bmatrix} C_{C_3} & C_{C_6} & C_{C_9} & C_{C_{12}} \\ C_{X_3} & C_{X_6} & C_{X_9} & C_{X_{12}} \\ C_{Y_3} & C_{Y_6} & C_{Y_9} & C_{Y_{12}} \\ C_{E_3} & C_{E_6} & C_{E_9} & C_{E_{12}} \end{bmatrix} \qquad \text{(F.3c)}$$

$$\tilde{S}_j = \begin{bmatrix} S_C \\ S_X \\ S_Y \\ S_E \end{bmatrix} \qquad \text{(F.3d)}$$

The elements in the above matrices are defined in Appendix D.

The form of the coefficient matrices and source term vectors at $j = 2$ and $j = J-1$ depend on the type of boundary conditions being used. In the following discussion, let $(\tilde{\tilde{B}}_2)_m$ represent the m'th row of $\tilde{\tilde{B}}_2$. This notation will also be used for $\tilde{\tilde{C}}_2$, $\tilde{\tilde{A}}_{J-1}$, and $\tilde{\tilde{B}}_{J-1}$.

ORIGINAL PAGE IS
OF POOR QUALITY

For a symmetry line at $j = 1$, the boundary conditions given in equations (3.19) are applied to equations (D.5)-(D.8). Each row of the matrix $\tilde{\tilde{B}}_2$ then has the form

$$(\tilde{\tilde{B}}_2)_m = \begin{bmatrix} C_{eq_2} + \frac{4}{3} C_{eq_1} \\ C_{eq_5} + \frac{4}{3} C_{eq_4} \\ C_{eq_8} \\ C_{eq_{11}} + \frac{4}{3} C_{eq_{10}} \end{bmatrix}^T \qquad \text{(F.4a)}$$

For convenience, $(\tilde{\tilde{B}}_2)_m$ has been written as the transpose of a column vector. In this equation, C_{eq} represents C_C, C_X, C_Y, and C_E for $m = 1, 2, 3$, and 4, respectively. This convention will be followed throughout this appendix. Each row of $\tilde{\tilde{C}}_2$ has the form

$$(\tilde{\tilde{C}}_2)_m = \begin{bmatrix} C_{eq_3} - \frac{1}{3} C_{eq_1} \\ C_{eq_6} - \frac{1}{3} C_{eq_4} \\ C_{eq_9} \\ C_{eq_{12}} - \frac{1}{3} C_{eq_{10}} \end{bmatrix}^T \qquad \text{(F.4b)}$$

The source term vector $\tilde{S}_2$ is unchanged from the form presented in equation (F.3d).

ORIGINAL PAGE IS
OF POOR QUALITY

At a wall with a specified temperature, the boundary conditions given by equations (3.20), (3.21), (3.22a), and (3.23) are applied to equations (D.5)-(D.8). For a solid surface at $j = 1$ with a specified temperature, then, each row of $\tilde{\tilde{B}}_2$ has the form

$$(\tilde{\tilde{B}}_2)_m = \begin{bmatrix} C_{eq_2} + \frac{C_{W_2}}{C_{W_1}} C_{eq_1} \\ C_{eq_5} + \frac{C_{W_5}}{C_{W_1}} C_{eq_1} \\ C_{eq_8} + \frac{C_{W_8}}{C_{W_1}} C_{eq_1} \\ C_{eq_{11}} + \frac{C_{W_{11}}}{C_{W_1}} C_{eq_1} \end{bmatrix}^T \qquad \text{(F.5a)}$$

and each row of $\tilde{\tilde{C}}_2$ has the form

$$(\tilde{\tilde{C}}_2)_m = \begin{bmatrix} C_{eq_3} + \frac{C_{W_3}}{C_{W_1}} C_{eq_1} \\ C_{eq_6} + \frac{C_{W_6}}{C_{W_1}} C_{eq_1} \\ C_{eq_9} + \frac{C_{W_9}}{C_{W_1}} C_{eq_1} \\ C_{eq_{12}} + \frac{C_{W_{12}}}{C_{W_1}} C_{eq_1} \end{bmatrix}^T \qquad \text{(F.5b)}$$

ORIGINAL PAGE IS
OF POOR QUALITY

Similarly, each element of the source term vector $\tilde{S}_2$ has the form

$$(\tilde{S}_2)_m = S_{eq} - \frac{S_W}{C_{W_1}} C_{eq_1} - \left(C_{eq_4} + \frac{C_{W_4}}{C_{W_1}} C_{eq_1}\right) u_{W_{i+1}} - \left(C_{eq_7} + \frac{C_{W_7}}{C_{W_1}} C_{eq_1}\right) v_{W_{i+1}} - \left(C_{eq_{10}} + \frac{C_{W_{10}}}{C_{W_1}} C_{eq_1}\right) T_{W_{i+1}} \qquad \text{(F.5c)}$$

For a specified wall temperature at $j = J$, each row of $\tilde{\tilde{A}}_{J-1}$ has the form

$$(\tilde{\tilde{A}}_{J-1})_m = \begin{bmatrix} C_{eq_1} + \frac{C_{W_3}}{C_{W_1}} C_{eq_3} \\ C_{eq_4} + \frac{C_{W_6}}{C_{W_1}} C_{eq_3} \\ C_{eq_7} + \frac{C_{W_9}}{C_{W_1}} C_{eq_3} \\ C_{eq_{10}} + \frac{C_{W_{12}}}{C_{W_1}} C_{eq_3} \end{bmatrix}^T \qquad \text{(F.6d)}$$

ORIGINAL PAGE IS
OF POOR QUALITY

and each row of $\tilde{\tilde{B}}_{J-1}$ has the form

$$(\tilde{\tilde{B}}_{J-1})_m = \begin{bmatrix} C_{eq_2} + \frac{C_{W_2}}{C_{W_1}} C_{eq_3} \\ C_{eq_5} + \frac{C_{W_5}}{C_{W_1}} C_{eq_3} \\ C_{eq_8} + \frac{C_{W_8}}{C_{W_1}} C_{eq_3} \\ C_{eq_{11}} + \frac{C_{W_{11}}}{C_{W_1}} C_{eq_3} \end{bmatrix}^T \tag{F.6b}$$

Each element of $\tilde{S}_{J-1}$ has the form

$$(\tilde{S}_{J-1})_m = S_{eq} - \frac{S_W}{C_{W_1}} C_{eq_3} - \left(C_{eq_6} + \frac{C_{W_4}}{C_{W_1}} C_{eq_3} \right) u_{W_{i+1}} - \left(C_{eq_9} + \frac{C_{W_7}}{C_{W_1}} C_{eq_3} \right) v_{W_{i+1}} - \left(C_{eq_{12}} + \frac{C_{W_{10}}}{C_{W_1}} C_{eq_3} \right) T_{W_{i+1}} \tag{F.6c}$$

At a wall with a specified temperature gradient normal to the wall, the boundary conditions are given by equations (3.20), (3.21),

ORIGINAL PAGE IS
OF POOR QUALITY

(3.22b), and (3.23). For a specified temperature gradient at the j = 1 wall then, each row of $\tilde{\tilde{B}}_2$ has the form

$$(\tilde{\tilde{B}}_2)_m = \begin{bmatrix} C_{eq_2} + \frac{C_{W_2}}{C_{W_1}} C_{eq_1} \\ C_{eq_5} + \frac{C_{W_5}}{C_{W_1}} C_{eq_1} \\ C_{eq_8} + \frac{C_{W_8}}{C_{W_1}} C_{eq_1} \\ C_{eq_{11}} + \frac{C_{W_{11}}}{C_{W_1}} C_{eq_1} + \frac{4}{3} C_{eq_{10}} \end{bmatrix}^T \qquad \text{(F.7a)}$$

and each row of $\tilde{\tilde{C}}_2$ has the form

$$(\tilde{\tilde{C}}_2)_m = \begin{bmatrix} C_{eq_3} + \frac{C_{W_3}}{C_{W_1}} C_{eq_1} \\ C_{eq_6} + \frac{C_{W_6}}{C_{W_1}} C_{eq_1} \\ C_{eq_9} + \frac{C_{W_9}}{C_{W_1}} C_{eq_1} \\ C_{eq_{12}} + \frac{C_{W_{12}}}{C_{W_1}} C_{eq_1} - \frac{1}{3} C_{eq_{10}} \end{bmatrix}^T \qquad \text{(F.7b)}$$

ORIGINAL PAGE IS
OF POOR QUALITY

Each element of $\tilde{S}_2$ has the form

$$(\tilde{S}_2)_m = S_{eq} - \frac{S_W}{C_{W_1}} C_{eq_1} - \left(C_{eq_4} + \frac{C_{W_4}}{C_{W_1}} C_{eq_1}\right) u_{W_{i+1}} - \left(C_{eq_7} + \frac{C_{W_7}}{C_{W_1}} C_{eq_1}\right) v_{W_{i+1}} + \frac{2}{3} C_{eq_{10}} \left(\frac{\partial T}{\partial Y}\right)_{W_{i+1}} \Delta Y \qquad \text{(F.7c)}$$

For a specified temperature gradient at the $j = J$ wall, each row of $\tilde{\tilde{A}}_{J-1}$ has the form

$$(\tilde{\tilde{A}}_{J-1})_m = \begin{bmatrix} C_{eq_1} + \frac{C_{W_3}}{C_{W_1}} C_{eq_3} \\ C_{eq_4} + \frac{C_{W_6}}{C_{W_1}} C_{eq_3} \\ C_{eq_7} + \frac{C_{W_9}}{C_{W_1}} C_{eq_3} \\ C_{eq_{10}} + \frac{C_{W_{12}}}{C_{W_1}} C_{eq_3} - \frac{1}{3} C_{eq_{12}} \end{bmatrix}^T \qquad \text{(F.8a)}$$

ORIGINAL PAGE IS
OF POOR QUALITY

and each row of $\tilde{\tilde{B}}_{J-1}$ has the form

$$(\tilde{\tilde{B}}_{J-1})_m = \begin{bmatrix} C_{eq_2} + \frac{C_{W_2}}{C_{W_1}} C_{eq_3} \\ C_{eq_5} + \frac{C_{W_5}}{C_{W_1}} C_{eq_3} \\ C_{eq_8} + \frac{C_{W_8}}{C_{W_1}} C_{eq_3} \\ C_{eq_{11}} + \frac{C_{W_{11}}}{C_{W_1}} C_{eq_3} + \frac{4}{3} C_{eq_{12}} \end{bmatrix}^T \qquad \text{(F.8b)}$$

Each element of $\tilde{S}_{J-1}$ has the form

$$(\tilde{S}_{J-1})_m = S_{eq} - \frac{S_W}{C_{W_1}} C_{eq_3} - \left(C_{eq_6} + \frac{C_{W_4}}{C_{W_1}} C_{eq_3} \right) u_{W_{i+1}} - \left(C_{eq_9} + \frac{C_{W_7}}{C_{W_1}} C_{eq_3} \right) v_{W_{i+1}} - \frac{2}{3} C_{eq_{12}} \left(\frac{\partial T}{\partial Y} \right)_{W_{i+1}} \Delta Y \qquad \text{(F.8c)}$$

When a wall function boundary condition is used for the streamwise velocity, and the temperature gradient normal to the wall is

ORIGINAL PAGE IS
OF POOR QUALITY

specified, the boundary conditions are given by equations (3.21), (3.22b), (3.23), and (3.24). Under these conditions at the j = 1 wall, each row of $\tilde{\tilde{B}}_2$ still has the form given in equation (F.7a). The form of each row of $\tilde{\tilde{C}}_2$ becomes

$$(\tilde{\tilde{C}}_2)_m = \begin{bmatrix} C_{eq_3} + \frac{C_{W_3}}{C_{W_1}} C_{eq_1} \\ C_{eq_4} + C_{eq_6} + \frac{C_{W_4} + C_{W_6}}{C_{W_1}} C_{eq_1} \\ C_{eq_9} + \frac{C_{W_9}}{C_{W_1}} C_{eq_1} \\ C_{eq_{12}} + \frac{C_{W_{12}}}{C_{W_1}} C_{eq_1} - \frac{1}{3} C_{eq_{10}} \end{bmatrix}^T \tag{F.9a}$$

In addition, the form of each element of $\tilde{S}_2$ becomes

$$(\tilde{S}_2)_m = S_{eq} - \frac{S_W}{C_{W_1}} C_{eq_1} - \left(C_{eq_4} + \frac{C_{W_4}}{C_{W_1}} C_{eq_1} \right) F_{u_W} - \left(C_{eq_7} + \frac{C_{W_7}}{C_{W_1}} C_{eq_1} \right) v_{W_{i+1}} + \frac{2}{3} C_{eq_{10}} \left(\frac{\partial T}{\partial Y} \right)_{W_{i+1}} \Delta Y \tag{F.9b}$$

ORIGINAL PAGE IS
OF POOR QUALITY

At the $j = J$ wall, each row of $\tilde{\tilde{B}}_{J-1}$ still has the form given in equation (F.8b). The form of each row of $\tilde{\tilde{A}}_{J-1}$ becomes

$$(\tilde{\tilde{A}}_{J-1})_m = \begin{bmatrix} C_{eq_1} + \frac{C_{W_3}}{C_{W_1}} C_{eq_3} \\ C_{eq_4} + C_{eq_6} + \frac{C_{W_4} + C_{W_6}}{C_{W_1}} C_{eq_3} \\ C_{eq_7} + \frac{C_{W_9}}{C_{W_1}} C_{eq_3} \\ C_{eq_{10}} + \frac{C_{W_{12}}}{C_{W_1}} C_{eq_3} - \frac{1}{3} C_{eq_{12}} \end{bmatrix}^T \qquad \text{(F.10a)}$$

and the form of each element of $\tilde{S}_{J-1}$ becomes

$$(\tilde{S}_{J-1})_m = S_{eq} - \frac{S_W}{C_{W_1}} C_{eq_3} - \left(C_{eq_6} + \frac{C_{W_4}}{C_{W_1}} C_{eq_3} \right) F_{u_W} - \left(C_{eq_9} + \frac{C_{W_7}}{C_{W_1}} C_{eq_3} \right) v_{W_{i+1}} - \frac{2}{3} C_{eq_{12}} \left(\frac{\partial T}{\partial Y} \right)_{W_{i+1}} \Delta Y \qquad \text{(F.10b)}$$

The parameter F_{u_W} appearing in equations (F.9b) and (F.10b) is defined by

$$F_{u_W} = (2\ \Delta Y) \left(\frac{h_2}{dY/d\eta} \right)_{j+1} \frac{1}{\kappa} u_{\tau_j} \frac{1}{y_{j+1}} \qquad \text{(F.11)}$$

ORIGINAL PAGE IS
OF POOR QUALITY

where the top sign is used for the $j = 1$ wall and the bottom sign is used for the $j = J$ wall.

When a wall function boundary condition is used for the streamwise velocity, and the wall temperature is to be specified, the boundary conditions are given by equations (3.21), (3.23) (3.24), and (3.25). Under these conditions at the $j = 1$ wall, each row of $\tilde{\tilde{B}}_2$ has the form

$$(\tilde{\tilde{B}}_2)_m = \begin{bmatrix} C_{eq_2} + \frac{C_{W_2}}{C_{W_1}} C_{eq_1} \\ C_{eq_5} + \frac{C_{W_5}}{C_{W_1}} C_{eq_1} \\ C_{eq_8} + \frac{C_{W_8}}{C_{W_1}} C_{eq_1} \\ C_{eq_{11}} + \frac{C_{W_{11}}}{C_{W_1}} C_{eq_1} - \left(C_{eq_{10}} + \frac{C_{W_{10}}}{C_{W_1}} C_{eq_1} \right) F_{T_W} \end{bmatrix}^T \qquad \text{(F.12a)}$$

ORIGINAL PAGE IS
OF POOR QUALITY

and each row of $\tilde{\tilde{C}}_2$ has the form

$$(\tilde{\tilde{C}}_2)_m = \begin{bmatrix} C_{eq_3} + \frac{C_{W_3}}{C_{W_1}} C_{eq_1} \\ C_{eq_4} + C_{eq_6} + \frac{C_{W_4} + C_{W_6}}{C_{W_1}} C_{eq_1} \\ C_{eq_9} + \frac{C_{W_9}}{C_{W_1}} C_{eq_1} \\ C_{eq_{10}} + C_{eq_{12}} + \frac{C_{W_{10}} + C_{W_{12}}}{C_{W_1}} C_{eq_1} \end{bmatrix}^T \qquad \text{(F.12b)}$$

In addition, the form of each element of $\tilde{S}_2$ becomes

$$(\tilde{S}_2)_m = S_{eq} - \frac{S_W}{C_{W_1}} C_{eq_1} - \left(C_{eq_4} + \frac{C_{W_4}}{C_{W_1}} C_{eq_1} \right) F_{u_W} - \left(C_{eq_7} + \frac{C_{W_7}}{C_{W_1}} C_{eq_1} \right) v_{W_{i+1}} - \left(C_{eq_{10}} + \frac{C_{W_{10}}}{C_{W_1}} C_{eq_1} \right) T_W F_{T_W} \qquad \text{(F.12c)}$$

ORIGINAL PAGE IS
OF POOR QUALITY

For these boundary conditions at the $j = J$ wall, each row of $\tilde{\tilde{A}}_{J-1}$ has the form

$$(\tilde{\tilde{A}}_{J-1})_m = \begin{bmatrix} C_{eq_1} + \frac{C_{W_3}}{C_{W_1}} C_{eq_3} \\ C_{eq_4} + C_{eq_6} + \frac{C_{W_4} + C_{W_6}}{C_{W_1}} C_{eq_3} \\ C_{eq_7} + \frac{C_{W_9}}{C_{W_1}} C_{eq_3} \\ C_{eq_{10}} + C_{eq_{12}} + \frac{C_{W_{10}} + C_{W_{12}}}{C_{W_1}} C_{eq_3} \end{bmatrix}^T \qquad \text{(F.13a)}$$

and each row of $\tilde{\tilde{B}}_{J-1}$ has the form

$$(\tilde{\tilde{B}}_{J-1})_m = \begin{bmatrix} C_{eq_2} + \frac{C_{W_2}}{C_{W_1}} C_{eq_3} \\ C_{eq_5} + \frac{C_{W_5}}{C_{W_1}} C_{eq_3} \\ C_{eq_8} + \frac{C_{W_8}}{C_{W_1}} C_{eq_3} \\ C_{eq_{11}} + \frac{C_{W_{11}}}{C_{W_1}} C_{eq_3} - \left(C_{eq_{12}} + \frac{C_{W_{10}}}{C_{W_1}} C_{eq_3} \right) F_{T_W} \end{bmatrix}^T \qquad \text{(F.13b)}$$

ORIGINAL PAGE IS
OF POOR QUALITY

The form of each element of $\tilde{S}_{J-1}$ becomes

$$(\tilde{S}_{J-1})_m = S_{eq} - \frac{S_W}{C_{W_1}} C_{eq_3} - \left(C_{eq_6} + \frac{C_{W_4}}{C_{W_1}} C_{eq_3} \right) F_{u_W} - \left(C_{eq_9} + \frac{C_{W_7}}{C_{W_1}} C_{eq_3} \right) v_{W_{i+1}} - \left(C_{eq_{12}} + \frac{C_{W_{10}}}{C_{W_1}} C_{eq_3} \right) T_W F_{T_W} \qquad \text{(F.13c)}$$

The parameter F_{T_W} is defined by

$$F_{T_W} = (2 \Delta Y) \left(\frac{h_2}{dY/dn} \right)_{j+1} \left[\kappa y_{j+1} \left(Pr_T \frac{1}{\kappa} \ln y^+_{j+1} + c_1 \right) \right]^{-1} \qquad \text{(F.14)}$$

APPENDIX G

DIFFERENCE EQUATIONS FOR VISCOUS PRESSURE CORRECTION

In this appendix, the difference equations used to compute the viscous pressure correction p' during the preliminary marching step are derived. First the streamwise momentum equation, presented in Section 2.2.1 as equation (2.14), is uncoupled from the continuity, cross-flow momentum, and energy equations and written in finite-difference form. The uncoupling is done by evaluating ρ, u, v, and T at the known station i. The "j" subscript has been omitted from all terms in the equation, since it is valid at any j-location. In addition, the "i+w" subscript has been omitted from the metric scale coefficients. The notation from Section 3.2 is used, so that $\Delta u = u^*_{i+1} - u_i$. The superscript * is used on u^* to distinguish it from the streamwise velocity to be computed during the main marching step. Note, however, that the variables at the known station i are those from the previous completely-coupled main marching step. The subscripts ξ and η denote partial differentiation. The resulting uncoupled streamwise momentum difference equation is as follows:

ORIGINAL PAGE IS
OF POOR QUALITY

$$\frac{1}{h_1}\rho_i u_i \frac{u^*_{i+1} - u_i}{\Delta\xi} + \frac{1}{h_2}\frac{dY}{d\eta}\rho_i v_i\left[\delta_Y u_i + w\,\delta_Y(\Delta u)\right] - \frac{h_{2_\xi}}{h_1 h_2}\rho_i v_i^2$$

$$+ \frac{h_{1_\eta}}{h_1 h_2}\rho_i v_i(u_i + w\,\Delta u) = -\frac{1}{h_1}(P_\xi + p'_\xi)_{i+w} + \frac{1}{Re_r}\frac{1}{h_1 h_2 h_3}$$

$$\times\left\{ h_3\frac{dY}{d\eta}\delta_Y(\mu v_\xi)_i + h_{3_\eta}\mu_i v_{\xi_i} - \frac{h_3 h_{2_\xi}}{h_2}\frac{dY}{d\eta}\delta_Y(\mu v)_i - \left(\frac{h_3 h_{2_\xi}}{h_2}\right)_\eta\right.$$

$$\times\,\mu_i v_i + \frac{h_1 h_3}{h_2}\frac{dY}{d\eta}\left[\delta_Y\left(\frac{dY}{d\eta}\mu_i\,\delta_Y u_i\right) + w\frac{dY}{d\eta}\mu_i\,\delta_Y^2(\Delta u) + w\,\delta_Y\right.$$

$$\times\left.\left(\frac{dY}{d\eta}\mu_i\right)\delta_Y(\Delta u)\right] + \left(\frac{h_1 h_3}{h_2}\right)_\eta\frac{dY}{d\eta}\mu_i\left[\delta_Y u_i + w\,\delta_Y(\Delta u)\right] - \frac{h_3 h_{1_\eta}}{h_2}$$

$$\times\;\frac{dY}{d\eta}\left[\delta_Y(\mu u)_i + w u_i\,\delta_Y(\Delta u) + w(\delta_Y\mu_i)\,\Delta u\right] - \left(\frac{h_3 h_{1_\eta}}{h_2}\right)_\eta\mu_i$$

$$\left.\times\,(u_i + w\,\Delta u)\right\} + \frac{1}{Re_r}\frac{h_{1_\eta}}{h_1 h_2}\left\{\frac{1}{h_1}\mu_i v_{\xi_i} - \frac{h_{2_\xi}}{h_1 h_2}\mu_i v_i + \frac{1}{h_2}\frac{dY}{d\eta}\mu_i\right.$$

$$\left.\times\left[\delta_Y u_i + w\,\delta_Y(\Delta u)\right] - \frac{h_{1_\eta}}{h_1 h_2}\mu_i(u_i + w\,\Delta u)\right\} - \frac{1}{Re_r}\frac{h_{2_\xi}}{h_1 h_2}$$

$$\times\;\left\{\frac{4}{3}\frac{1}{h_2}\frac{dY}{d\eta}\mu_i\,\delta_Y v_i - \frac{2}{3}\frac{1}{h_2}\left(\frac{h_{1_\eta}}{h_1} + \frac{h_{3_\eta}}{h_3}\right)\mu_i v_i - \frac{2}{3}\frac{1}{h_1}\mu_i\right.$$

Continued on next page

ORIGINAL PAGE IS
OF POOR QUALITY

$$\times \frac{u^*_{i+1} - u_i}{\Delta\xi} + \frac{2}{3}\frac{1}{h_1}\left(2\frac{h_{2_\xi}}{h_2} - \frac{h_{3_\xi}}{h_3}\right)\mu_i(u_i + w\,\Delta u)\Bigg\} - \frac{1}{Re_r}$$

$$\times \frac{h_{3_\xi}}{h_1 h_3}\Bigg\{-\frac{2}{3}\frac{1}{h_1}\mu_i\frac{u^*_{i+1} - u_i}{\Delta\xi} + \frac{2}{3}\frac{1}{h_1}\left(2\frac{h_{3_\xi}}{h_3} - \frac{h_{2_\xi}}{h_2}\right)$$

$$\times \mu_i(u_i + w\,\Delta u) - \frac{2}{3}\frac{1}{h_2}\frac{dY}{dn}\mu_i\,\delta_Y v_i + \frac{2}{3}\frac{1}{h_2}\left(2\frac{h_{3_n}}{h_3} - \frac{h_{1_n}}{h_1}\right)\mu_i v_i\Bigg\} \tag{G.1}$$

After collecting terms and applying the boundary conditions, equation (G.1) can be written as

$$b_2 u^*_2 + c_2 u^*_3 + d_2 p'_\xi = s_{x_2}$$

$$a_j u^*_{j-1} + b_j u^*_j + c_j u^*_{j+1} + d_j p'_\xi = s_{x_j} \qquad (3 \le j \le J-2) \tag{G.2}$$

$$a_{J-1} u^*_{J-2} + b_{J-1} u^*_{J-1} + d_{J-1} p'_\xi = s_{x_{J-1}}$$

where, for $2 \le j \le J-1$,

$$d_j = \frac{1}{h_1}\Delta\xi$$

ORIGINAL PAGE IS
OF POOR QUALITY

Now, for $2 \le j \le J-1$, let

$$a_j' = -\frac{1}{h_2}\frac{dY}{dn} w \rho_i v_i \frac{\Delta\xi}{2\Delta Y} + \frac{1}{Re_r}\frac{1}{h_1 h_2 h_3}\frac{dY}{dn} w\left[\frac{h_1 h_3}{h_2}\delta_Y\left(\frac{dY}{dn}\mu_i\right)\right.$$

$$\left. + \left(\frac{h_1 h_3}{h_2}\right)_n \mu_i - \frac{h_3 h_{1_n}}{h_2}\mu_i\right]\frac{\Delta\xi}{2\Delta Y} + \frac{1}{Re_r}\frac{h_{1_n}}{h_1 h_2^2}\frac{dY}{dn} w\mu_i \frac{\Delta\xi}{2\Delta Y}$$

$$- \frac{1}{Re_r}\frac{1}{h_2^2}\left(\frac{dY}{dn}\right)^2 w\mu_i \frac{\Delta\xi}{(\Delta Y)^2}$$

$$b_j' = \frac{1}{h_1}\rho_i u_i - \frac{1}{Re_r}\left(\frac{h_{2_\xi}}{h_1 h_2} + \frac{h_{3_\xi}}{h_1 h_3}\right)\frac{2}{3}\frac{1}{h_1}\mu_i + \frac{h_{1_n}}{h_1 h_2} w\rho_i v_i \Delta\xi$$

$$+ \frac{1}{Re_r}\frac{1}{h_1 h_2 h_3} w\left[\frac{h_3 h_{1_n}}{h_2}\frac{dY}{dn}\delta_Y\mu_i + \left(\frac{h_3 h_{1_n}}{h_2}\right)_n \mu_i\right]\Delta\xi + \frac{1}{Re_r}$$

$$\times\left[\left(\frac{h_{1_n}}{h_1 h_2}\right)^2 + \frac{2}{3}\frac{h_{2_\xi}}{h_1^2 h_2}\left(2\frac{h_{2_\xi}}{h_2} - \frac{h_{3_\xi}}{h_3}\right) + \frac{2}{3}\frac{h_{3_\xi}}{h_1^2 h_3}\left(2\frac{h_{3_\xi}}{h_3}\right.\right.$$

$$\left.\left. - \frac{h_{2_\xi}}{h_2}\right)\right] w\mu_i \Delta\xi + \frac{2}{Re_r}\frac{1}{h_2^2}\left(\frac{dY}{dn}\right)^2 w\mu_i \frac{\Delta\xi}{(\Delta Y)^2}$$

$$c_j' = -a_j' - \frac{2}{Re_r}\frac{1}{h_2^2}\left(\frac{dY}{dn}\right)^2 w\mu_i \frac{\Delta\xi}{(\Delta Y)^2}$$

ORIGINAL PAGE IS
OF POOR QUALITY

$$S'_{X_j} = \frac{1}{h_1}\rho_i u_i^2 - \frac{1}{h_2}\frac{dY}{d\eta}(1-w)\rho_i v_i(\delta_Y u_i)\Delta\xi + \frac{h_{2_\xi}}{h_1 h_2}\rho_i v_i^2\Delta\xi$$

$$- \frac{h_{1_\eta}}{h_1 h_2}(1-w)\rho_i u_i v_i \Delta\xi - \frac{1}{h_1}\left(\frac{\partial P}{\partial\xi}\right)_{i+w} + \frac{1}{Re_r}\frac{1}{h_1 h_2 h_3}\left\{h_3\frac{dY}{d\eta}\right.$$

$$\times \delta_Y(\mu v_\xi)_i + h_{3_\eta}\mu_i v_{\xi_i} - \frac{h_3 h_{2_\xi}}{h_2}\frac{dY}{d\eta}\delta_Y(\mu v)_i - \left(\frac{h_3 h_{2_\xi}}{h_2}\right)_\eta \mu_i v_i$$

$$+ \frac{h_1 h_3}{h_2}\frac{dY}{d\eta}\left[\delta_Y\left(\frac{dY}{d\eta}\mu_i\,\delta_Y u_i\right) - w\frac{dY}{d\eta}\mu_i\,\delta_Y^2 u_i - w\,\delta_Y\left(\frac{dY}{d\eta}\mu_i\right)u_i\right]$$

$$+ \left(\frac{h_1 h_3}{h_2}\right)_\eta \frac{dY}{d\eta}(1-w)\mu_i\,\delta_Y u_i - \frac{h_3 h_{1_\eta}}{h_2}\frac{dY}{d\eta}\left[(1-w)\mu_i\,\delta_Y u_i\right.$$

$$\left.\left. + (1-w)(\delta_Y\mu_i)u_i\right] - \left(\frac{h_3 h_{1_\eta}}{h_2}\right)_\eta (1-w)\mu_i u_i\right\}\Delta\xi + \frac{1}{Re_r}\frac{h_{1_\eta}}{h_1 h_2}$$

$$\times\left[\frac{1}{h_1}\mu_i v_{\xi_i} - \frac{h_{2_\xi}}{h_1 h_2}\mu_i v_i + \frac{1}{h_2}\frac{dY}{d\eta}(1-w)\mu_i\,\delta_Y u_i - \frac{h_{1_\eta}}{h_1 h_2}(1-w)\right.$$

$$\left.\times\,\mu_i u_i\right]\Delta\xi - \frac{1}{Re_r}\frac{h_{2_\xi}}{h_1 h_2}\left[\frac{4}{3}\frac{1}{h_2}\frac{dY}{d\eta}\mu_i\,\delta_Y v_i - \frac{2}{3}\frac{1}{h_2}\left(\frac{h_{1_\eta}}{h_1} + \frac{h_{3_\eta}}{h_3}\right)\mu_i v_i\right.$$

$$\left. + \frac{2}{3}\frac{1}{h_1}\mu_i\frac{u_i}{\Delta\xi} + \frac{2}{3}\frac{1}{h_1}\left(2\frac{h_{2_\xi}}{h_2} - \frac{h_{3_\xi}}{h_3}\right)(1-w)\mu_i u_i\right]\Delta\xi$$

$$- \frac{1}{Re_r}\frac{h_{3_\xi}}{h_1 h_3}\left[\frac{2}{3}\frac{1}{h_1}\mu_i\frac{u_i}{\Delta\xi} + \frac{2}{3}\frac{1}{h_1}\left(2\frac{h_{3_\xi}}{h_3} - \frac{h_{2_\xi}}{h_2}\right)(1-w)\mu_i u_i\right.$$

Continued on next page

ORIGINAL PAGE IS
OF POOR QUALITY

$$- \frac{2}{3} \frac{1}{h_2} \frac{dY}{d\eta} \mu_i \, \delta_Y v_i + \frac{2}{3} \frac{1}{h_2} \left(2 \frac{h_{3_\eta}}{h_3} - \frac{h_{1_\eta}}{h_1} \right) \mu_i v_i \Bigg] \Delta\xi$$

For $3 \leq j \leq J-2$, the coefficients in equation (G.2) are simply given by

$$a_j = a'_j$$

$$b_j = b'_j$$

$$c_j = c'_j$$

$$s_{X_j} = s'_{X_j}$$

However, the forms of the coefficients b_2, c_2, a_{J-1}, and b_{J-1}, and the source terms s_{X_2} and $s_{X_{J-1}}$ depend on the type of boundary condition being used. For a symmetry line at $j = 1$, using equation (3.19) gives

$$b_2 = b'_2 + \frac{4}{3} a'_2$$

$$c_2 = c'_2 - \frac{1}{3} a'_2$$

$$s_{X_2} = s'_{X_2}$$

ORIGINAL PAGE IS
OF POOR QUALITY

For a solid wall at $j = 1$ with $u_1 = u_W$,

$$b_2 = b_2'$$

$$c_2 = c_2'$$

$$s_{X_2} = s'_{X_2} - a_2' u_W$$

For a wall function boundary condition at $j = 1$, using equation (3.24) gives

$$b_2 = b_2'$$

$$c_2 = a_2' + c_2'$$

$$s_{X_2} = s'_{X_2} + a_2' F_{u_W}$$

where F_{u_W} is defined by equation (F.11). For $u_J = u_W$ at $j = J$,

$$a_{J-1} = a'_{J-1}$$

$$b_{J-1} = b'_{J-1}$$

$$s_{X_{J-1}} = s'_{X_{J-1}} - c'_{J-1} u_W$$

And finally, for a wall function boundary condition at $j = J$,

$$a_{J-1} = a'_{J-1} + c'_{J-1}$$

$$b_{J-1} = b'_{J-1}$$

$$s_{X_{J-1}} = s'_{X_{J-1}} + c'_{J-1} F_{u_W}$$

ORIGINAL PAGE IS
OF POOR QUALITY

The other equation used to compute the viscous pressure correction is the total mass flow rate equation, derived in Section 3.5.2. It is repeated here.

$$\int_0^1 \frac{1}{RT_i}\left[-p'_{\xi_{i-1+w}}\,u_i\,\Delta\xi + \left(P_{i+1} + p'_i + p'_{\xi_{i-1+w}}\,\Delta\xi\right) u^*_{i+1} + u_i p'_{\xi_{i+w}}\,\Delta\xi\right]\left(\frac{h_2 h_3}{\partial Y/d\eta}\right)_{i+1}(2\pi)^\omega\,dY = \dot{m} \qquad (G.3)$$

The unknowns in this equation are u^*_{i+1} and $p'_{\xi_{i+w}}$. By moving the known terms to the right side, equation (G.3) can be rewritten as

$$\int_0^1 \frac{1}{RT_i}\left[\left(P_{i+1} + p'_i + p'_{\xi_{i-1+w}}\,\Delta\xi\right) u^*_{i+1} + u_i p'_{\xi_{i+w}}\,\Delta\xi\right]\left(\frac{h_2 h_3}{dY/d\eta}\right)_{i+1}(2\pi)^\omega\,dY = \dot{m}$$

$$+\int_0^1 \frac{1}{RT_i}\,p'_{\xi_{i-1+w}}\,u_i\,\Delta\xi\left(\frac{h_2 h_3}{dY/d\eta}\right)_{i+1}(2\pi)^\omega\,dY \qquad (G.4)$$

Equation (G.4) is to be integrated numerically from $j = 1$ to $j = J$ using Simpson's rule. Since Simpson's rule requires an odd number of grid points, if J is even the integration from $J-1$ to J is done by trapezoidal rule. When the integration is performed, and the boundary conditions are applied, the resulting equation can be written as

$$e_2 u^*_2 + e_3 u^*_3 + \ldots + e_{J-2} u^*_{J-2} + e_{J-1} u^*_{J-1} + f p'_\xi = s_M \qquad (G.5)$$

ORIGINAL PAGE IS
OF POOR QUALITY

where

$$f = \frac{3}{(2\pi)^{\omega}\,\Delta Y}\int_0^1 \frac{1}{RT_i}\,u_i\,\Delta\xi\left(\frac{h_2h_3}{dY/d\eta}\right)_{i+1}(2\pi)^{\omega}\,dY$$

Now, for $1 \le j \le J$, let

$$e_j' = \frac{1}{RT_i}\left(P_{i+1} + p_i' + p'_{\xi_{i-1+w}}\,\Delta\xi\right)\left(\frac{h_2h_3}{dY/d\eta}\right)_{i+1}$$

$$s_m' = \frac{3}{(2\pi)^{\omega}\,\Delta Y}\left[\dot{m} + \int_0^1 \frac{1}{RT_i}\,p'_{\xi_{i-1+w}}\,u_i\,\Delta\xi\left(\frac{h_2h_3}{dY/d\eta}\right)_{i+1}(2\pi)^{\omega}\,dY\right]$$

Then for even j's from 4 to J-3, the coefficients in equation (G.5) are given by

$$e_j = 4e_j'$$

and for odd j's from 5 to J-3,

$$e_j = 2e_j'$$

The exact forms of e_2 and e_3 depend on the type of boundary condition used at j = 1. For a symmetry line at j = 1,

$$e_2 = 4e_2' + \frac{4}{3}e_1'$$

$$e_3 = 2e_3' - \frac{1}{3}e_1'$$

For a solid surface at j = 1 with $u_1 = u_w$,

$$e_2 = 4e_2'$$

$$e_3 = 2e_3'$$

ORIGINAL PAGE IS
OF POOR QUALITY

And for a wall function boundary condition at $j = 1$,

$$e_2 = 4e'_2$$

$$e_3 = e'_1 + 2e'_3$$

The forms of e_{J-2} and e_{J-1} depend on the boundary condition used at $j = J$, and on whether J is odd or even. For J odd and $u_J = u_W$,

$$e_{J-2} = 2e'_{J-2}$$

$$e_{J-1} = 4e'_{J-1}$$

For J odd with a wall function boundary condition at $j = J$,

$$e_{J-2} = 2e'_{J-2} + e'_J$$

$$e_{J-1} = 4e'_{J-1}$$

For J even and $u_J = u_W$,

$$e_{J-2} = 4e'_{J-2}$$

$$e_{J-1} = \frac{5}{2} e'_{J-1}$$

For J even with a wall function boundary condition at $j = J$,

$$e_{J-2} = 4e'_{J-2} + \frac{3}{2} e'_J$$

$$e_{J-1} = \frac{5}{2} e'_{J-1}$$

The form of the source term s_M depends on the types of boundary conditions used at $j = 1$ and at $j = J$, and on whether

ORIGINAL PAGE IS
OF POOR QUALITY

J is odd or even. First, for J odd with symmetry conditions at j = 1,

$$s_m = s'_m - e'_J F'_J$$

where $F'_J = u_J$ for a specified velocity boundary condition at j = J, and $F'_J = -F_{u_J}$ for a wall function boundary condition at j = J. For J odd with a solid surface at j = 1,

$$s_M = s'_M - e'_1 F'_1 - e'_J F'_J$$

where $F'_1 = u_1$ for a specified velocity boundary condition at j = 1, and $F'_1 = -F_{u_1}$ for a wall function boundary condition at j = 1. For J even with a symmetry line at j = 1,

$$s_m = s'_m - \frac{3}{2} e'_J F'_J$$

And finally, for J even with a solid surface at j = 1,

$$s_M = s'_M - e'_1 F'_1 - \frac{3}{2} e'_J F'_J$$

ORIGINAL PAGE IS
OF POOR QUALITY

APPENDIX H

JEFFERY-HAMEL FLOW STREAMWISE PRESSURE GRADIENT

One of the classical examples of viscous duct flow is laminar incompressible flow in a two-dimensional wedge-shaped channel, known as Jeffery-Hamel flow. When self-similarity is assumed, an exact solution to the Navier-Stokes equations exists for this flow. The streamlines are radial, intersecting at a line source (for diverging flow) or sink (for converging flow). The solution for the velocity, derived in terms of Jacobian elliptic functions, is given by Millsaps and Pohlhausen (Ref. 60). From Reference 60, the velocity profile for converging Jeffery-Hamel flow is given by

$$F(\varphi) = 2\,[m^2(k^2 - 2) - 1] + 6\,m^2(1 - k^2)\,dn^{-2}(m\varphi, k) \qquad (H.1)$$

where

$$F(\varphi) = \frac{uR_s}{\nu} \qquad (H.2)$$

$$m^2 = \frac{1 + Re_0/2}{1 - 2k^2} \qquad (H.3)$$

and k is the largest number satisfying the equation

$$sn^2(m\alpha, k) = \frac{Re_0(1 - 2\,k^2)}{2k^2\left[3k^2 - 3 + \frac{Re_0}{2}\,(k^2 - 2)\right]} \qquad (H.4)$$

ORIGINAL PAGE IS
OF POOR QUALITY

Here $sn(m_\alpha,k)$ and $dn(m_\varphi,k)$ are Jacobian elliptic functions, which are evaluated by the Arithmetic-Geometric Mean method of Reference 77. The Reynolds number Re_0 is given by

$$Re_0 = \frac{u_{CL} R_S}{\nu}$$

The polar coordinates R_S and φ are defined in Figure 4-16, u_{CL} is the centerline velocity at a given R_S, and α is the half-angle of the duct. For the case studied here ($Re_0 = -5000$, $\alpha = 5$ degrees) the value of k is 0.99988175.

The radial momentum equation for purely radial flow, in the coordinate system of Figure 4-16, is

$$u \frac{\partial u}{\partial R_S} = -\frac{1}{\rho}\frac{\partial p}{\partial R_S} + \nu \left(\frac{\partial^2 u}{\partial R_S^2} + \frac{1}{R_S}\frac{\partial u}{\partial R_S} + \frac{1}{R_S^2}\frac{\partial^2 u}{\partial \varphi^2} - \frac{u}{R_S^2} \right) \qquad \text{(H.5)}$$

Substituting equation (H.2) for u gives

$$\frac{\partial p}{\partial R_S} = \frac{\rho \nu^2}{R_S^3} \left(F^2 + \frac{d^2F}{d\varphi^2} \right) \qquad \text{(H.6)}$$

Using derivatives of Jacobian elliptic functions as given by Reference 77, the second derivative on the right-hand side of equation (H.6) is given by

$$\frac{d^2F}{d\varphi^2} = 12m^4(1 - k^2)k\, dn^{-2}(m_\varphi,k) \Big[- sn^2(m_\varphi,k)\, dn^2(m_\varphi,k)$$

$$+ cn^2(m_\varphi,k)\, dn^2(m_\varphi,k) + 3k\, sn^2(m_\varphi,k)\, cn^2(m_\varphi,k) \Big]$$

Here $cn(m\varphi,k)$ is also a Jacobian elliptic function.

Since the computational streamwise coordinate ξ is given by

$$\xi = R_{S_1} - R_S$$

the exact streamwise pressure gradient is

$$\frac{\partial p}{\partial \xi} = -\frac{\rho v^2}{R_S^3}\left(F^2 + \frac{d^2F}{d\varphi^2}\right) \qquad \text{(H.7)}$$